EFFECTS OF MICROSTRUCTURAL AND MECHANICAL TESTING VARIABLES ON THE TOUGHNESS OF QUENCHED AND TEMPERED 4340 STEEL

by

Kanti P. Datta
B. Tech (Hons), I.I.T., Kharagpur, India
M. Tech., I.I.T., Kharagpur, India

A thesis submitted to the faculty
of the Oregon Graduate Center
in partial fulfillment of the
requirements for the degree
Doctor of Philosophy
in
Materials Science

September 1979

This dissertation has been examined and approved by the following Examination Committee:

W. E. Wood, Thesis Advisor
Associate Professor
Chairman
Department of Materials Science

N. G. Eror
Associate Professor
Department of Materials Science

R. A. Elliott
Associate Professor
Department of Applied Physics
and Electronic Science

D. G. Atteridge
Senior Research Scientist
Battelle - Northwest
Richland, Washington

DEDICATION

This is dedicated to the memory of my father, whose spirit left the material plane during the course of this work.

ACKNOWLEDGEMENT

I wish to express my appreciation to the faculty, staff and students of the Oregon Graduate Center for the opportunity of participating in the Center's unique program of graduate education. Gratefully acknowledged is the financial support provided by the Center in the form of a research fellowship.

I would like to thank my thesis committee, Dr. W.E. Wood, Dr. N. G. Eror, Dr. R.A. Elliott, and Dr. D. Atteridge for going through the manuscript and giving helpful suggestions. In addition, I would like to thank Mr. D. Ireland and Dr. D. Atteridge for the help in carrying out the experiments at Effects Technology, Santa Barbara, and Dr. V.C. Kannan of Bell Laboratories for critical discussions and encouragement. Thanks are also due to Mr. John Biskey for the experimental help in the initial stages.

Finally, I would like to thank Mrs. Janijo Weidner for her many pages of flawless typing and Mrs. Barbara Ryall for many of her excellent line drawings.

TABLE OF CONTENTS

TABLE OF CONTENTS (Cont'd)

TABLE OF CONTENTS (Cont'd)

TABLE OF CONTENTS (Cont'd)

ABSTRACT

The effects of notch root radii on the toughness of quenched and tempered 4340 steel were studied in greater details by instrumented and slow-bend Charpy tests. Also studied was the effect of tempering after both high and conventional austenitizing temperatures by fracture toughness, slow-bend Charpy and instrumented Charpy tests. The effects of bainitic isothermal transformations from high temperature austenitization of 4340 steel were studied by fracture toughness and tensile tests. Microstructural investigation was carried out by optical, transmission and scanning electron microscopy as well as X-ray diffraction.

The effects of notch root radii on the toughness results showed that initially the toughness increased as the notch-root radius increased and then after a critical notch-root radius was reached, the toughness dropped. The loss in toughness was coincident with an intergranular fracture initiation mode. Also, the critical root radius at which the drop in toughness was noticed was strongly temperature and strain rate dependent but independent of the prior austenitic grain size. The critical stress or strain model applies for the initial rise of the toughness with notch root radius. Beyond the critical notch root radius, fracture criteria based on 'strain energy density' is consistent with the observed drop in toughness. A physical model involving double slip band for the intergranular fracture initiation mode is also discussed.

A new explanation for the differences in toughness behavior between the sharp crack and blunt notch behavior for the two heat-treatments is provided. ε-carbide precipitation in as-quenched martensite from high temperature austenitization is proposed to improve the toughness in 'sharp crack' testing. In blunt notch testing, the importance of grain size is stressed. Here, larger grain size resulted in inferior toughness.

Finally the results indicated that the limited bainitic heat-treatments from high austenitizing temperature studied in this investigation were not conducive to either toughness or tensile strength. The impairment of mechanical properties is attributed to large bainitic ferrite grain size. The tempering behavior from high austenitizing temperature showed that up to a tempering temperature of about 175°C, toughness increased continuously; however, toughness dropped at a tempering temperature as low as 225°C for the high austenitizing case, whereas no such drop was observed in that tempering temperature range for the low austenitizing temperature case. SEM, TEM and X-ray studies have indicated that the loss in toughness was associated with a change in fracture mode, i.e. from microvoid coalescence to intergranular fracture, and was also coincident with cementite precipitation. It is believed that the prior austenite grain boundary segregation coupled with cementite precipitation triggered the above embrittlement.

INTRODUCTION

Making of iron and steel for use to mankind's advantage dates back to antiquity. Evidences of use of metals in pre-historic days are not wanting. However, production of steels and later alloy steels in an organized way started only in the last century, when cementation and crucible processes were invented. Thereafter, followed a series of more advanced processes such as the Bessemer process, the open hearth process, the basic oxygen process and finally the electric furnace process of steel making. As the processes of steel making were improved steadily, so also was the development of steel itself. Apart from carbon steels with different carbon contents for various uses, alloy steels, which contain one or more other elements to give them special qualities, were also developed. For example, today we have aluminum steel which is smooth and has a high tensile strength. Chromium steel is most widely used in automobile and airplane parts. Nickel steel has the tensile strength of high carbon steel without brittleness. Nickel-chromium steel possesses a shock resistant quality that makes it suitable for armor plate. 4340 is such a low alloy (Ni-Cr-Mo) ultra-high strength and apart from other applications, is widely used for the landing gear of aircraft as it has a comparatively high strength to weight ratio. Modification in the alloy contents or in the processing variables of such alloy steels is still underway for achieving higher strength and toughness to meet today's ever increasing demands.

As the need for newer, stronger, and purer materials in general and steel in particular has increased, so also has the need increased to guarantee safety against catastrophic failures, especially in this space-age world. That has led to different testing methods to assess a materials resistance against fracture (also known as toughness), i.e. Charpy, Izod, tension, fatigue to name only a few. As all the above testing methods have some limitations, efforts have been directed to more realistically assessing material's resistance to fracture, thus paving the way for fracture mechanics, which has given the designers a powerful tool to deal with fracture problems. By using the plane strain fracture toughness, K_{Ic}, it is now possible to predict the fracture resistance of brittle structural components in the presence of flaws and defects, which are inherently present in any structural material.

As mentioned before, low alloy ultra high strength steels offer the advantage of a high strength to weight ratio. Such steels are often chosen according to their relative fracture toughness at different strength levels. However, at high strength levels, the use of these materials is limited by their low fracture toughness. Maraging steels, as a class of alloys, exhibit one of the best combinations of strength and toughness available, better than conventionally treated low alloy steels such as 4140 and 4340. However, cost limits their uses except where absolutely necessary. Recent investigations have proved that the long associated poor fracture toughness of these very high strength low alloy steels can be significantly improved approaching the values obtained for the maraging

steels without the high cost. This has been achieved by altering only the heat-treatment procedures (i.e. high temperature austenitization). Furthermore, the fracture toughness levels have been achieved without a reduction in strength. Later investigations on such modifications in heat-treatment point out that the enhanced toughness, as reported earlier, is only an apparent one resulting from a change in mechanical variable (i.e. notch root radius), rather than arising out of improved microstructural features. In fact, it has been argued that the proposed heat-treatment modification produced a microstructure, which is essentially detrimental.

The arguement in favor of notch root radius on the enhancement of toughness has been based on a limited data. The purpose of the present investigation was to evaluate the notch root radius effects on the toughness of 4340 steel after high temperature austenitization (1200°C) in greater details. This involves studying (a) a greater range of notch root radii, (b) larger number of test conditions, and (c) for more number of heat-treatments, than has been attempted before. The second purpose of this investigation was to study the tempering behavior of as-quenched 4340 steel after austenitization at 1200°C; for tempering in general renders still higher toughness. From the standpoint of strength and toughness, bainitic matrices are sometimes as good or better than the martensitic matrices. Hence a few exploratory bainitic heat-treatments of 4340 steel after high temperature austenitization were also studied along with the above objectives.

1.1 Review of Related Work: The relationship between microstructural features and mechanical properties of metals has been a major study for the metallurgists for a long time. For a brief review of martensite and bainite and their impacts on strength, the reader is referred to the appendices. Recently it has been reported (1) that a high austenitizing temperature (1200°C) instead of the conventional austenitizing temperature (870°C) for 4340 steel can produce almost two-fold increase in K_{Ic} without the reduction in yield strength in as-quenched condition (For a detailed description of the K_{Ic} testing the reader is referred to the appendix). Concommitant with the increase in K_{Ic}, fairly continuous 100-200 Å thick films of retained austenite were observed between the martensite laths. Additionally, specimens austenitized at 870°C contained twinned martensite plates while those austenitized at 1200°C showed no twinning. The improvement in K_{Ic} in the latter case has thus been attributed to (a) increased amount of retained austenite, (b) absence of twins in the martensitic laths. One discouraging feature of the modified heat-treatment is that concommitant with the increase in K_{Ic} value, Charpy value is not increased proportionately. In fact, Charpy value either decreased slightly or remained the same for 4340 steel (For a detailed description of the Charpy test the reader is referred to the appendix.) It has been proposed (2) that the discrepancy in the toughness behavior of the two heat-treatments in two types of testing can be related to a notch root radius effect (i.e. fracture toughness specimen contains a fatigue pre-crack and Charpy specimen has a notch root radius of .01 inch).

It has been shown (2) that in the pre-cracked condition the high austenitizing treatment gives better toughness than the conventional austenitizing treatment. However, in the blunt notch testing condition, the conventional austenitizing treatment gives better toughness than the high austenitizing treatment (see Fig. 1.1). Thus it has been argued that the high toughness associated with high austenitizing treatment in pre-cracked testing condition can be related to an increase in the limiting root radius ρ_o, which may be thought to be equal to the prior austenitic grain-size. (For a description of the limiting root radius, see the appendix). It has also been argued (2) that the modified heat-treatment lowers the critical fracture stress and hence in blunt notch testing condition the toughness properties are poor. The decrease in critical fracture stress has been attributed to segregation of impurities such as S&P at high austenitizing temperatures. Thus the increase in K_{Ic} toughness is only an apparent one, resulting primarily from increased grain-size. Also, although it has been shown by TEM that retained austenite in as-quenched condition is significantly higher for the high temperature austenitization case (1), it has been claimed by magnetic and X-ray techniques (3) that retained austenite percentage remained unchanged from conventional to high austenitizing temperature (i.e. about 6%. See Fig.1.2). However, at yield, the retained austenite percentage dropped below 2%. Thus the retained austenite contribution to improved K_{Ic} has been discounted (3).

1.2 General Microstructure/Toughness Consideration: Characterization of the substructure and the morphology of martensites in steel alloys has been attempted by many investigators for several decades. In general,

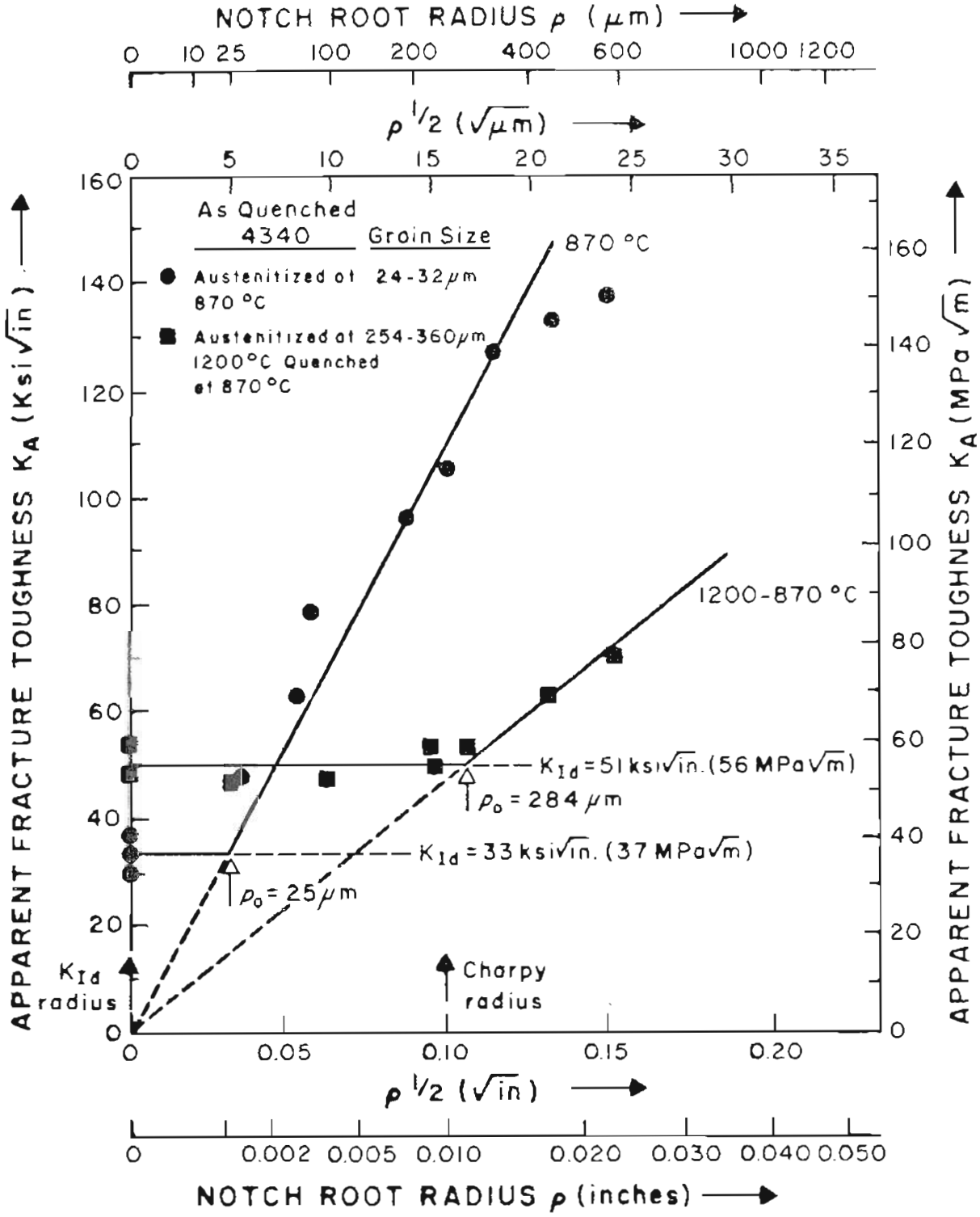

Fig. 1.1 The relationship between toughness, measured by the apparent dynamic fracture toughness (K_A) from instrumented Charpy tests, and notch root radius (ρ) in oil quenched AISI 4340. for the 1200-870°C and 870°C structure, ρ_o is the "limiting" root radius, K_{Id} the dynamic fracture toughness. (2)

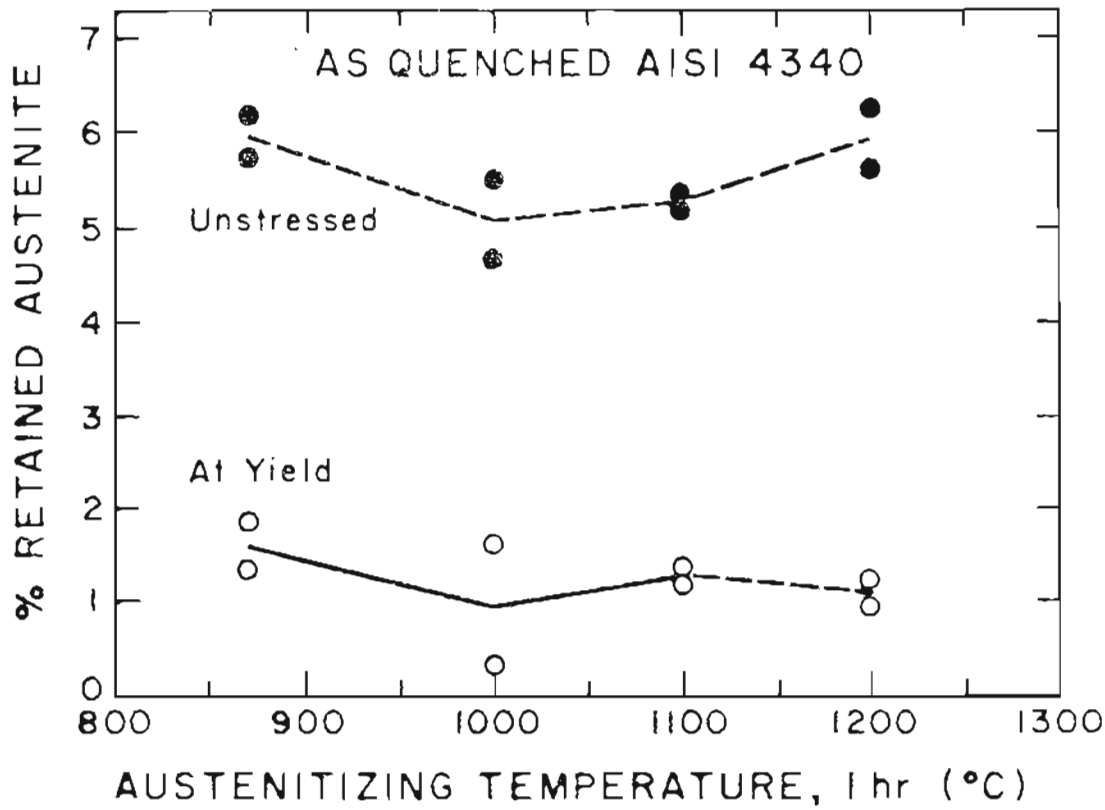

Fig. 1.2 Variation of percentage of retained austenite, measured by magnetic saturation technique, with austenitizing temperature for as-quenched (untempered) 4340 steel. Plotted are initial (unstressed) levels and amounts untransformed at yield (0.2 pct strain). (Ritchie et al.)

two forms of martensites have been recognized: (a) lath martensites which have been found in low carbon and 18-8 stainless steel and which are dislocated. (b) Plate martensites which have been found in high carbon and high nickel steels, which are internally twinned. Among the factors (4) favoring the formation of twinned martensites are (a) low M_s, (b) high stacking fault energy of the parent austenite. Later investigation (5) supported only the first factor and discounted the second one. Another interesting aspect (6) between lath and plate martensite is the enthalpy of transformation; the stored energy in lath martensite being ~1150 J/mole higher than in twinned martensite. This also supports the earlier contention that lath martensites will be favoured for a higher M_s and twinned martensites will be favoured for a lower M_s.

The relative strength and toughness of lath and plate martensite have been compared by several investigators. Kelly and Nutting (4) have suggested that the available deformation systems are reduced by a factor of four in the presence of twins. This decrease in the number of possible deformation systems will result in both an increase in the strength and a decrease in ductility and toughness. On Fe-Ni alloys Yokota and Lai (7) have demonstrated that lath martensites possess superior toughness properties compared to plate martensites at the same yield strength level. However, Zackay et al. (8) showed a one-to-one relation between the austenitic grain diameter and the length of the largest martensitic plates/laths (see Fig. 1.3) and it has been shown that the strength of martensite decreased with increase in martensitic plate/lath size but the ductility is unaffected by the lath/plate size. With regard to martensitic laths

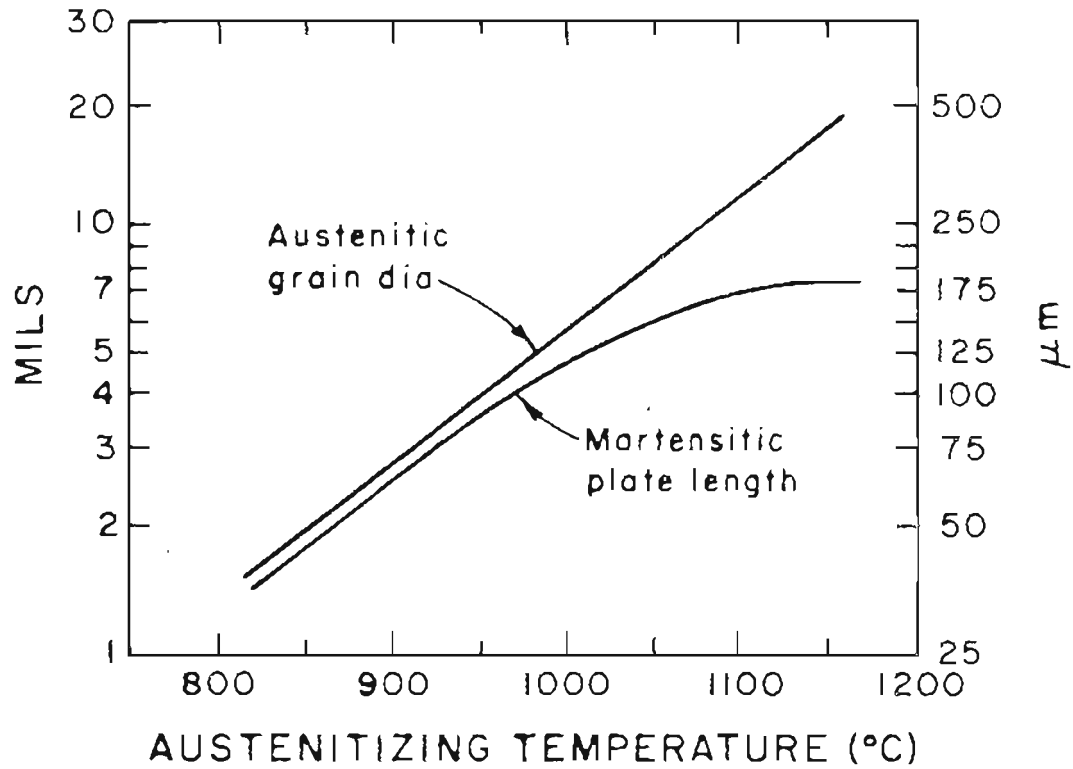

Fig. 1.3. Relation between austenite grain size and maximum martensite plate length (Zackay et al.)

from high temperature austenitization, we have thus two competing factors for the enhancement of toughness. Since the laths are dislocated and not twinned, toughness should increase; however, the toughness should decrease, because of the concomitant increase of lath size.

The tempering of martensites in steels is an aging process which is normally considered to occur in three stages (9-11): (a) the decomposition of martensite and the precipitation of ε-carbide, (b) the transformation of retained austenite to ferrite and cementite, (c) the transformation of ε-carbide to cementite. While earlier investigations (4) failed to identify the carbide during the early stage of tempering, Murphy and Whitman (12) have unambiguously identified ε-carbide in a high carbon steel, a nickel steel and a silicon steel.

The effect of the morphology of as-quenched martensite has been first discussed by Kelly and Nutting (4). They reported that the lath martensite (low carbon steel) was partially tempered during the quenched. Tempering between 100°-300°C produced little change in the size of the precipitates. At 300°C they were identified as cementite and at 400°C they showed signs of growth. In contrast twinned martensite (high carbon steel) showed no carbide after quenching and no change was detected after tempering at 100°C. Tempering at 200° resulted in the appearance of carbides along the twins in the martensite. At 300°C, the carbides were identified as cementite. Thus the main differences in the tempering behavior of a high carbon and a low carbon steel stem from the differences in the martensitic morphology of the two steels. The mechanical properties of lath and plate martensites after tempering up to 540°C have been

investigated by Huang and Thomas (13) in 0.25 pct C steels with varying amounts of nickel and manganese. They found that at equivalent yield and ultimate tensile strength levels, the tempered martensite of lower Mn steels (lath martensites) showed better impact toughness than the tempered martensites of higher Mn steels (plate martensite). Also it has been reported by Smith and Heheman (14) that the yield strength of 4340 steel drops when martensite and bainite are tempered beyond 300°C. This decrease in yield strength has been attributed to the coarsening of carbide precipitates.

A bainitic heat-treatment is often employed to get high toughness in low alloy high strength steels. The reasons are mainly two-fold; (a) bainite is very similar to tempered martensite, (b) bainite heat-treatment is relatively free from quench cracks normally associated with martensitic transformation. In general, two forms of bainite have been recognized; (a) upper bainite, where iron carbides (cementite) precipitate between the ferrite laths, (b) lower bainite where iron carbide (ε-carbide) precipitate inside the ferrite laths. Quantitative relationships between the microstructure and strength of bainite are difficult to define because of the many interacting factors. However, it is qualitatively known that a large bainitic ferrite grain size and a long inter-carbide spacing are detrimental to strength. For this reason, lower bainite is generally stronger than upper bainite. The reasons normally attributed for the high strength of bainite (15) are (a) dispersion hardening by precipitated carbides, (b) high dislocation density of bainitic ferrite, (c) solution hardening effect of carbon in solid solution in ferrite,

(d) Fine bainitic ferrite grain-size. Irvine and Pickering (15) have demonstrated that a .5/.6% C - 1% Cr - 1/2% Mo-B steel can be raised to 255 k s.i. tensile strength by a bainitic treatment. In fact, it has been argued (16) that the morphology of lower bainite can be favourably compared with that of tempered martensite structure. However, Lai (17) observed two variants of ε-carbide in lower bainite. Lai (19) has also demonstrated that the proeutectoid ferrite and upper bainite have to be avoided to achieve high fracture toughness in low alloy ultra-high strength steels. Another interesting fact for the bainitic reaction is that no partition of alloying elements takes place (18) between austenite and bainite in Si, Mn, Ni, Mo and Cr steels.

1.3 Experimental Approach: - As stated earlier, a high austenitizing treatment (1200°C) instead of the conventional austenitizing treatment (870°C) for 4340 steel in as-quenched condition can produce almost two-fold increase in K_{Ic}, whereas Charpy values are not improved proportionately. The microscopical features attributed to such improvement in K_{Ic} are (a) increased amount of retained austenite, (b) absence of twins in the martensitic laths. On the other hand such improvement in K_{Ic} and decrease in Charpy has been related to an increase in the limiting root radius, which has been hypothesized to be equal to the prior austenitic grain-size. The root radius effect has been based on very limited data (up to 0.03" by instrumented Charpy and 0.01" by slow-bend Charpy and at room temperature only). Therefore, there is further need to emplore the notch root radius effects in greater details. In this investigation we have chosen four heat-treatments namely (a) 1200°C/AQ, (b) 870°C/AQ, (c) 1200°C/AQ + tempering at 175°C, (d) 870°C/AQ + tempering at 175°C. The reason for the additional two heat-treatments is that the highest toughness for

the 1200°C austenitizing treatment has been achieved at a tempering temperature of 175°C (20). The conventional 870°C austenitizing followed by tempering at 175°C is also studied along with for comparison. Secondly, ε-carbides start participating in the martensitic plates for the conventional austenitizing treatment around that temperature and hence such comparison will be made on the basis of a more even microstructural feature. The tests were planned to be carried out by instrumented and slow-bend Charpy tests and at room and liquid nitrogen temperatures. The reason for choosing another test temperature (liquid nitrogen) is that 4340 steel is often used as landing gear of aircraft and the service temperature may be well below room temperature. However, mechanical testing to evaluate toughness is carried out at room temperature only. Since the temperature of the landing gear, when it hits the ground, is not known, liquid nitrogen temperature as an additional test temperature was chosen. In reality, the service temperature will be between the room and liquid nitrogen temperatures. Initially, root radii varying from pre-crack to .04 inch have been used. They were later expanded to include two more root radii (.07 inch and 0.10 inch) for the room temperature instrumented Charpy testing.

A comparison of the resistance against fracture between plane strain fracture toughness testing and Charpy testing between the modified and conventional austenitizing treatments in both as-quenched and tempered (up to 230°C) was conducted. In summary, the differences between the two types of testing were examined and their effects on the measured toughness were analyzed. (For a detailed comparison between the

two tests see the appendix). In addition to as-quenched structure between the two austenitizing treatments, the tempered structure were also examined. The reasons are as follows. First, tempering, in general, renders higher toughness. Secondly, as stated earlier, the tempering characteristics of lath and plate martensites differ and hence it may be interesting to see the toughness behavior in the tempered structure after the two austenitizing treatments. Thirdly, retained austenite generally disintegrates to ferrite and cementite during the second stage of tempering; whether that has any effect on the toughness or not is worth noting, since retained austenite has been proposed to contribute to enhanced toughness. The tempering temperature has been limited to 280°C (below 300°C) since the yield strength of tempered martensite starts dropping beyond 300°C (14).

As stated before, a bainitic treatment is often employed to get the high toughness in low alloy high strength steels. The reasons are mainly two-fold, (a) lower bainite is very similar to tempered martensite, (b) bainitic treatment is relatively free from quench cracks normally associated with martensitic transformations. Since high temperature austenitization gives high toughness for 4340 steel in as-quenched condition, the next logical choice for achieving higher toughness is the bainitic treatment from high temperature austenitization, which has never been attempted before. The following experiments were planned based on the TTT diagram from 1200°C austenitization for 4340 steel (shown in Fig. 1.4 [ref. 21]). The comparison was made between the bainitic transformation and direct martensitic transformation after high temperature

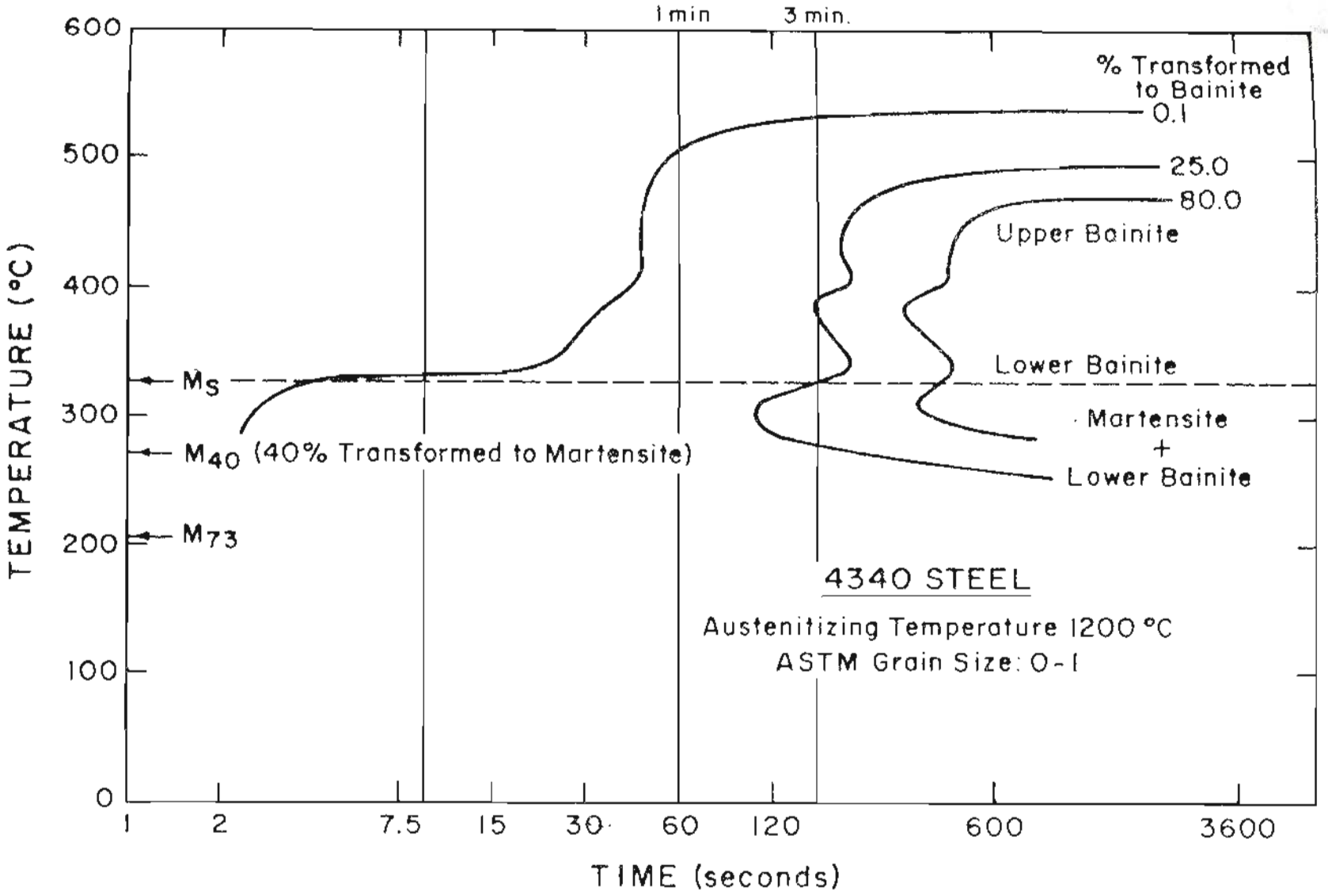

Fig. 1.4 Isothermal transformation curve for alloy 4340 austenitized at 1200°C.

austenitization. The lower bainitic region was only planned to be explored as it has been reported that the proeutectoid ferrite and upper bainite have to be avoided for achieving high toughness (19). Three temperatures namely, (a) 350°C, (b) 335°C, (c) 300°C have been chosen for the bainitic studies. As seen from the TTT diagram, the first two temperatures are above M_s and the last temperature is below M_s. The difference between the two treatments is that in the former first bainite is formed followed by martensite on subsequent quenching; in the latter first martensite followed by bainite subsequently followed by martensite on quenching. Bainitic treatments are carried out for varying lengths of time to have a duplex structure (bainite and martensite) in different proportions. Also, the resultant structure is tempered to have as-quenched martensite tempered. As before, the tempering temperature has been limited to 280°C.

1.4 Statement of Purpose: - Recently it has been documented that the plane strain fracture toughness of 4340 steel can be improved by almost two-fold (1) in the as-quenched condition when austenitized at 1200°C instead of conventional 870°C. The reasons (1) attributed for such enhancement in toughness are (a) retained austenite between the martensitic laths, (b) dislocated martensite instead of twinned martensite. One discouraging feature of the modified heat-treatment is that the Charpy value is not improved concommitant with the observed increase in fracture toughness result. Such discrepancy in results in two types of testing has been related to notch root radius effects. (2,3) The argument in favor of a notch root radius has been based on a very limited data. In this investigation the effects of notch root radii on the toughness of 4340

steel after modified and conventional heat-treatment have been studied in much greater details; (a) broader range of notch root radii (pre-crack to 0.100 inch root radius), (b)larger number of test conditions (high and low strain rates and room and liquid nitrogen temperatures), (c) more number of heat-treatments including both as-quenched and tempered microstructures. Next, the tempering behavior of the steel (4340), after austenitizing at 1200°C has been studied. Since tempering, in general, renders still higher toughness. Also as the tempering behavior of lath and plate martensites differ, a comparison between the tempering of as-quenched 4340 steel after both conventional and high austenitizing treatments has been made. Tempering in this investigation has been limited to below 300°C (280°C) because the yield strength of tempered martensite of 4340 steel drops beyond a tempering temperature of 300°C.(14)

From the standpoint of strength and toughness, bainitic matrices are sometimes as good as or better than the martensitic matrices. Hence a few bainitic heat treatments from high temperature austenitization (1200°C) have been attempted for the 4340 steel to explore higher toughness. Such attempt has been limited to lower bainitic regions since it has been demonstrated (19) that for high toughness in low alloy ultrahigh strength steels both preeutectoid ferrite and upper bainite have to be avoided.

2. EXPERIMENTAL PROCEDURE

In this section the experimental procedures will be described.

2.1 Materials and Specimen Preparation: - The alloy used in this investigation was aircraft quality 4340 steel plate with the following chemical composition:

C	Mn	Si	S	P	Cr	Ni	Mo	Cu	V	Fe
.40	.69	.32	.015	.015	.69	1.87	.20	.16	-	balance

The materials were received in the hot rolled condition in the form of 0.625" thick plates. The location of the specimens with respect to the orientation of the plates is given in Figure 2.1. The dimensions of the fracture toughness specimens (both compact tension and three point bend specimens) and also Charpy specimen are given in Fig. 2.2. A grinding wheel was used to produce specimens of variable root radii using coolant and light grinding passes. Prior to testing, the root radius of the notch was checked with a comparator. In addition to pre-cracked and standard (.010" root radius) Charpy specimens, specimens of root radii (.004", .006", 0.020", 0.030", 0.040", .07" and 0.1") were also prepared.

2.2 Heat Treatment - An argon atmosphere tube furnace was utilized for all high temperature austenitization treatments. This furnace maintained a temperature within $\pm$ 5°C. The furnace was sealed at both ends and austenitizing was carried out in an argon atmosphere for 1 hour. The material being austenitized was then quenched by removing the bottom and dropping it through the bottom and directly into the agitated oil bath

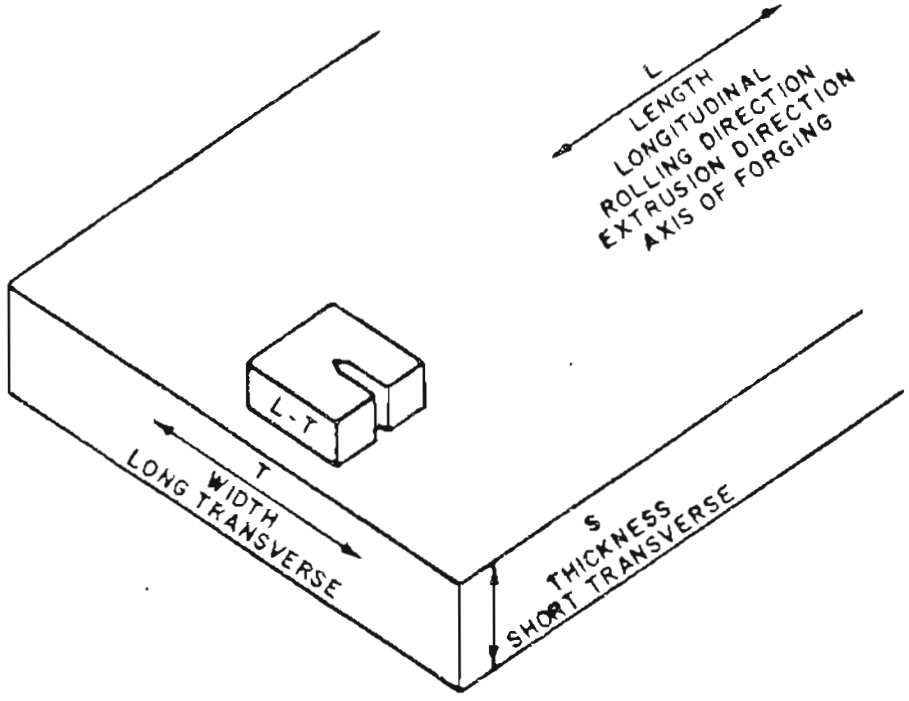

(a) Orientation of compact tension specimen

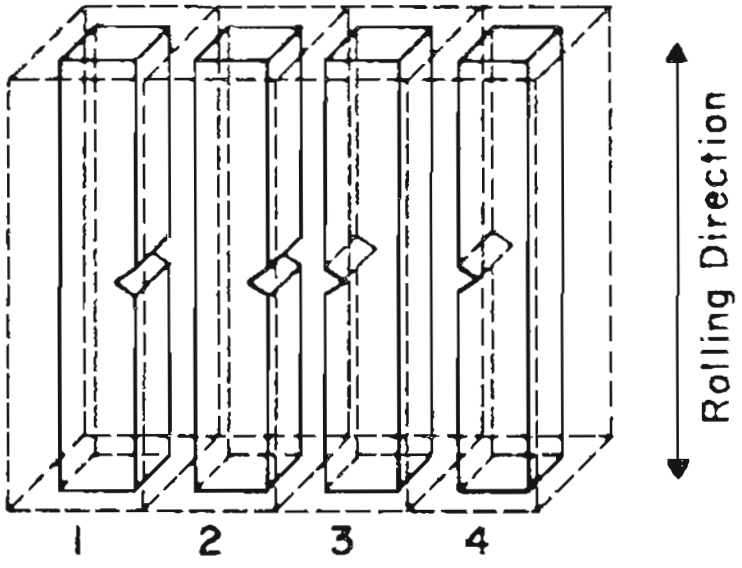

(b) Orientation of charpy specimen. The same orientation known as L-TS is employed for three-point bend specimen.

Fig. 2.1

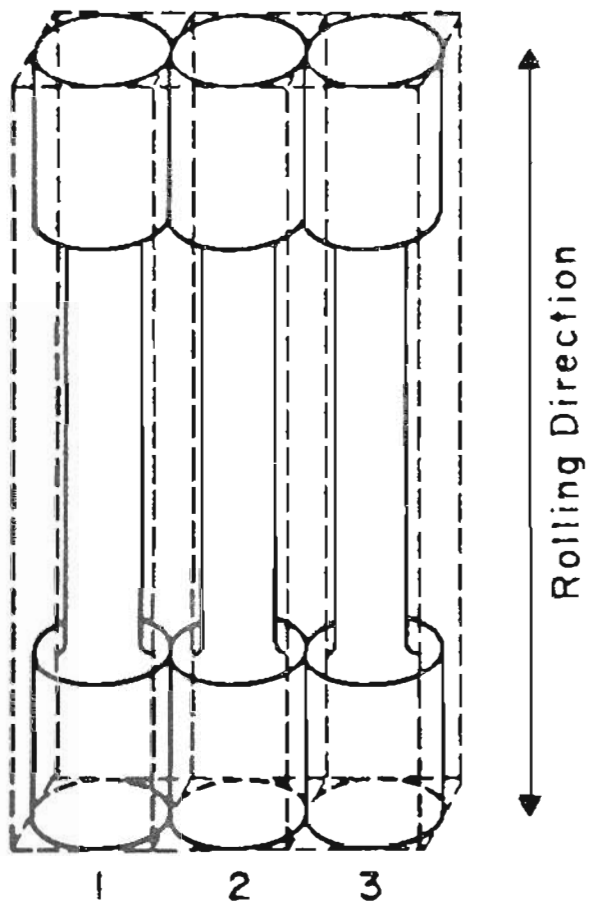

(c) Orientation of tensile specimen.

Fig. 2.1 (cont'd)

below. The bainitic treatment from austenitizing temperature was done in a salt bath and then quenched in an agitated oil bath at room temperature. All tempering was done in an agitated salt bath for one hour followed by quenching in an agitated oil bath at room temperature.

2.3 Testing Method

2.3.1 Fracture Toughness Testing

The room temperature longitudinal plane strain fracture toughness was determined using the ASTM specified (114) compact tension testing specimen, Fig. 2.2a. All specimens were machined from 5/8 in. thick bar stock to final dimensions except for the thickness of an 0.008 in. slot. After the heat-treatment an .008 in. thick slot was machined in order to act as a notch for introducing a fatigue crack. A 22,000 lbs Instron Lawrence dynamic test system was used for all testing including fatigue pre-cracking at 6 hz. All fatigue cracks were fatigued at least 0.10 inch and fatigue loads were kept within ASTM recommendations (115). Fracture toughness testing was carried out at a cross head speed of 0.1 cm/min.

The stress intensity for the compact tension specimen has been determined by Brown and Srawley (46) and can be expressed as a function of specimen geometry and loading to result in the following equation

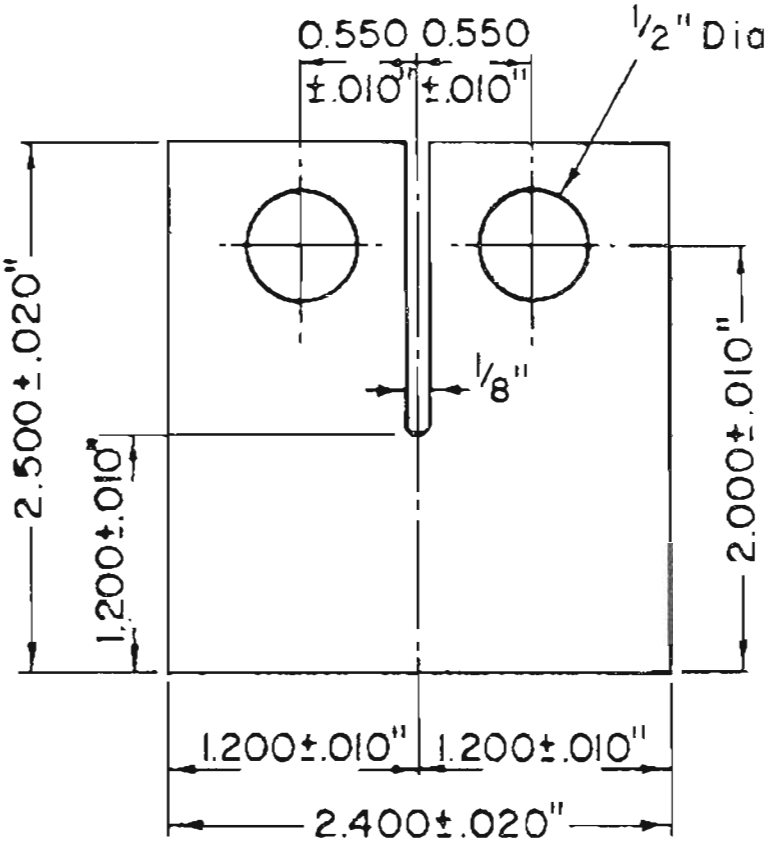

(a) Dimensions of compact tension specimen

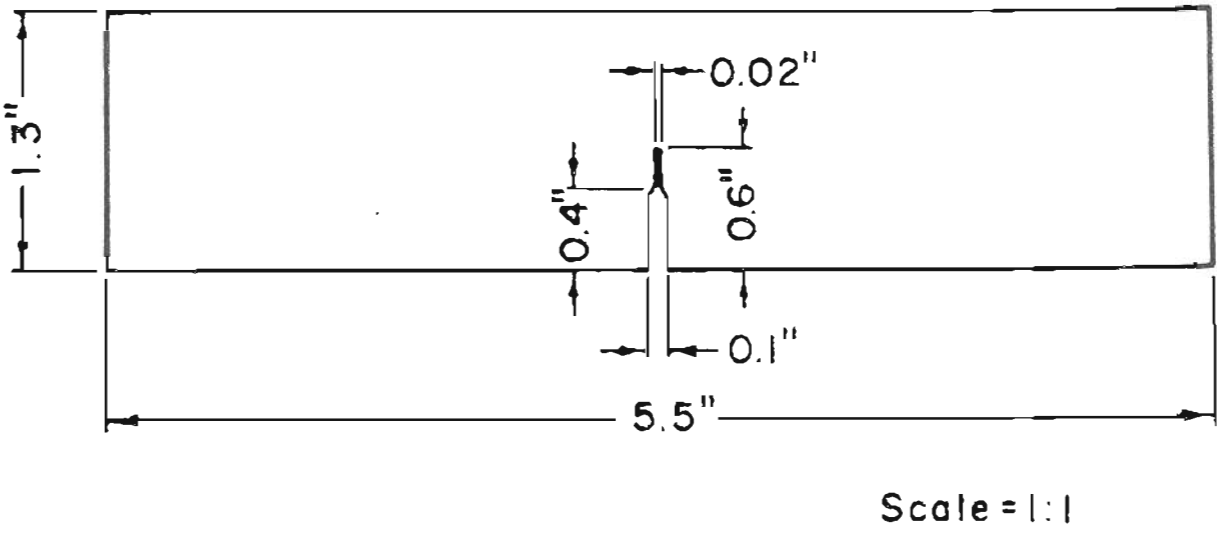

(b) Dimensions of three-point bend specimen

Fig. 2.2

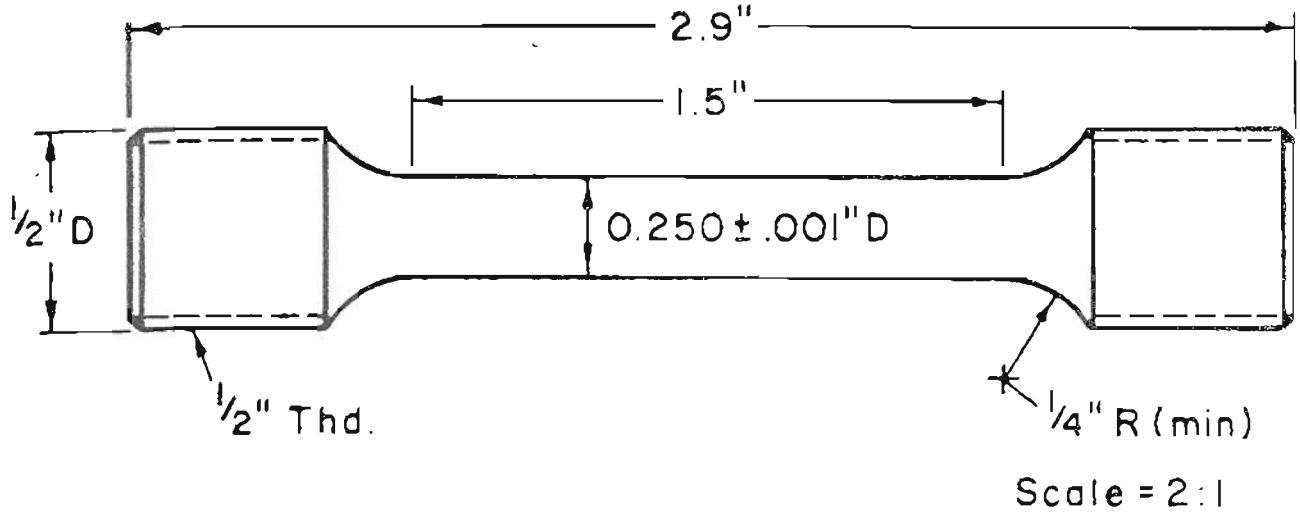

(c) Dimensions of tensile specimen

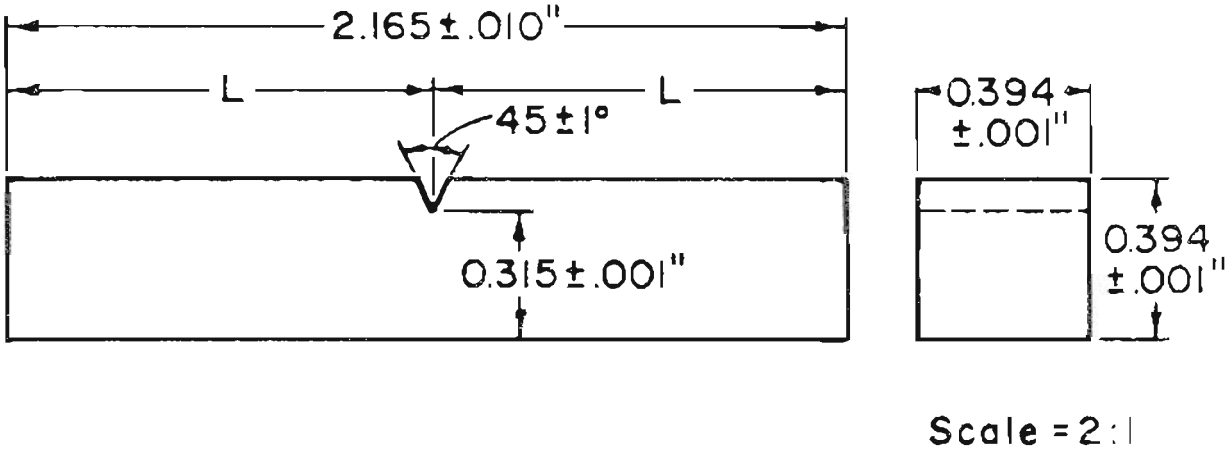

(d) Dimensions of Charpy specimen

Fig. 2.2 (cont'd)

$$K = \frac{P}{BW^{1/2}} \quad f\left(\frac{a}{w}\right)$$

$$f\left(\frac{a}{w}\right) = 29.6\left(\frac{a}{w}\right)^{1/2} - 185.5\left(\frac{a}{w}\right)^{3/2} + 655.7\left(\frac{a}{w}\right)^{5.2} \ldots\ldots \qquad (2.1)$$

$$-1017\left(\frac{a}{w}\right)^{7/2} + 638.9\left(\frac{a}{w}\right)^{9/2}$$ where K is the stress intensity, P the load, B the thickness, w the specimen width and a the crack length.

A crack opening displacement (COD) gauge was used to follow the crack length during each test. With the use of a crack-opening-displacement vs crack length calibration curve, (Fig. 2.3) for this particular specimen geometry, the crack length during each test could be determined from the crack-opening-displacement measured with the COD gauges. Hence the stress intensities K_{Ic} and K_Q were determined using Eq. 2.1 in accordance with the ASTM standards.

2.3.2 Tensile Testing

The room temperature longitudinal tensile properties were determined using a 1 inch gauge length, 0.250 inch diameter ASTM specified round specimen shown in Fig. 2.2c. Machining was done prior to heat treatment. A 100,000 lbs capacity MTS machine was used to test the specimen at a loading rate of 0.1 cm/min. The yield strength was determined on a micro yield strength level, using a strain gauge extensometer.

2.3.3 Instrumented Charpy Impact Testing

The dynamic tests were performed by an instrumented Charpy impact machine with 120 ft. lb. capacity. The instrumented tup was part of a commercial Dynatup system developed by Effects Technology, Inc.,

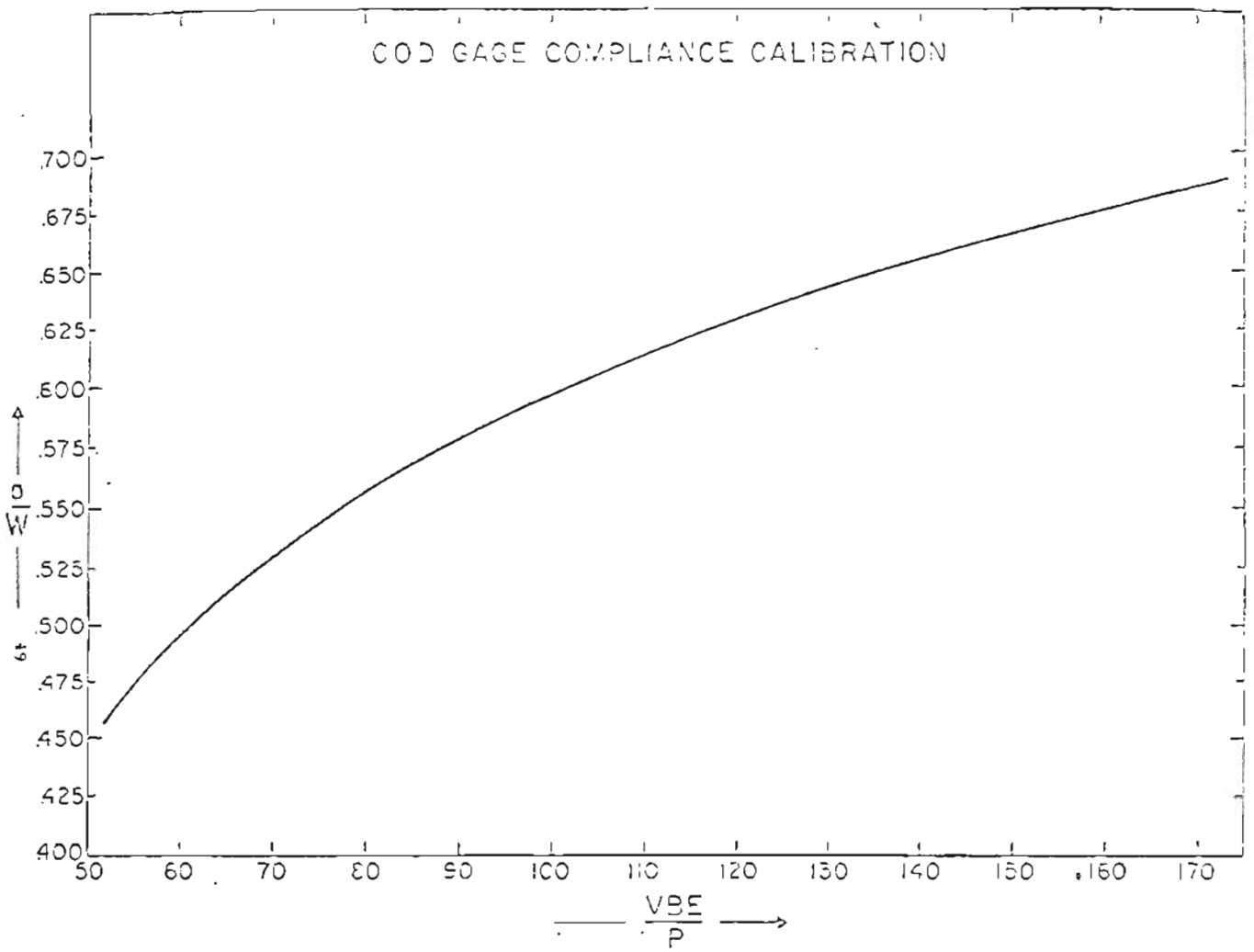

Fig. 2.3. Crack opening displacement and crack-length calibration,

Santa Barbara. On impact, the dynamic load on the specimen is measured through an electrical signal sent by the strain gauges on the tup of a Charpy hammer. This electrical signal is related to the load through a proportionality constant, P_d having units of lbs/v. To assure the reliability of dynamic load measurements, two methods can be used to calibrate the system. The first method is to compare the impact energy (W_t) recorded from the Charpy machine dial to the energy measured from the area (A) under the trace of load-time curve recorded by the oscilloscope. The area measured in units of square inches can be converted to energy W_c with units of ft-lb from the following equation:

$$Wc = A\ C_x Cy\ Pd\ \bar{v}/C_a, \tag{2.2}$$

where Ca = area of one square division on the oscilloscope record.

C_x is the time sweep rate per division.

C_y is the vertical sensitivity per division and

$\bar{v}$ is the effective velocity of the tup during the entire impact. Equating W_t to W_c and rearranging gives the following relation from which Pd can be calculated:

$$Pd = W_t\ ca/C_x C_y\ \bar{v}\ A. \tag{2.3}$$

Accurate calculation of the effective velocity is difficult. However, for low values of impact energy the difference between the initial velocity Vo, and the final velocity, Vf, is relatively small,

and the effective velocity can be estimated to be a simple average of the two velocities. Thus,

$$\bar{v} = (v_f + v_o)/2. \tag{2.4}$$

A material with an impact energy value of about 20 ft-lbs is suitable for this calibration purpose, since for values lower than this, the percent of error in measuring the area under the load-time trace would increase, and at larger impact energies, Eq. 2.4 would not apply.

The initial velocity at impact is given by $v_o = (2\ gh)^{1/2}$ where g is the acceleration of gravity and h is the drop height of the pendulum hammer. The final velocity is determined by the same relationship where h is the maximum rise height of the hammer after the impact.

The second method of calibration involves testing a material for which dynamic properties are known. For example 7075 T-6 aluminum, which has a dynamic fracture toughness of about 23 ksi$\sqrt{\text{in}}$ may be used. Pre-cracked specimens may be broken with the impact hammer and the value of P_d may be calculated. The dynatup was equipped with an internal calibration system so that once P_d was known the system was easily calibrated before testing.

In our case, most of the instrumented impact testing was done at Effects Technology, Inc., Santa Barbara. A few were carried out at Battelle Memorial, Richland,at an earlier date. The system located

at Effects Technology was also equipped with a microprocessor so that the fracture toughness data could be printed out shortly after the test.

2.3.4. Three Point Slow Bend Testing with Charpy Specimens

The slow bending tests were performed with a specially constructed three-point bending fixture as shown in Fig. 2.4. The bend jig was attached to the bottom of the cross-head of the Instron Universal testing machine. All the slow bend tests were conducted at a cross-head speed of 0.1 cm/min.

The fracture loads were used to calculate the stress intensity factors from the fracture mechanics formula for the three-point bending (46).

$$K = \frac{6YM}{BM^2} (a)^{1/2}, \quad \text{where}$$

$$Y = 1.93-3.07 \left(\frac{a}{w}\right) + 14.53 (a/w)^2 - 25.11 \left(\frac{a}{w}\right)^3 + 25.8 (a/w)^4 \qquad (2.5)$$

and M is the applied moment. In case of precracked specimens, it was done in the same fixture.

2.3.5 Three-Point Slow Bend Testing with Fracture Toughness Specimens Configuration

The room temperature longitudinal plane strain fracture toughness was determined using the ASTM specified 3-point bend specimens. All specimens were machined from 5/8 inch thick bar stock to

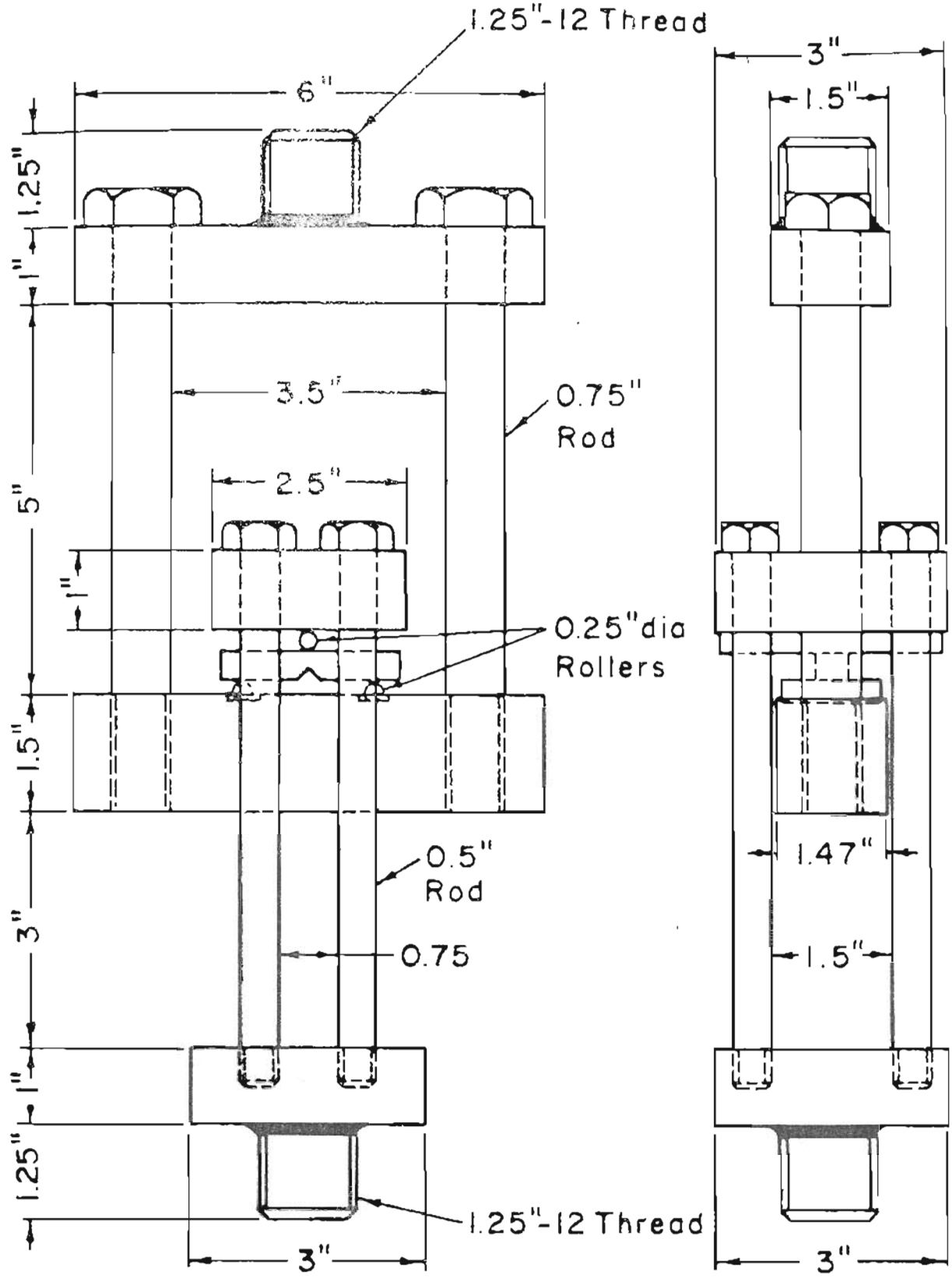

Fig. 2.4. Testing fixture for slow-bend Charpy specimen.

final dimensions. Pre-cracking and testing was done in a similar fixture as shown in Fig. 2.5. in an universal Instron testing machine. All fatigue cracks were at least .05 inch long and fatigue loads were kept within ASTM recommendations.

The stress intensity factor can be expressed as a function of specimen geometry and can be expressed using Equation 2.5.

2.4 Electron Microscopy

2.4.1 Scanning Electron Microscopy

Scanning electron microscopy was carried out using a Hitachi scanning electron microscopy at 25 Kv (secondary electron volt). For each specimen the region adiacent to the fatigue pre-crack was examined, since this is the region of crack initiation in all types of specimens. In order to preserve the fracture surface from oxidation or corrosion, the fracture surface was coated with the Dem-Kote spray. Before examining the fracture surface the spray was removed by using acetone.

2.4.2 Transmission Electron Microscopy

Sections for transmission electron microscopy were taken from the midsection of the K_{Ic} specimens. Thin foil preparation was carried out using both the window technique and the jet polishing technique, (Fischione unit). Two electrolytes, glacial acetic acid plus perchloric acid and glacial acetic acid plus chromium trioxide, were used. The best results were obtained from the latter in conjunction with the window

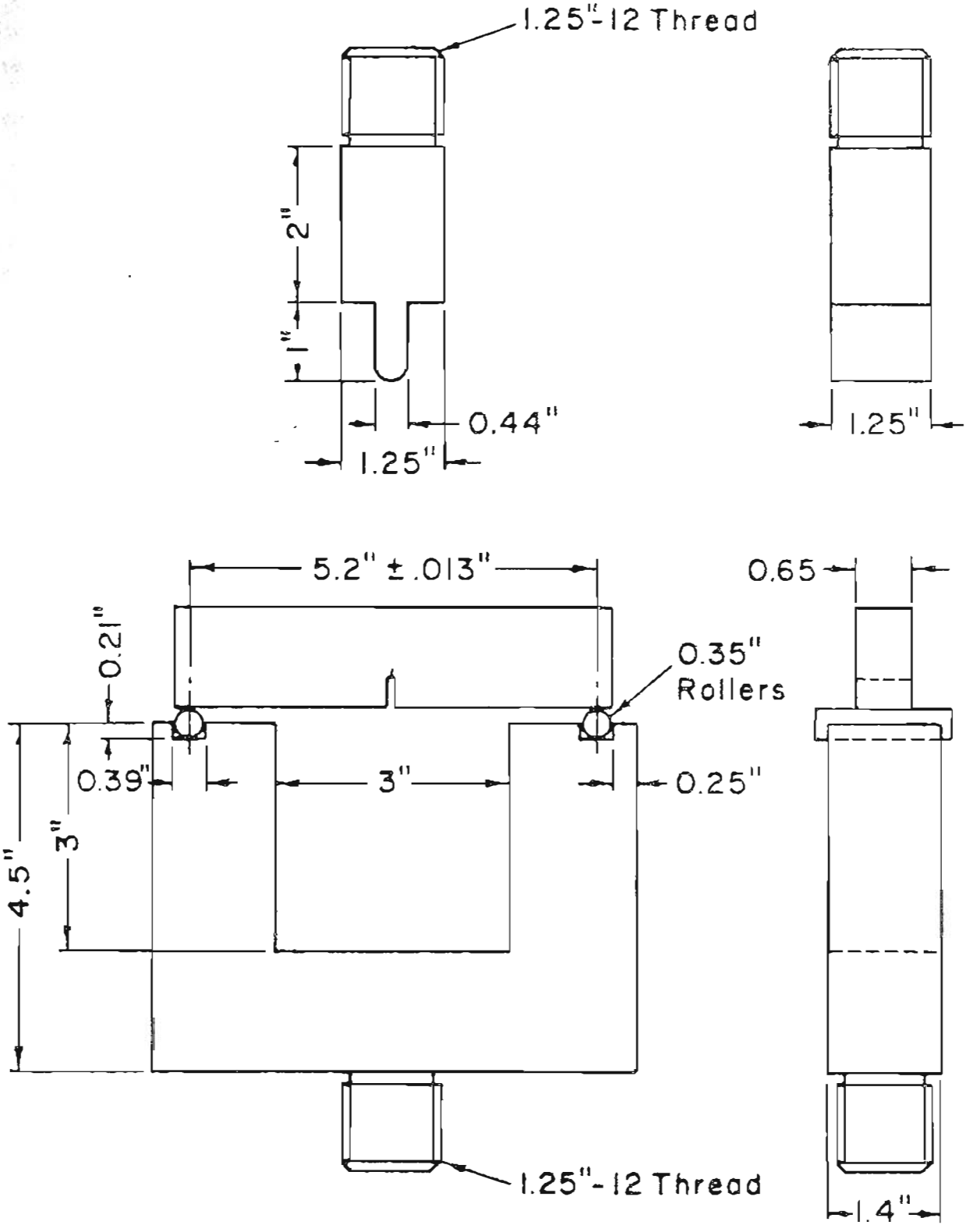

Fig. 2.5 Testing fixture for three-point bend specimen

technique. The exact composition of the electrolyte and the polishing conditions are given below:

Electrolyte:

Galacial Acetic Acid	135 ml
Chromium Trioxide	25 gms
Water	7 ml

Polishing Conditions:

Temperature	10-15°C
Voltage	25 volts
Current density	0.1-0.2 amp/cm^2

The starting material was obtained in 10-15 mil thickness sections by cutting heat treated specimens with a 1/32" abrasive wheel. Sections were cut while flooded with water. A very low cutting rate was employed. These 10-15 mil sections were then carefully ground to about 5 mils thickness. From this thickness, final polishing by either the window or the jet polishing technique was carried out. Electron microscope studies were made in a Hitachi electron microscope using 100 kv.

2.5 X-ray Diffraction:- Powders for X-ray diffraction were taken by filing from K_{Ic} samples. Care was taken to see that powders were not contaminated by filings or oxidation product. Cobalt K_α radiation was used for X-ray diffraction. This analysis was carried out at Tektronix on a computerized system.

3. RESULTS

In this section the results will be described. Results are divided into two categories (a) mechanical results and (b) microscopy.

3.1 Mechanical Results: -As indicated in the introduction, the effects of notch root radii on the toughness of quenched and tempered 4340 steel were studied in the initial phase. In the second phase a comparison was made between the tempering behavior of 4340 steel after both high (1200°C) and conventional (870°C) austenitizing treatments. The third phase was directed to explore the possibility of achieving higher toughness in the bainitic region after high temperature austenitization. Accordingly the mechanical results are subdivided into three groups. (a) The effect of notch-root radius on the toughness, (b) comparison of tempering behaviour after both high (1200°C) and conventional (870°) austenitizing treatments, (c) mechanical properties in the bainitic region after high temperature austenitization.

3.1.1 The Effect of Notch Root Radius on the Toughness

Charpy specimens of varying root radii (up to 0.1") were tested at room temperature by slow-bend Charpy (slow strain rate) and by instrumented Charpy (high strain rate) at room and liquid nitrogen temperatures. Prior to notching, the specimens were heat-treated and prior to testing all the root radii were checked in a comparator. The results are as described below. As described in the appendix the toughness obtained by such tests is known as the apparent toughness, since they do not conform to ASTM specifications.

3.1.1.1 Room Temperature Instrumented Charpy Test

The room temperature instrumented Charpy data having various root radii are given in Table 3-1. Root radii up to 0.1" (100 mil) were tried. Four different heat treatments were given to these specimens of various root radii, namely (a) 1200°/AQ, (b) 1200°C/AQ followed by tempering at 175°C, (c) 870°C/AQ, (d) 870°C/AQ followed by tempering at 175°C. The corresponding results are shown in Fig. 3.1. The noticeable feature is that the toughness increased with the increase in root radius up to 0.04" root radius. However, beyond that point there was a plateau up to the root radius .07" for the three heat-treatments namely (a) 1200°C/AQ followed by tempering at 175°C, (b) 870°C/AQ, (c) 870°C/AQ followed by tempering at 175°C. The toughness, however, increases again with further increase in root radius. For the other heat treatments, namely 1200°C/AQ, a substantial drop in toughness was observed at the root radius of .07". However, when the root radius was increased still further to 0.1", the toughness again increased as observed in the other cases. It should be pointed out, however, that except for the last heat treatment (i.e. 1200°C/AQ) for all other heat treatments general yielding occurred during the test at root radii of .04 inch and larger. For the last heat treatment, general yielding took place at the root radius of 0.1 inch.

3.1.1.2 Room Temperature Slow Bend Test

The room temperature slow bend Charpy data having various root radii are given in Table 3-2. Root radii up to 0.04 inch were studied. The same four heat treatments as described before were

TABLE 3-1

ROOM TEMPERATURE TOUGHNESS OF 4340 STEEL BY INSTRUMENTED CHARPY SPECIMEN HAVING VARIOUS ROOT RADII

SPECIMEN ID	AUSTENITISING TREATMENT °C/1H	TEMPERING TEMPERATURE °C/1H	ROOT RADIUS INCH	K_Q(APP) KSI$\sqrt{IN}$	MPA$\sqrt{M}$
A-31	1200	AQ	.004	89.89	98.70
A-32	"	"	.004	90.52	100.17
A-33	"	"	.006	100.84	110.72
A-34	"	"	.006	99.85	109.63
A-35	"	"	.02	115.100	126.38
A-36	"	"	.02	111.45	122.37
A-37	"	"	.03	133.68	146.78
A-38	"	"	.03	126.38	138.76
A-39	"	"	.04	141.97	155.88
A-40	"	"	.04	128.70	141.31
A-389	"	"	.07	95.52	104.89
A-390	"	"	.07	88.56	97.24
A-381	"	"	.10	127.38	139.86
A-382	"	"	.10	132.02	144.96
A-41	1200	175	.004	105.65	116.00
A-42	"	"	.004	105.65	116.00
A-43	"	"	.006	116.27	127.66
A-44	"	"	.006	119.42	131.12
A-45	"	"	.02	126.05	138.40
A-46	"	"	.02	125.55	137.85
A-47	"	"	.03	148.43	162.98
A-48	"	"	.03	146.45	160.80
A-49	"	"	.04	148.43	162.98
A-50	"	"	.04	140.81	154.61
A-391	"	"	.07	142.96	156.98
A-392	"	"	.07	132.67	145.68
A-383	"	"	.10	150.26	164.99
A-384	"	"	.10	144.63	158.80
A-71	870	AQ	.004	96.52	105.98
A-72	"	"	.004	97.85	107.44
A-73	"	"	.006	110.13	120.92
A-74	"	"	.006	101.50	111.45
A-75	"	"	.02	141.64	155.52
A-76	"	"	.02	152.59	167.54
A-77	"	"	.03	156.56	171.91
A-78	"	"	.03	159.55	175.19
A-79	"	"	.04	166.18	182.47
A-80	"	"	.04	159.22	174.82
A-385	"	"	.07	152.58	167.54
A-386	"	"	.07	144.95	159.16
A-377	"	"	.10	148.43	162.98
A-378	"	"	.10	169.17	185.75

TABLE 3-1 (CON'T)

ROOM TEMPERATURE TOUGHNESS OF 4340 STEEL BY INSTRUMENTED CHARPY SPECIMEN HAVING VARIOUS ROOT RADII

SPECIMEN ID	AUSTENITISING TREATMENT °C/1H	TEMPERING TEMPERATURE °C/1H	ROOT RADIUS INCH	K(APP) KSI√IN	K(APP) MPA√M
A-81	870	175	.004	117.09	128.57
A-82	"	"	.004	115.76	127.11
A-83	"	"	.006	125.05	137.31
A-84	"	"	.006	127.04	139.49
A-85	"	"	.03	151.58	166.44
A-86	"	"	.02	154.91	170.09
A-87	"	"	.03	167.51	183.93
A-88	"	"	.03	173.48	190.46
A-89	"	"	.04	172.49	189.39
A-90	"	"	.04	177.79	195.22
A-387	"	"	.07	164.85	181.01
A-388	"	"	.07	159.88	175.55
A-379	"	"	.10	180.12	197.77
A-380	"	"	.10	176.14	193.40

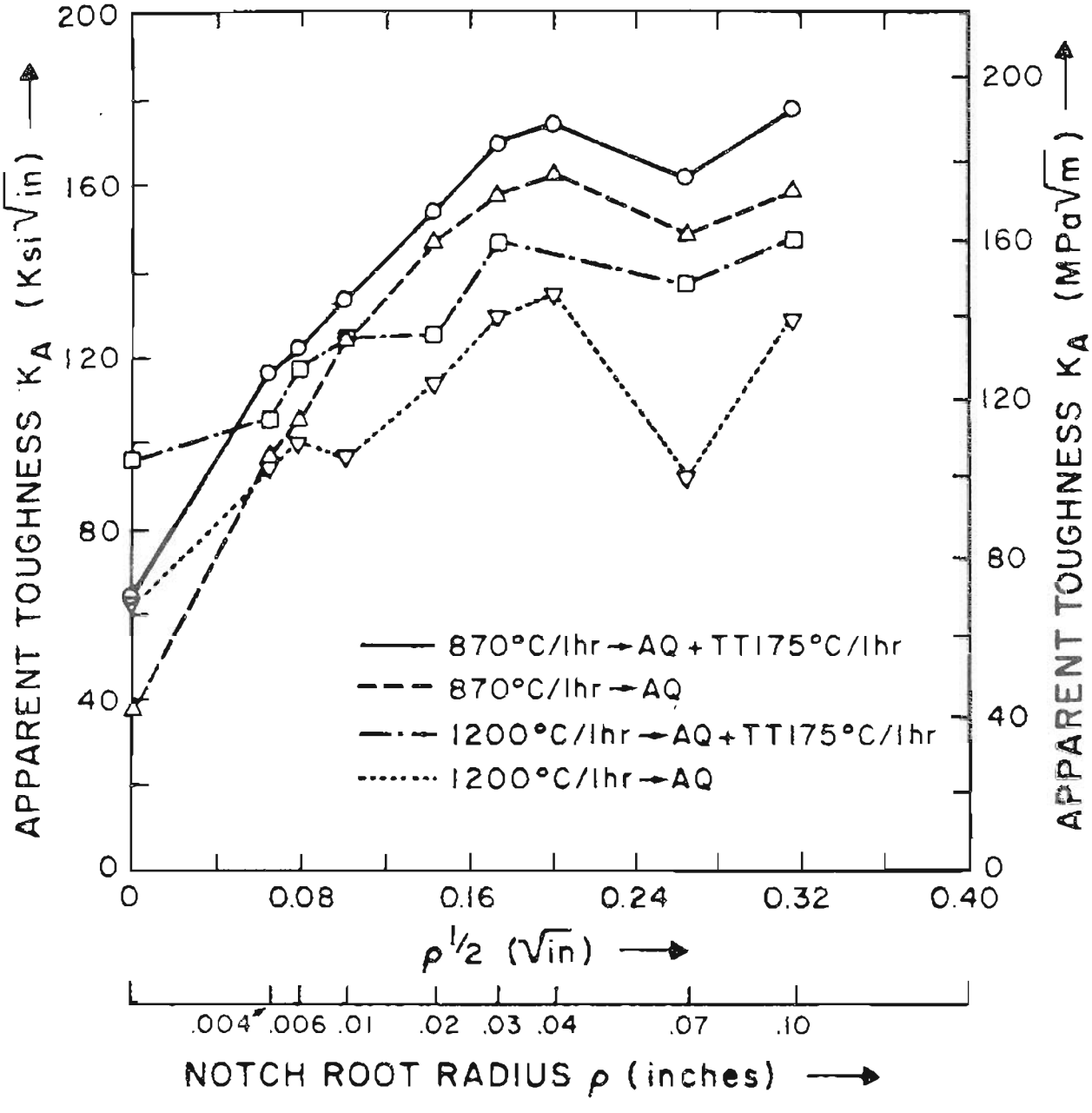

Fig. 3.1 Effect of notch root radius on the toughness of 4340 steel given different heat-treatments by instrumented Charpy test at room temperature.

TABLE 3-2

ROOM TEMPERATURE TOUGHNESS DATA OF 4340 STEEL BY SLOW-BEND CHARPY SPECIMENS HAVING VARIOUS ROOT RADII

SPECIMEN ID	AUSTENITISING TREATMENT °C/1H	TEMPERING TEMPERATURE °C/1H	ROOT RADIUS INCH	$K_{(APP)}$ KSI$\sqrt{IN}$	$K_{(APP)}$ MPA$\sqrt{M}$
A-151	1200	AQ	.004	65.47	71.88
A-152	"	AQ	.004	78.23	77.11
A-153	"	AQ	.006	78.23	77.11
A-154	"	AQ	.006	67.85	74.49
A-155	"	AQ	.02	53.56	58.81
A-156	"	AQ	.02	52.37	57.50
A-157	"	AQ	.03	55.95	61.43
A-158	"	AQ	.03	49.99	54.89
A-159	"	AQ	.04	59.514	65.35
A-160	"	AQ	.04	57.134	62.73
A-161	1200	175	.004	86.89	95.41
A-162	"	175	.004	95.223	104.55
A-163	"	175	.006	99.984	109.78
A-164	"	175	.006	104.75	115.02
A-165	"	175	.02	53.563	58.81
A-166	"	175	.02	85.701	94.09
A-177	"	175	.03	92.843	101.94
A-168	"	175	.03	95.223	104.55
A-199	"	175	.04	103.57	113.71
A-170	"	175	.04	97.604	107.17
A-171	870	AQ	.004	38.09	41.82
A-172	"	AQ	.004	47.61	52.28
A-173	"	AQ	.006	45.23	49.66
A-174	"	AQ	.006	44.184	48.51
A-175	"	AQ	.02	35.709	39.21
A-176	"	AQ	.02	36.89	40.51
A-177	"	AQ	.03	33.33	36.59
A-178	"	AQ	.03	38.09	41.82
A-179	"	AQ	.04	42.85	47.05
A-180	"	AQ	.04	40.946	44.96
A-181	870	175	.004	113.070	124.16
A-182	"	175	.004	117.839	129.39
A-183	"	175	.006	92.843	101.94
A-184	"	175	.006	108.317	118.93
A-185	"	175	.02	116.65	128.08
A-186	"	175	.02	114.27	125.47
A-187	"	175	.03	96.423	105.87
A-188	"	175	.03	90.462	99.33
A-189	"	175	.04	73.798	81.03
A-190	"	175	.04	70.47	77.37

given to these specimens of various root radii. The corresponding results are depicted in Fig. 3.2. The noticeable feature in this figure is that the toughness abruptly dropped for all the heat-treatments when the root radius exceeded 0.01 inch. For root radii less than .01" the toughness increased with the increase in root radius for all heat-treatments. However, for the heat-treatment 870/AO followed by tempering at 175°C the increase in the toughness was most marked. Beyond that root radius, the toughness levels off, though the trend is for a little increase in the toughness for all the heat treatments.

3.1.1.3 Liquid Nitrogen Instrumented Charpy Test

The liquid nitrogen instrumented Charpy data having various root radii are given in Table 3-3. Root radii varying from zero (i.e. pre-cracked) up to 0.04 inch were studied. The same four heat-treatments as described in earlier sections were given to these specimens having various root radii. The results are depicted in Figs. 3.3 and 3.4. The important point here is again the drop in toughness when the notch root radius was increased beyond .006" and levelling off of the toughness beyond that radius.

In summary, the toughness increased initially with the increase in notch root radius, as predicted by different models described in the appendix. However, after a critical root radius was reached, the toughness dropped, in contrast to all previously reported literature. Also, the critical root radius at which such drop in toughness is noticed is strongly temperature and strain-rate dependent.

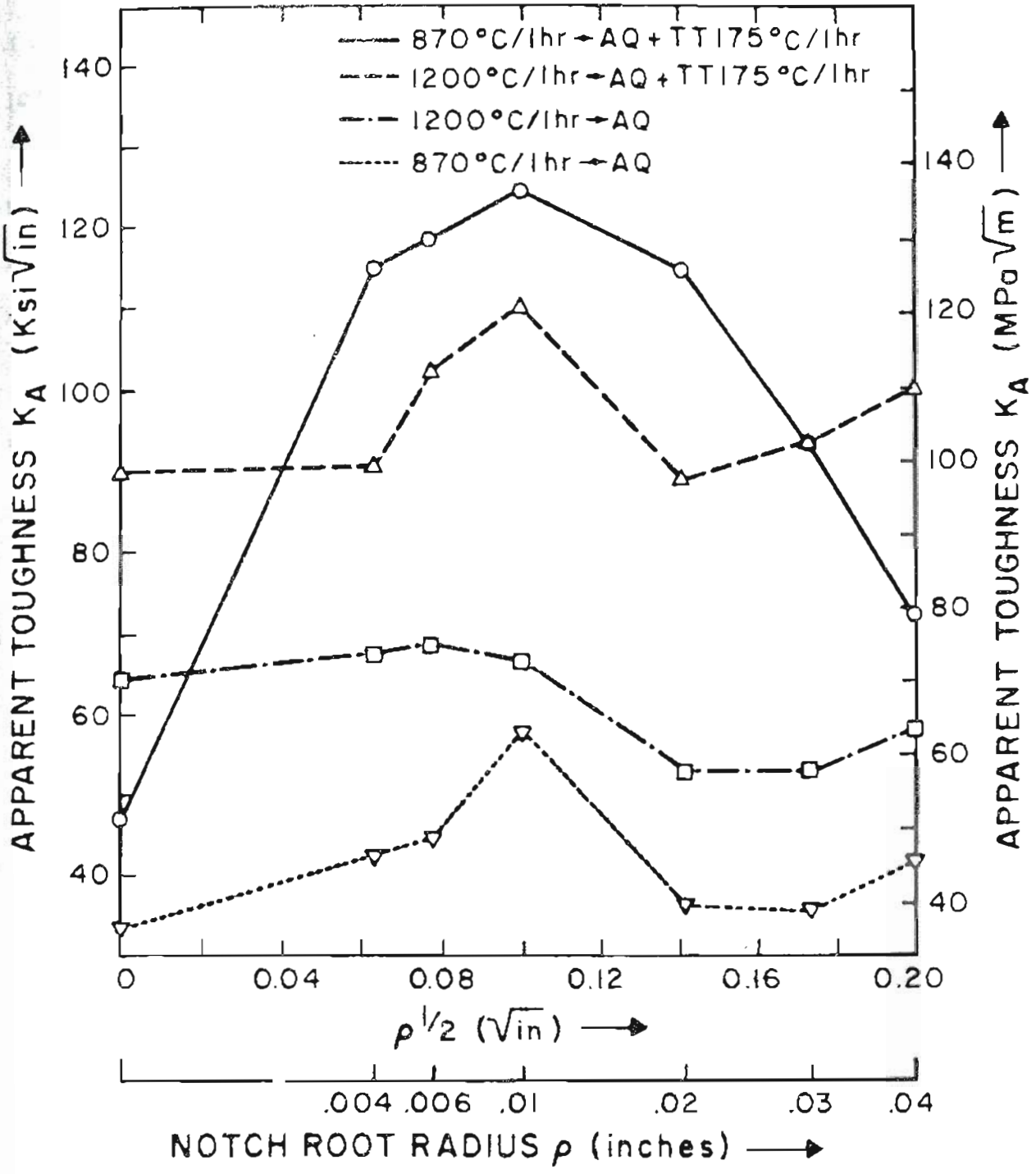

Fig. 3.2 Effect of notch root radius on the toughness of 4340 steel given different heat-treatment by slow-bend Charpy test at room temperature.

TABLE 3-3

LIQUID NITROGEN TOUGHNESS DATA OF 4340 STEEL BY INSTRUMENTED CHARPY SPECIMEN HAVING VARIOUS ROOT RADII

SPECIMEN ID --	AUSTENITISING TREATMENT 'C/1H	TEMPERING TEMPERATURE 'C/1H	ROOT RADIUS INCH -	K(APP) KSI$\sqrt{IN}$ -	K(APP) MPA$\sqrt{M}$ -
A-299	1200	AQ	.004	42.79	46.98
A-300	"	AQ	.004	54.06	59.36
A-301	"	AQ	.006	37.81	41.52
A-302	"	AQ	.006	39.13	42.97
A-303	"	AQ	.02	24.87	27.31
A-304	"	AQ	.02	29.85	32.78
A-305	"	AQ	.03	31.51	34.60
A-306	"	AQ	.03	29.19	32.05
A-307	"	AQ	.04	31.51	34.60
A-308	"	AQ	.04	26.20	28.77
A-309	1200	175	.004	62.02	68.10
A-310	"	175	.004	65.01	71.38
A-311	"	175	.006	63.02	69.20
A-312	"	175	.006	68.66	75.39
A-313	"	175	.02	43.114	47.34
A-314	"	175	.02	48.09	52.81
A-315	"	175	.03	46.44	50.99
A-316	"	175	.03	57.05	62.64
A-317	"	175	.04	44.12	48.444
A-318	"	175	.04	51.08	56.09

TABLE 3-3 (CONT'D)

LIQUID NITROGEN TOUGHNESS DATA OF 4340 STEEL BY INSTRUMENTED CHARPY SPECIMEN HAVING VARIOUS ROOT RADII

SPECIMEN ID	AUSTENITISING TREATMENT °C/1H	TEMPERING TEMPERATURE °C/1H	ROOT RADIUS INCH	K(APP) KSI $\sqrt{IN}$	K(APP) MPA $\sqrt{M}$
--				-	-
A-319	870	AQ	.020	42.79	46.98
A-320	"	AQ	.020	42.95	47.16
A-321	"	AQ	.030	40.63	44.61
A-322	"	AQ	.030	42.95	47.16
A-323	"	AQ	.02	28.02	30.77
A-324	"	AQ	.02	25.04	27.49
A-325	"	AQ	.03	25.87	28.40
A-326	"	AQ	.03	39.64	43.52
A-327	"	AQ	.04	22.71	24.94
A-328	"	AQ	.04	21.06	23.12
A-329	870	175	.020	65.01	71.38
A-330	"	175	.020	62.69	68.83
A-331	"	175	.030	60.70	66.65
A-332	"	175	.030	51.91	57.00
A-333	"	175	.02	41.62	45.70
A-334	"	175	.02	47.43	52.08
A-335	"	175	.03	42.12	46.25
A-337	"	175	.04	30.51	33.50
A-338	"	175	.04	29.35	32.23
		175.			

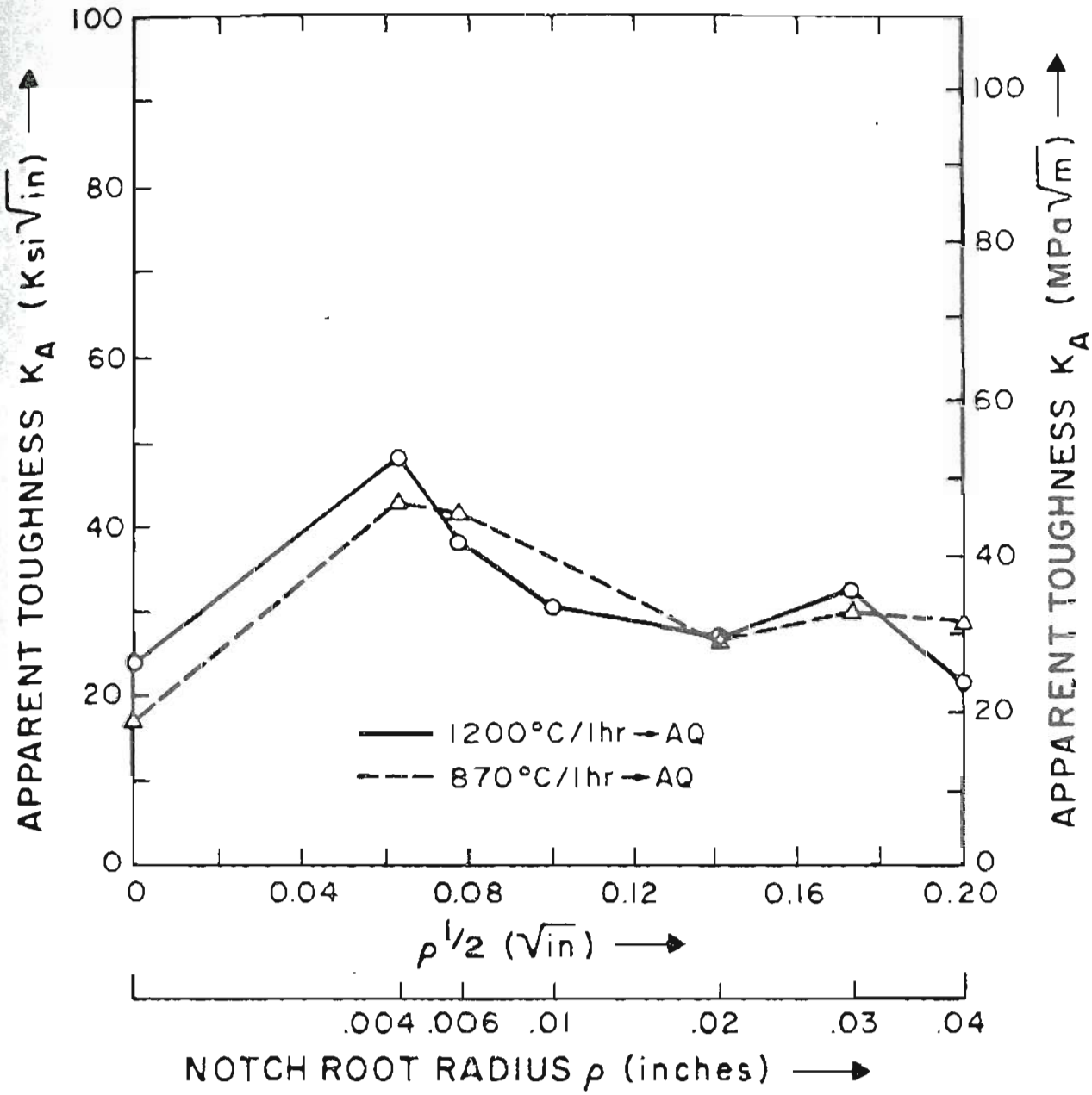

Fig. 3.3. Effect of notch root radius on the toughness of 4340 steel given different heat-treatments by instrumented Charpy test at liquid nitrogen temperature.

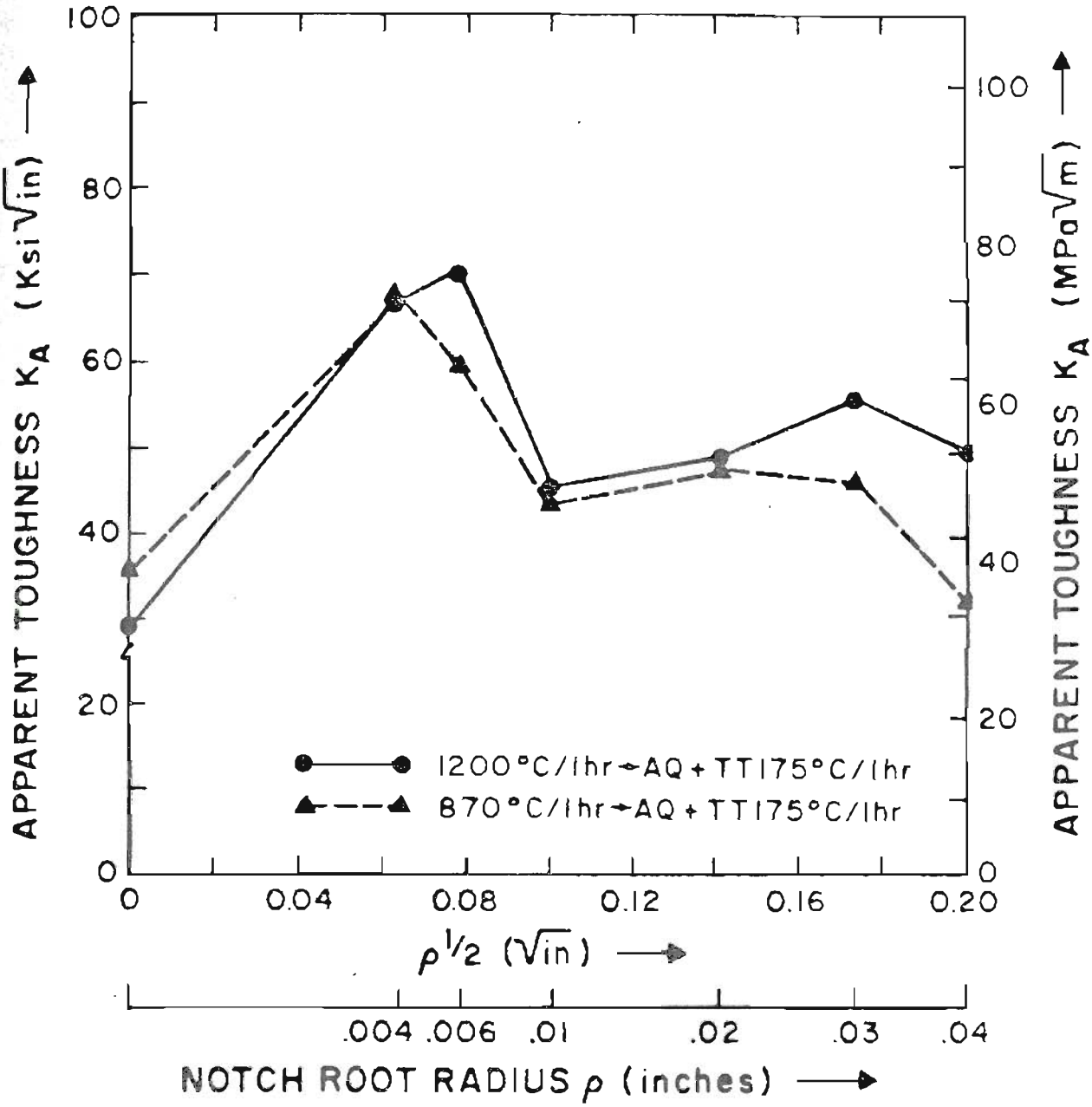

Fig. 3.4 . Effect of notch root radius on the toughness of 4340 steel given different heat-treatments by instrumented Charpy test at liquid nitrogen temperature.

3.1.2 Comparison of Tempering Behavior After Both High (1200°C) and Conventional (870°C) Austenitizing Treatments

In view of the differences between fracture toughness test and Charpy V-notch test, the following experiments were planned to study the above tempering behavior. Firstly, pre-cracked Charpy specimens were tested under slow-bend condition, the strain-rate approaching that of the K_{Ic} testing. Secondly, the fracture toughness test involving three-point bend specimens was performed. Thirdly, both V-notch Charpy specimens and three-point bend specimens with a root radius of 0.01 inch were tested to evaluate the root radius effect. The results are described as below.

3.1.2.1 Slow Bend Pre-Cracked Charpy Test

The room temperature slow-bend pre-cracked Charpy test results are given in Table 3-4a. The pre-cracked length was measured by a travelling microscope and the a/w ratio is reported in the table for each specimen. Since to ensure plane strain condition the a/w ratio is normally kept between 0.45 to 0.55, these tests failed to meet the ASTM criterion for valid fracture toughness test. Hence, the toughness, as measured in this program is treated as the apparent toughness.

Figure 3.5 shows the apparent toughness as a function of tempering temperature for two austenitizing treatments namely 870°C and 1200°. It is seen very clearly that in the pre-cracked condition, the high austenitizing treatment was unquestionably better up

TABLE 3-4

ROOM TEMPERATURE SLOW-BEND CHARPY TESTING DATA FOR 4340 STEEL

(A) PRE-CRACKED

SPECIMEN ID	AUSTENITISING TREATMENT 'C/1H	TEMPERING TEMPERATURE 'C/1H	A/W - -	K(APP) KSI √IN --	K(APP) MPA √M --
A 121	1200	AQ	.3	64.552	70.80
A 123	"	150	263	90 259	99.101
A 124	"	150	.3	79.230	86 99
A 125	"	175	.275	84.52	92.80
A 126	"	175	.263	95.90	105 29
A 127	"	200	.3	71.544	78 55
A 128	"	200	.2625	83 21	91.36
A 263	"	225	.2794	59.75	65 606
A 264	"	225	.3848	60. 66	66.605
A 130	"	280	.3	52.881	58.06
A 131	870	AQ	3	32.66	35.86
A 132	"	AQ	.3	34.217	37.57
A 133	"	150	.3	39.666	43.55
A 134	"	150	.3125	38.563	42.34
A 135	"	175	.275	53.195	58.400
A 136	"	175	.3	41.994	46.109
A 137	"	200	.3125	51 418	56 46
A 138	"	200	.3	55.220	60.63
A 139	"	280	.2875	57.97	63.65
A 140	"	280	.3	55.22	60.63

(B) V-NOTCH

A 191	1200	AQ	.2	66.656	73.100
A 192	"	AQ	"	67.856	74.505
A 193	"	150	"	99.984	109.82
A 194	"	150	"	103.565	113.714
A 195	"	175	"	109.507	120 239
A 196	"	175	"	111.807	122.852
A 197	"	200	"	102.365	112.396
A 198	"	200	"	109.507	120.230
A 267	"	225	"	96.41	105.86
A 268	"	225	"	92.85	101.95
A 199	"	280	"	77.369	84.95
A 200	"	280	"	85.701	94.10
A 201	870	AQ	.2	57.134	62.73
A 202	"	AQ	"	57.134	62.73
A 203	"	150	"	109.51	120.24
A 204	"	150	"	100.32	110.932
A 205	"	175	"	126.17	138.535
A 206	"	175	"	123.79	135.92
A 207	"	200	"	130 932	143.76
A 208	"	200	"	129.74	142.46
A 259	"	225	"	126.10	138.55

TABLE 3-4 (CON'T)

ROOM TEMPERATURE SLOW-BEND CHARPY TESTING DATA FOR 4340 STEEL

(B) V-NOTCH

SPECIMEN ID	AUSTENITISING TREATMENT	TEMPERING TEMPERATURE	A/W	K(APP)	
--	'C/1H	'C/1H	-	KSI√IN	MPA√M
A 26E	''	225	''	119.83	130.69
A 20E	''	250	''	122.60	134.62
A 21E	''	280	''	119.829	130.69

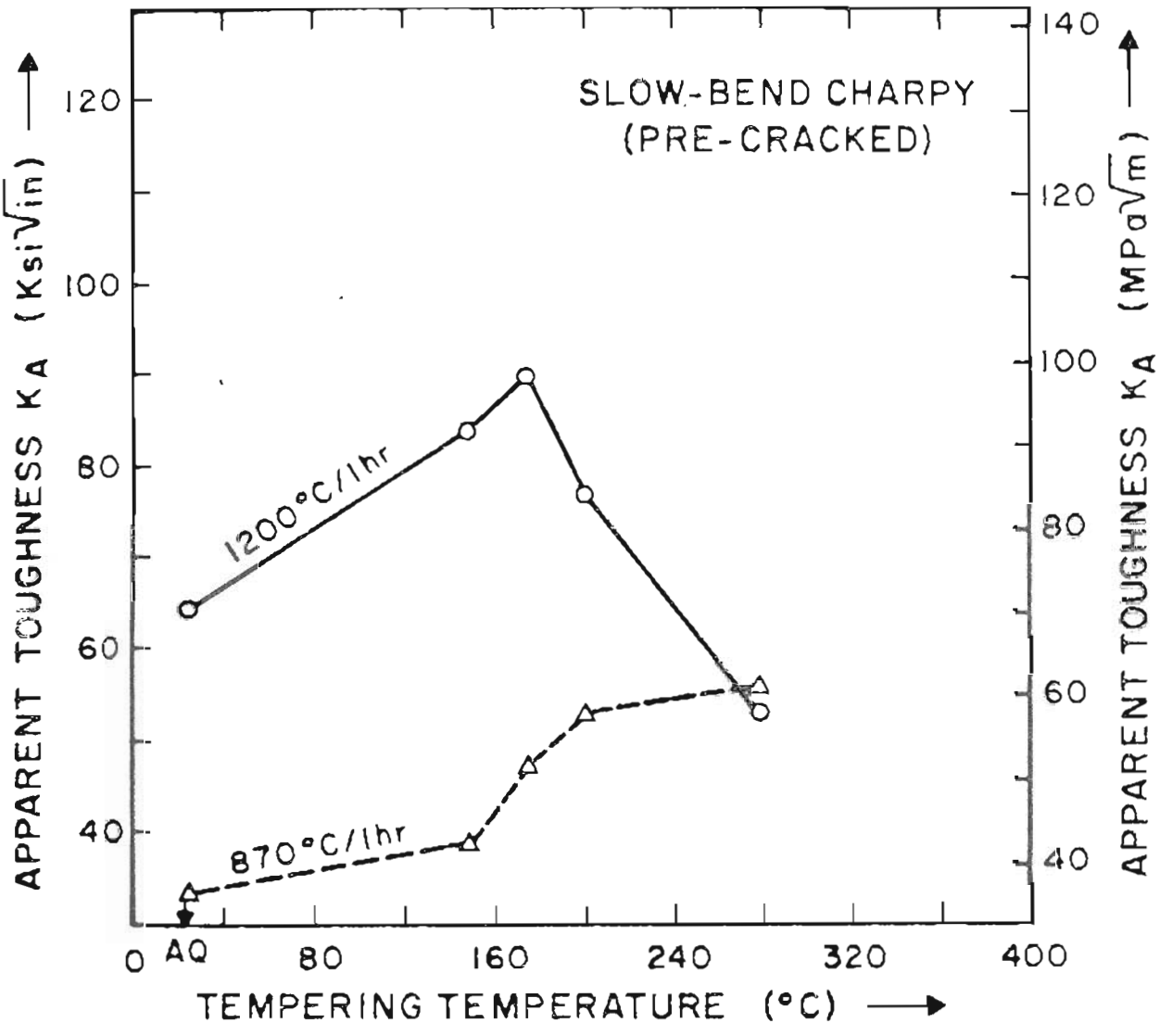

Fig. 3.5 Effect of tempering temperature on the toughness of 4340 steel, given both high and low austenitizing treatments by slow-bend pre-cracked Charpy test.

to a tempering temperature of about 200°C. However, the toughness dropped abruptly when the tempering temperature was further increased for the high austenitizing case whereas no such drop in toughness occurred for the lower austenitizing treatment for this tempering temperature range.

3.1.2.2 Instrumented Pre-cracked Charpy Test

The room temperature pre-cracked instrumented Charpy test results are tabulated in Table 3.5a and also depicted in Fig. 3.6 as a function of the tempering temperature for both high and low austenitizing temperatures. Two important results follow. Firstly, in the pre-cracked condition the high austenitizing treatment resulted in superior toughness properties up to a tempering temperature of about 200°C. Secondly, there was a drastic drop in toughness or 'temper embrittlement' beyond a tempering temperature of 225°C for the high austenitizing case, whereas no such drop was observed for the lower austenitizing temperature. Before the embrittlement, toughness, of course, increased with the increase in tempering temperature as in slow-bend Charpy tests. This also shows that the strain-rate has insignificant effect on the toughness behavior of the steel in question.

3.1.2.3 Three-Point Bend Plane Strain Fracture Toughness Test

The room temperature longitudinal fracture toughness data for three-point bend specimen are given in Table 3-6. The corresponding results are shown in Fig. 3.7. As in the previous cases the same two trends are noticeable, i.e. in the pre-cracked condition the

TABLE 3-5

ROOM TEMPERATURE INSTRUMENTED CHARPY TEST FOR 4340 STEEL

(A) PRE-CRACKED

SPECIMEN ID	AUSTENITISING TREATMENT °C/1H	TEMPERING TEMPERATURE °C/1H	A/W - -	K(APP) KSI$\sqrt{IN}$ -	K(APP) MPA$\sqrt{M}$ -
A 221	1200	AQ	.3	59.87	68.74
A 222	"	AQ	.3	67.57	74.19
A 223	"	150	.3	70.19	77.07
A 5	"	175	.2632	80.12	96.76
A 6	"	175	.2375	90.69	100.36
A 7	"	200	.2375	79.595	87.395
A 261	"	225	.3	68.78	75.52
A 262	"	225	.3	71.62	78.64
A 9	"	280	.225	59.10	64.90
A 10	"	280	.225	60.82	66.78
A 239	870	AQ	.3	37.55	41.23
A 12	"	AQ	.21	41.21	45.25
A 14	"	150	.227	60.07	65.96
A 16	"	175	.21	65.23	71.62
A 17	"	200	.217	77.15	84.71
A 19	"	280	.236	73.824	81.06

(B) V-NOTCH

A 91	1200	AQ	.2	99.24	100 97
A 92	"	AQ	.2	94.27	103.51
A 93	"	150	.2	125.34	137.62
A 94	"	150	.2	124.69	136.90
A 95	"	175	.2	123.95	136.098
A 96	"	175	.2	125.21	137.48
A 97	"	200	.2	122.49	134.49
A 98	"	200	.2	121.90	133.94
A 265	"	225	.2	102.34	112.37
A 266	"	225	.2	106.35	116.774
A 99	"	280	.2	95.68	105.06
A 100	"	280	.2	79.35	87.12
A 241	870	AQ	.2	86.32	94.77
A 242	"	AQ	.2	100.80	110.77
A 103	"	150	.2	120.40	132.203
A 104	"	150	.2	122.66	134.68
A 105	"	175	.2	140.65	154.43
A 106	"	175	.2	127.12	130.58
A 108	"	200	.2	141.71	155.59
A 109	"	200	.2	119.22	130.899
A 110	"	280	.2	129.56	142.26

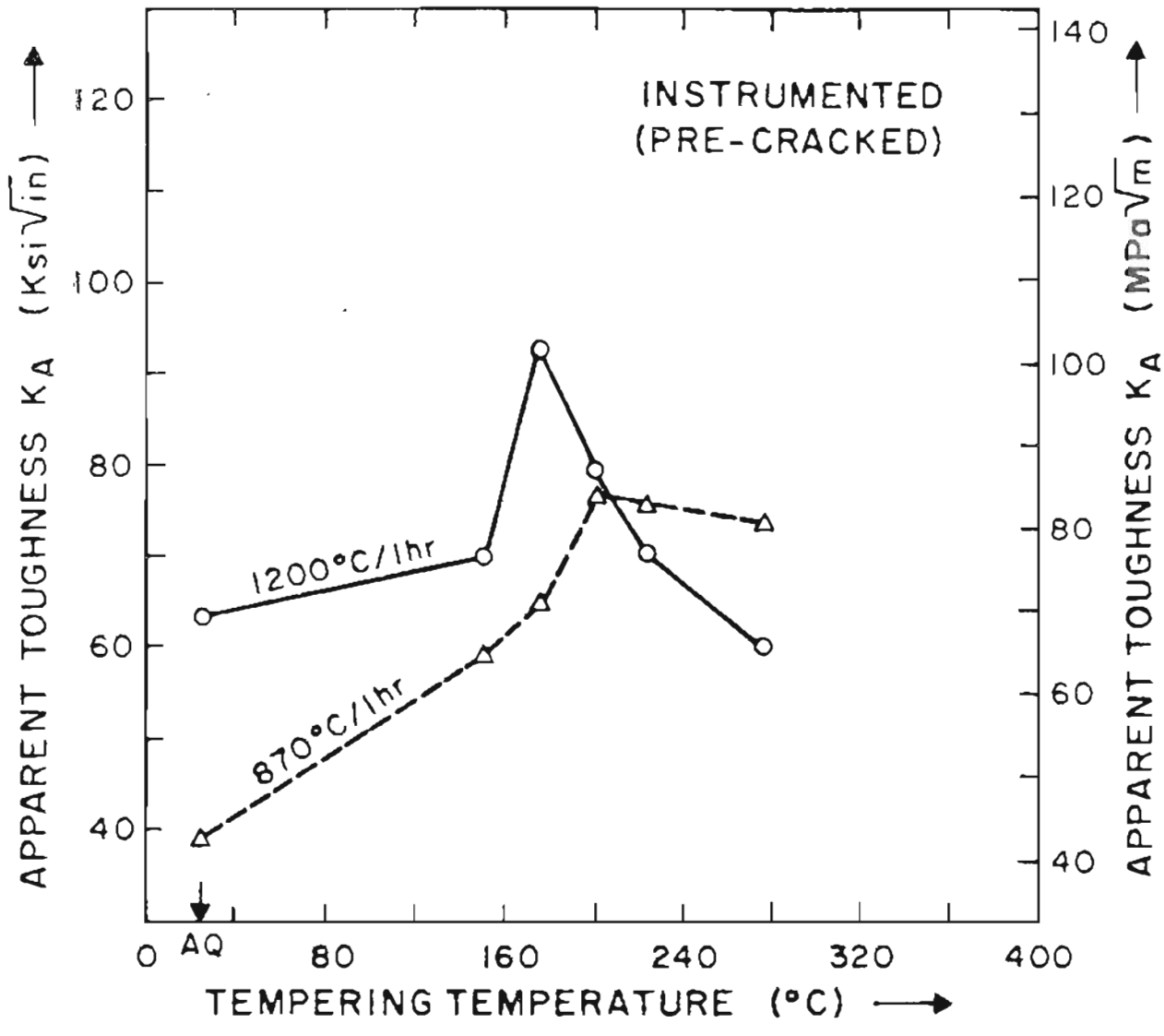

Fig. 3.6 Effect of tempering temperature on the toughness of 4340 steel given both high and low austenitizing treatments by pre-cracked instrumented Charpy test.

TABLE 3-6

ROOM TEMPERATURE BEND SPECIMEN FRACTURE TOUGHNESS DATA FOR 4340 STEEL

SPECIMEN ID	AUSTENITISING TREATMENT	TEMPERING TEMPERATURE	A/W	$K_{(IC)}$ KSI $\sqrt{IN}$	$K_{(IC)}$ MPA $\sqrt{M}$
--	'C/1H	'C/1H	-	-	-
T-2	870	AQ	.52	38.214	41.96
T-5	"	175	.575	65.938	72.40
T-6	"	175	.49	74.553	81.86
T-17	"	280	.52	83.12	91.27
T-9	1200	AQ	.55	77.63	85.24
T-10	"	AQ	.57	66.44	72.95
T-13	"	175	.5	98.44	108.00
T-14	"	175	.56	112.0	122.92
T-19	"	280	.49	68.81	75.55

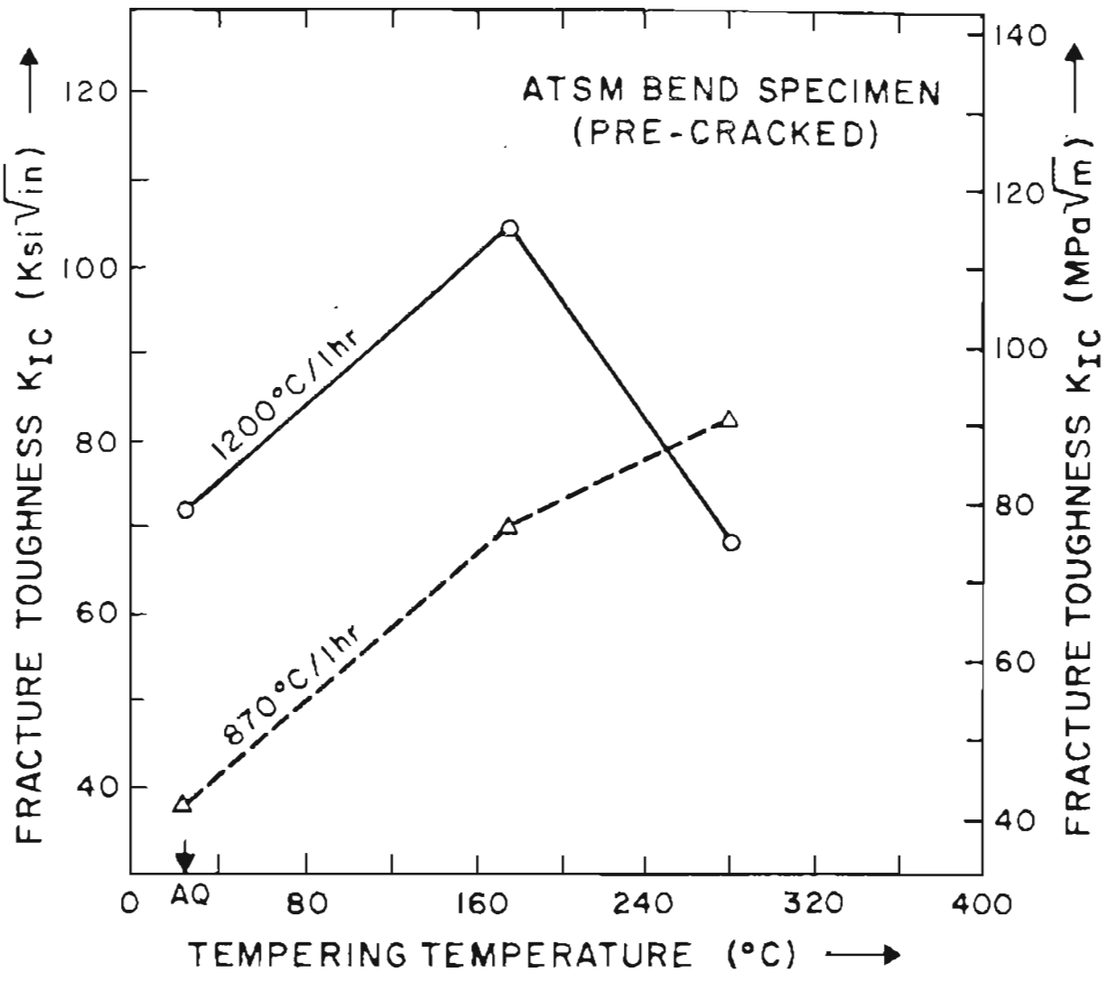

Fig. 3.7 Effect of tempering temperature on the toughness of 4340 steel given both high and low austenitizing treatments by three-point bend fracture toughness specimen.

Charpy toughness for the lower austenitizing treatment was similar to that of the higher austenitizing treatment up to a tempering temperature of about 150°C; however, beyond that tempering temperature the lower

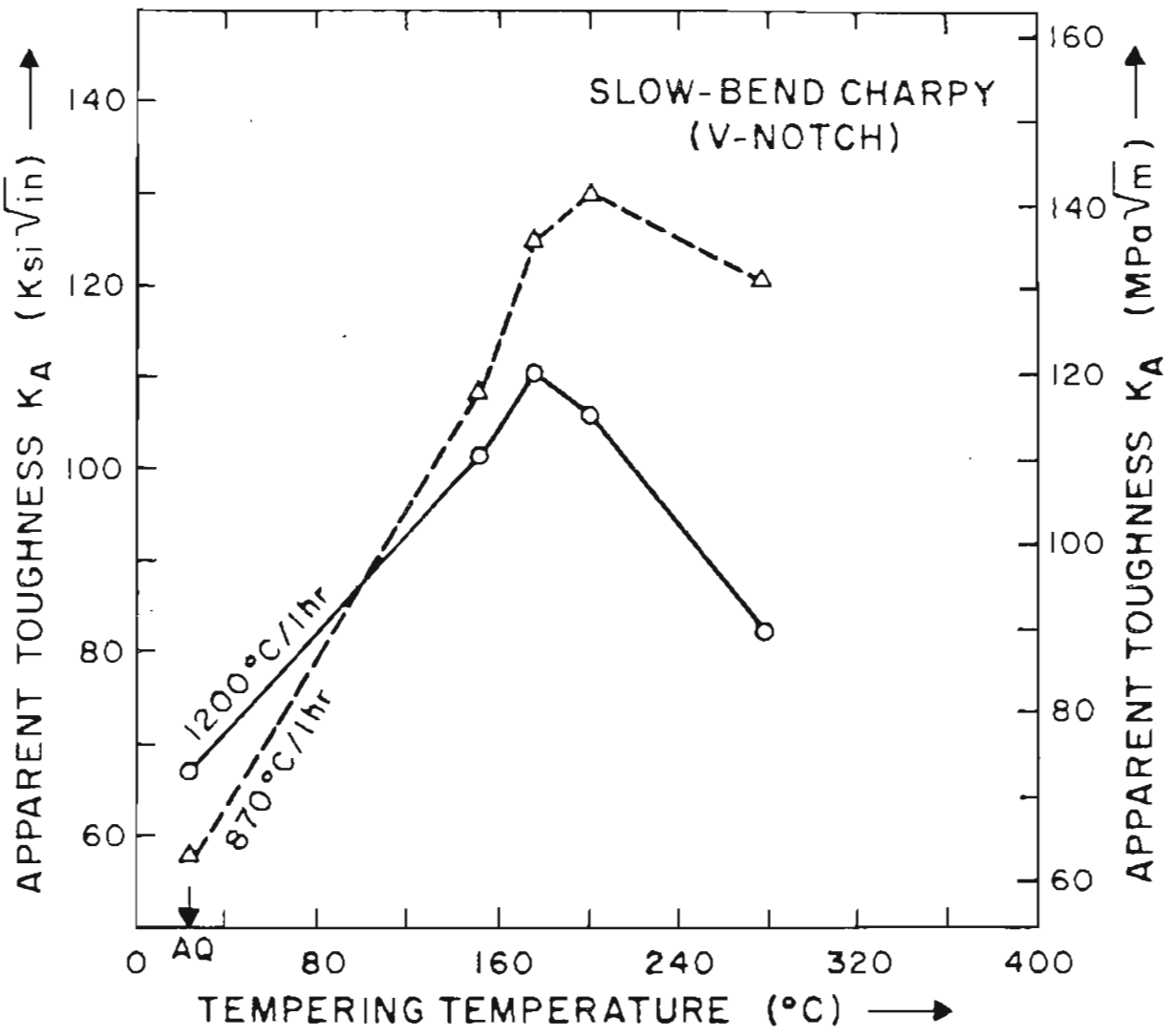

Fig. 3.8 Effect of tempering temperature on the toughness of 4340 Steel given both high and low austenitizing treatments by slow-bend V-notch Charpy test.

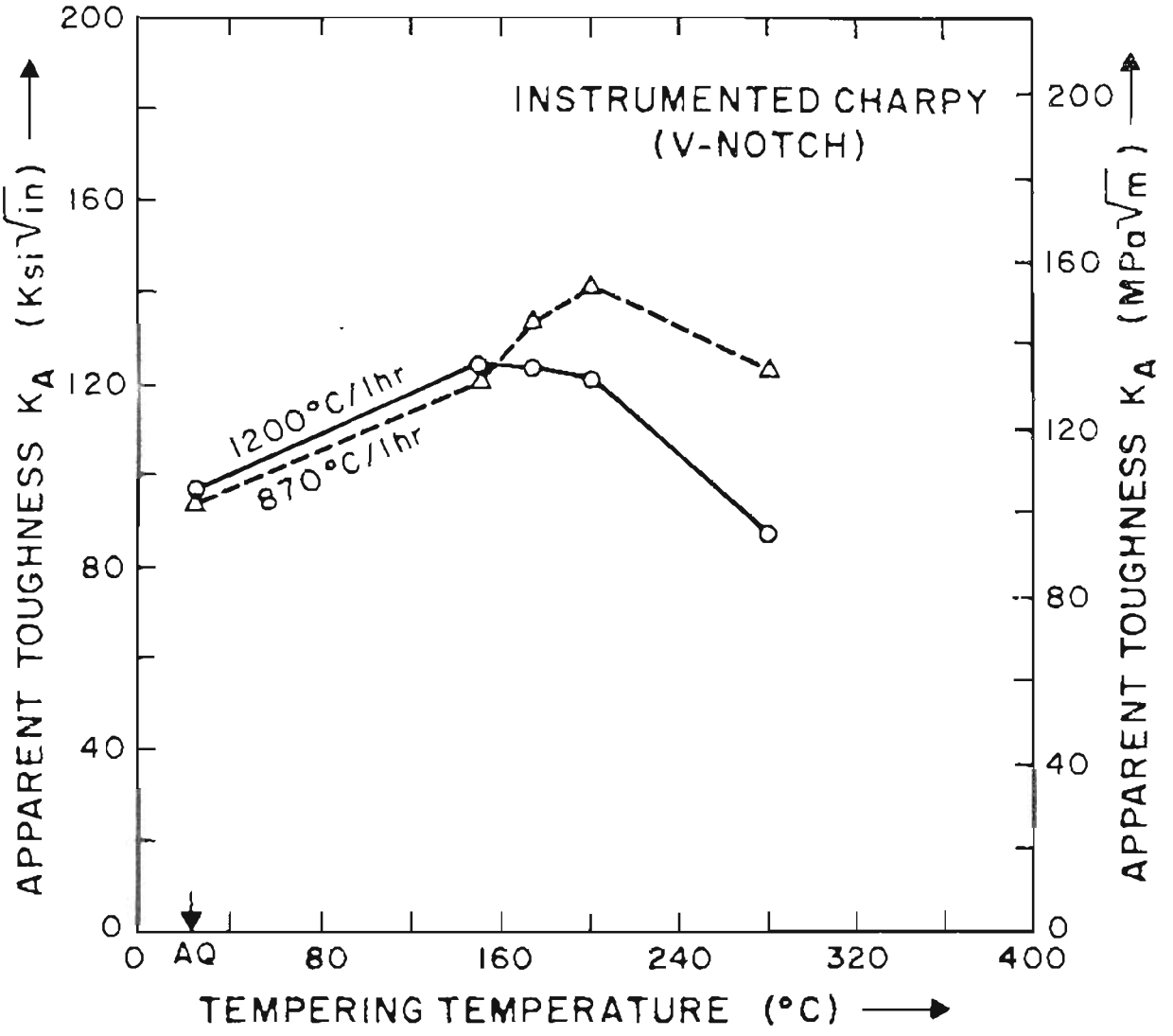

Fig. 3.9 Effect of tempering temperature on the toughness of 4340 steel given both high and low austenitizing treatments by V-notch instrumented Charpy test.

austenitizing treatment gave superior properties. Also, the 'toughness drop' which occurred in the pre-cracked testing condition for the higher austenitizing case occurred in the V-notch testing condition as well. While because of low energy tear made of fracture Charpy V-notch energy is not considered significant in this investigation, the corresponding values are shown in Table 3-7 and Fig. 3.10.

3.1.2.6 Blunt Notch ASTM Bend Specimen Fracture Toughness Test

The toughness data by blunt notch ASTM bend specimens are tabulated in Table 3-8 and are shown in Fig. 3.11. The trends were exactly the same as in the previous cases. The results in Fig. 3.8, 3.9 and 3.11 indicate that there was no difference in the toughness behavior with changes in method of loading, specimen thickness, $\frac{a}{w}$ ratio and the strain-rate. However, the toughness for the lower austenitizing treatment appeared to be superior when the crack tip is blunt instead of being pre-cracked. In other words there exists a root radius effect in the toughness behavior of the two heat treatments as established earlier (2,3).

3.1.3 Mechanical Properties in the Bainitic Region

Bainitic microstructures have been observed to provide good mechanical properties in both medium carbon and high carbon steels. However, most of the mechanical tests reported so far are conventional in nature, i.e. Charpy impact test, tensile test and the determination of transition temperature. High strength steels like 4340 fail by a low

TABLE 3-7

ROOM TEMPERATURE CHARPY V-NOTCH ENERGY FOR 4340 STEEL

HEAT-TREATMENT	AVG. CHARPY ENERGY FT-LBS	JOULES
870°C/1-AQ	8.69	11.775
870°C/1H-AQ+TT 150°C/1H	9.485	12.75
870°C/1H-AQ+TT 175°C/1H	10.85	14.71
870°C/1H-AQ+TT 200°C/1H	11.57	15.68
870°C/1H-AQ+TT 280°C/1H	10.13	13.74
1200°C/1H-AQ	8.136	11.83
1200°C/1H-AQ+ TT150°C/1H	10.85	14.71
1200°C/1H-AQ+ TT175°C/1H	13.39	18.15
1200°C/1H-AQ+ TT280°C/1H	10.85	14.71
1200°C/1H-AQ+ TT280°C/1H	6.144	8.33

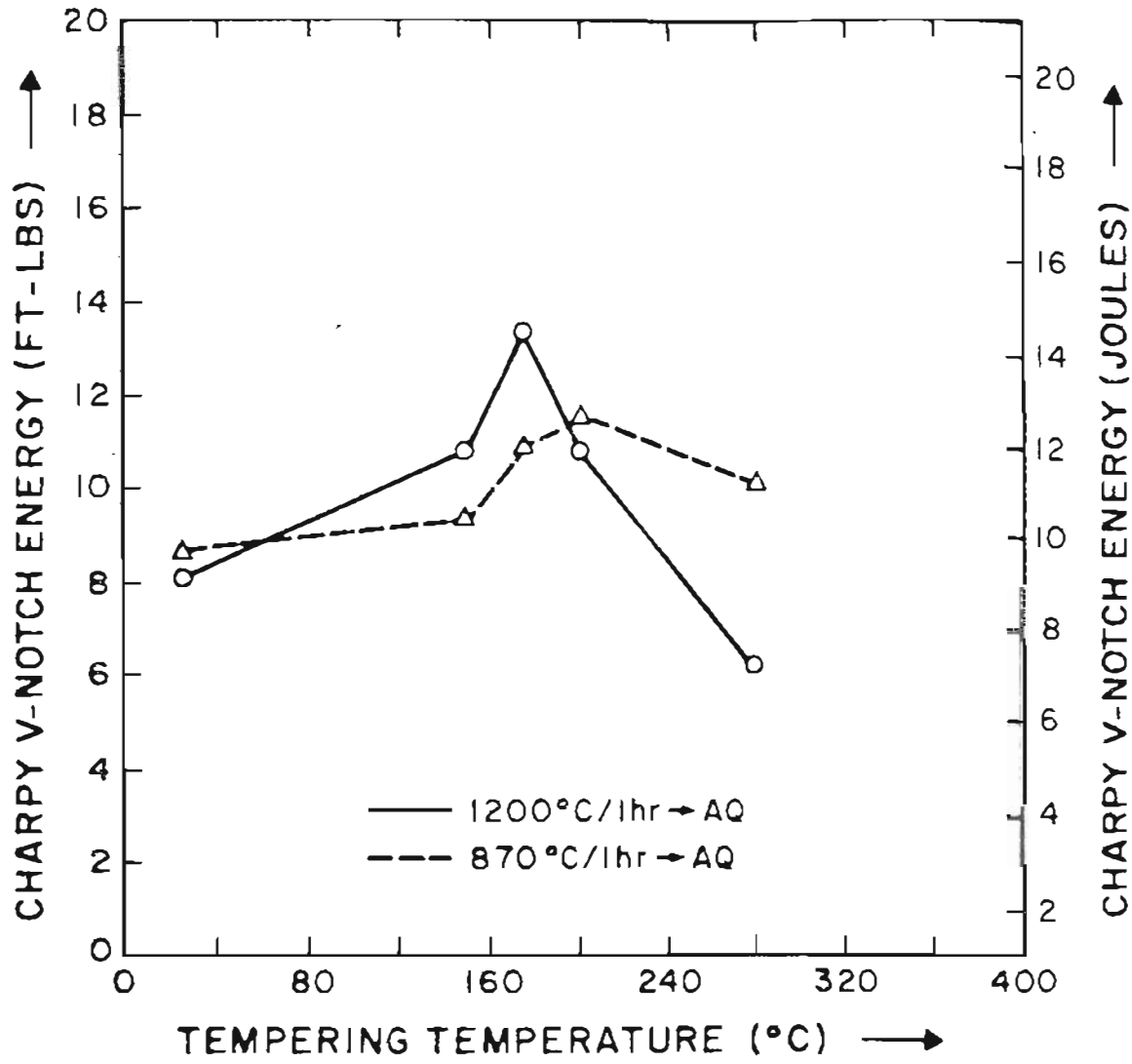

Fig. 3.10. Effect of tempering temperature on the Charpy V-notch energy of 4340 steel for both high and low austenitizing treatments.

TABLE 3-8

ROOM TEMPERATURE BEND SPECIMEN FRACTURE TOUGHNSS (BLUNT NOTCH)
FOR 434B STEEL

SPECIMEN ID	AUSTENITISING TREATMENT 'C/1H	TEMPERING TEMPERATURE 'C/1H	A/W	K(APP) KSI√IN	K(APP) MPA√M
--			-	-	-
T-3	87B	AQ	.44	88.78	97.48
T-4	"	AQ	.47	83.11	91.25
T-7	"	175	.47	169.47	186.88
T-8	"	175	.48	171.75	188.58
T-18	"	28B	.47	149.92	164.61
T-11	12BB	AQ	.47	99.48	189.142
T-12	"	AQ	.48	185.87	116.25
T-15	"	175	.48	148.86	154.43
T-16	"	175	.475	148.65	154.43
T-28	"	28B	.47	93.697	182.88

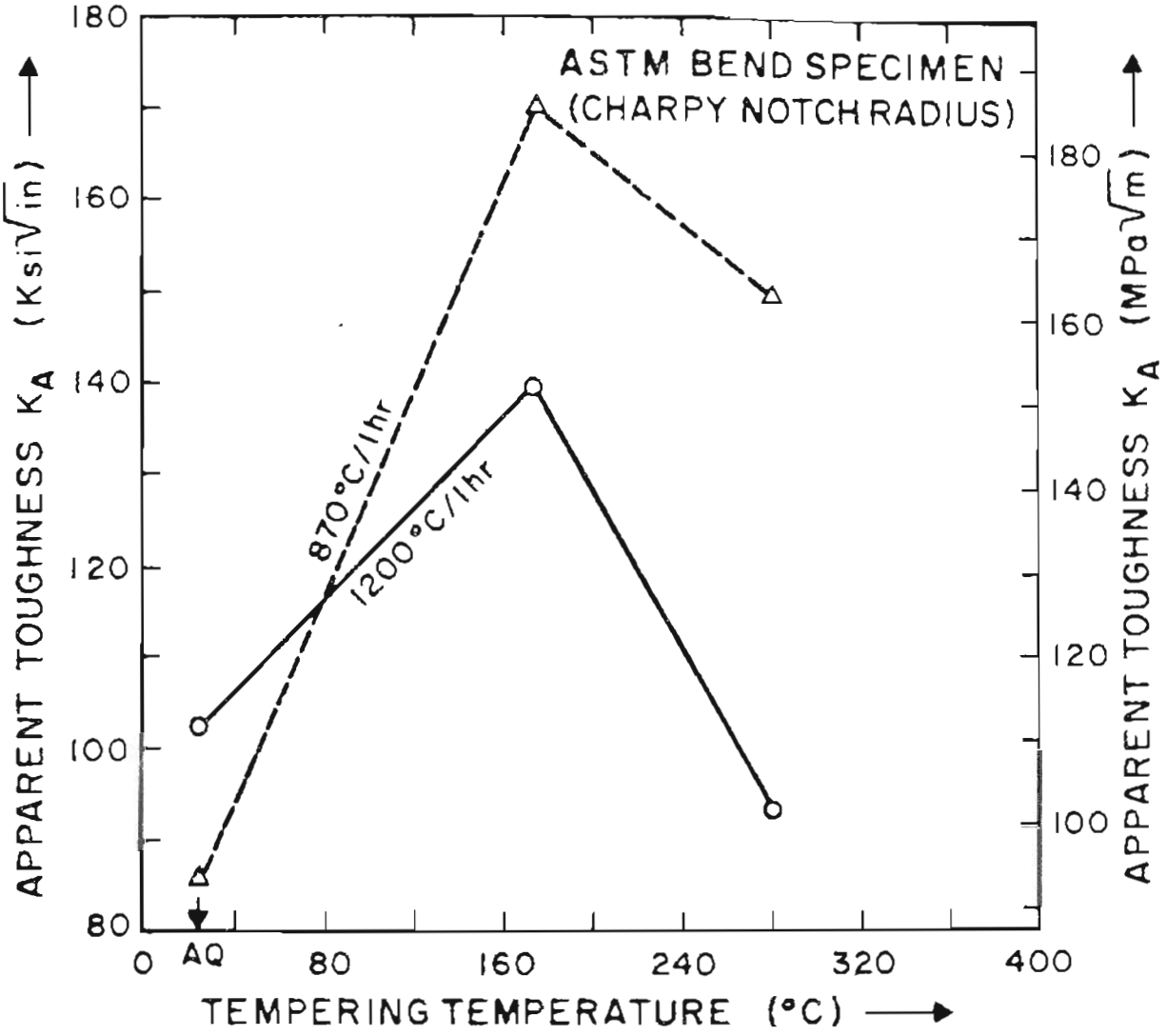

Fig. 3.11 Effect of tempering temperature on the toughness of 4340 steel for both high and low austenitizing treatments by 3-point bend fracture toughness test (with specimen having blunt notch radius = Charpy notch radius).

energy tear mode (61) in Charpy testing and hence any small change in the Charpy value may not correspond to subtle microstructural difference. Also, in recent years fracture toughness tests are considered to provide a more scientific basis for determining the material's resistance against fracture. In order to evaluate the mechanical properties in the bainitic region for the steel austenitized at 1200°C fracture toughness tests and the corresponding tensile tests were conducted.

3.1.3.1 Fracture Toughness Tests

The room temperature longitudinal plane strain fracture toughness results for different heat treatment in the bainitic region are given in Table 3-9. In these tables the ratio P_m/P_Q is determined from the load vs crack opening displacement curve generated during the test. This is shown schematically in Fig. 3.12. These ratios are included in the tables since they are a new restriction placed on the determination of the validity of K_{Ic}. The ASTM now specifies (115) that this ratio must be less than or equal to 1.10. However, it was demonstrated (116) that significant difference in the calculated fracture toughness does not arise, even though P_m/P_Q ratio exceeds 1.10. Normally the two conditions which have to be met for a valid K_{Ic} are

1. $P_m/P_Q \leq 1.10$.
2. $B \geq 2.5 \, (K_{Ic}/\sigma_{ys})^2$.

Three bainitic isothermal transformation temperatures were chosen, based on the TTT diagram of 4340 steel austenitized at 1200°C, namely 350°C, 335°C and 300°C. Specimens were held at these temperatures for varying lengths of time before quenching in

TABLE 3-9

ROOM TEMPERATURE LONGITUDINAL FRACTURE TOUGHNESS DATA FOR 4340 STEEL

SPECIMEN ID -	AUSTENITISING TREATMENT °C/H	TEMPERING TEMPERATURE °C/1HR	K(IC) KSI√IN -	K(IC) MPA√M -	K(MAX) KSI√IN -	K(MAX) MPA√M -	PM/PQ -
AC 156	1200/1-350/1MIN	AQ	70.4	77.3	84.3	92.56	1.15*
AC 160	"	AQ	63.8	70.85	82.2	90.25	1.17*
AC 132	"	175	90.55	99.42	91.8	100.79	1.01
AC 133	"	175	78.8	86.52	87.5	96.08	1.04
AC 134	"	200	81.4	89.37	88.7	97.39	1.06
AC 135	"	200	80.0	87.84	98.8	100.48	1.08
AC 216	1200/1-350/5MIN	AQ	53.2	58.41	75.9	83.34	1.2
AC 217	"	AQ	60.7	66.65	-	-	1.03
AC 218	"	175	87.2	95.75	-	-	1.02
AC 219	"	175	79.6	87.4	-	-	1.03
AC 136	"	200	77.0	84.55	94.2	103.43	1.06
AC 220	1200/1-350/30MIN	175	60.0	65.88	61.5	67.52	1.09
AC 221	"	175	58.8	64.56	59.4	65.22	1.01
AC 64	1200/1-335/3MIN	AQ	58.2	63.90	66.3	72.79	1.06
AC 65	"	AQ	60.5	66.43	66.8	73.35	1.03
AC 73	"	175	80.2	88.06	82.1	90.15	1.01
AC 70	"	200	74.5	81.80	82.7	90.81	1.03
AC 71	"	200	78.2	85.86	79.7	87.51	1.00
AC 74	"	200	68.5	75.21	81.4	89.37	1.06
AC 222	1200/1-335/5MIN	AQ	62.0	68.95	69.7	76.53	1.09
AC 137	"	175	69.4	76.20	89.1	97.83	1.14*
AC 157	"	175	70.7	77.63	93.0	103.0	1.17*
AC 75	"	200	82.7	90.8	80.7	97.39	1.01
AC 210	1200/1-335/10MIN	AQ	53.0	59.07	66.4	72.91	1.09
AC 211	"	AQ	52.7	57.86	63.7	69.94	1.08
AC 212	"	175	62.2	68.29	74.7	82.01	1.13
AC 213	"	200	66.0	72.47	83.6	91.79	1.06
AC 214	"	200	63.3	69.5	77.9	85.53	1.12*
AC 215	"	200	80.9	88.82	80.9	88.82	1.00
AC 223	1200/1-335/30MIN	175	54.5	59.84	55.1	60.49	1.04
AC 66	1200/1-335/60MIN	AQ	43.5	47.76	50.7	55.67	1.08
AC 67	"	AQ	45.9	50.40	45.9	50.40	1.00
AC 68	"	200	53.9	59.18	58.1	63.79	1.01
AC 69	"	200	47.2	61.83	57.4	63.02	1.10
AC 139	1200/1-315/3MIN	200	80.0	87.84	80.2	96.84	1.08
AC 140	"	200	76.0	84.33	90.3	99.15	1.02
AC 82	1200/1-300/3MIN	200	79.2	86.96	80.0	97.5	1.05
AC 83	"	200	80.4	88.28	84.7	93.00	1.03

TABLE 3-9 (CON'T)

ROOM TEMPERATURE LONGITUDINAL FRACTURE TOUGHNESS DATA FOR 4340 STEEL

SPECIMEN ID	AUSTENITISING TREATMENT °C/h	TEMPERING TEMPERATURE °C/1HR	K(IC) KSI√IN	K(IC) MPA√M	K(MAX) KSI√IN	K(MAX) MPA√M	PM/PQ -
-			-	-	-	-	-
AC 80	1200/1-300/60MIN	200	62.5	68.63	62.5	68.63	1.00
AC 81	"	200	65.4	71.81	65.4	71.81	1.00

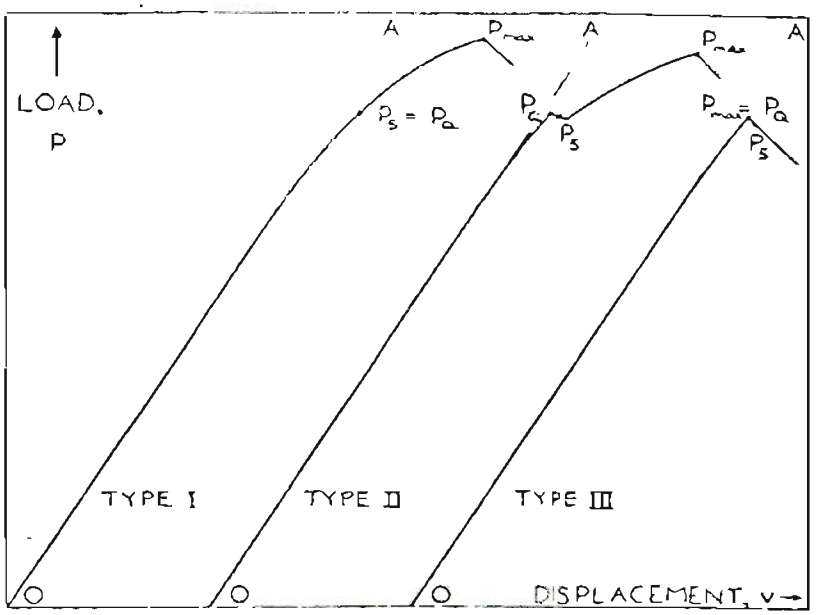

Fig. 3.12. Principal types of load - displacement Records.

an agitated oil bath. They were subsequently tempered in a salt bath for 1 hour. The results are shown in Table 3-9 and Figs. 3.13, 3.14 and 3.15. The toughness values as a function of the tempering temperatures for different bainitic treatments are depicted in Figs. 3.13 and 3.14. It is shown that as the holding time for any isothermal transformation temperature increases, the toughness decreases. Also, up to about 200°C tempering temperature, the toughness slightly increases from the as-quenched value. Fig. 3.15 shows the toughness value as a function of the holding time at 300°C, which is subsequently tempered at 200°C. It also shows that the toughness decreases as the holding time at the isothermal transformation temperature increases. From these figures, it is clear that the above isothermal transformation treatment is not beneficial to high toughness when the steel is austenitized at 1200°C.

3.1.3.2 Tensile Test

The room temperature longitudinal properties were determined using a strain gauge extensometer. The results are shown in Table 3-10. Figs 3.16, 3.17, and 3.18 show the ultimate tensile strengths as a function of tempering temperature for different bainitic treatments. As shown in Fig. 3.16 the ultimate tensile strengths of the steel for different holding times and for different tempering temperature remain almost the same. Fig. 3.17 shows that although the ultimate tensile strength of 4340 remains the same, if given the bainitic treatment at 335°C for 5 or 60 minutes, the strength is almost two-fold higher for the steel given the bainitic treatment at 335°C for a holding time of only two

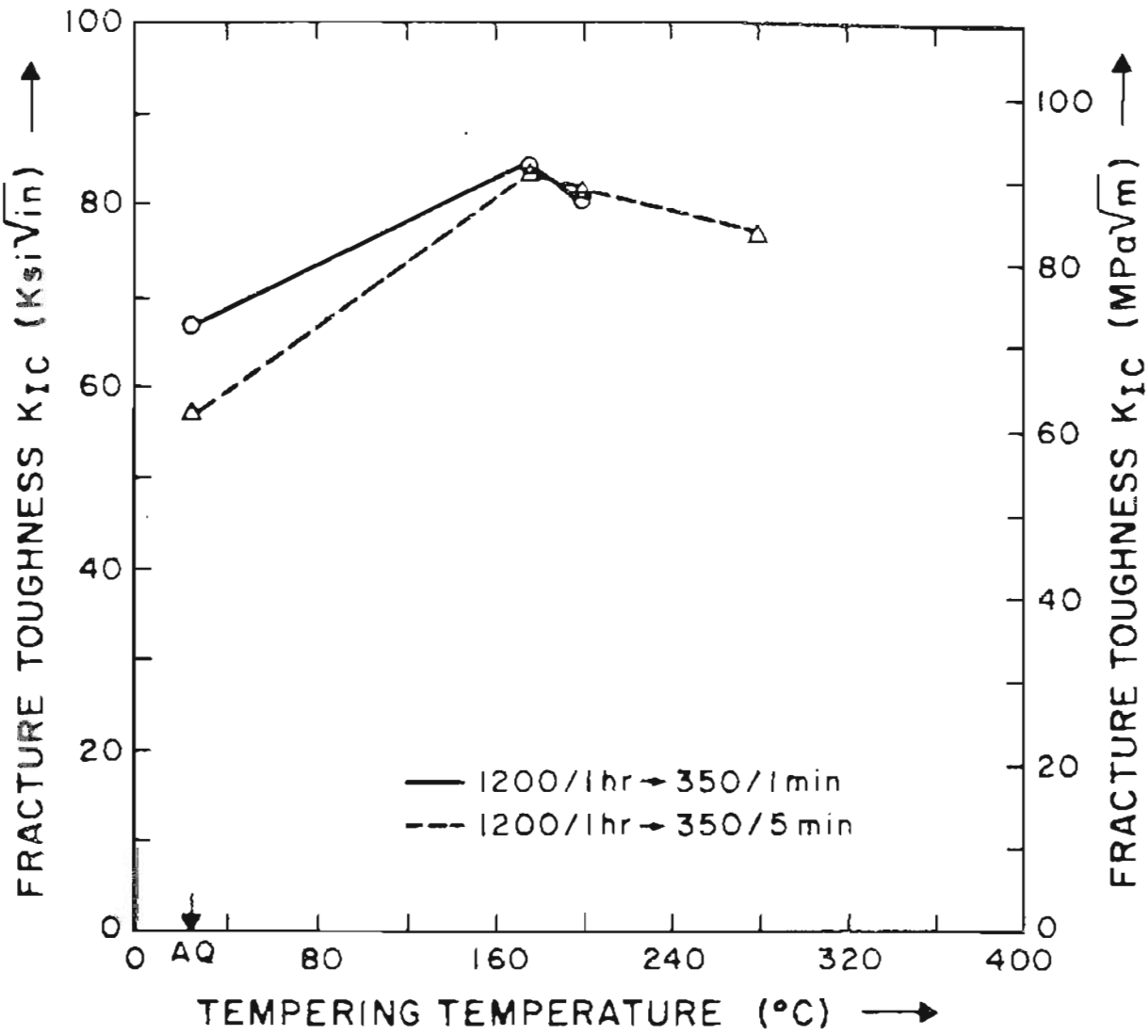

Fig. 3.13 Effect of tempering temperature on the toughness of high temperature austenitized 4340 steel given the bainitic treatment at 350°C for different lengths of holding time.

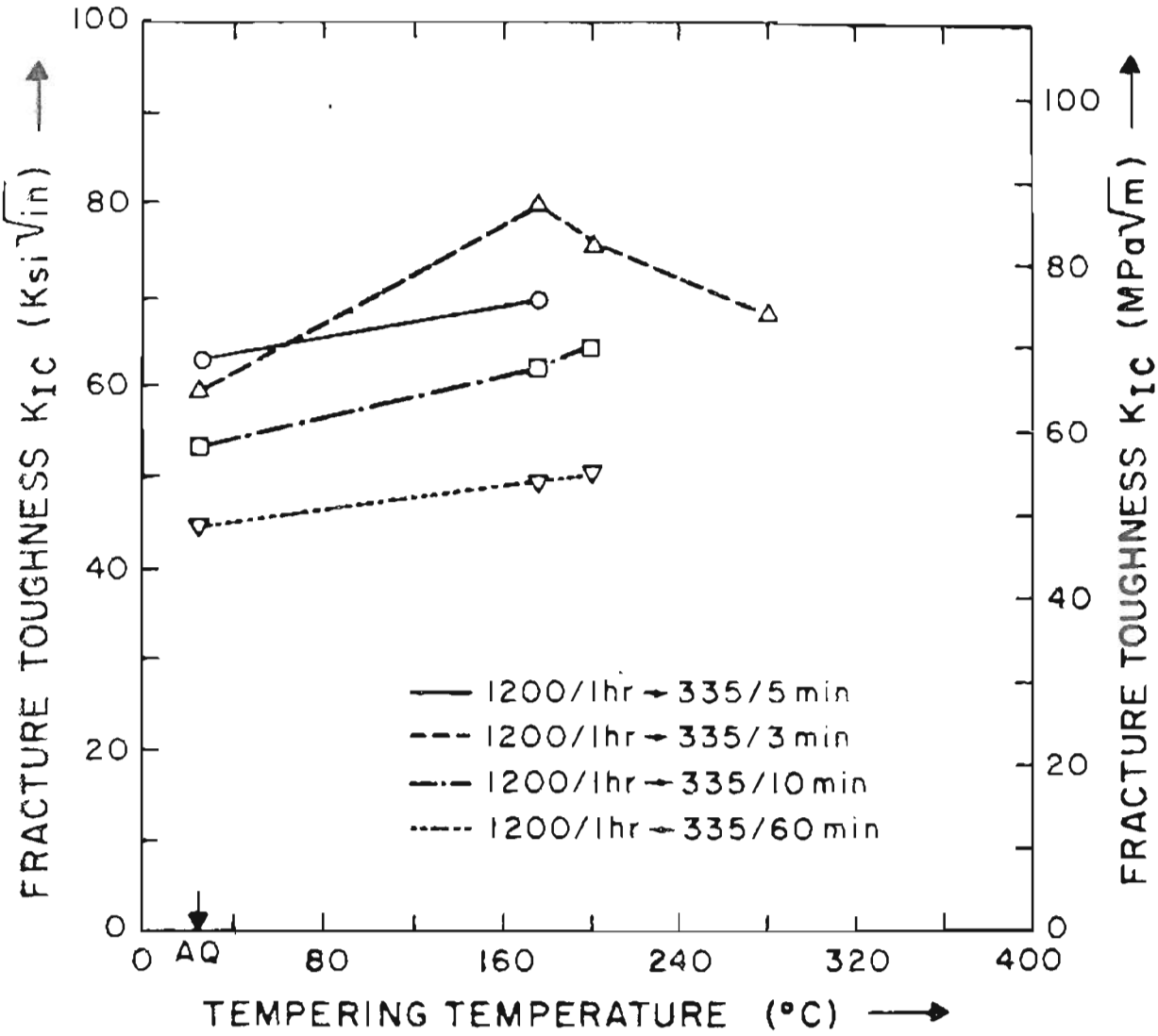

Fig. 3.14 Effect of tempering temperature on the toughness of high temperature austenitized 4340 steel given the bainitic treatment at 335°C for different lengths of holding time.

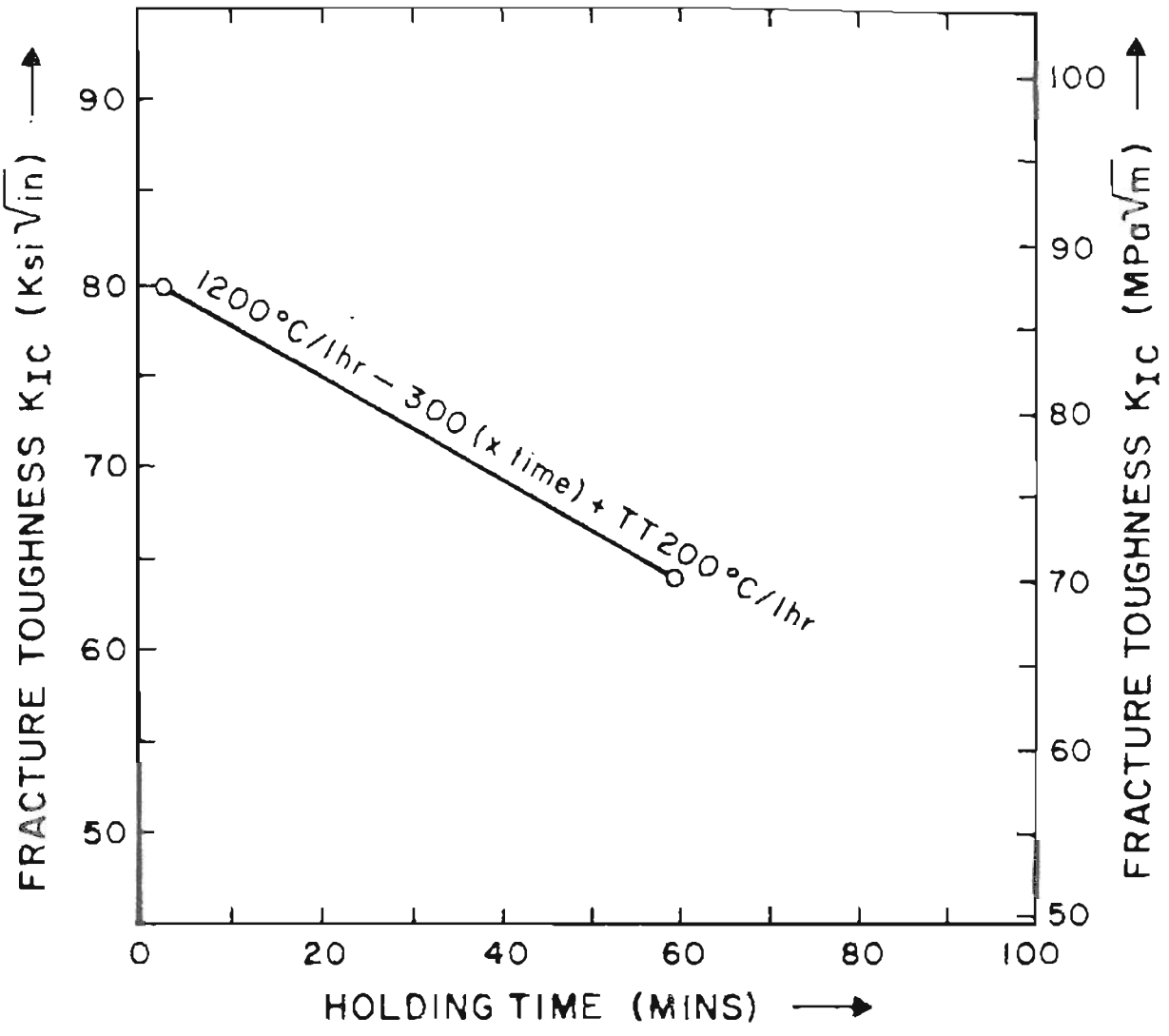

Fig. 3.15 Effect of holding time at the bainitic temperature of 300°C on the toughness of high temperature austenitization 4340 steel, which is subsequently tempered at 200°C.

TABLE 3-10

ROOM TEMPERATURE LONGITUDINAL TENSILE DATA FOR 4340 STEEL

SPECIMEN ID	AUSTENITISING TREATMENT °C/1H	TEMPERING TEMPERATURE °C/1H	σ(YS) KSI	σ(YS) MN/M^2	σ(ULT) KSI	σ(ULT) MN/M^2	EL %	RA %
C 71	1200/1-350/5MT	AQ	115	792.93	149	1027.36	4.8	18.3
C 72	"	AQ	125	861.88	162	1116 92	6 4	18.9
C 73	"	175	121	834.3	160	1103.2	7.5	27.5
C 74	"	175	122	841.2	155	1068.73	5.9	29.9
C 75	"	200	127	875.67	152	1048.04	8.0	38.0
C 76	1200/1-350/30MT	AQ	110	758.45	142	979.09	10.1	38.5
C 77	"	AQ	114	786.03	146	1006.67	9.2	31.2
C 78	"	175	100	744.66	148	1020.46	11.9	35.7
C 79	"	175	114	786.03	147	1013.57	11.1	35.9
C 90	"	200	110	758.45	145	999.78	10.0	38.5
C 81	1200/1-350/1H	AQ	117	806.72	147	1013.57	10.6	38.0
C 82	"	AQ	112	772.24	146	1006.67	9.2	30.6
C 83	"	175	112	772.24	147	1013.57	11.0	34 7
C 84	"	175	113	779.14	146	1006.67	11.9	35.9
C 85	"	200	116	799.82	146	1006.67	10.9	36.4
C 49	1200/1H-335/2MT	AQ	195	1344.53	294	2027.13	2.5	5.4
C 50	"	AQ	204	1406.58	297	2047.82	2.4	4.7
C 51	"	175	195	1344.53	265	1827.18	6.3	10.8
C 52	"	175	212	1461.74	265	1829.18	6.3	7.8
C 53	"	200	209	1441.06	258	1778.91	6.3	13.0
C 54	"	200	194	1337.63	228	1572.06	5.3	12.3
C 56	1200/1H-335/5MT	AQ	127	875.67	169	1165.26	9.3	24.4
C 57	"	AQ	126	868.77	170	1172.15	9.3	25.2
C 58	"	175	121	834.30	164	1130.78	10.3	33.3
C 59	"	175	129	889.46	168	1158.36	7.8	28 6
C 60	"	200	131	903.25	166	1144.57	12.3	33.9
C 61	1200/1-335/30MT	AQ	122	841.19	156	1075.62	12.7	35.7
C 62	"	AQ	113	779.14	150	1034.25	8.7	37.0
C 63	"	175	120	827.4	156	1075.62	10.3	33.9
C 64	"	175	120	827.4	152	1048.04	13.1	43.9
C 66	1200/1-335/60MT	AQ	121	834.30	153	1054.94	13.3	39.7
C 67	"	AQ	121	834.30	154	1061.83	11.9	32.6
C 68	"	175	124	854.98	156	1075.62	13.6	37.6
C 69	"	175	117	806.72	153	1054.94	14.3	36.0
C 70	"	200	127	875.67	153	1054.94	12.5	38.1
C 34	1200/1H-300/5MT	AQ	142	979.09	200	1379	3.9	14.9
C 35	"	AQ	146	1006.67	194	1337.03	4.4	21.1
C 36	"	175	150	1034.25	186	1902.47	7.5	38.4
C 37	"	175	136	937.72	185	1275.58	10.3	41.0
C 38	"	200	163	1123.09	189	1303.16	8.0	36.6

TABLE 3-10 (CON'T)

ROOM TEMPERATURE LONGITUDINAL TENSILE DATA FOR 4340 STEEL

SPECIMEN ID	AUSTENITISING TREATMENT °C/1H	TEMPERING TEMPERATURE °C/1H	σ(YS) KSI	σ(YS) MN/M^2	σ(ULT) KSI	σ(ULT) MN/M^2	EL %	RA %
-	-	-	-	-	-	-	-	-
C 39	1200/1-300/30MT	AQ	146	1006.67	182	1254.89	12.9	55.6
C 40	"	AQ	146	1006.67	182	1254.89	12.8	44.3
C 41	"	175	143	985 99	183	1261.99	13.9	39.9
C 42	"	175	147	1013.57	180	1241.1	11.4	52.9
C 43	"	200	146	1006.67	183	1261.79	12.5	46.8
C 44	1200/1-300/60MT	AQ	144	992.80	168	1158.36	15.6	44.9
C 45	"	AQ	147	1013.57	180	1241.1	16.6	47.3
C 46	"	175	143	985.99	178	1227.31	14.7	58.2
C 47	"	175	147	1013.57	179	1234.21	11.9	44.6
C 48	"	200	148	1020.5	180	1241.1	12.6	48.9

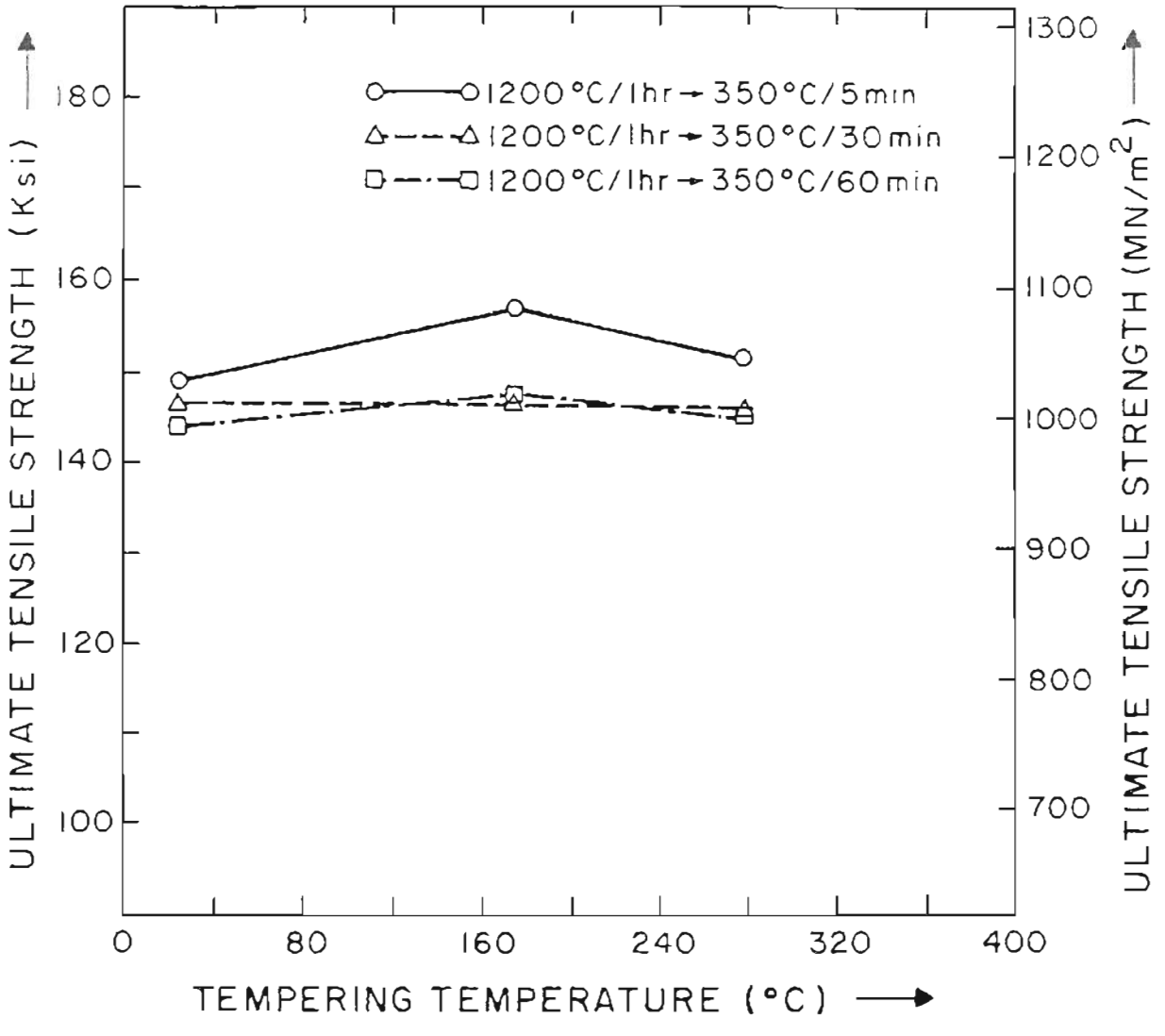

Fig. 3.16. Effect of tempering temperature on the ultimate tensile strength of high temperature austenitized 4340 steel given the bainitic treatment at 350°C for different lengths of holding time.

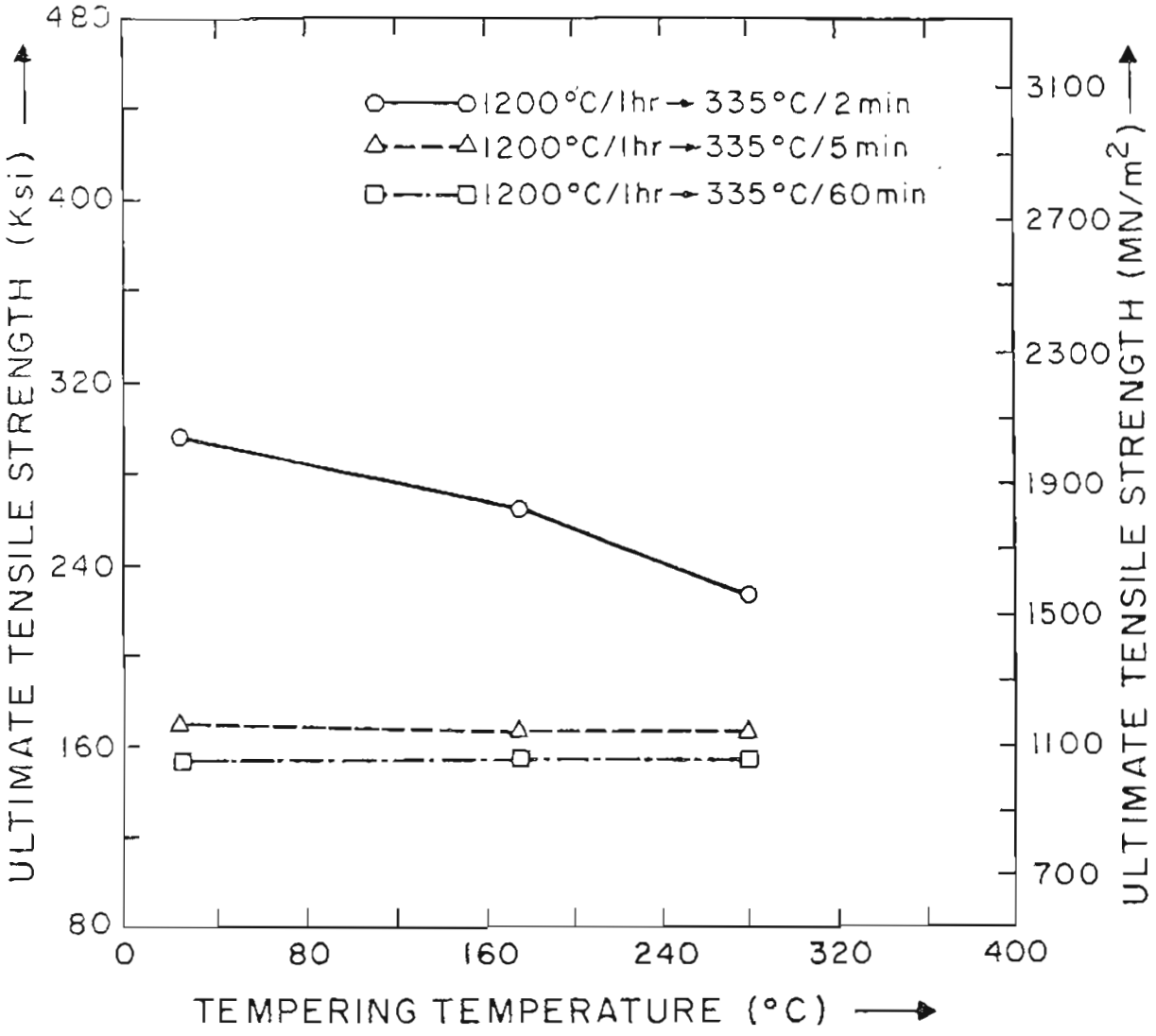

Fig. 3.17 Effect of tempering temperature on the ultimate tensile strengths of high temperature austenitized 4340 steel given the bainitic treatment at 335°C for different lengths of holding time.

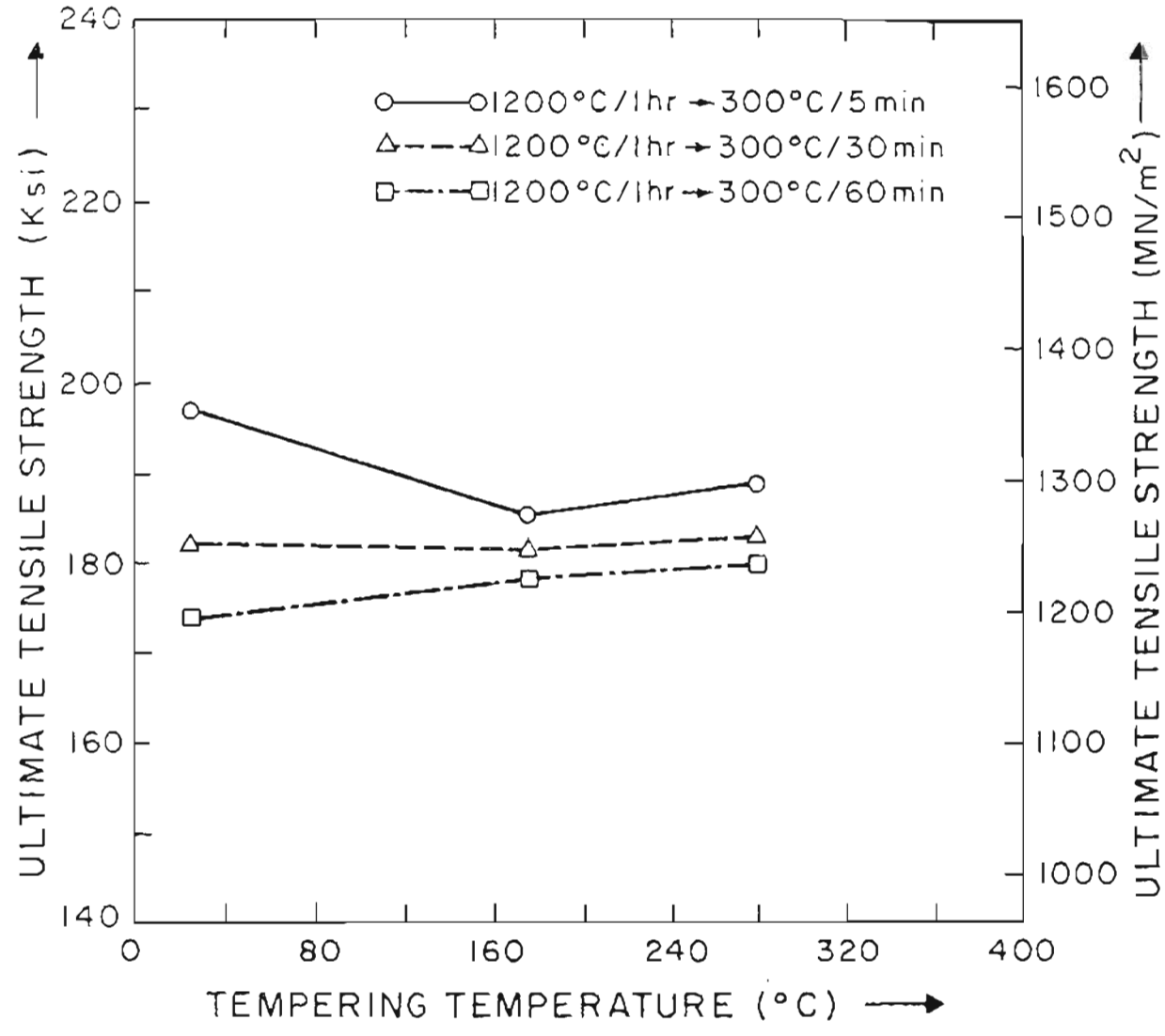

Fig. 3.18 Effect of tempering temperature on the ultimate tensile strengths of high temperature austenitized 4340 steel given the bainitic treatment at 300°C for different lengths of holding time.

two minutes. Also, while there is change in the strength level for different tempering temperatures, if the bainitic holding time is 5 minutes or greater, there is a decrease in the strength as the tempering temperature is increased for the 2 minute case. Fig. 3.18 demonstrates again that the tensile strength remains more or less the same if the bainitic treatment at 300°C exceeds 5 minutes and also the strength is far less than the as-quenched case (20). Thus as in fracture toughness results, the tensile properties are also impaired for all isothermal transformation temperatures studied, if the holding time is about 5 minutes or more.

3.1.4 Summary of Mechanical Test Results

The mechanical testing results are summarized as follows. (a) For different heat treatments and consequently microstructures, as studied in this investigation, toughness increased first with the increase in root radius and then it decreased. The root radius, at which such phenomena occurs, was strongly temperature and strain-rate dependent, but independent of the prior austenitic grain-size. (b) For different methods of testing studied in this investigation, in pre-cracked specimens, the higher austenitizing treatment gave superior toughness than that of the lower austenitizing treatment in as-quenched condition. (c) For different methods of testing studied in this investigation in both pre-cracked and blunt-notch testing condition, 'temper embrittlement' occurred as low as 225°C for the high austenitizing treatments; for the lower austenitizing temperature no similar drop in toughness occurred. (d) The limited bainitic isothermal transformation of 4340 steel when austenitized at 1200°C studied in this investigation was not conducive to improved toughness.

Since toughness was not improved for the bainitic treatment, no further microstructural examination was pursued. The second two observations certainly indicate that there must be essential microstructural differences between the higher and lower austenitizing treatments and necessitates such examination as optical, transmission and scanning electron microscopy. As for the first observation, mechanical parameters rather than microstructural parameters may dictate the fracture morphology and hence necessitates the scanning examination; in the next section microscopy results are presented.

3.2 Microscopy: - Microscopical examination is sub-divided into three categories (a) optical microscopy, (b) transmission electron microscopy, (c) scanning electron microscopy.

3.2.1. Optical Microscopy

Fig. 3.19 shows the microstructure of 4340 in as-received (as rolled) condition. The banded structure which is evident resulted from the segregation of carbon and alloying elements during casting and subsequent rolling operation. Fig. 3.20 shows the microstructure of 4340 in as quenched condition when austenitized at 870°C. While the banded structure is not observed, the fine grain-size (ASTM 9) is evident. Some dark etching plates are also visible, there are most likely auto-tempered martensite plates. Fig. 3.21 shows the microstructure of 4340 in as-quenched condition, when austenitized at 1200°C. The most marked difference as noted between Fig. 3.20 and Fig. 3.21 is the grain size. The grain-size of Fig. 3.21 is estimated to be ASTM 1. More dark etching plates

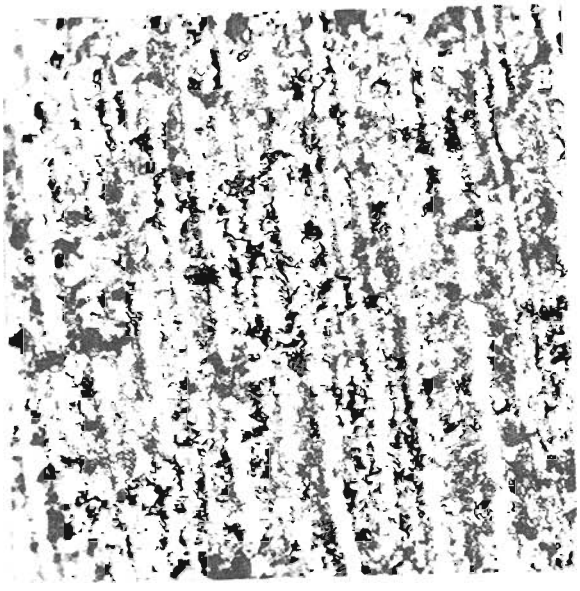

100X.

Figure 3.19. As received structure of 4340 steel. The banded structure is evident.

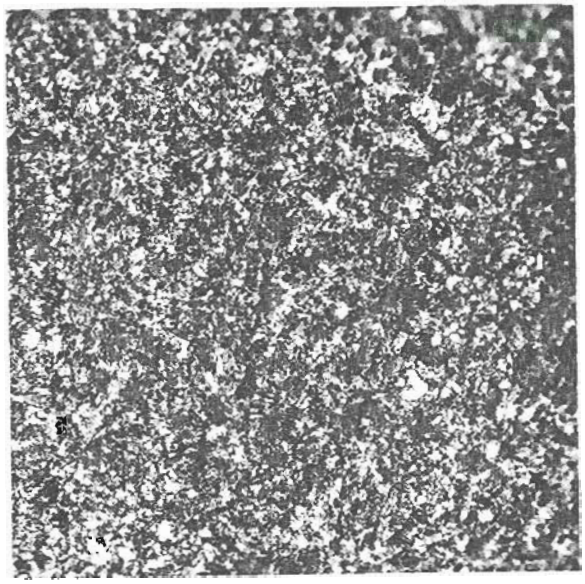

(a) 100X

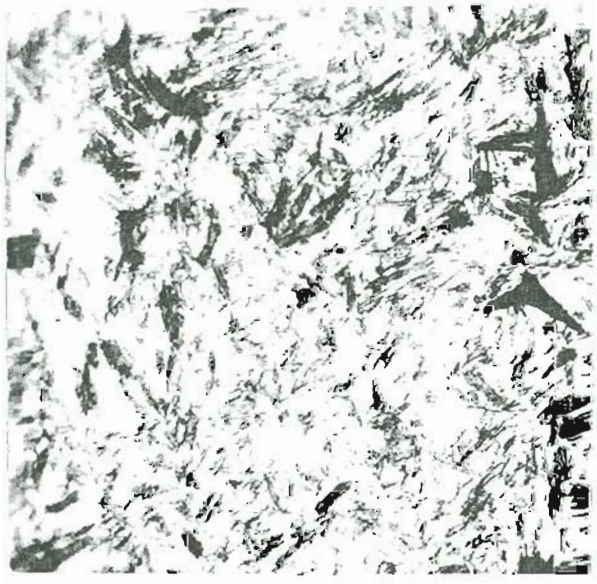

(b) 1000X

Fig. 3.20 Optical micrograph of as-quenched sample austenitized at 870°C (1143°K).

(a) At low magnification ASTM grain size is found to be 7-8
(b) At high magnification, some dark plates representative of auto-tempered martensite in a martensitic matrix (white).

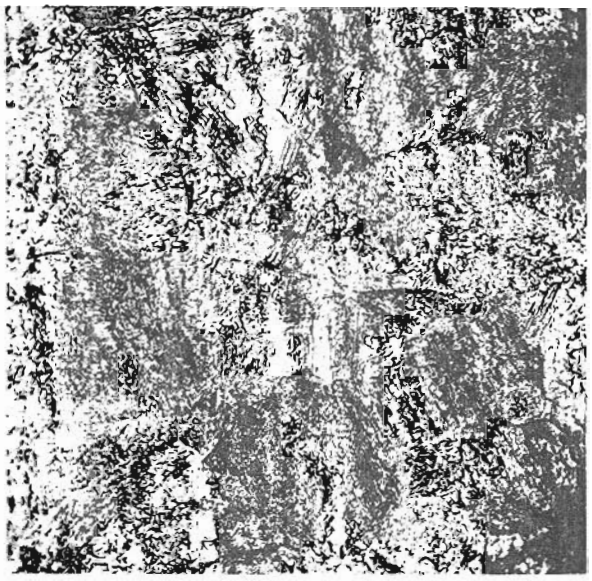

(a) 100X

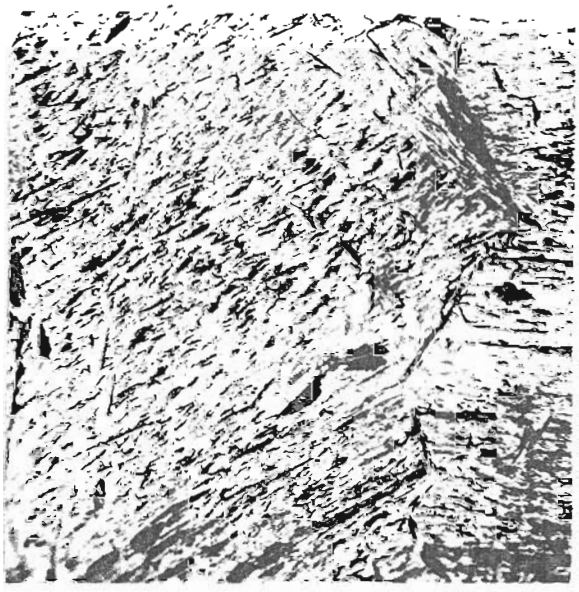

(b) 400X

(c) 1000X

Figure 3.21. Optical micrograph of as quenched sample austenitized at 1200°C (1473°K) (a) At low magnification ASTM grain-size is found to be 1, (b) At high magnification more dark plates are found in the structure, (c) At still higher magnification the relative proportions of autotempered martensite and martensite (white) are compared.

representative of auto-tempered martensite are visible in the microstructure. This is not surprising, since the material has been quenched from 1200°C. The grain-size determination for different austenitizing treatment has been carried out elsewhere (20) and the summary is written as below.

Solution Treatment	Grain Size
As received	9
870°C/1 hr	9
1000°C/1 hr	9
1100°C/1 hr	5.5
1150°C/1 hr	3
1200°/15 min	1
1200°C/30 min	1
1200°C/1 hr	1

In short, the high austenitizing treatment resulted in grain size, which was ten times larger (i.e. one order of greater magnitude) than that of the conventionally treated 4340 steel. Also, more dark plates representative of autotempered martensitic plates are observed for the higher austenitizing case than for the lower austenitizing case.

Fig. 3.22 shows the microstructure of 4340 given in bainitic treatment from higher austenitizing temperature (1200°C). The bainitic heat-treatment consists of holding the steel at 335°C for 3 minutes from the austenitizing temperature and then quench in an agitated oil bath. The structure consists of lower bainite (dark constituent) in a matrix of martensite (white constituent). In comparison, Fig. 3.23 shows the microstructure of 4340 given a bainitic treatment from a lower austenitizing temperature (870°C). The bainitic temperature was 315°C and the holding time was 3 minutes. The latter treatment resulted in significantly

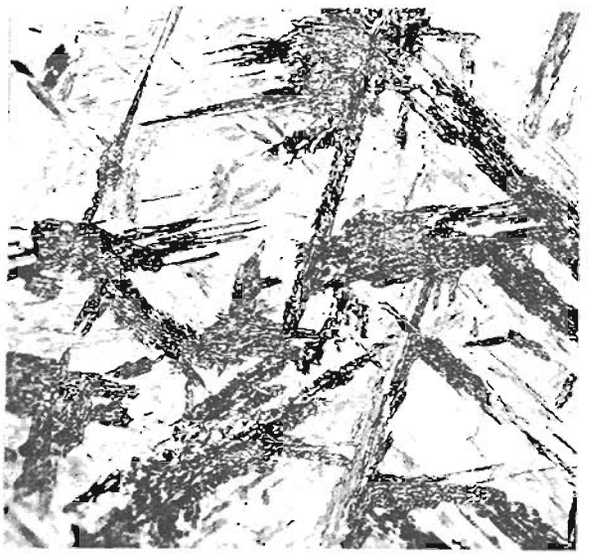

(a) 500X

(b) 1000X

Figure 3.22. 4340 steel given a bainitic treatment at 335°C for 3 minutes after austenitizing at 1200°C.

(a) Lower bainite (dark) in a matrix of martensite (white).
(b) At high magnification the relative proportions are compared.

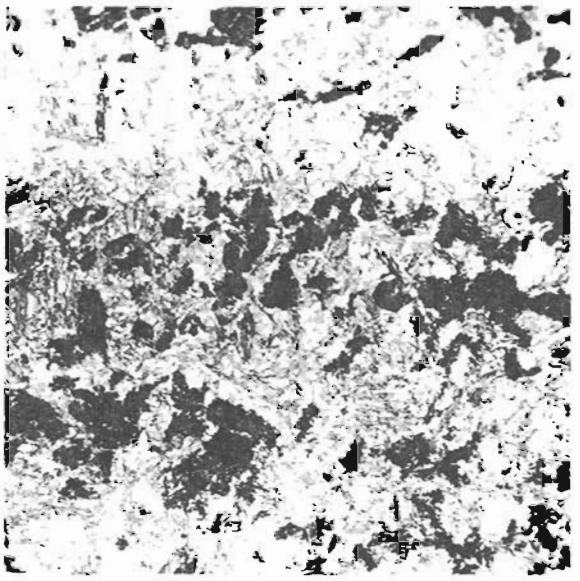

(a) 500X

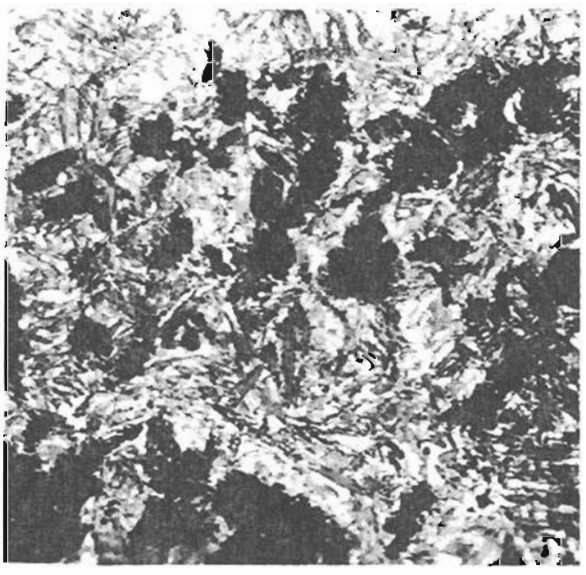

(b) 1000X

Figure 3.23. 4340 steel given a bainitic treatment at 315°C for 3 minutes after austenitizing at 870°C. (a) Lower bainite (dark) in a matrix of martensite (white), (b) At higher magnification the relative proportions are compared.

less bainite. Also, the bainite is not resolvable because of the finer grain size. The carbon replica pictures shown in Figs. 3.24 and 3.25 also show clearly that more carbide particles have precipitated in the higher austenitizing bainitic treatment than in the lower austenitizing bainitic treatment. In other words, the bainitic reaction is accelerated in the higher austenitizing case relative to the lower austenitizing case (also clear from the respective TTT diagrams, Fig. 3.26 a and b).

3.2.2 Electron Microscopy and X-ray Diffraction

Fig. 3.27 a shows the bright-field electron micrograph of as quenched 4340 steel, austenitized at 1200°C. The small ε-carbide particles are seen inside the martensitic laths and also by the use of the selected area diffraction pattern as shown in Fig. 3.27 c. The spots due to ε-carbide are consistent with previous work (17). In contrast, Fig. 3.28 shows the bright-field electron micrograph of as quenched 4340 steel, austenitized at 870°C. The martensite lath size seems to be smaller and in particular contain fewer ε-carbides or no ε-carbides. The other important microstructural differences between higher and lower austenitizing treatments, namely absence of twins and more retained austenite for the higher austenitizing treatment have been documented elsewhere (1). Summarizing then, higher austenitizing treatment prodoces more ε-carbide, more retained austenite and less twins.

Fig. 3.29 and Fig. 3.30 show electron microscopy results for 4340 steel austenitized at 1200°C and tempered at 175°C and at 225°C respectively. After tempering at 175°C, the microstructure consisted of lath martensite with a high density of dislocation and ε-carbide as well

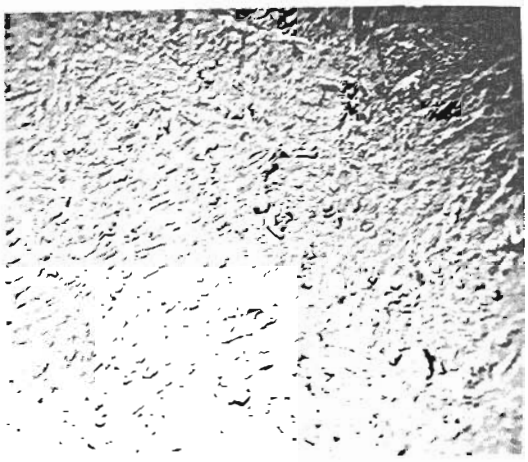

(a) 2.4K

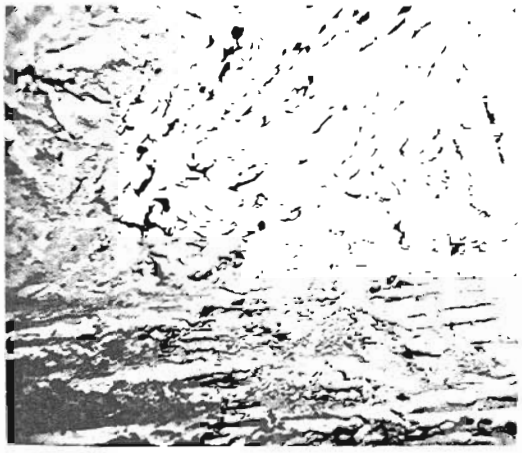

(b) 6 K.

Fig. 3.24. Carbon replica pictures of samples austenitized at 870°C and given the bainitic treatment for 3 min at 315°C (588°K). (a) At low magnification, (b) at high magnification. Carbide particles in a matrix of ferrite and martensite.

(a) 6K

(b) 10K

Fig. 3.25. Carbon replica pictures of samples austenitized at 1200°C and given the bainitic treatment of 3 min at 335°C. (a) At low magnification, (b) at high magnification. More carbide particles in a matrix of ferrite and martensite.

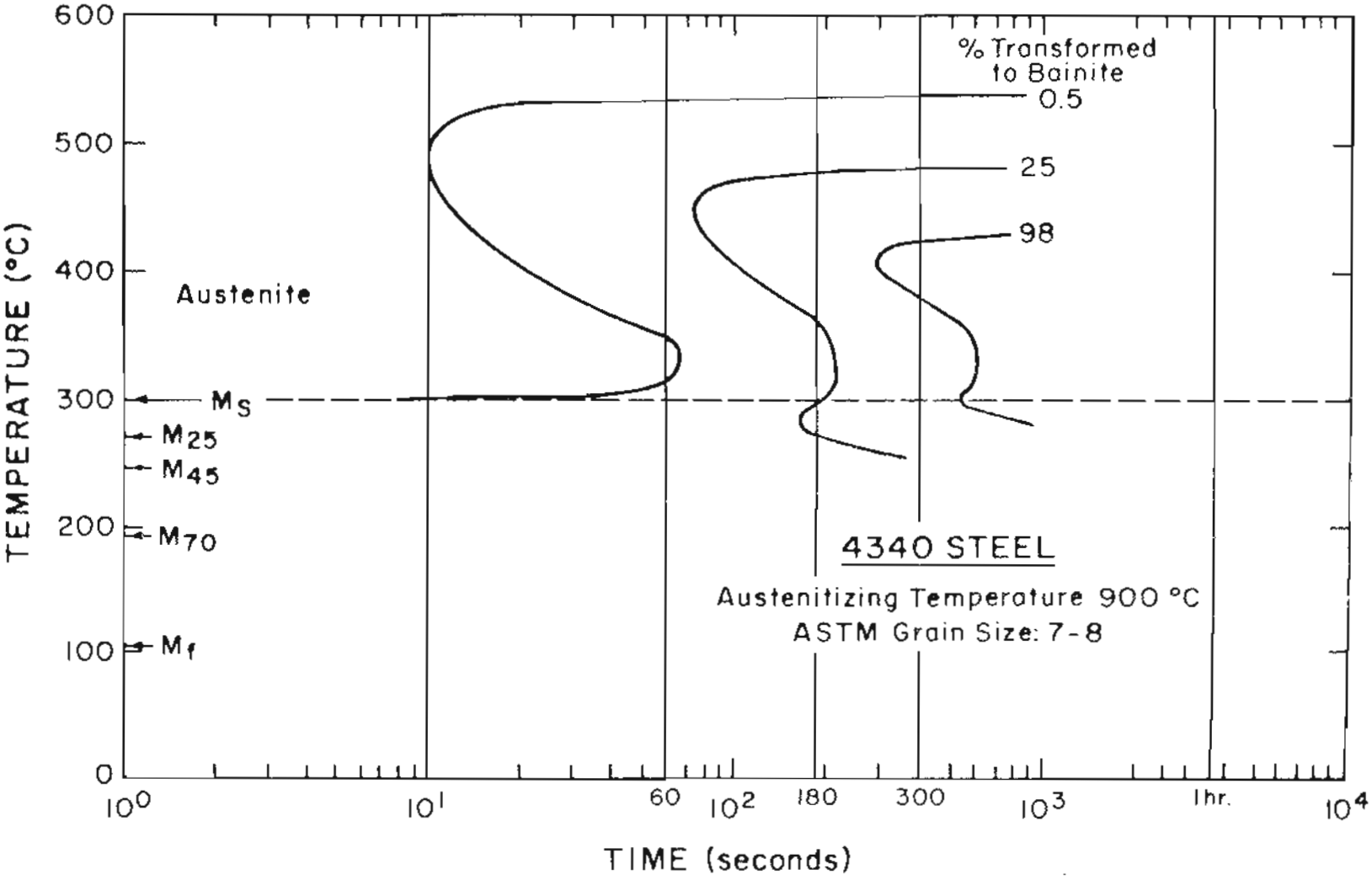

Fig. 3.26 (a) Isothermal transformation curve for alloy 4340 austenitized at 900°C.

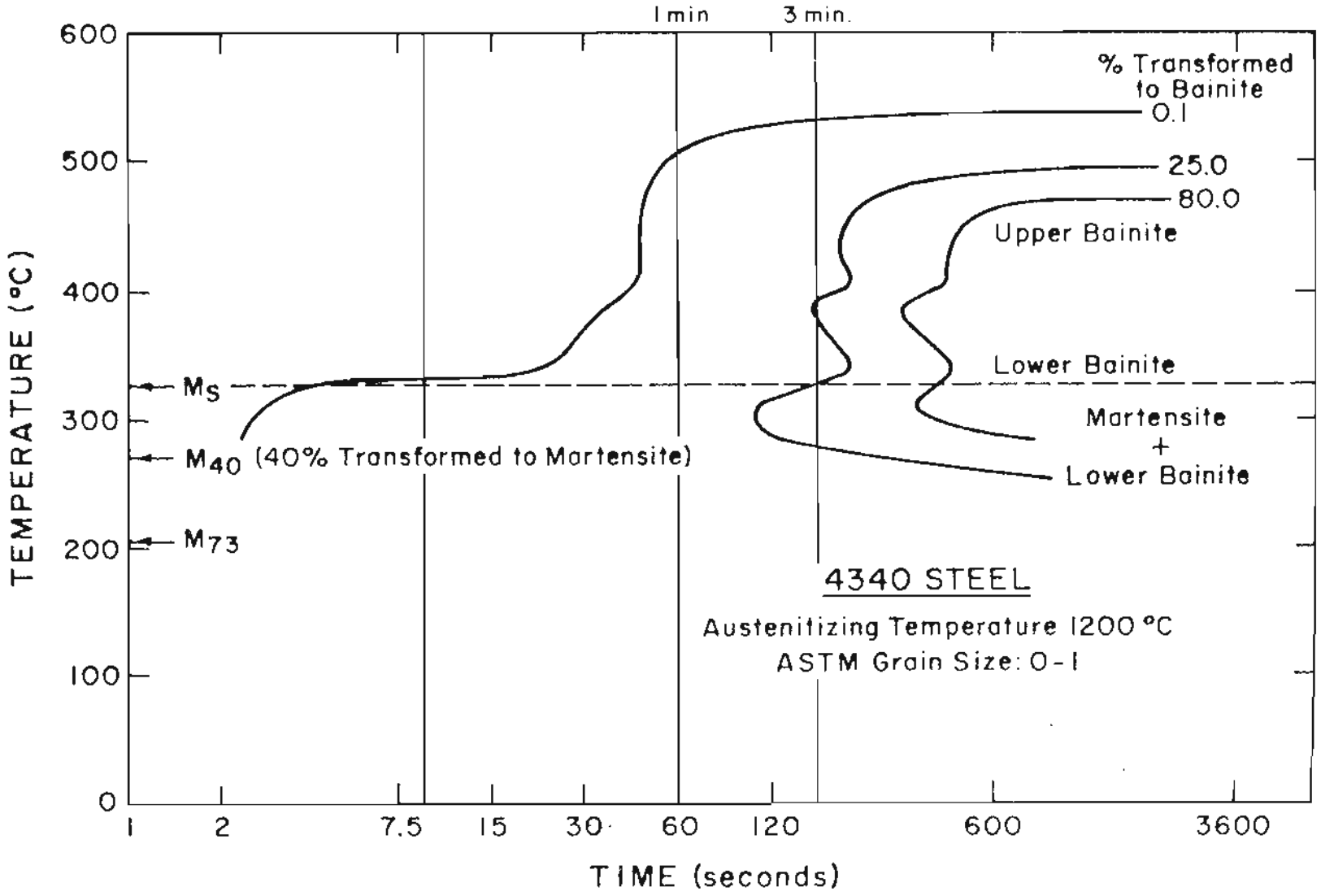

Fig. 3.26 (b) Isothermal transformation curve for alloy 4340 austenitized at 1200°C.

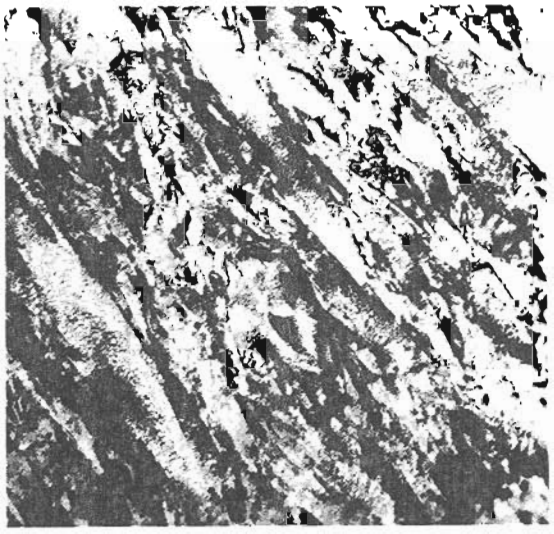

(a) 10K

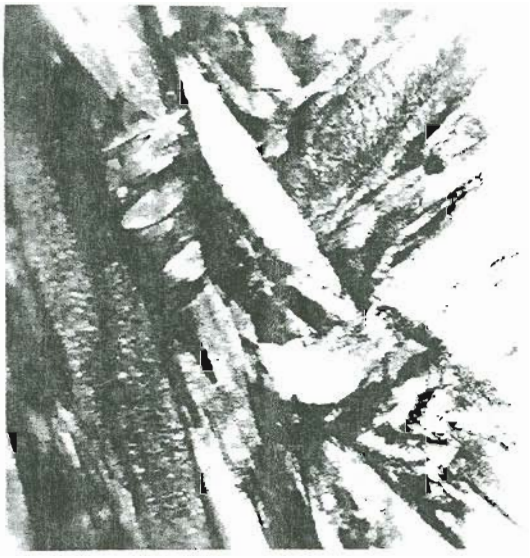

(b) 30K

Fig. 3.27. (a) and (b). B.F. image of as-quenched sample austenitized at 1200°C, showing the presence of ϵ-carbide and retained austenite

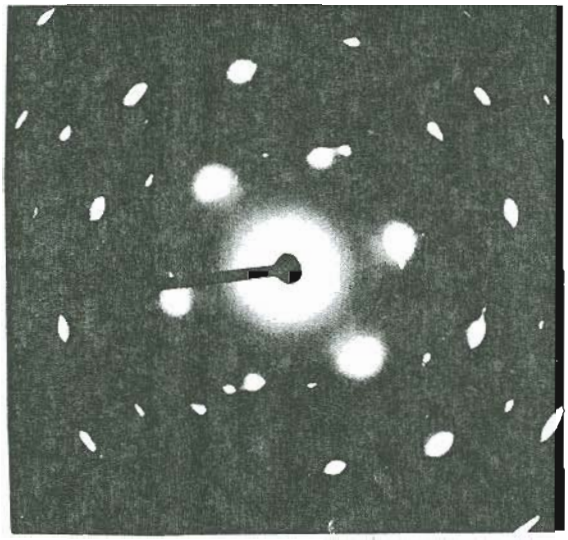

(c)

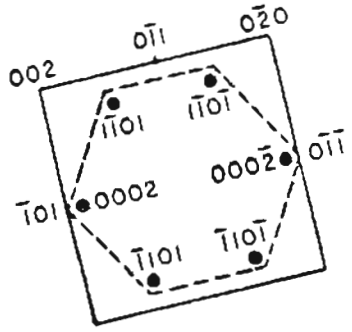

(d)

Fig. 3.27 (cont'd) (c) Selected area diffraction pattern, (d) schematic diagram of the SADP. Note the matrix. Zone areas are $\langle 100\rangle_\alpha$ and $\langle 111\rangle_\alpha$. Spots due to ϵ-carbide (Z.A. $\langle 11\bar{2}0\rangle_\epsilon$) are consistent with previous work.[103]

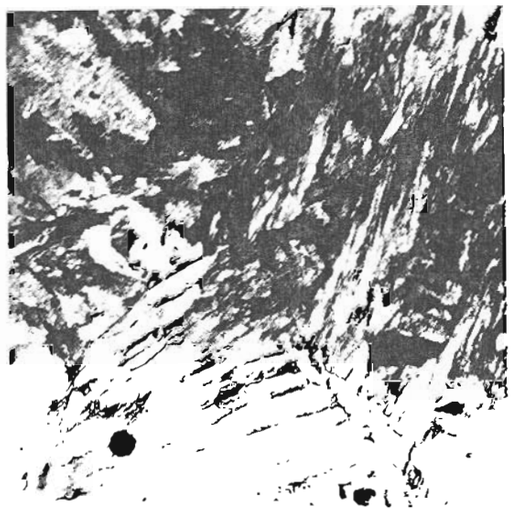

(a) 10K

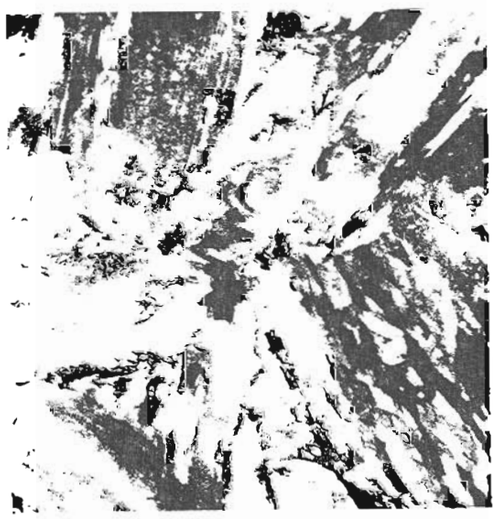

(b) 16K

Fig. 3.28. (a) and (b) B.F. image of as-quenched sample austenitized at 870°C, showing little or no ϵ-carbide.

(a) 18K

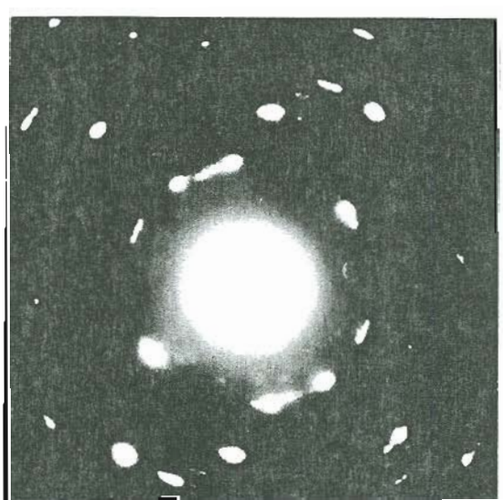

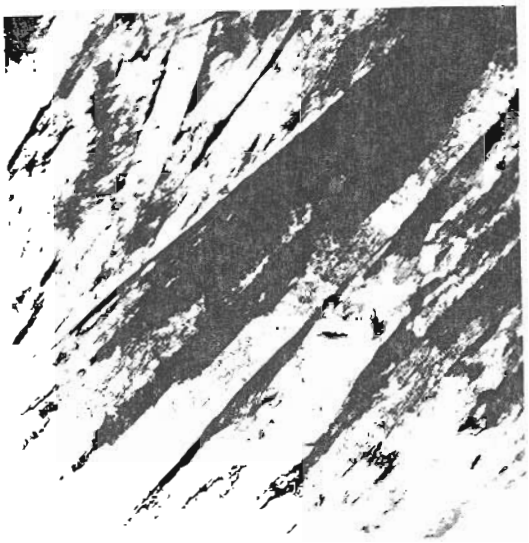

(a) 18K

(b)

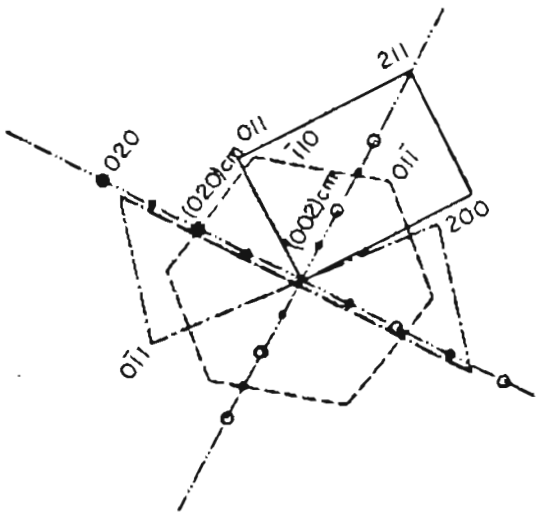

(c)

Fig. 3.30. (a) BF image of samples austenitized at 1200°C and tempered at 225°C, (b) selected area diffraction, (c) schematics of SADP. Note the matrix zone areas $\langle 110\rangle_\alpha$, $\langle 111\rangle_\alpha$, $(01\bar{1})_\alpha$, spots due to cementite (Z.A. $\langle 100\rangle_{cm}$) are also indexed which obey Bagaryatski relationship $(001)_{cm}$ 11 $(211)_\alpha$, $(100)_{cm}$ 11 $(0\bar{1}1)_\alpha$ $(010)_{cm}$ 11 $(\bar{1}11)$.

as retained austenite at the interlath boundaries. After tempering at 225°C, although no ε-carbide was found, interlath retained austenite was still present. Also, the selected area diffraction pattern shown in Figs. 3.30 b and c revealed the presence of cementite phase, which obeyed the Bagaryatski relationship, i.e. $(100)_{cm} || (0\bar{1}1)$, $(010)_{cm} || (\bar{1}11)$, $(001)_{cm} || (211)$. Since dark field analysis did not clearly delineate the cementite, X-ray powder photographs were obtained using cobalt K_α radiation and the obtained data are given in Table 3-11. The as-quenched samples and the samples tempered at 175°C gave diffracted lines with nearly the same d-spacings: however, the diffracted lines of as-quenched samples were very broad compared to the sharp lines of tempered samples due to the large amount of the internal strains in the as-quenched case. The powder pattern of samples tempered at 225°C contained an extra line which corresponded to the 030 line of Fe_3C. The ε-carbide particles were extremely small and line broadening probably prevented their analysis. Similarly, the amount of retained austenite was insufficient to result in a measurable intensity. Two unknown, diffuse lines in all three samples were observed with d-spacings about 2.23Å and 1.87Å. These lines coincide with d-spacings of compounds such as Fe-P, Ni_2P, Mn_4N and Al_3V, which may have resulted from the original steel manufacturing process.

3.2.3 Scanning Electron Microscopy

Fig. 3.31 shows the fractograph of as quenched 4340 precracked steel austenitized at 1200°C. At low magnification the fracture surface is found to be uneven. However, at high magnification the fracture initiation is found to be microvoid coalescence. This is also consistent with observation before (1,117).

Table 3.11 Measured Interplanar Spacings (Å) for 4340 Solutioned at 1200°C and Tempered at Various Temperatures.

As Quenched	175°C/1 hr	225°C/1 hr.	Possible Indices
2.237 (diffuse)	2.229 (diffuse)	2.236 (diffuse)	
2.043 (broad)	2.044 (sharp)	2.034 (sharp)	$(110)_\alpha$
1.891 (diffuse)	1.856 (diffuse)	1.873 (diffuse)	
-	-	1.709	(030) Fe_3C
1.451 (broad)	1.434 (sharp)	1.433 (sharp)	$(200)_\alpha$.

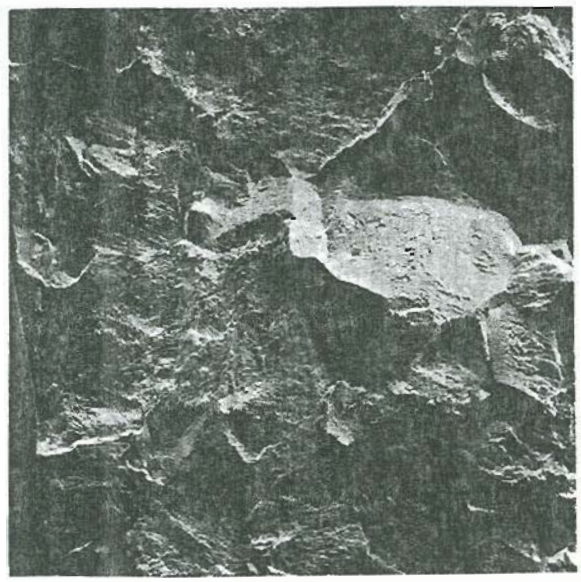

(a) 50X

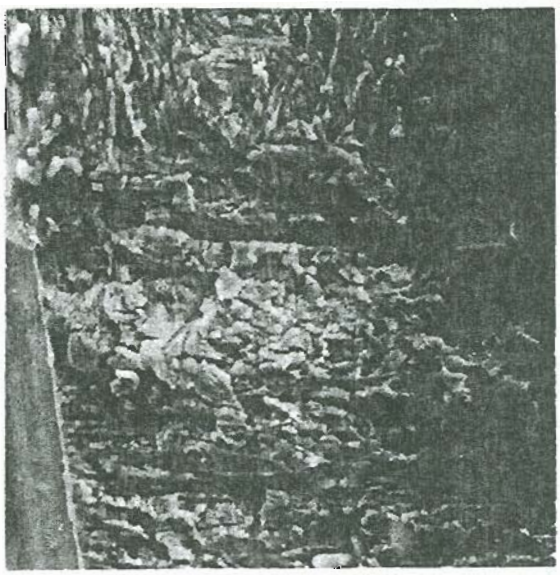

(b) 1000X

(c) 1000X

Fi-ure 3.31. SEM micrograph of as quenched sample austenitized at 1200°C, (a) At low magnification intergranular nature, (b) fatigue crack zone near the notch, (c) fatigue zone changing to microvoid, coalescence, which is the fracture initiation mode.

Fig. 3.32 shows the fractograph of as quenched pre-cracked 4340 steel austenitized at 870°C. Here the fracture initiation mode, in contrast, has been found to be quasi-cleavage/intergranular cleavage type. The high toughness associated with higher austenitizing treatment in the pre-cracked condition is thus consistent with the observed change in fracture mode.

Fig. 3.33 shows the fractograph of as quenched pre-cracked 4340 austenitized at 1200°C followed by tempering at 175°C. The fracture morphology exhibited a fine dimpled structure, typical of ductile rupture. However, for this treatment, the intergranular nature of the fracture surface was absent. On the other hand, the fractograph shown in Fig. 3.34 obtained from the samples austenitized at 1200°C and tempered at 225°C, exhibited an integranular brittle fracture. Similarly as shown in Fig. 3.35 the SEM fractograph of sample austenitized at 1200°C and tempered at 280°C also showed an intergranular brittle fracture.

Fig. 3.36 to 3.49 shows the fracture morphology for different notch root radii. The effect of notch root radius on the toughness has been studied (a) at liquid nitrogen temperature and high strain rate, (b) at room temperature and slow strain rate, (c) at room temperature and high strain rate and (d) also as a function of microstructures. Apart from the fracture initiation mode, the extent of shear lip is also shown in some of the pictures. The mode of fracture for both initiation and propagation is described under each heading. It may be pointed out in this context that the major portion of the fracture surface is quasi-cleavage. However, the fracture initiation mode, which has a direct

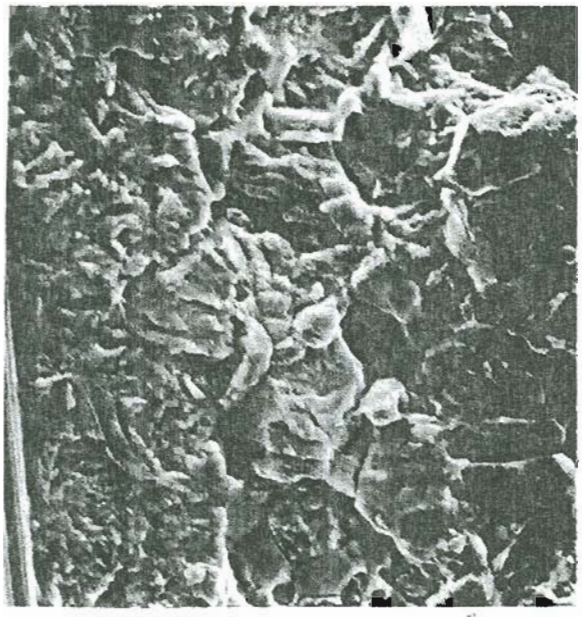

(a) 900X

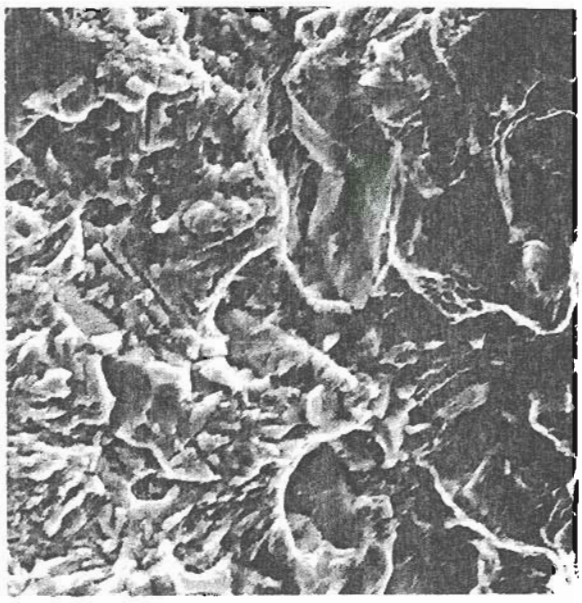

(b) 1000X

Figure 3.32. SEM micrographs of as quenched sample austenitized at 1143°K. (a) notch, fatigue zone and intergranular/quasi-cleavage mode, (b) fatigue zone changing to intergranular/quasi-cleavage mode, which is the fracture initiation mode.

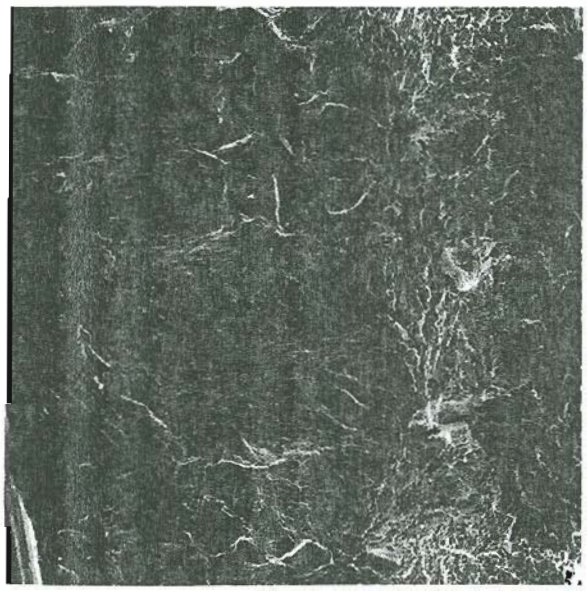

(a) 50X

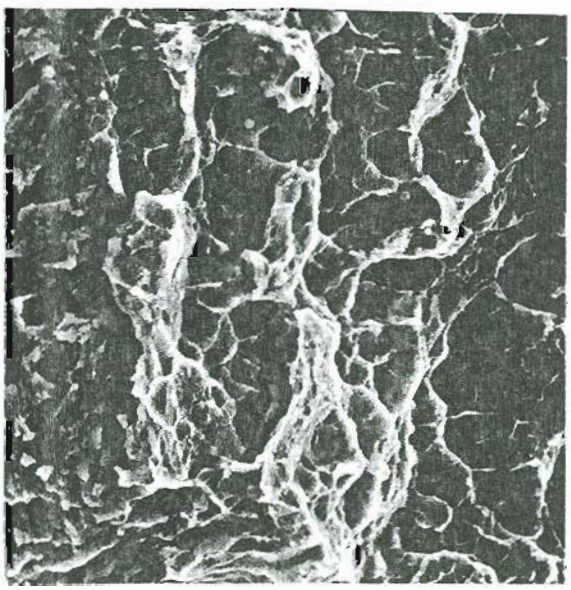

(b) 1000X

Figure 3.33. SEM micrographs of samples austenitized at 1200°C (1473°K) and tempered at 175°C (448°K). (a) At low magnification absence of intergranular nature of fracture surface. (b) At high magnification fatigue zone, changing to micro-void coalescence, which is the fracture initiation mode.

(a) 100X

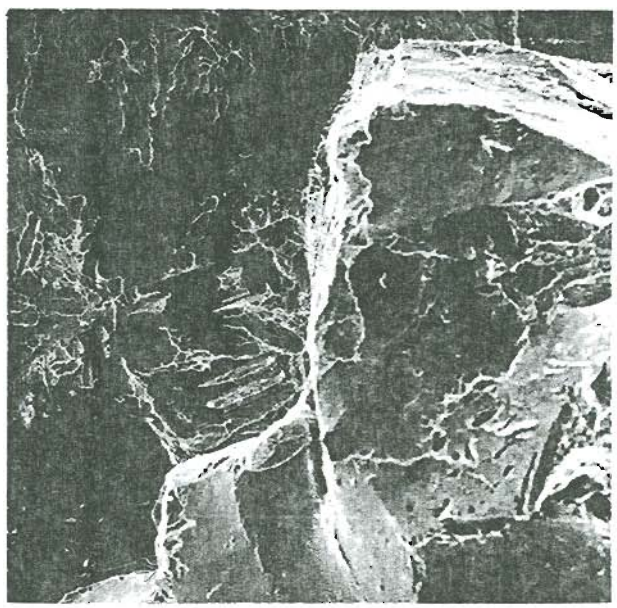

(b) 200X

Figure 3.34. SEM micrographs of samples austenitized at 1200°C (1473°K) and tempered at 225°C (498°K). (a) Intergranular fracture mode, (b) at high magnification tearing marks on the intergranular facets.

(a) 100X

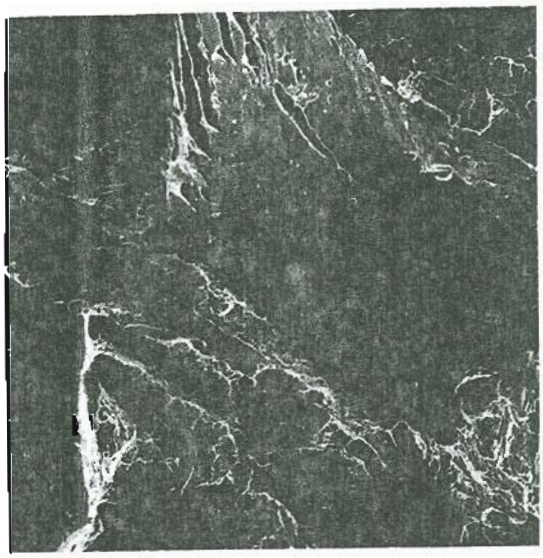

(b) 200X

Figure 3.35. SEM micrographs of samples austenitized at 1200 °C (1473° K) and tempered at 280° C (553° K). (a) Intergranular fracture mode, (b) At high magnification tearing marks on the intergranular facets.

correspondence with the fracture toughness value, is different for different samples. Summarizing all the results, schematic SEM observations can be made under two cases.

Case 1 - Toughness Increases with Notch Root Radius: - For this case schematic fractographic representation looks like the following:

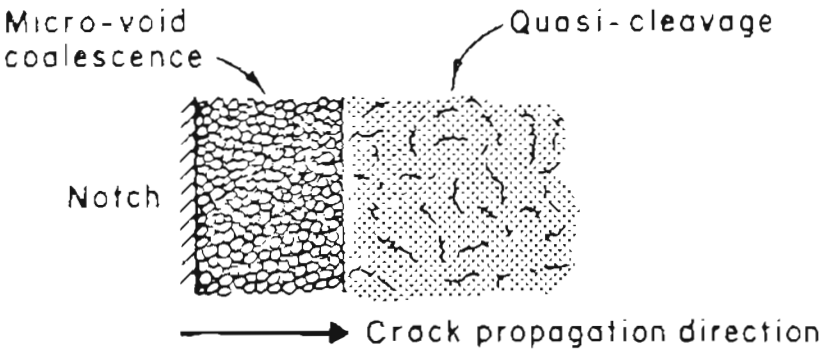

In this case, the fracture initiation is always by microvoid coalescence, which later changes to quasi-cleavage as the crack propagates. The microvoid region is about 40 microns for the instrumented Charpy test conducted at liquid nitrogen temperature and is apparently independent of prior austenitic grain size.

Case 2 - Toughness Decreases as the Notch Root Radius is Increased Beyond a Critical Value. - The schematic fractographic observation in this case looks like below:

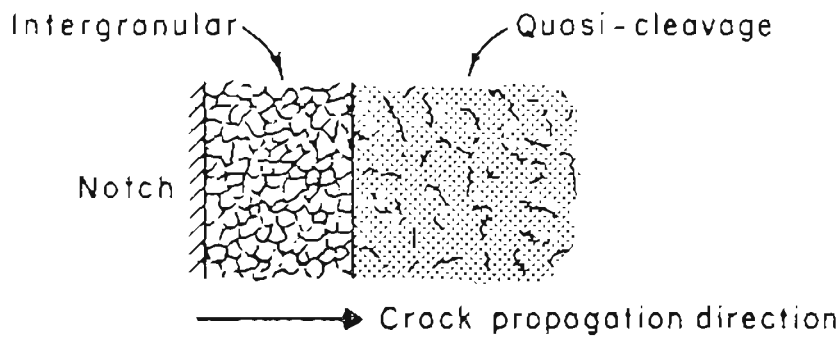

In this case, when the toughness drops, the mode of fracture initiation changes to intergranular mode, which later changes to quasi-cleavage as the crack propagates. However, this intergranular region is strongly heat-treatment dependent, i.e. about 150 microns for 870°C case (in other words 5-6 grains) compared to about 300 micron for 1200°C (or about 1 grain).

In essence, the fractographic observation is consistent with the toughness data.

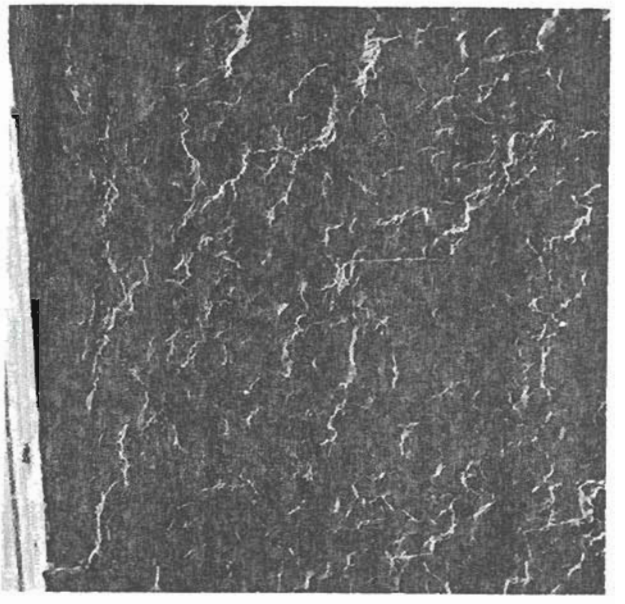

(a) 200X

(b) 750X

Figure 3.36. SEM micrograph of as quenched sample austenitized at 870°C. It is tested at liquid nitrogen temperature (instrumented Charpy) and it has a fatigue pre-crack. (a) At low magnification, the notch fatigue-zone and the intergranular zone is visible, (b) at high magnification, fatigue zone changing to intergranular/quasi-cleavage zone, which is the fracture initiation zone.

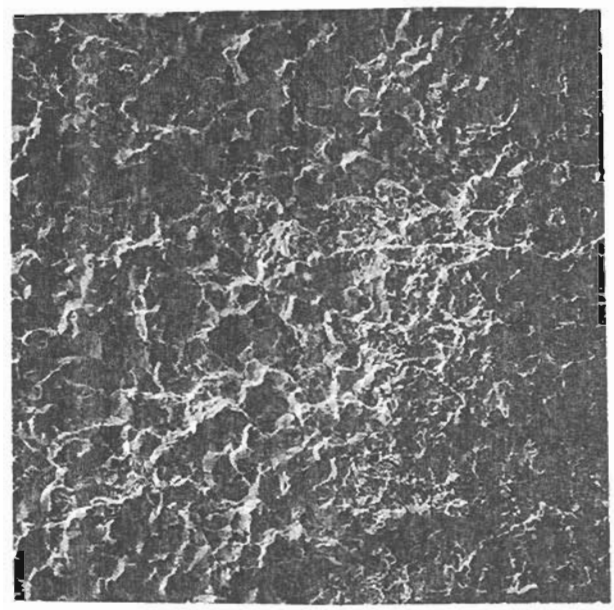

(c) 200X

(d) 800X

Figure 3.36. (continuation)

(c) At low magnification, the intergranular zone changing to quasi-cleavage, (d) At high magnification, intergranular zone changing to quasi-cleavage.

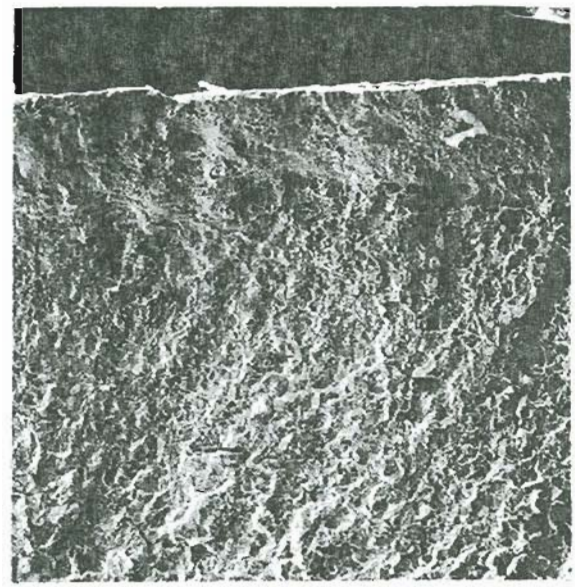

(e) 50X

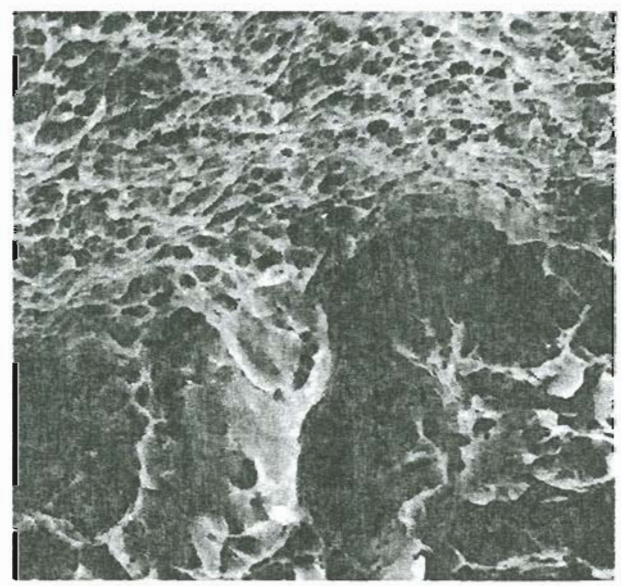

(f) 1500X

Figure 3.36 (continuation).

(e) At low magnification, it shows the extent of shear lip, (f) At high magnification, it shows the microvoid coalescence (shear lip)/quasi-cleavage interface.

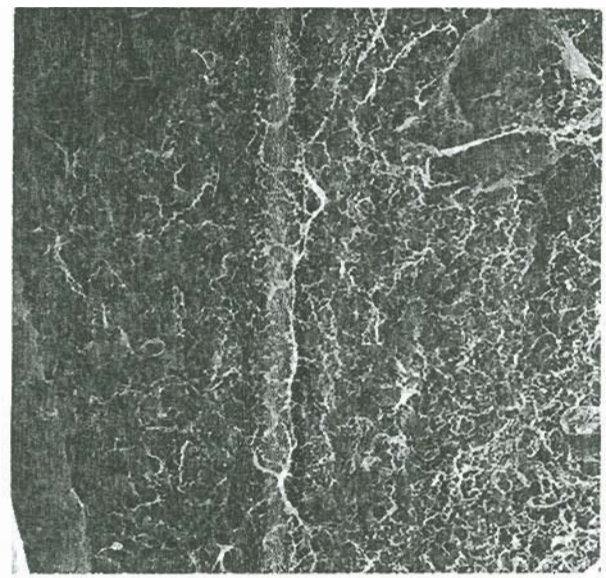

(a) 200X

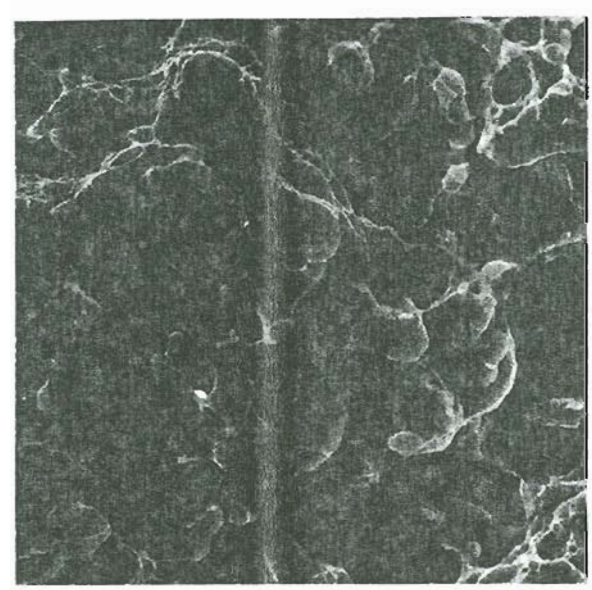

(b) 2000X

Figure 3.37. SEM micrographs of as-quenched sample austenitized at 870°C. It is tested at liquid nitrogen temperature (instrumented Charpy) and it has a notch root-radius of .004 inch. (a) At low magnification, the initiation mode is found to be microvoid, which changes into quasi-cleavage mode, (b) At high magnification the quasi-cleavage mode is seen.

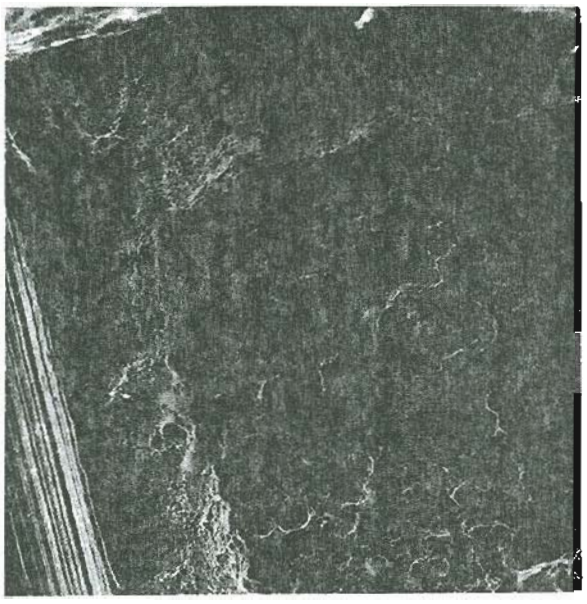

(c) 200X

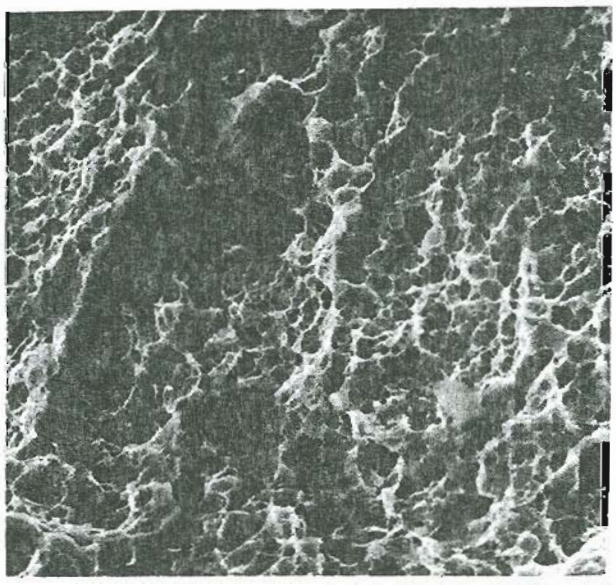

(d) 2000X

Figure 3.37 (continuation).

(c) At low magnification the relative magnitudes of shear lip zone and fracture initiation zone are compared. (d) At higher magnification, microvoid coalescence in the shear lip zone is evident.

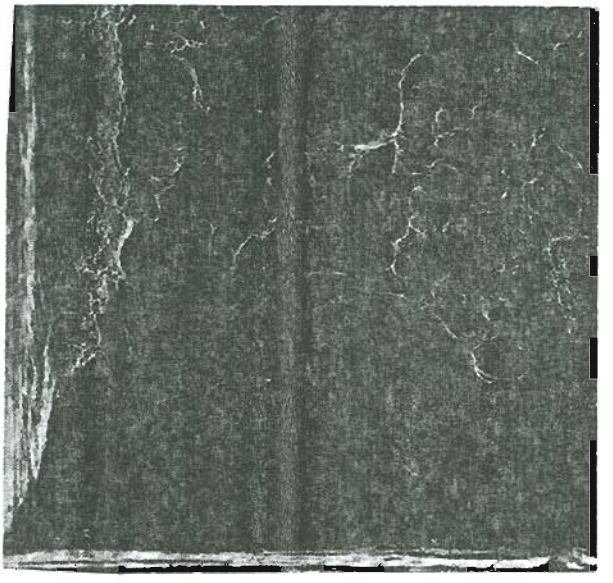

(a) 200X

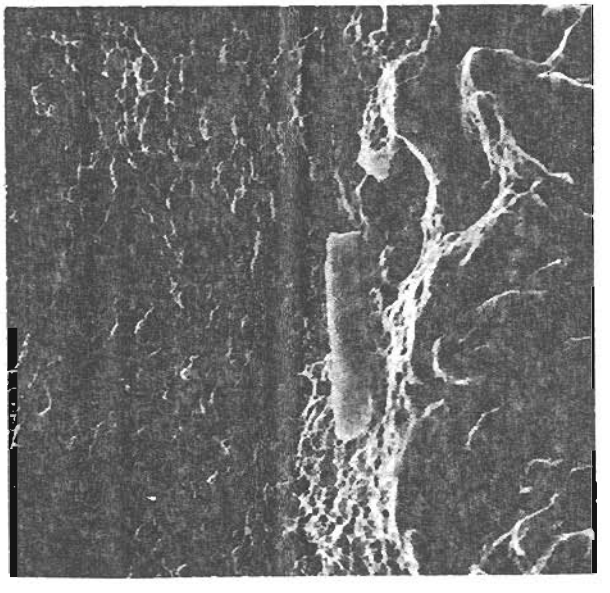

(b) 2000X

Figure 3.38. SEM micrographs of as-quenched sample austenitized at 870°C . It is tested at liquid nitrogen temperature (instrumented Charpy) and has a notch root radius of .006 inch. (a) At low magnification the relative magnitudes of shear lip zone and the fracture initiation zone are compared. (b) At high magnification it shows how micro-void zone (fracture initiation) changes to quasi-cleavage zone (fracture propagation).

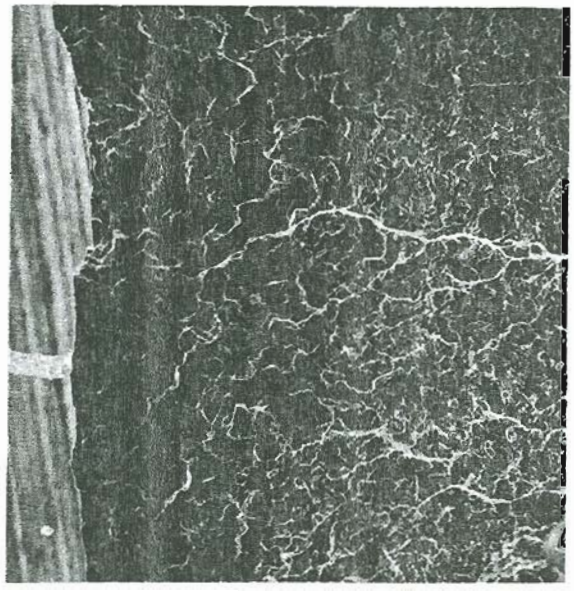

(a) 200X

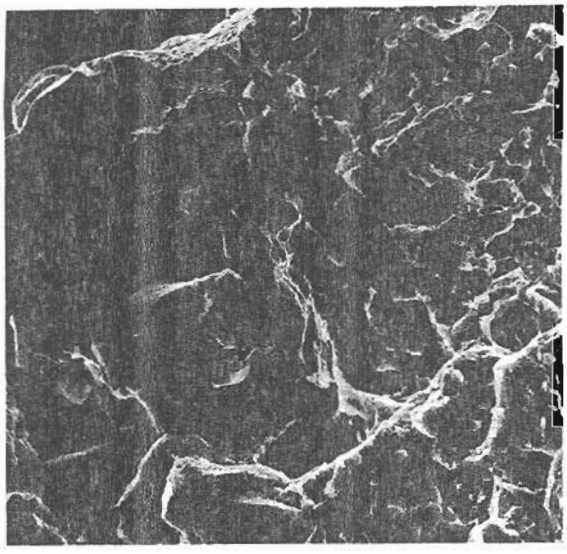

(b) 1000X

Figure 3.39. SEM micrographs of as-quenched sample austenitized at 870°C . It is tested at liquid nitrogen temperature (instrumented Charpy test) and it has a root radius of .02". (a) At low magnification the fracture initiation mode is found to be intergranular. (b) At high magnification the intergranular mode later changes into quasi-cleavage mode.

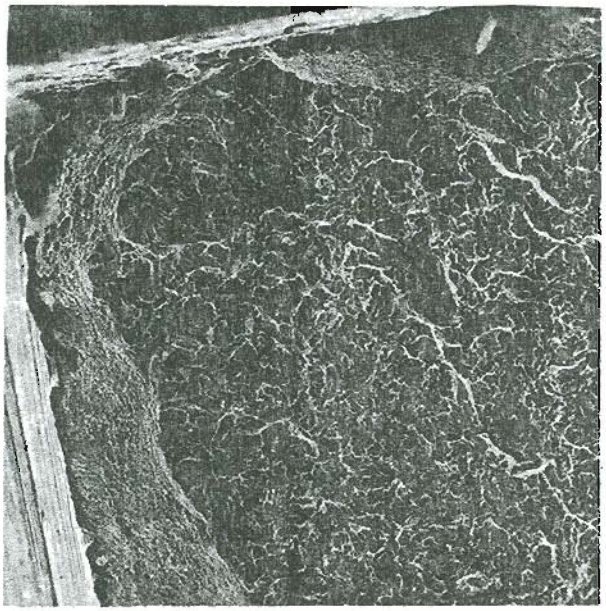

(e) 200X

Figure 3.39 (continuation)

(c) It shows that very near the surface, where plane stress condition exists, the fracture initiation mode is still micro-void coalescence. The shear lip zone is also visible.

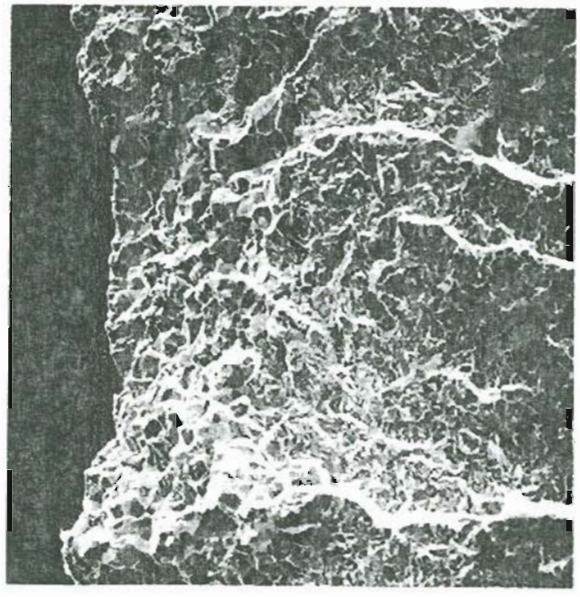

(a) 200X

(b) 1000X

Figure 3.40. SEM micrographs of as-quenched sample austenitized at 870°C. It is tested at liquid nitrogen temperature (instrumented Charpy) and it has a notch root radius of .03". (a) At low magnification the fracture initiation mode is found to be intergranular. (b) At high magnification the interface between the intergranular mode and the quasi-cleavage mode is shown.

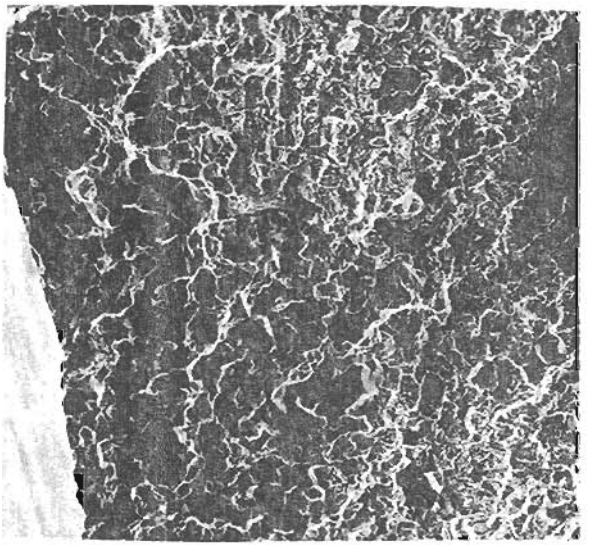

(a) 200X

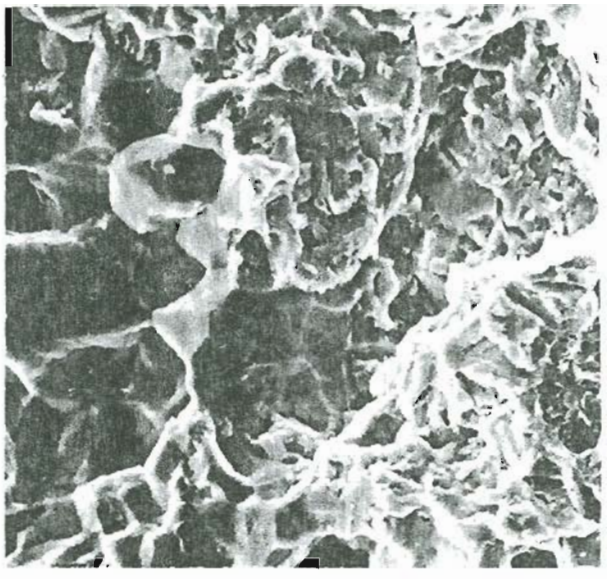

(b) 1000X

Figure 3.41. Same as Figure 3.40 except it has a notch root radius of .04 inch. (a) At low magnification the fracture initiation mode again is found to be intergranular, which later changes into quasi-cleavage. (b) The interface between the intergranular and the quasi-cleavage is shown at high magnification. Thus the drop in toughness with increase in notch root radius is associated with intergranular fracture mode initiation.

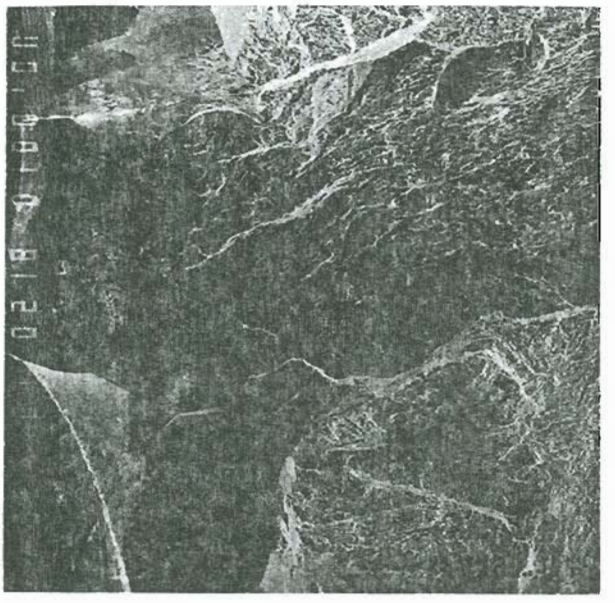

(a) 100X

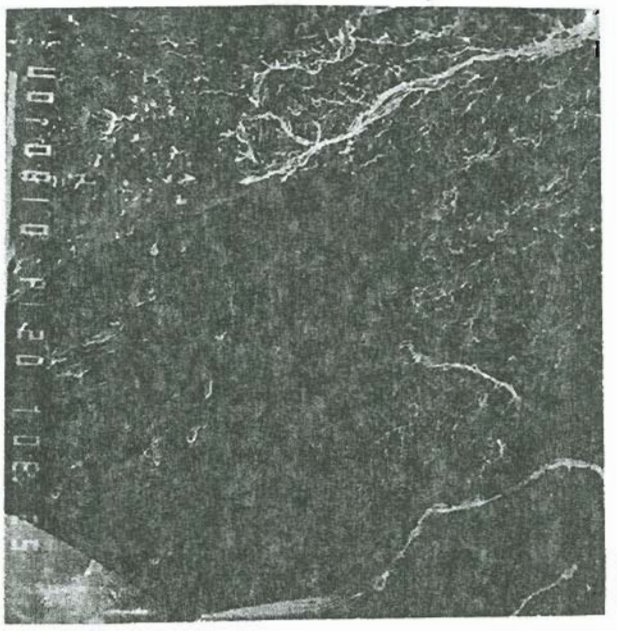

(b) 300X

Figure 3.42. SEM micrographs of as-quenched sample austenitized at 1200°C. It is tested at liquid nitrogen temperature (instrumented Charpy) and it has a notch root radius of .02". (a) At low magnification, the intergranular fracture mode is evident, which later changes to quasi-cleavage, (b) The same view at high magnification.

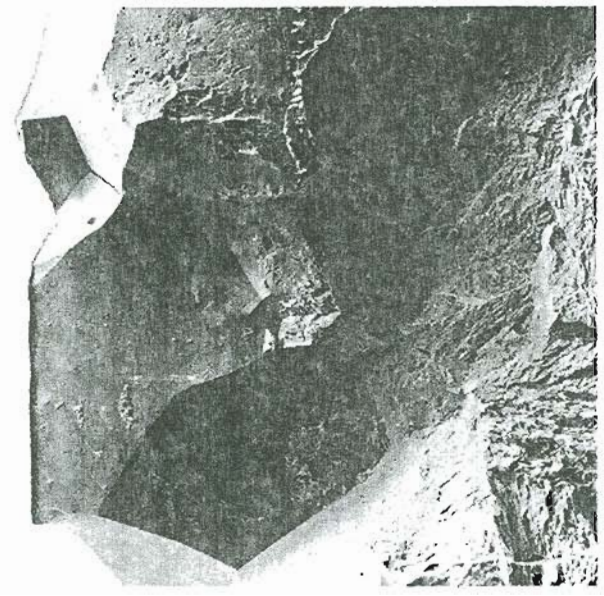

(a) 100X

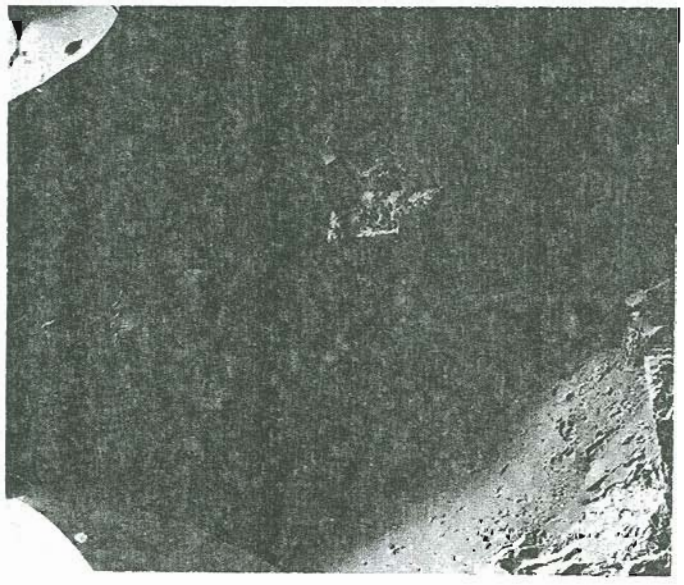

(b) 150X

Figure 3.43 Same as Figure 3-42 except that it has a notch root radius of .03 inches. (a) At low magnification the intergranular fracture mode is seen, which later changes to quasi-cleavage. (b) The same view at a little higher magnification. Thus the drop in toughness which occurs at the same notch root radius is independent of grain-size.

(a) 500X

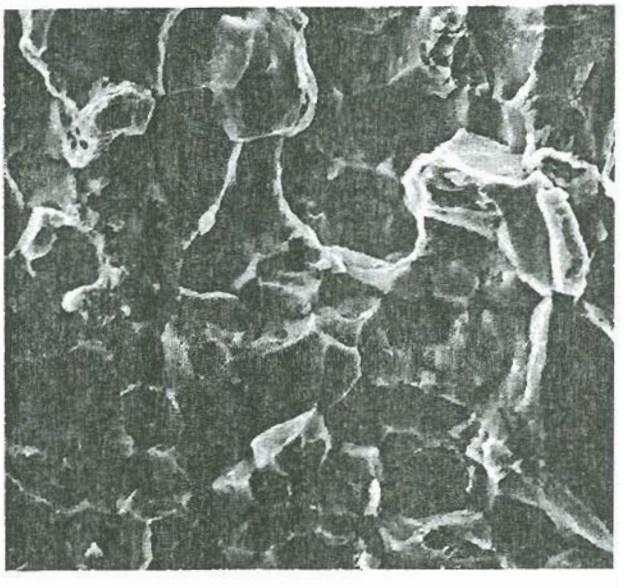

(b) 1000X

Figure 3.44. SEM micrographs of as-quenched samples austenitized at 870° C. It is tested at room temperature (slow-bend test) and it has a notch root radius of .03 inch. Both (a) and (b) show intergranular fracture mode.

(a) 100X

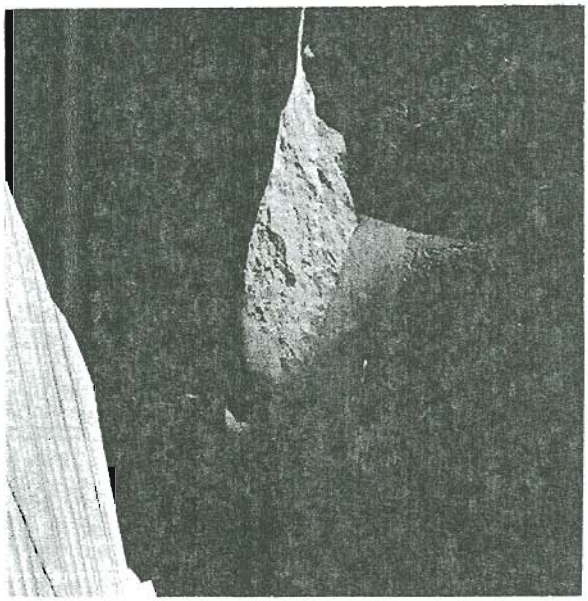

(b) 100X

Figure 3.45. SEM micrographs of samples of as-quenched at 1200°C It is tested at room temperature (slow-bend test) and it has a notch-root radius of .04 inches. (a) Intergranular initiation mode at the edge, (b) intergranular initiation mode at the center.

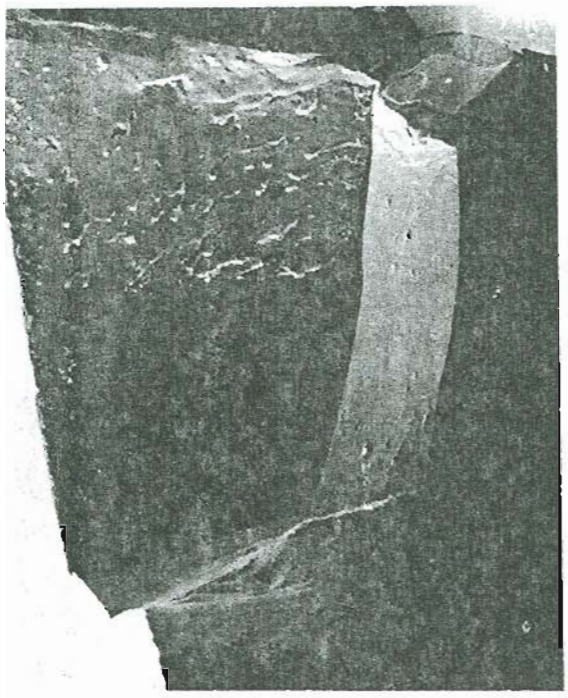

(c) 300X

Figure 3.45 (continuation); (c) At still higher magnification the the intergranular fracture mode is shown. Thus, again, the grain-size does not affect the notch root radius, when the drop in toughness is observed.

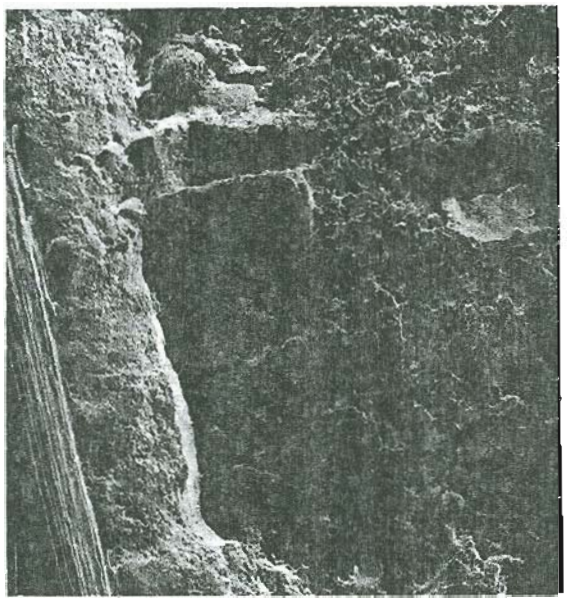

(a) 100X

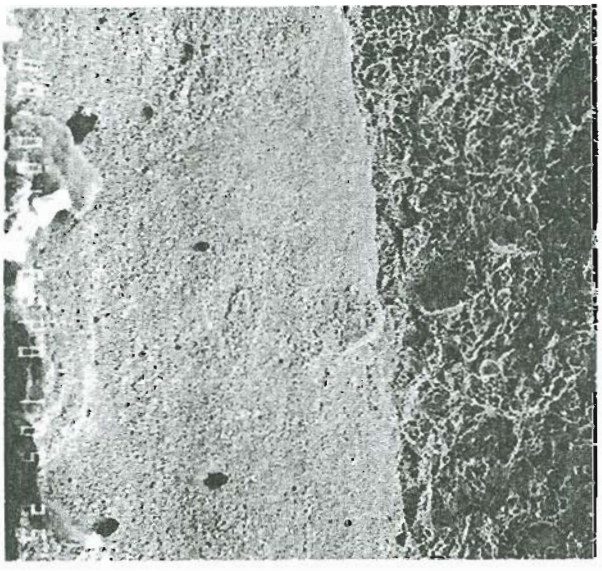

(b) 200X

Figure 3.46: SEM micrographs of as-quenched samples austenitized at 1143°K. It is tested at room temperature (instrumented Charpy test). (a) With notch root radius of .004 inch, the fracture initiation mode is microvoid coalescence, (b) with notch root radius of .04 inch: the fracture initiation mode is again microvoid coalescence; however, the zone extends a little further than in the previous case.

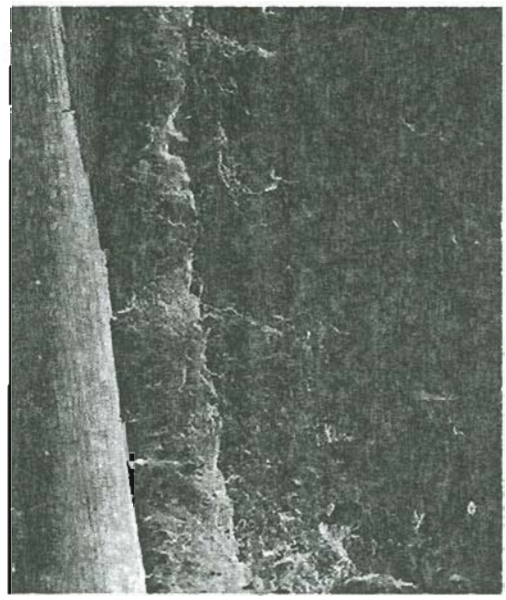

(a) 20X

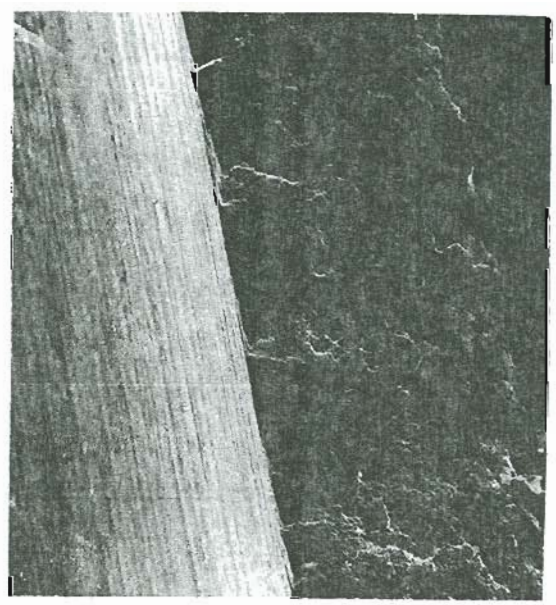

(b) 50X

Figure 3.47: Same as Figure 3.46 except different notch root radii. (a) With notch root radius of .07 inch, the fracture initiation mode is found to be microvoid coalescence, which later changes into quasi-cleavage mode. (b) With notch root radius of 0.1 inch the same fracture initiation mode (i.e. microvoid coalescence).

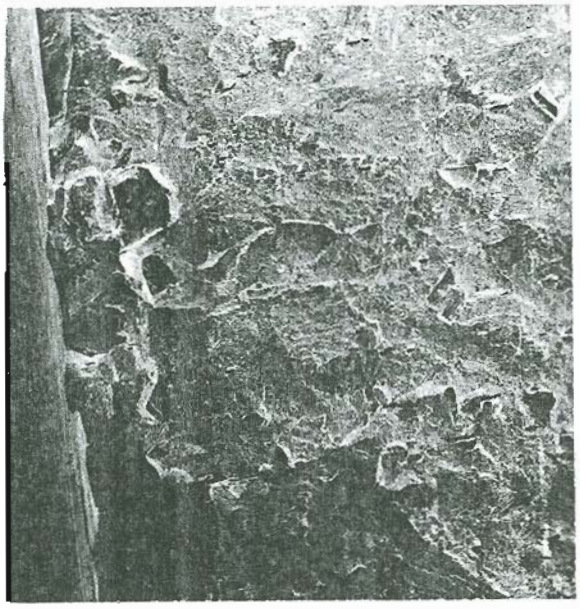

(a) 20X

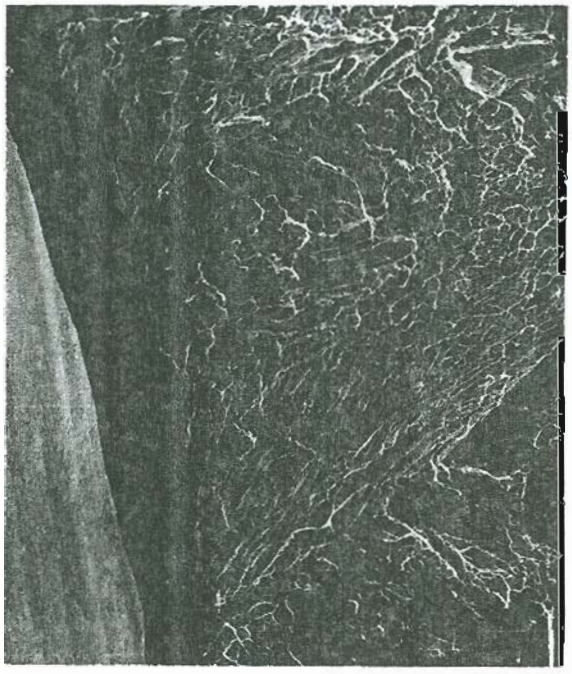

(b) 200X

Figure 3.48. SEM micrographs of as-quenched samples austenitized at 1200°C. It is tested at room temperature (instrumented Charpy) and has a notch root radius of .07 inch. (a) At low magnification the intergranular fracture mode initiation at the centre is observed; however, at the sides the initiation mode is microvoid (the left top corner). (b) At high magnification, the intergranular region is visible, which later changes into quasi-cleavage.

(a) 20X

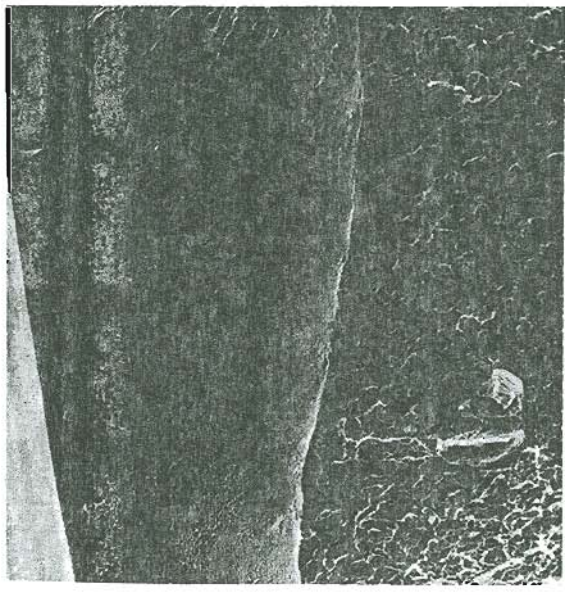

(b) 200X

Figure 3.49. Same as Figure 3.48 except it has a notch root radius of .10 inch. (a) At low magnification the fracture surface is found to be rough. (b) At high magnification the fracture mode is found to be microvoid coalescence, which later changes into quasi-cleavage mode.

4. DISCUSSION

4.1 The Effect of Notch Root Radius on the Toughness: - Early investigations have reported (62,63) that the elastic strain energy release rate is relatively insensitive to tip-root radius in the range from a mathematical 'sharp' crack to macroscopic root radii. This is also expected from Irwin's formula (64) $K = \lim_{\rho \to 0} \frac{1}{2} \sigma_m (\pi\rho)^{1/2}$, where σ_m = maximum stress at the notch, ρ = notch root radius. In this relationship K will become insensitive to root radius, whenever, σ_m is inversely proportional to $\rho^{1/2}$. However, present data and other experimental fracture data show that this is not always the case. Fracture toughness values can be significantly lower for a fatigue pre-cracked specimen than for a small but finite root radius specimen. (65) Malkin et al (68) found that the apparent toughness increases with the square-root of the root radius for mild steel. Similar increases in toughness with increase in root radius have been observed by other investigators, namely Rack (66) in unaged β-titanium alloy, Myers,et al.(67) in monocrystalline silicon, Ritchi et al. (2) in 4340 quenched and tempered steel. The theoretical relationships of fracture toughness with notch root radius also predict an increase in fracture toughness value with increase in root radius.

The longitudinal stress distribution ahead of a blunt notch of radius ρ is given by slip-line field theory(37)

$$\sigma_{yy} = \sigma_y [1 + \ln (1 + R/\rho)] \qquad \text{(Eqn.4.1)}$$

The relative stress distribution ahead of blunt notches of different root radii are shown in Fig. 4.1. It is observed that stresses ahead of the notch are higher as the notch root radius decreases.

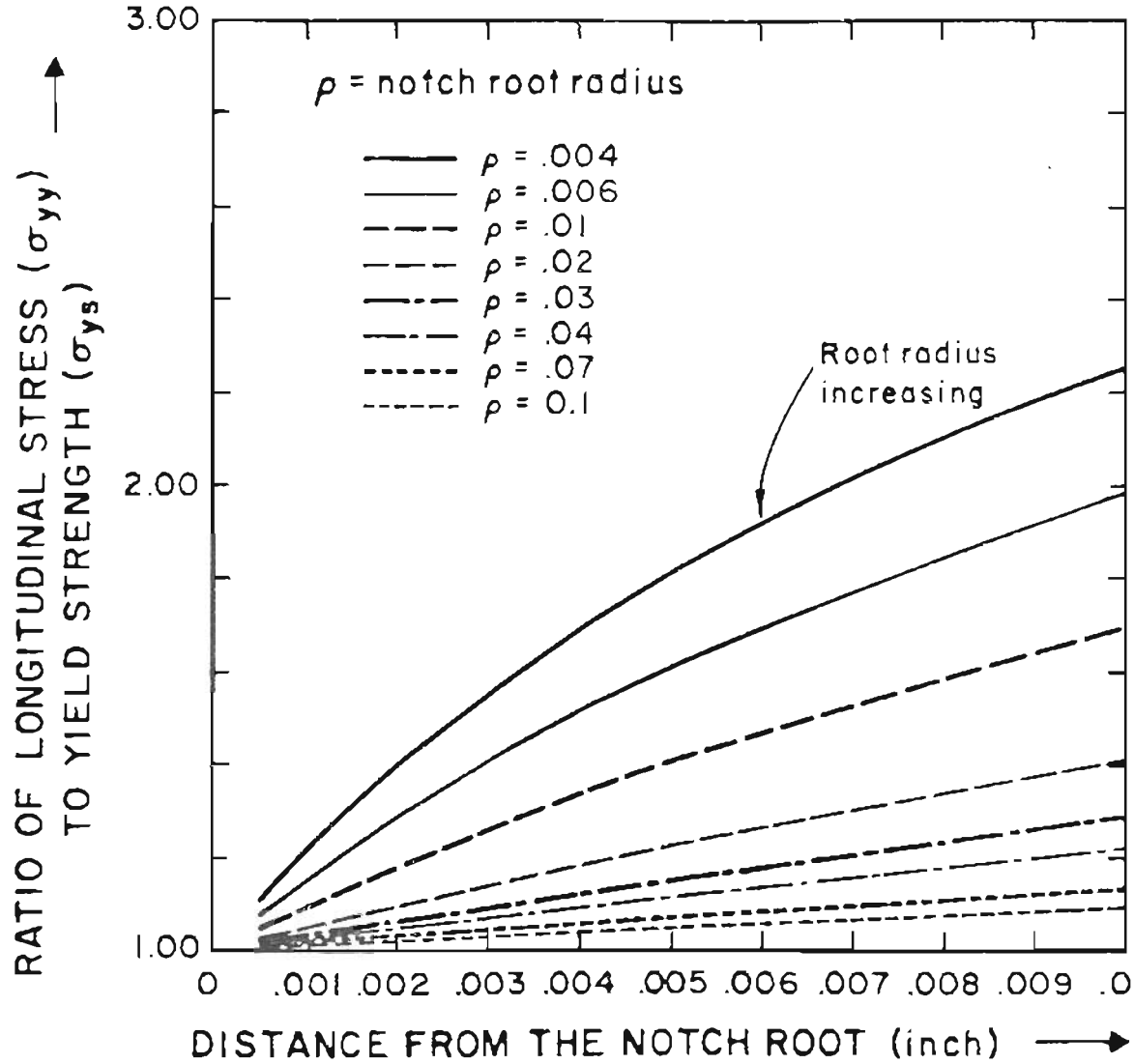

Fig. 4.1 Stress distribution ahead of blunt notches of various root radii by slip-line field theory.

Greager and Paris (73) have calculated the near-field notch tip stresses for very slender elliptical crack having a 'small' root radius for a mode 1 loading, the stresses are

$$\sigma_x = -\frac{K_I}{2\pi r}\frac{\rho}{2r}\cos\frac{3\theta}{2} + \frac{K_I}{2\pi r}\cos\frac{\theta}{2}\left[1-\sin\frac{\theta}{2}\sin\frac{3\theta}{2}\right]$$

$$\sigma_y = \frac{K_I}{2\pi r}\frac{\rho}{2r}\cos\frac{3\theta}{2} + \frac{K_I}{2\pi r}\cos\frac{\theta}{2}\left[1+\sin\frac{\theta}{2}\sin\frac{3\theta}{2}\right] \qquad 4.2$$

$$\tau_{xy} = -\frac{K_I}{2\pi r}\frac{\rho}{2r}\sin\frac{3\theta}{2} + \frac{K_I}{2\pi r}\sin\frac{\theta}{2}\cos\frac{\theta}{2}\cos\frac{3\theta}{2}$$

For $\theta = 0°$, the relative stress distribution for identical stress-intensity factor is plotted in Figs. 4.2 and 4.3 as a function of the distance from the notch-tip for root radii ranging from .004" to 0.1". It is seen that the σ_y stresses ahead of the notch tip are quite similar beyond a distance of .005" for different notch root radii. However, before that distance, the stress increases as the notch root radius decreases. The σ_x stress distribution ahead of the notch root similarly increases, as the notch root radius decreases.

From the foregoing discussion, it is apparent that the toughness should increase as the notch radius increases, if a critical stress criterion applies for a crack initiation. From a critical strain model also, it has been postulated by many investigators (68,3) that toughness follows a linear relation with the square root of notch-root radius.

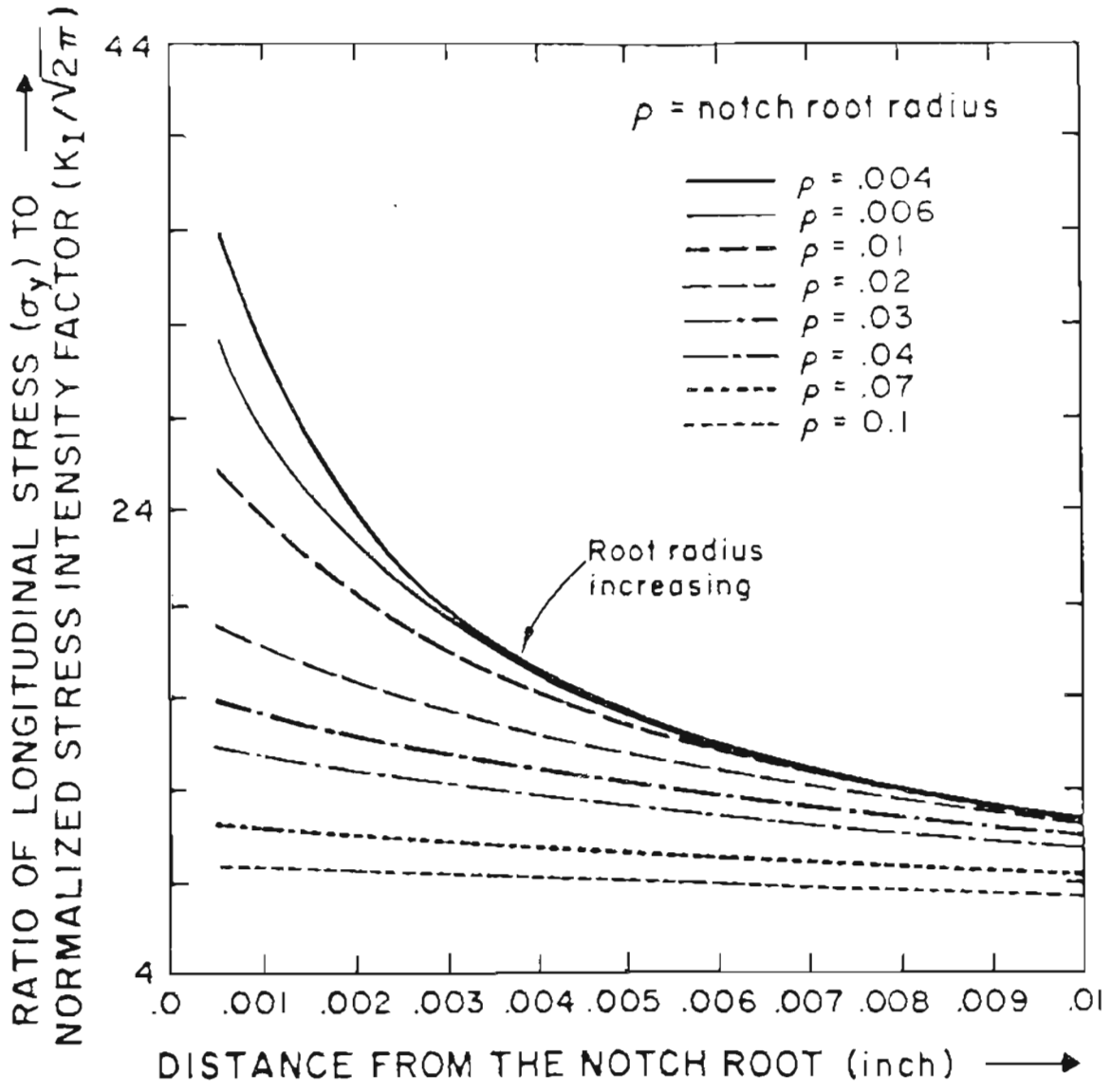

Fig. 4.2 Variation of σ_y with distance from the notch-root ($\theta = 0^\circ$) for different notch root radii for a mode 1 stress intensity factor K_I.

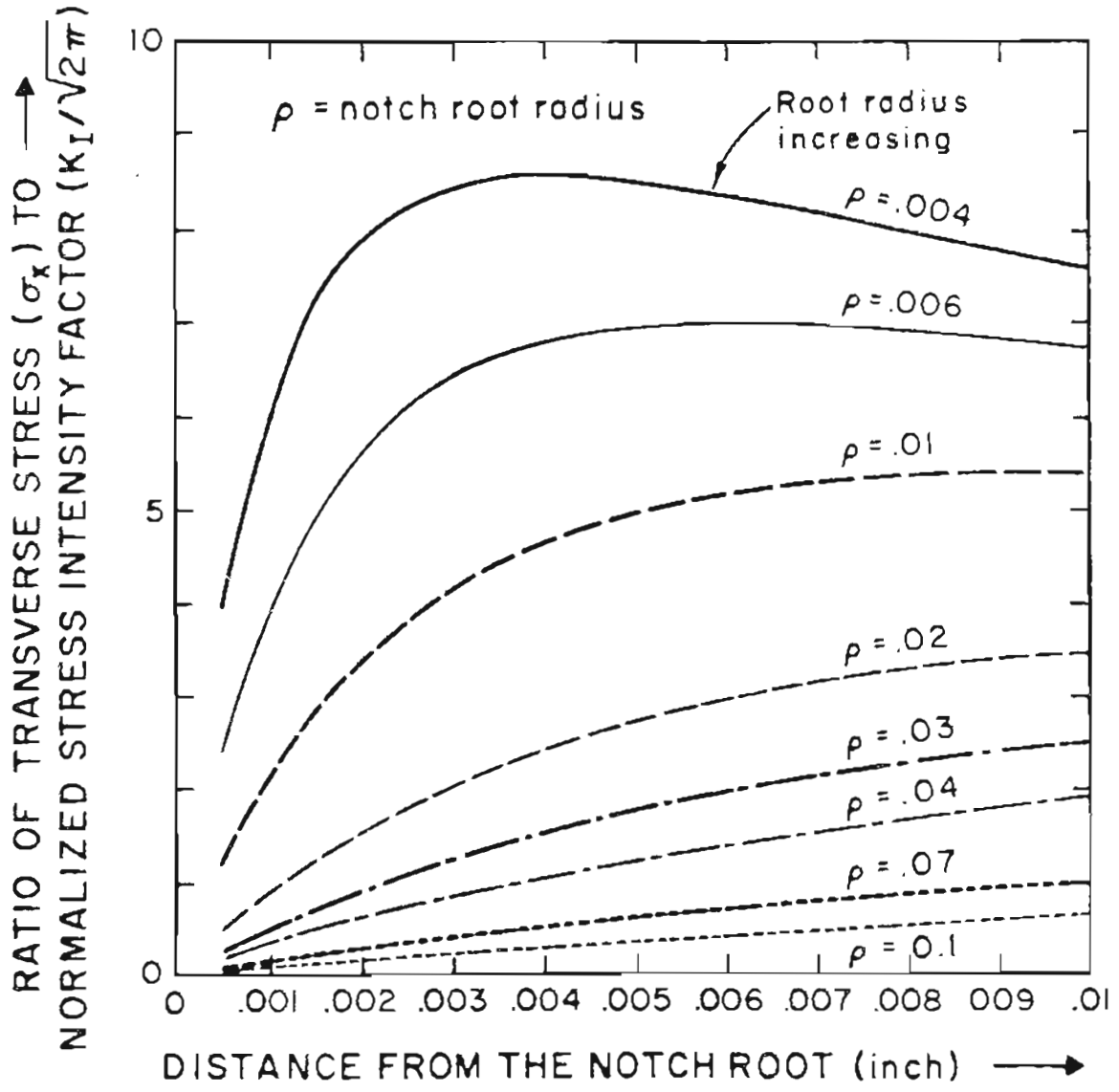

Fig. 4.3 Variation of σ_x with distance from the notch-root ($0=\mathring{0}$) for different notch-root radii for a mode 1 stress intensity factor K_I.

The results in this investigation, on the contrary, indicate that there exists a critical notch root radius, above which the toughness drops. Below that critical root radius, however, the toughness increases with the increase in notch root radius. The drop in toughness above the critical notch root radius is associated with an intergranular mode of fracture. The critical root radius at which such phenomenon occurs is also independent of the prior grain-size.

The relative sizes of the plastic zone for notches of varying root radii are shown in Figs. 4.4 i, ii and iii with grain-sizes incorporated for the two heat-treatments. It is seen that plastic zone size increases with increase in notch-root radius. In Figs. 4.5 a and b the relative size of the intergranular region with respect to plastic zone size is shown. It is seen that the intergranular zone is only a fraction of the plastic zone size. Hence the plastic zone size does not seem to play a role at this anomaly of the toughness behavior. Also, as stated earlier, the root radius at which this phenomenon occurs is independent of the grain-size and hence grain-size also does not seem to play a role in this anomalous behavior. Recently Sih et al. (118-120) have proposed a strain energy density theory for the initiation of a crack. In this theory the total strain energy density S is defined as

$$S = \frac{dU}{dA} = \frac{1-\nu^2}{2E}\left[\sigma_x^2 - \left(\frac{2\nu}{1-\nu}\right)\sigma_x\sigma_y + \sigma_y^2 + \left(\frac{2}{1-\nu}\right)\tau_{x_\tau}^2\right] \qquad (4.3)$$

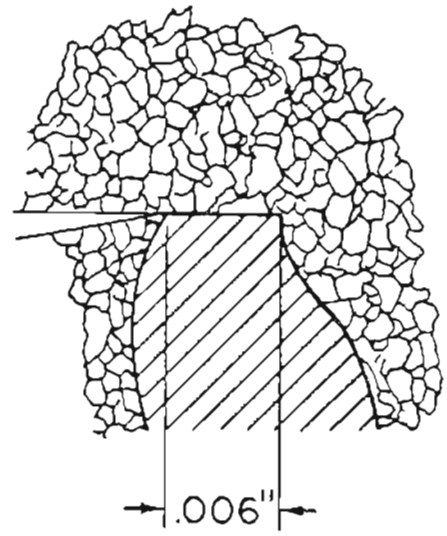

(a)

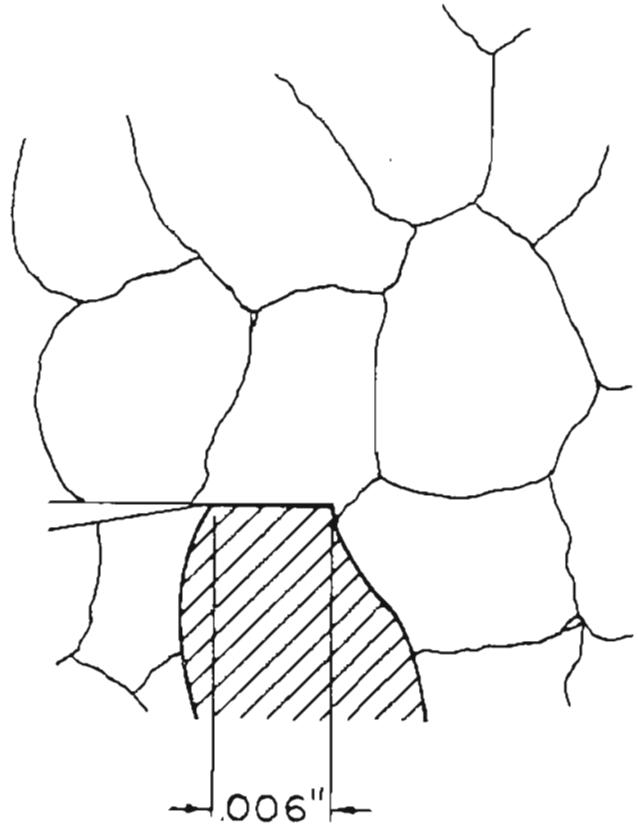

(b)

Fig. 4.4 (i) Plastic zone size for sharp-carck for $\frac{K}{\sigma_{ys}} \approx 0.25$. The relative grain sizes for both (a) low and (b) high austenitizing temperatures are superimposed. Scale 100X

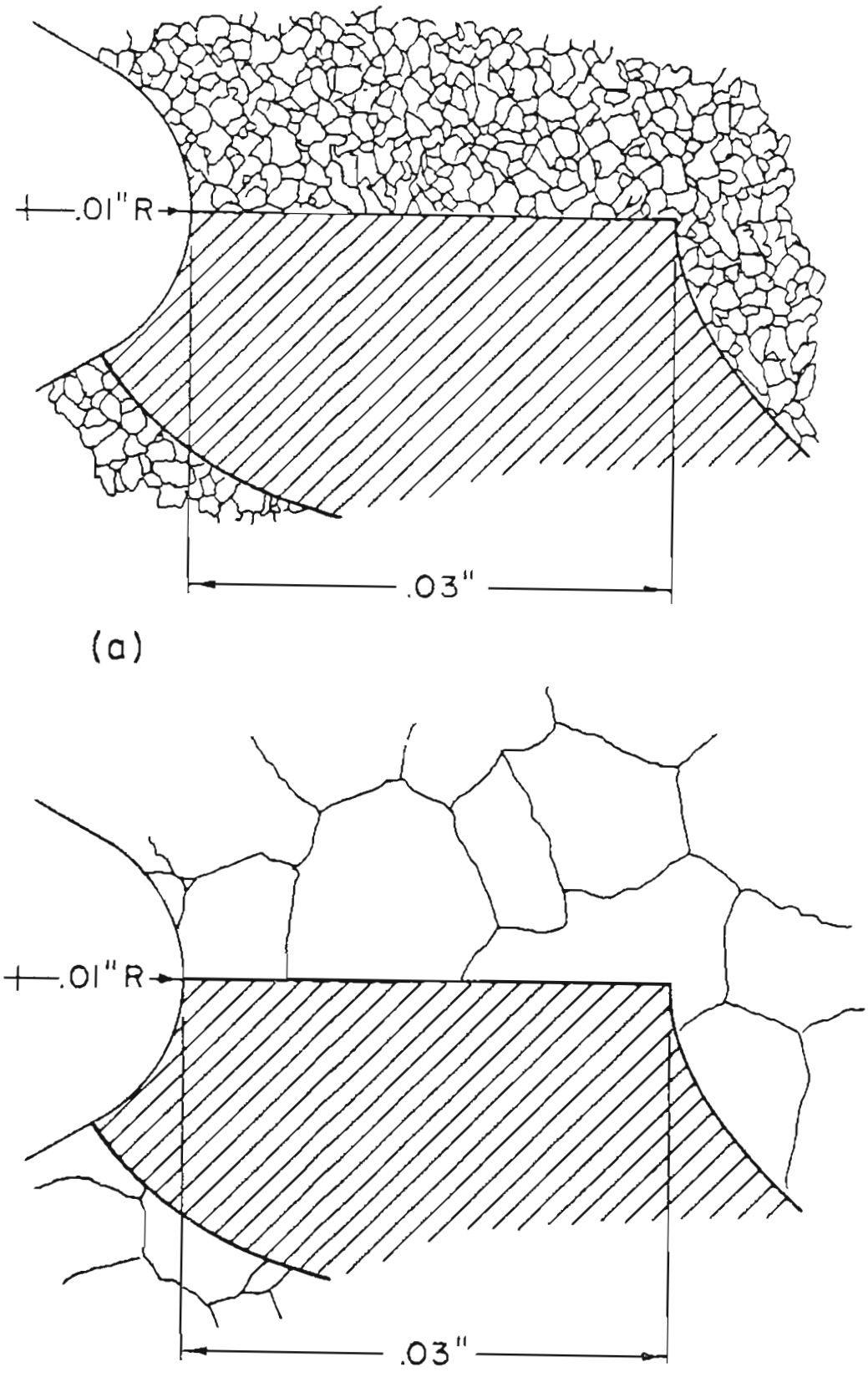

Fig. 4.4 (ii) Plastic zone size for a blunt notch of root radius .01" for $PF/P_{Gy} \simeq 0.7$. The relative grain-sizes for both (a) low and (b) high austenitizing temperatures are superimposed. Scale 100X.

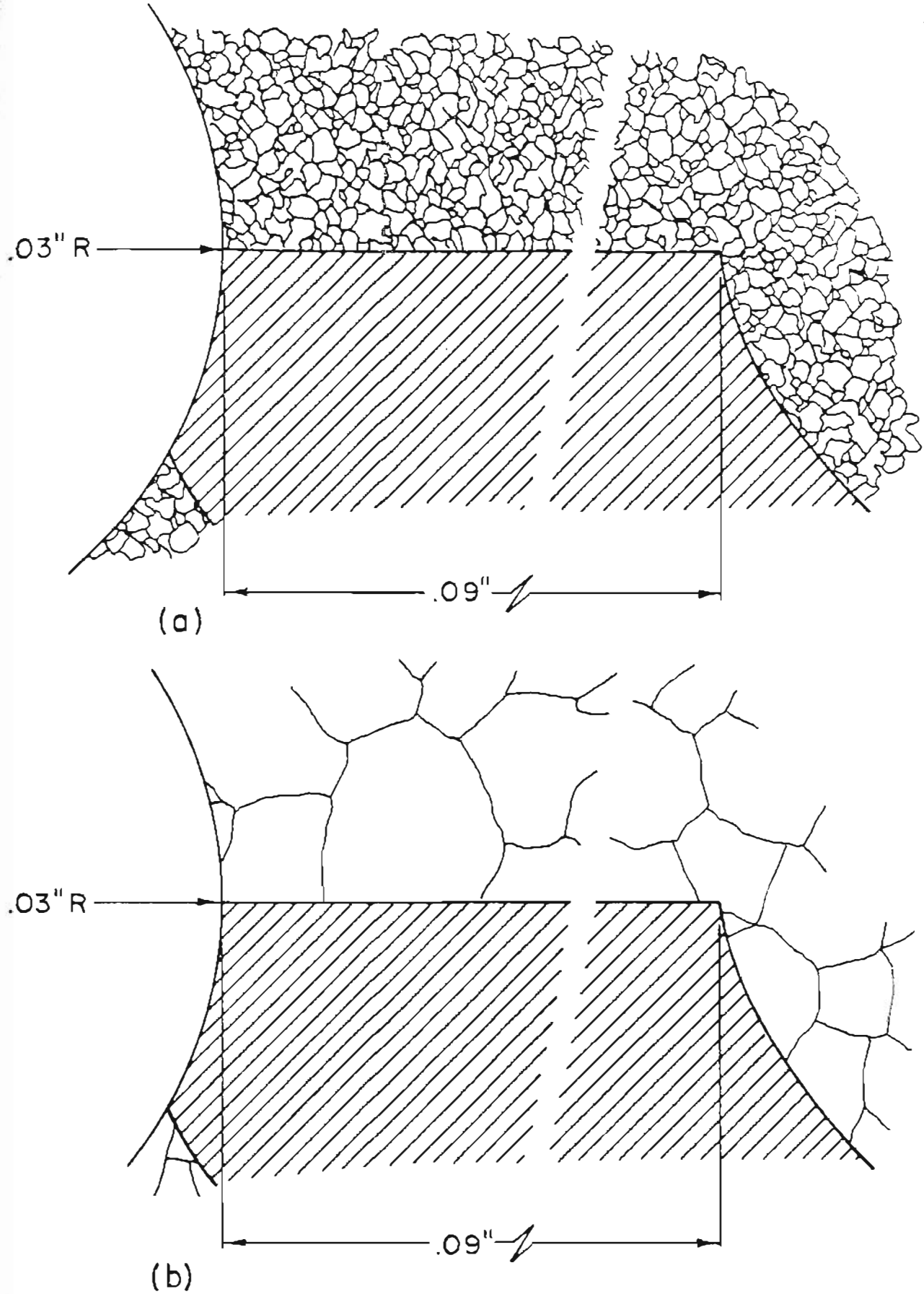

Fig. 4.4 (iii) Plastic zone size for a blunt notch of root radius .03" for $PF/P_{Gy} \approx 0.7$. The relative grain-sizes for both (a) low and (b) high austenitizing temperatures are superimposed. Scale 100X.

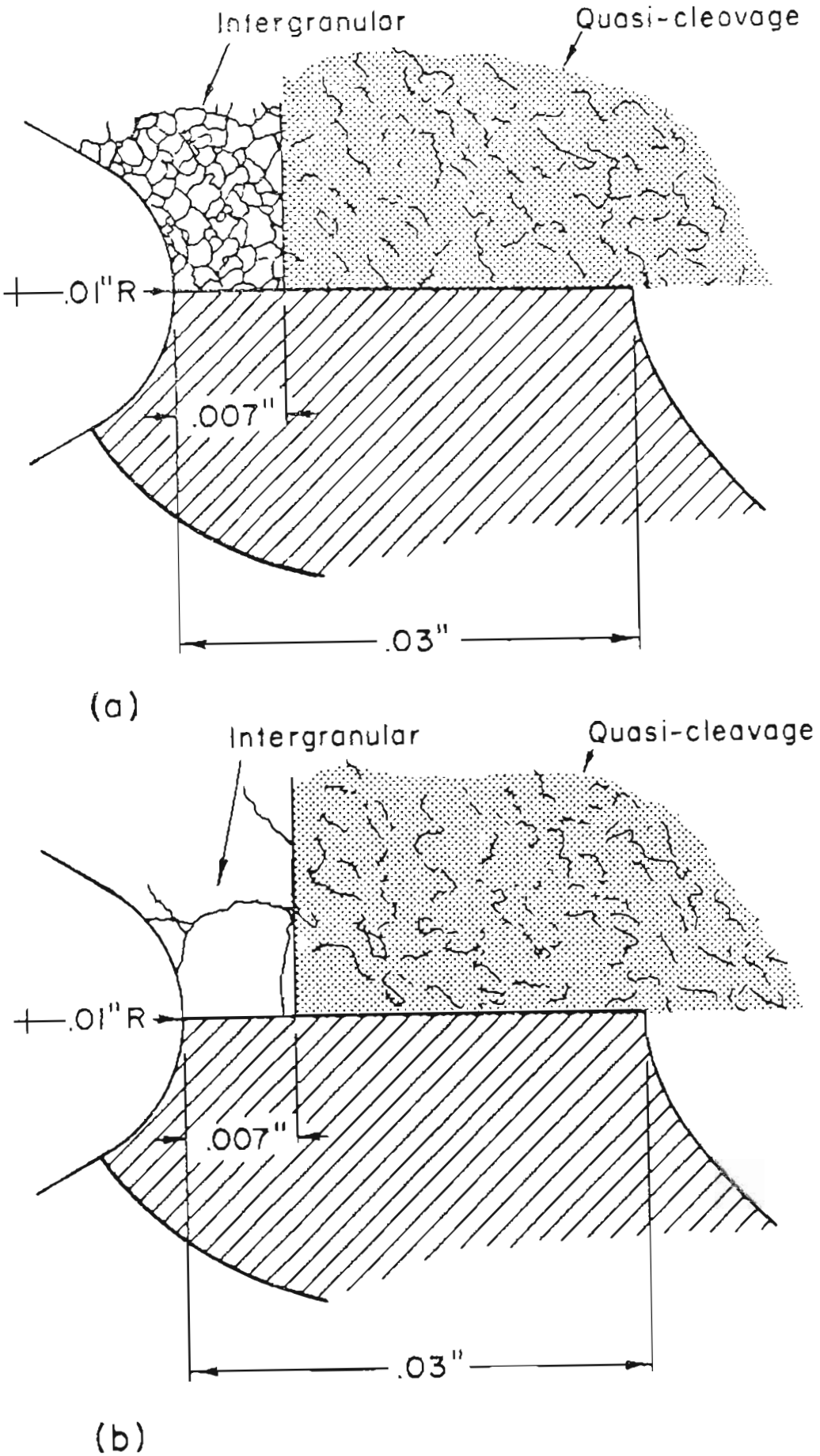

Fig. 4.5 (i) Relative fracture mode zones for a blunt notch of root radius .01". The plastic zone size is superimposed. (a) for low grain-size material, (b) for high grain-size material.

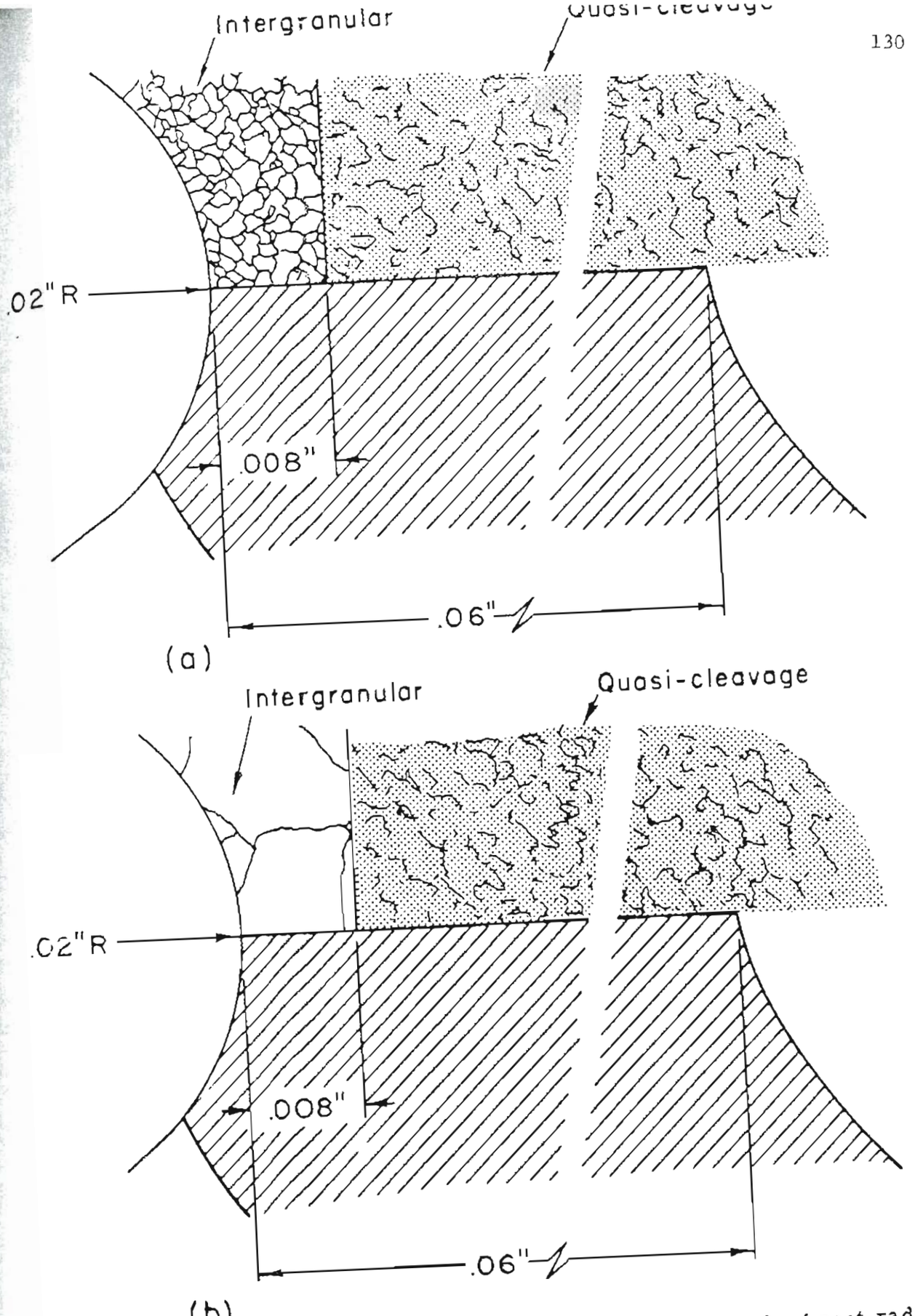

Fig. 4.5 (ii) Relative fracture mode zones for a blunt notch of root radius .02". The plastic zone size is superimposed, (a) for low grain size material, (b) for high grain-size material.

According to this theory, fracture will occur when S assumes a critical value S_c at $\theta = \theta_c$. It also has been demonstrated (121) that for a mode 1 fracture, $\theta_c = 0°$, and is independent of notch-root radius.

Greager and Paris's equations for a mode 1 stress distribution for $\theta = 0°$, were used for calculating the strain-energy density function in the present investigation and the strain energy density as a function of the distance from the notch tip is shown in Fig. 4.6 for different notch root radii. It is seen that just ahead of the notch, the strain energy density for larger root radius is much higher than that for smaller root radius. In other words, if the critical strain energy density is applied to the initiation of fracture, the toughness should decrease as the notch root radius increases.

Thus, we have two competing situations. Both the critical stress and the critical strain models predict higher toughness with larger root radii and the critical strain energy density model predicts lower toughness with larger root radii. In this investigation, the critical stress model operates initially until a critical root radius is reached. Above this critical root radius the strain-energy density theory seems to be applicable.

It is a difficult question to answer why the fracture initiation mode is intergranular. The strain energy density theory is based on a continuum mechanics approach and does not consider microscopic aspects of fracture. Therefore, this question can be answered only in a quanitative way. In a recent paper on 'grain boundary fragility' Hondrous and

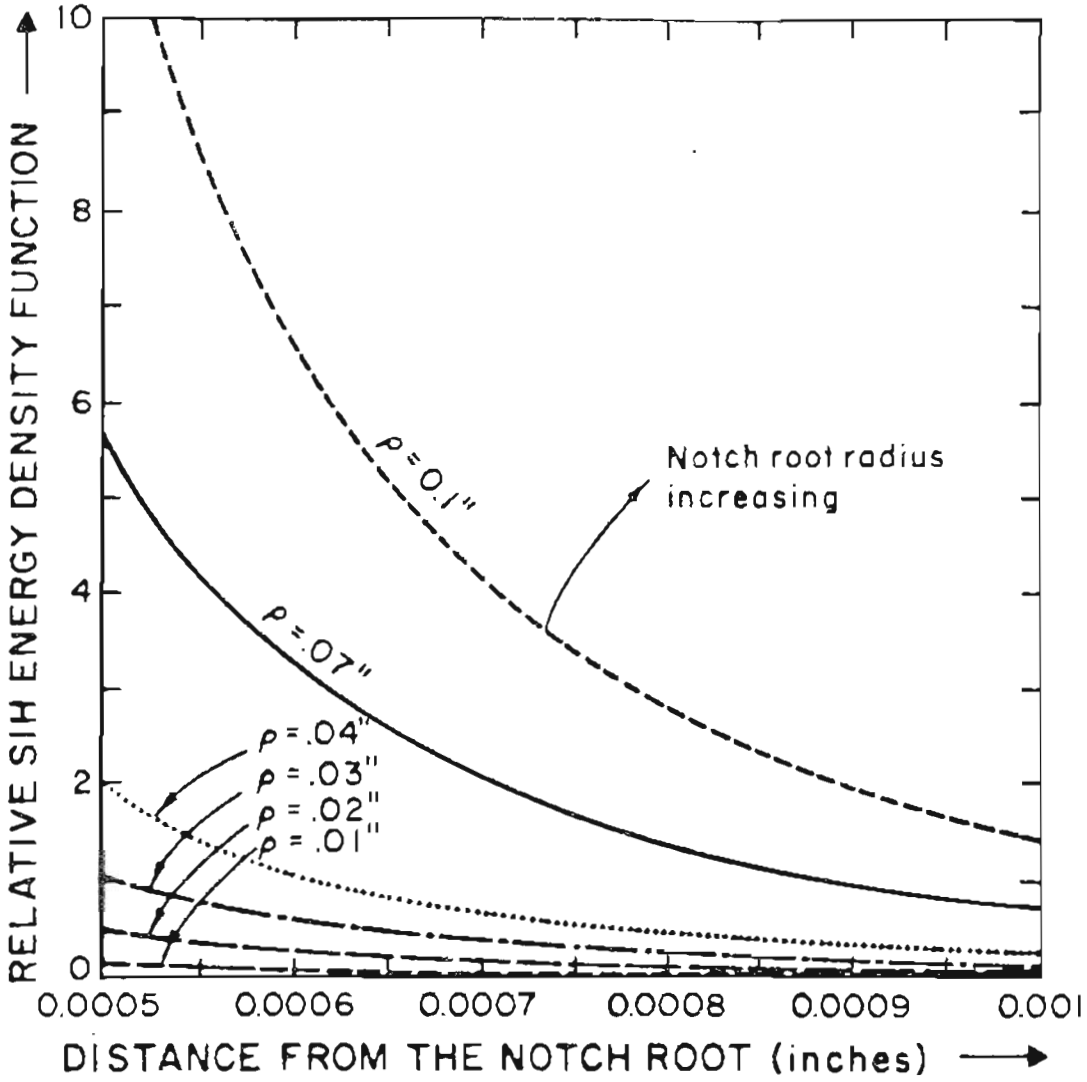

Fig. 4.6 Variation of relative Sih energy density function ahead of the notch for different notch root radii.

McLean (122) tried to explain the grain boundary decohesion, which may be caused by impurity segregation, particle/matrix interaction, stress system and stress magnification requirements. In the present investigation the first two may be ruled out since the variable is purely a mechanical parameter, i.e. notch root radius: also the effect is seen for a variety of heat-treatments. Hence, the last factor, i.e. the stress system, is changed so as to cause the intergranular mode of fracture. The grain boundary even with segregation and second phase particles is normally strong enough not to rupture unless the applied stress is locally magnified a great deal. In plastic polycrystals the largest stress magnifications occur at the heads of slip bands. According to Hondrous and McLean, in order for the intergranular fracture to occur two conditions have to be met

$$\begin{aligned} &\sigma_c > \sigma_m \quad \text{Condition 1} \\ &\sigma_c/\tau_c > \sigma_m/\tau_m \quad \text{Condition 2} \end{aligned} \tag{4.4}$$

where σ_c is the maximum tensile component of the stress concentration and σ_m is the cohesive strength of the metal. τ_c = shear component of the stress concentration τ_m = shear resistance of the material.

In this model, even though the first requirement is easily satisfied, the second requirement is not, when a single slip band model is considered. When a double slip band is considered, (shown in Fig. 4.7) τ_c is considerably decreased, making the second condition easier to satisfy. Hence it may seem plausible that after a critical root radius

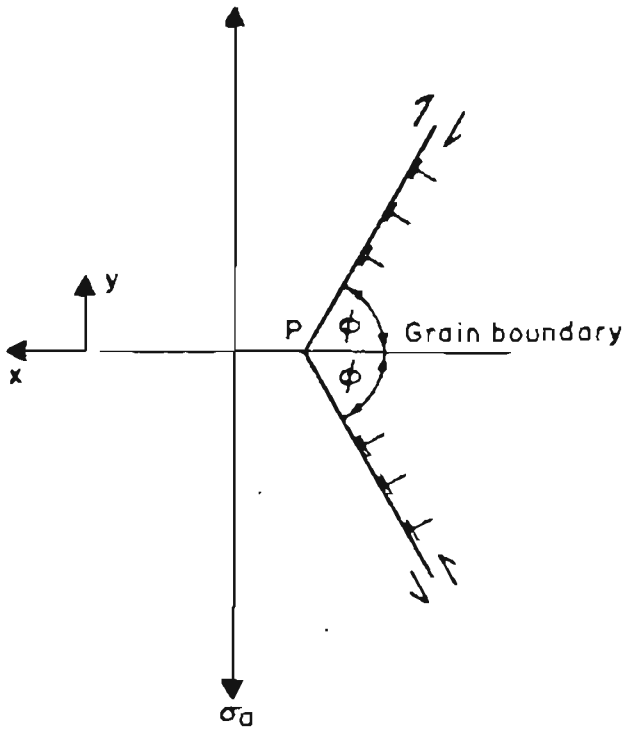

Fig. 4.7 (a) Schematic diagram of two slip bands meeting along a grain boundary at P.[122]

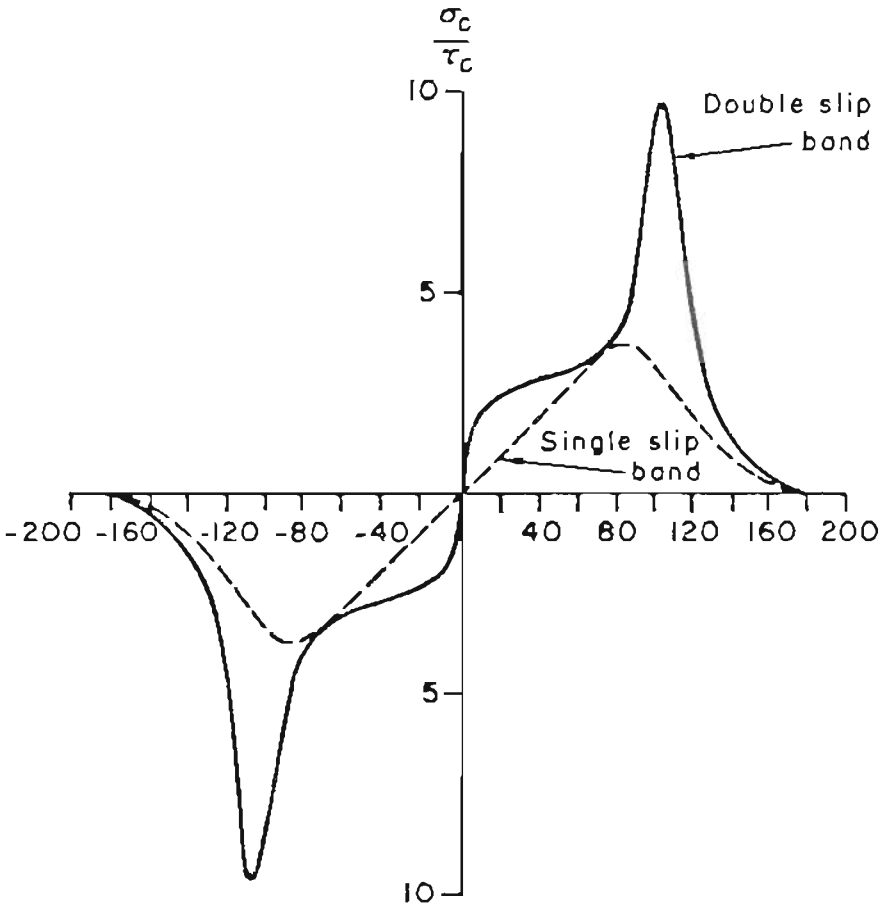

Fig. 4.7 (b), The ratio σ_c/τ_c for the single slip board (dashed line) and for the double slip band (full line): this ratio is equal to the that of condition 2.[122]

is reached double or multiple slip bands operate just ahead of the notch, reducing τ_c. Thus, both the requirements are satisfied, thereby making intergranular fracture possible. Dislocation movement, it may be noted, is strongly temperature and strain-rate dependent and that is why the critical root radius at which intergranular fracture and drop in toughness occurs is also temperature and strain-rate dependent.

4.2 Sharp Crack and Blunt Notch Behavior of the Above Two Heat-Treatments. The results in this investigation, as well as others have demonstrated that the sharp crack and blunt-notch toughness behavior for the two heat treatments is quite different. In fact, the apparent toughness from blunt notch specimens is better for the lower austenitizing treatment than for the higher austenitizing treatment in as-quenched condition. This discrepancy in the sharp crack and blunt notch behavior for the high austenitizing treatment in the as-quenched condition has been related to higher limiting root radius (ρ_o, which has been hypothesized to be equal to the prior austenite grain size) and lower fracture stress (σ^*_f) (2,3)

It must be borne in mind that the limiting root radius is a fictitious root radius, which has been introduced to satisfy the result for pre-cracked condition, since the model predicts a zero toughness for pre-cracked specimen. (See the appendix). If limiting root radius is made equal to the grain size, the toughness from pre-cracked condition up to a root radius of the prior austenite grain size should remain constant. In other words, for the 1200°C austenite treatment in as-quenched condition which produces a grain size of 250μ (or .010"), toughness should remain constant from 'sharp' crack to about .010" root radius. The results,

in this investigation, replotted in Figs. 4.8 and 4.9 do not show this behavior in a variety of testing conditions. Hence, the explanation based on limiting root radius for the improvement in toughness does not seem to be valid.

The stress distribution ahead of a sharp crack and a blunt notch (shown in Fig. 4.10) has been discussed quite extensively, (123,124). The salient points are (1) the maximum stress intensification ahead of a 'sharp' crack occurs very close to the crack tip. This distance from the crack tip is given by $2\delta_t = K^2/E\sigma_{\gamma s}$ and for a $K = 50$ ksi$\sqrt{\text{in}}$ and $\sigma_{\gamma s} = 200$ ksi, $2\delta_t = .0005$ inch (2) the maximum stress intensification ahead of blunt notch occurs at the plastic/elastic interface (slip-line field theory) or behind the plastic/elastic interface (finite element method) but in either case well away from the notch, i.e. for a root radius of .010" the plastic/elastic interface is roughly at .030" distance from the notch.

From a dislocation model a crack can be conceived of a continuous group of edge dislocations. (32) Physically, a crack will propagate only when the dislocations which are created ahead of the crack tip can join the main group of dislocations (schematically shown in Figs. 4.11 and 4.12). From this, it is clear that in pre-cracked condition, for the crack to propagate, the dislocation source need not cross any grain boundary even in low austenitizing treatment (for which the grain diameter .001"). On the other hand, in the blunt notch testing condition the dislocation source has to cross a number of grain boundaries to join the

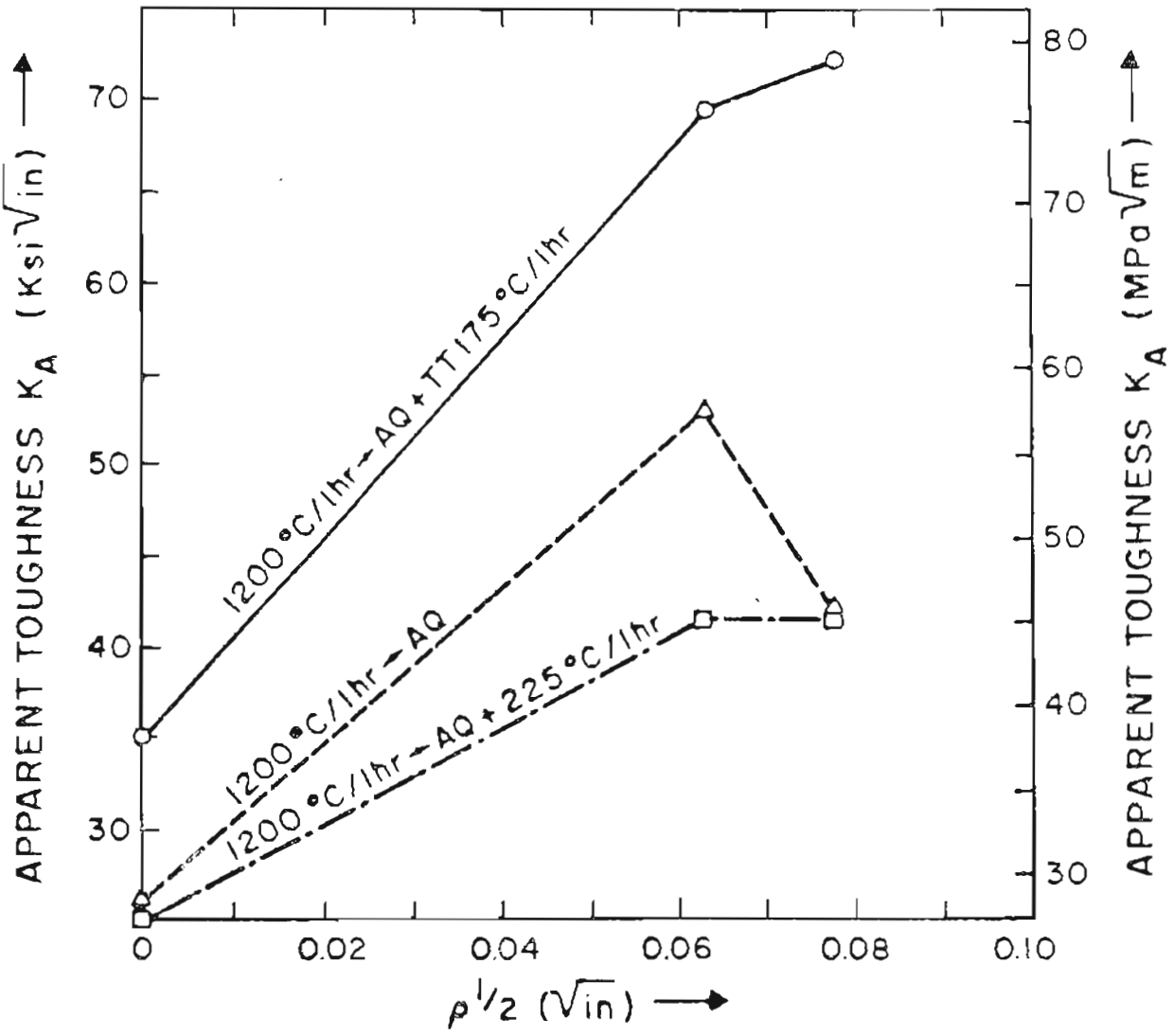

Fig. 4.8 Effect of notch root radius on the toughness of 4340 steel given different heat-treatments by instrumented Charpy test at liquid nitrogen temperature.

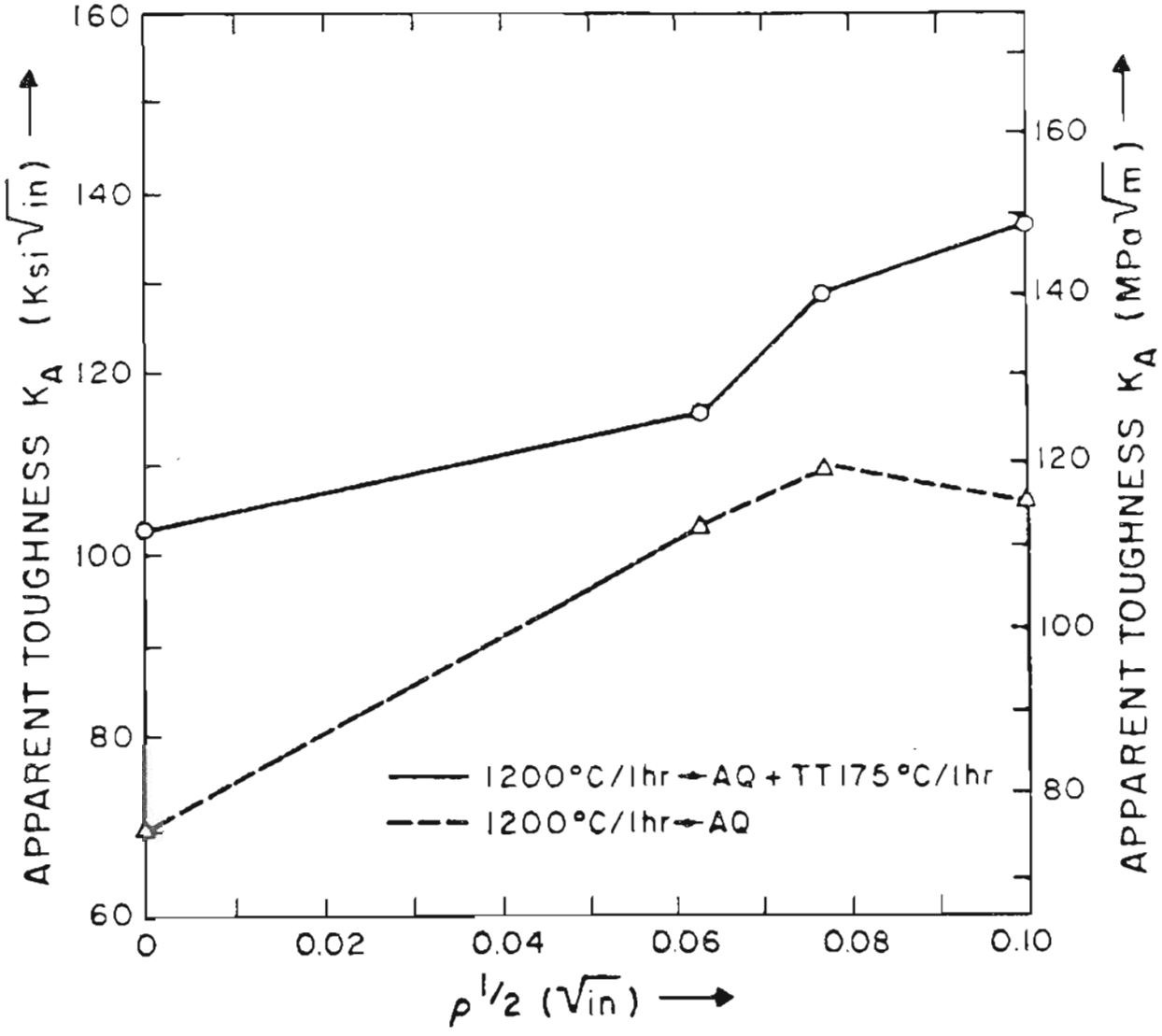

Fig. 4.9 Effect of notch-root radius on the toughness of 4340 steel given different heat-treatments by instrumented Charpy test at room temperature.

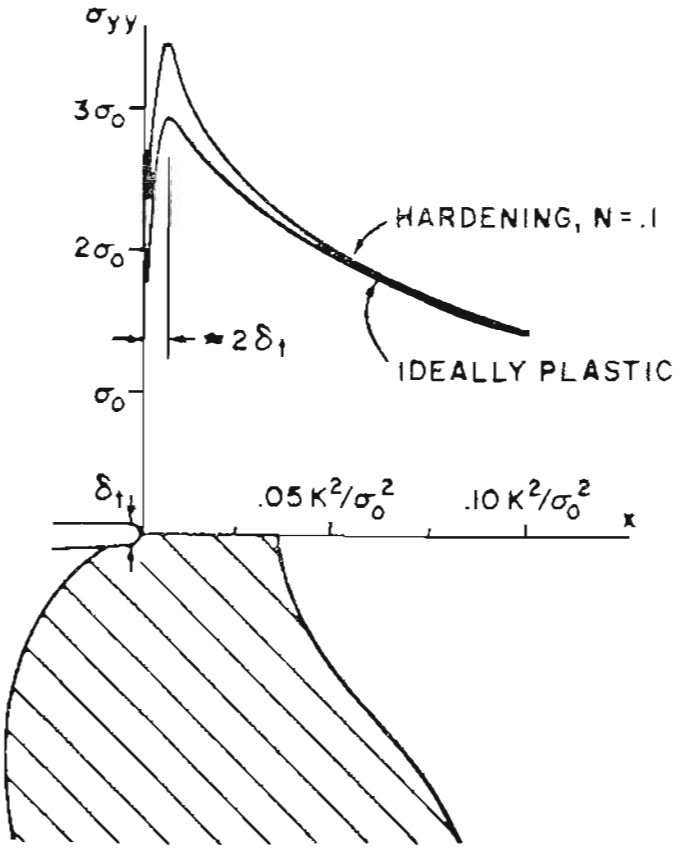

Fig. 4.10 (a). Distribution of normal stress as a function of position ahead of an initially sharp crack tip. Cross hatching schematically indicates plastic zone shape.

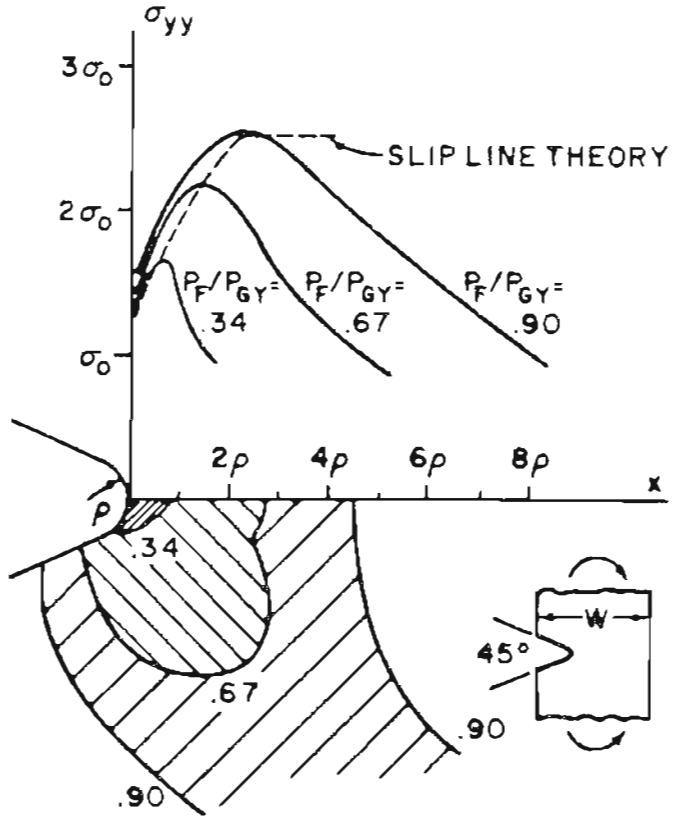

Fig. 4.10(b) Distribution of normal stress as a function of position ahead of an initially blunt crack tip. Cross hatching schematically indicates plastic zone shape.

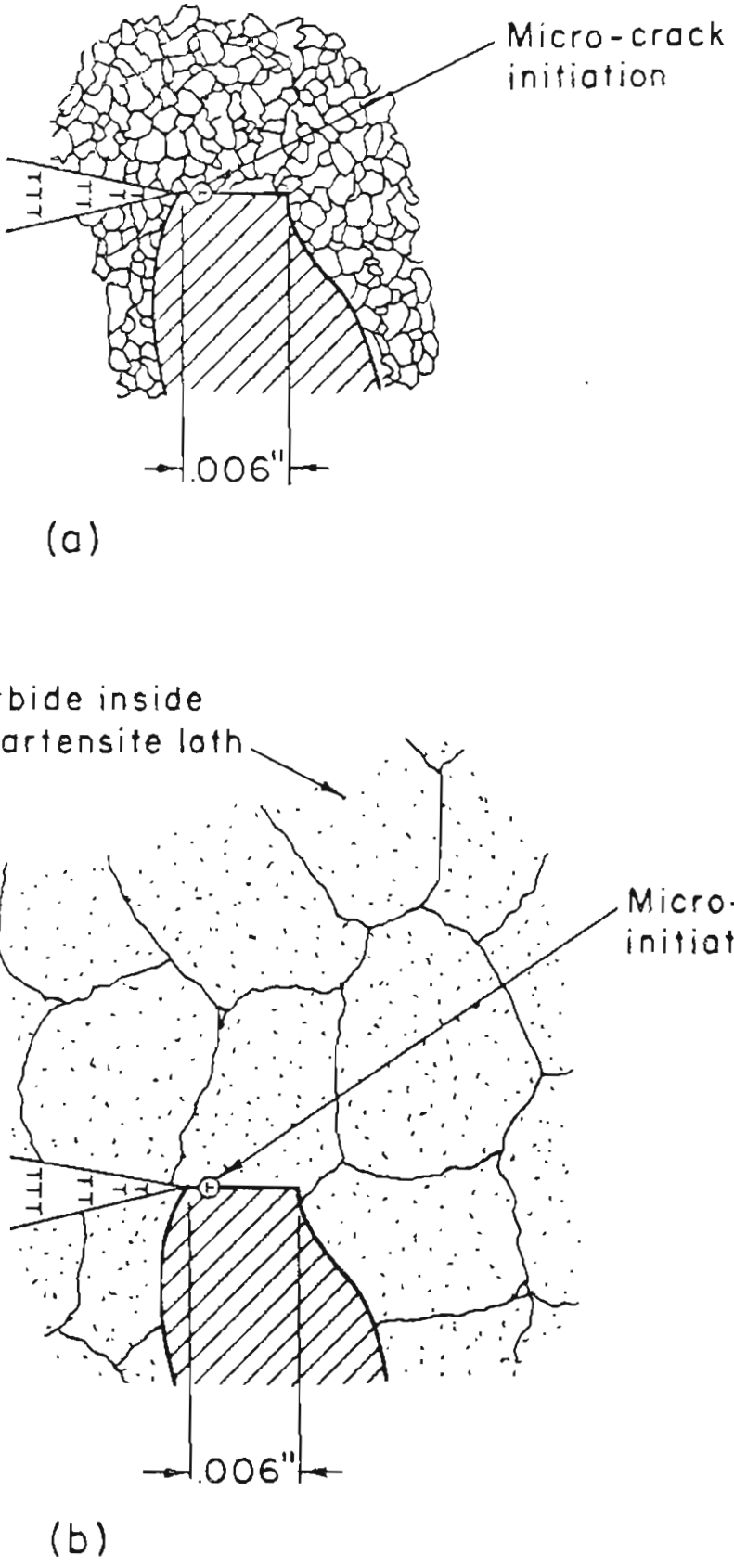

Fig.4.11. Schematic crack nucleation site for sharp-crack testing condition, (a) for low grain size material, (b) for high grain size material.

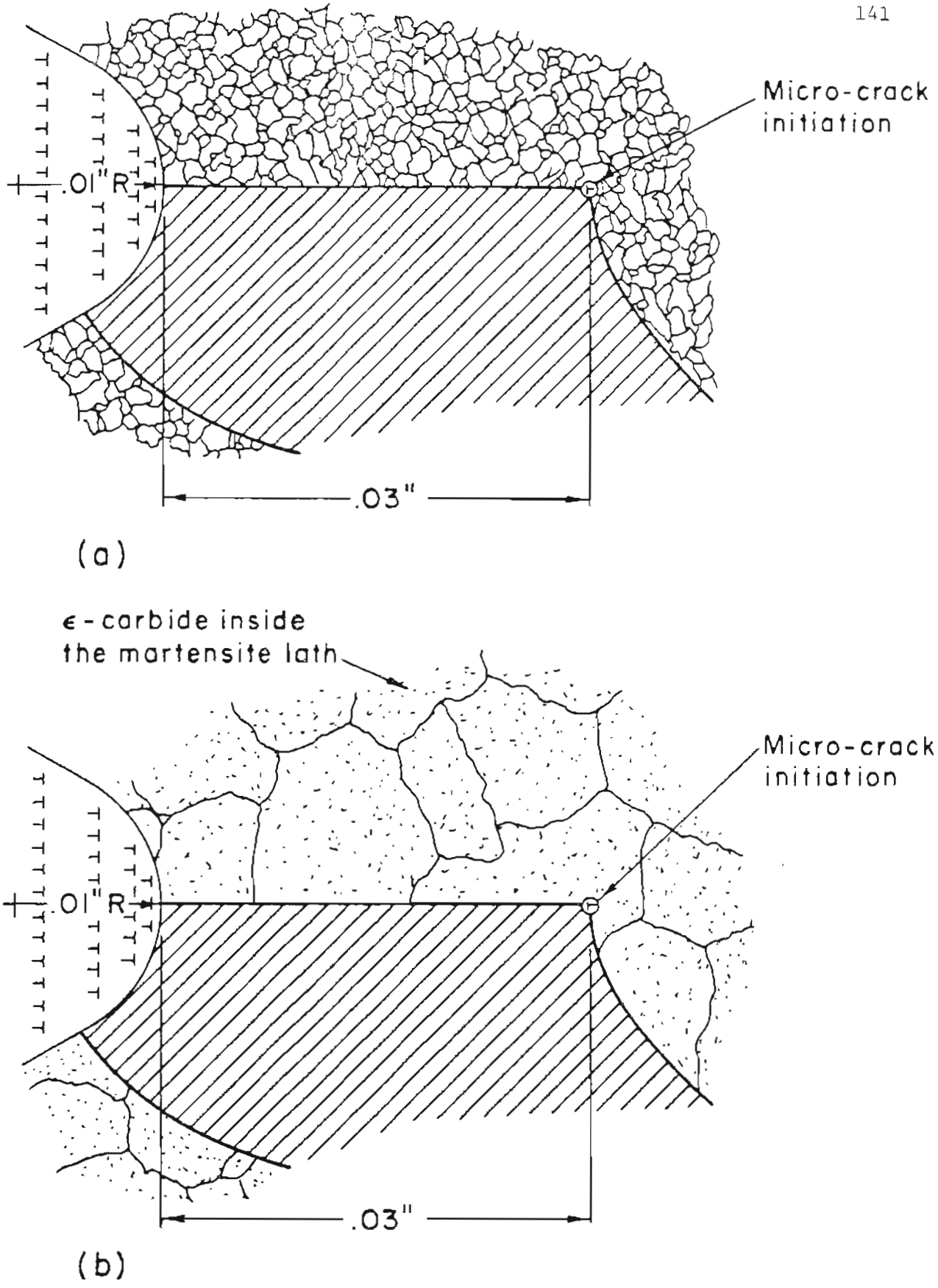

Fig. 4.12 Schematic crack nucleation site for blunt-notch testing condition (i.e. Charpy testing), (a) for low grain-size material, (b) for high grain-size material.

main crack: but, ten times fewer grain boundaries for high austenitizing temperature than for low austenitizing temperature. Grain boundaries are natural obstacles for the propagation of dislocation and an inverse of square root of grain-size relationship has been obtained for both yield stress and fracture stress (125, 126). Hence, based on the same argument, if the fracture stress to create a source of dislocation for the initiation of crack is taken as σ_f^*, the actual fracture stress σ_f will be

$$\sigma_f = \sigma_f^* \qquad \text{(for pre-cracked condition)}$$
$$\text{and} \qquad \sigma_f = \sigma_f^* + kd^{-1/2} \qquad \text{(for blunt notch condition)} \tag{4.5}$$

where k is a constant.

These equations also point out that in the pre-cracked condition the fracture stress is independent of grain size, whereas in blunt notch condition it is inversely related to the square root of the grain size. Also in the blunt notch condition, the fracture stress is always higher than in the pre-cracked conditions since d is a positive quantity. This is also consistent with the experiments.

In the light of this discussion, the anomaly of pre-cracked and blunt notch toughness between high temperature and low temperature austenitizing -reatment of 4340 steel can be resolved. For the high austenitizing treatment σ_f^* is higher because carbon distribution leading to more ε-carbide precipitation takes place earlier for the high temperature austenitization than in the low temperature austenitization (described in section 4.3 in more details). Hence, in the pre-cracked

condition the fracture stress, σ_f is higher. However, for the same heat-treatment in the blunt notch condition, even though σ_f^* is higher, the second term is considerably lower, (i.e. $kd^{-1/2}$) leading to lower fracture stress σ_f. Thus in Charpy testing which has a blunt notch the lower austenitizing temperature produces a higher toughness because of smaller grain size. Also, the highest toughness for a blunt notch will be obtained when both σ_f^* is high and the grain size is small, i.e. for a 4340 steel which has been austenitized at 870°C and subsequently tempered at 175°C leading to fine precipitates of ε-carbide. The variation of fracture toughness with notch root radius for this heat-treatment is shown in Fig.4.13. and the blunt notch toughness will be lowest when both σ_f^* is low and grain size is high, i.e. for a 1200°C → 870°C step quench treatment. Here the grain size is the same as that for the direct quench for 1200°C. Fig. 4.13 shows the toughness as a function of root radius for this treatment (the 870°C and 1200°C treated results are also shown). Thus the above discussion explains the toughness behavior observed for both sharp crack and blunt notch testing conditions for a variety of heat-treatments.

4.3 The Effect of Microstructure on the Toughness: - The effect of microstructures on mechanical properties has been studied by material scientists for many years. This investigation studied the key aspects of microstructural features of high temperature austenitization of 4340 steel in both as-quenched and tempered condition and their contribution to toughness. The effects of microstructures on the toughness have been divided into two groups; (a) the effect of bainitic heat-treatment on the toughness, (b) the effect of martensitic heat-treatment on the toughness.

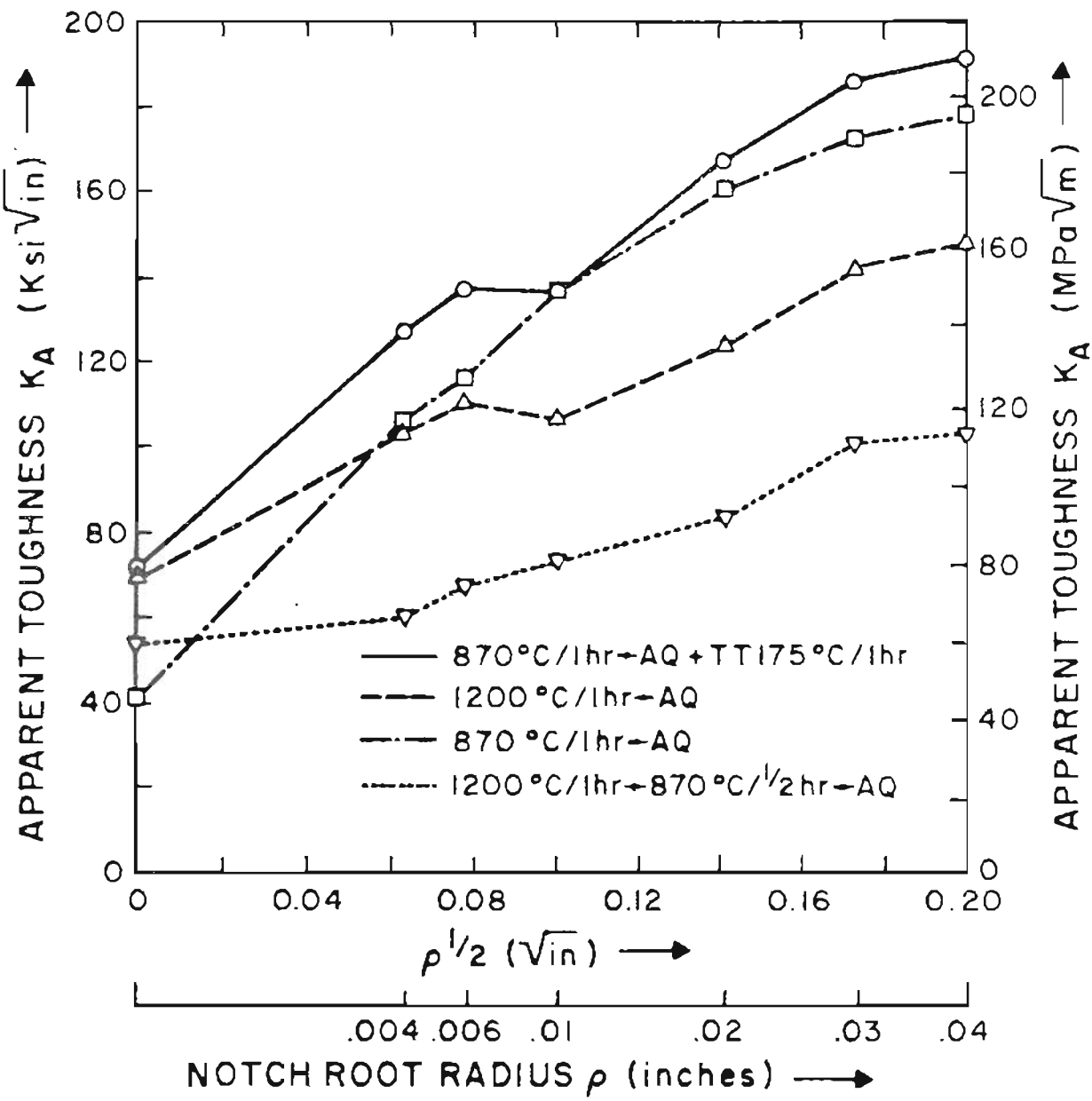

Fig. 4.13 Effect of notch root radius on the toughness of 4340 steel given different heat-treatments by instrumented Charpy test at room temperature.

4.3.1 The Effect of Bainitic Heat Treatment on the Toughness

The mechanism of bainite formation, even though postulated as long as 40 years ago, still is a matter of controversy, and has been summarized in a recent debate. (127). While it has been accepted that bainite is a two-phase structure of ferrite and carbide and that carbide is within the ferrite lath in lower bainite and at the ferrite lath boundaries in upper bainite, the mechanism of formation of such structures has not been agreed upon. While the growth of the ferritic component of bainite is usually attributed to a shear mechanism (127), Kinsman and Aaronson (127) proposed a ledge mechanism involving diffusion. Also, as for the source of bainitic carbide precipitation, Heheman (127) postulated an invariant metastable eutectoic reaction $\gamma \rightarrow \alpha$ + ε-carbide, which later changes to cementite, while Kinsman and Aaronson (127) concluded that precipitation from austenite at the austenite/ferrite boundaries is the primary source of bainitic carbide precipitation. It seems that both the mechanisms may be operative at two extremes of lower and upper bainite. In Lower bainite the carbon may be taken into the ferrite and subsequently precipitated behind the ferrite-austenite interface, while in upper bainite the ferrite grows into the austenite matrix pushing carbon ahead of it until carbide is nucleated in the carbon-enriched regions between the ferrite grains (128). As for the strengthening mechanism, Pickering (129) has stressed the importance of bainitic ferrite grain size. (shown in Fig. 4.14). The bainitic ferrite grain size depends upon the size of the untransformed austenite region in which the bainitic ferrite can grow.

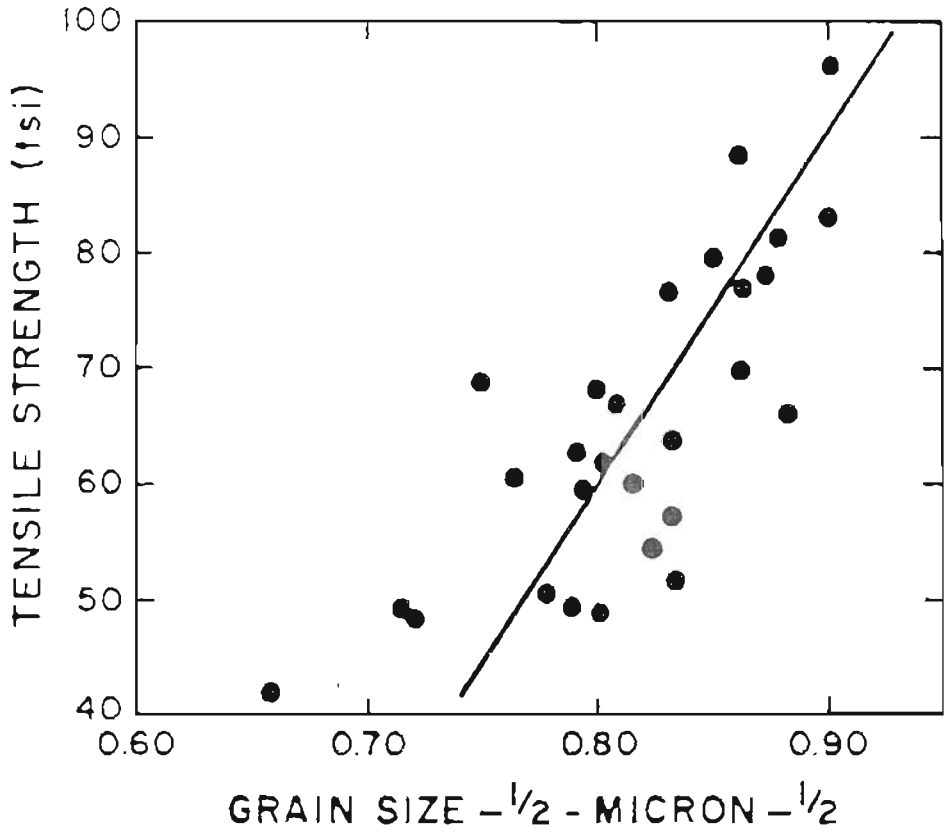

Fig. 4.14 Effect of grain size on strength of bainite steels

As stated in Sec. 3.1.3, the bainitic treatment from a 1200°C austenitizing treatment does not produce high toughness. Two facts are important, when the steel is austenitized at 1200°C, instead of the conventional 870°C, i.e. (a) higher Ms temperature, (b) higher prior austenite grain size. Higher Ms temperature also indicates higher diffusion of carbon at the bainitic holding temperature which is helpful for the growth of bainitic plates. The size of the bainitic plate depends on structural inhomogeneity such as the grain boundary or another bainite plate which will halt its growth. It is then not unreasonable to assume that both these factors combine to give a large bainitic ferrite size. As stated earlier, a large bainitic ferrite size is detrimental to strength and hence the poor toughness by the bainitic treatment from a high austenitizing temperature can thus be attributed to a large bainitic ferrite size.

4.3.2. The Effect of Martensitic Heat Treatment (as Quenched and Quenched and Tempered) on the Toughness

In pre-cracked fracture toughness and Charpy specimens, it has been shown that higher austenitizing treatment renders better toughness than lower austenitizing treatment in as-quenched condition and also after tempering up to a temperature of 200°C independent of the test method. The stress distributions ahead of a sharp crack and blunt notch are significantly different (this point was discussed in greater details in Section 4.2) (123,124). However, in the pre-cracked condition, the stress distribution is the same, independent of heat treatment the specimens has undergone. Hence, the toughness difference in the as-quenched

condition between the 870°C and 1200°C austenitizing treatments are due to essential microstructural differences.

The fracture toughness variation of this and other alloys given similar heat-treatment has been variously correlated with the amount of retained austenite, the extent of twinning, segregation of trace elements and grain size. Transmission electron microscopy results (1) have documented the presence of more retained austenite and very few twins in the 1200°C austenitizing treatment compared to extensive twinning and less retained austenite in the 870°C austenitizing treatment. Magnetic measurement of the amount of retained austenite (3) on the other hand has indicated that there was no difference in the amount of retained austenite in the above two treatments. Initial studies have shown that there was no segregation above a austenitizing temperature of 1100°C (130,131); however, recent studies have detected the segregation of P and N at high austenitizing temperatures (132), and segregation of P at 1300°C (133). High temperature austenitization always produces a grain-size which is one order higher than that in the conventional austenitizing treatment (i.e. 250 μm against 25 μm).

With respect to time temperature transformation diagrams from low and high austenitizing temperatures the two most noticeable features are (a) higher Ms temperature for higher austenitizing temperature, (b) shorter time for the bainitic transformation from higher austenitizing temperature.

The Ms temperature of a steel depends predominantly on three factors (134,) (a) the equilibrium temperature (To), (b) the strain

and surface energy of nucleation (F_N) and the existence of sites for heterogeneous nucleation, i.e. grain boundaries, (c) the stress which has to be overcome to shear the austenite into martensite requires additional energy (if heterogeneous nucleii are available)F_τ.

The energy needed for the start of martensite formation

$$\Delta F_{\alpha r} > F_N + F_\tau$$

This corresponds to an undercooling

$$\Delta T = T_o - M_s = \frac{F_N + F_\tau}{\Delta s_{\alpha\gamma}}$$

$\Delta s_{\alpha\gamma}$ is the transformation entropy and the difference in specific heats is neglected.

Higher Ms temperatures mean lower ΔT and hence either lower value of the combined term ($F_N + F_\tau$) or higher value of $\Delta s_{\alpha r}$. High austenitizing temperature gives higher grain size or lower grain boundary areas. Hence, F_N will be lower. Similarly F_τ will also be lower for high austenitizing treatment, since it produces mostly dislocated martensite in the as-quenched state in contrast to twinned martensite in the conventionally treated specimen (1). $\Delta s_{\alpha r}$ may also be higher, because transformation takes place at a higher temperature.

A higher Ms temperature also results in higher diffusivity of carbon atoms in martensite during quench. The role of carbon in austenite and carbon precipitation in subsequent transformation has been extensively documented (10,135). The stable phases of Fe-C alloys at high

(>723°C) and low (<723°C) temperatures are γ-iron with carbon in solid solution and α-iron and graphite respectively. However, at low temperatures carbon forms a metastable compound cementite (Fe_3C) which for all practical purposes can be taken as the stable phase. When austenite is transformed into martensite, carbon atoms which are in solid solution in γ-Fe and randomly distributed, first segregate to the lower energy dislocation sites. As the tempering proceeds, the first phase to precipitate is ε-carbide, which forms along $\langle 100 \rangle_\alpha$ with a definite orientation relationship. At still higher tempering temperatures cementite begins to precipitate. Also the transition from ε-carbide to cementite does not occur in situ. Therefore, the important point above is that even though cementite is the final phase, the process goes from carbon in dislocation sites to clustering of carbon atoms to precipitation of ε-carbide and finally to precipitation of cementite. From internal friction measurements (136), it has also been shown that carbon segregation to dislocation sites occurs earlier in the higher austenitizing case than in the lower austenitizing treatments. The experimental observations in this investigation have demonstrated (a) a shorter time for the start of bainitic transformation from the higher austenitizing temperature, (b) more carbide particles in bainitic structure given similar holding time at the bainitic transformation temperature from a higher austenitizing temperature, (c) evidence of ε-carbide particles in the as-quenched martensitic lath from the higher austenitizing temperature. These strongly indicate carbon redistribution (specifically ε-carbide precipitation) is an essential feature for the two heat treatments and hence may contribute to the observed

variation in toughness behavior. The other two important microstructural features in as-quenched condition for the two heat treatments are reported to be (a) more retained austenite, (b) less twins (1) for the higher austenitizing treatment. However, it was stated earlier, retained austenite measurement by an X-ray technique (3) for both the treatments has produced identical results for the two heat-treatments. As discussed before, absence of twins may be closely related to higher Ms temperature and consequent carbon segregation leading to ε-carbon precipitation.

ε-carbide precipitation in the martensite lath is consistent with the microvoid coalescence fracture morphology of high temperature austenitized as quenched sample, (117,137). Initiation of the void takes place at the carbide/matrix interface, which grows on subsequent loading and finally when the coalescence of the microvoid takes place, fracture occurs. In contrast, the fracture morphology of conventional temperature austenitized, as-quenched sample, is quasi-cleavage, and/or intergranular cleavage, which again is consistent on the basis of lack of such carbide particles. This difference in fracture morphology on the basis of ε-carbide particles also explains the high fracture toughness for the high temperature austenitized as-quenched sample.

Finally, as will be seen shortly, that the entire process of carbon redistribution is accelerated by high temperature austenitization, is also reflected by the tempering behavior of such steels. A consistent drop in toughness by all fracture tests was observed for the high temperature austenitizing treatment for a tempering temperature of as low

as 225°C, which is concommitant with the precipitation of cementite. While tempered martensite embrittlement has been a subject of many investigations (138,139) in recent years, the present results differs significantly from all reported literature. Firstly, the decrease in toughness value by all methods of testing is considerably higher. Secondly, tempered martensite embrittlement (TME) is normally characterized by transgranular fracture (138,139) while the present results show an entirely intergranular brittle fracture. Thirdly, destabilization of retained austenite (138,139) constitutes a major mechanism of TME, whereas the present embrittlement is coincident with predominantly cementite precipitation.

The fracture toughness variation of this and other alloys given similar heat-treatment has been variously correlated with the amount of retained austenite (1, 139), the extent of twinning, (1) segregation of trace elements (132) and grain size (1,2,3). The presence of twins in this investigation was found to be a function of the prior austenitizing temperature and not the subsequent tempering temperature. Also, it has been documented that 4340 steel austenitized at 1200°C and directly quenched produces mostly dislocated lath martensite and not twinned martensite. Grain size may in some cases affect the toughness, but grain size both before and after the embrittlement treatment in high temperature austenitization was the same and cannot be responsible for the observed behavior. The exact role of retained austenite and the amount present has been elusive, since the amounts present are small and accurate analysis difficult. Transmission electron microscopy results have well documented

the presence of retained austenite after a 1200°C austenitizing treatment (1). These studies have also shown a noticeable lack of retained austenite after the conventional 870°C treatment. Magnetic measurements (3) of the amount of retained austenite on the other hand have indicated that the stability was apparently the same whether in the as-quenched or in the tempered condition. Collectively, the past results as well as the present study indicate that the presence, distribution and stability of retained austenite in samples austenitized at 1200°C does not control the variation in fracture properties, when tempered at these low tempering temperatures.

The present results indicate that cementite precipitation is a necessary condition for the onset of tempered martensite embrittlement. The fact that the addition of silicon (20) increases the embrittlement tempering temperature range (for 300M austenitization at 1200°C) suggests that the mechanism for TME is one of cementite precipitation. However, cementite precipitation alone cannot be solely responsible for embrittlement, since embrittlement does not occur in high purity steels (140); neither does it account for the intergranular nature of the fracture surface, since cementite does not precipitate in grain boundary alone. Impurity segregation of trace elements such as S, P,N or even substitutional elements like Cr, Mn, etc. in conjunction with cementite precipitation near the prior austenite grain boundaries has been proposed by several workers to explain the change in fracture mode (132, 140, 141). Segregation of P after precipitation of cementite was also proposed by some (142). Earlier investigations (130, 131) showed that no segregation occurs beyond

an austenitizing temperature of 1100°C. However, recent investigations (132) have indicated segregation of P and N at 1160°C and segregation of P at 1300°C (133). The present results tend to support the segregation of impurities at the austenitizing temperature. Since the embrittlement is absent in high purity steels, it seems plausible that the impurity effects are inherited from the austenite and the cementite precipitation triggers the embrittlement by providing additional slip barrier at the already impurity-weakened boundaries. That also explains why the fracture is intergranular. In summary, segregation at the prior austenite grain boundary and the cementite precipitation during tempering lead to the above embrittlement.

5. SUMMARY AND CONCLUSIONS

High temperature austenitization of low alloy high strength steel like 4340 has been of considerable interest in recent years. The objective of such modification is to achieve a high toughness while maintaining the same level of yield strength. The present investigation studied different aspects of high temperature austenitization of 4340 steel carried out in several phases.

In the first stage the notch root radius effect on the toughness of 4340 after conventional and high temperature austenitizing in both as-quenched and tempered condition has been studied in greater details than has been attempted before. This involved greater range of notch root radii, greater number of prior heat-treatments, carrying out tests at high and low strain rates and also at room and liquid nitrogen temperatures. In the second phase, tempering behavior of 4340 steel after high temperature austenitization has been studied, since tempering in general, renders still higher toughness. In the last stage a few exploratory bainitic heat treatments from high temperature austenitization have been attempted, as bainitic microstructures are sometimes better or as good as martensitic microstructures.

1. The variation of toughness with notch root radius for various heat-treatments showed that the toughness initially increased with increasing notch root radius. Thereafter, when a critical notch root radius was reached, toughness decreased with a further increase in the notch-root radius. The drop in toughness is also associated with an

intergranular fracture initiation mode. The critical root radius, at which such phenomena occurs, is strain-rate and temperature dependent but independent of prior austenitic grain size. It is also independent of the plastic zone size.

2. The initial increase in toughness with increasing notch root radius up to the critical root radius is consistent with a critical stress or strain model; the critical strain-energy density fracture criterion is applicable beyond the critical notch root radius, when the toughness drops. The intergranular fracture mode may be possible due to double slip bands operating ahead of the notch-root.

3. In pre-cracked specimens, i.e. slow-bend Charpy, instrumented Charpy and fracture toughness tests the high temperature austenitization always produced a higher toughness than did the conventional austenitization temperature in as-quenched condition as well as up to a tempering temperature of 200°C. The improvement in toughness in as-quenched condition from high temperature austenitization is also associated with a microvoid coalescence fracture initiation mode. It is believed that ε-carbide precipitation from high temperature austenitization in as-quenched condition is the primary cause for such fracture initiation mode and consequently higher toughness.

4. In blunt notch testing conditions, i.e. slow bend Charpy V-notch, instrumented Charpy V-notch on ASTM bend specimens with a blunt notch root radius equal to Charpy notch root radius, the conventional austenitization temperature produced a slightly better toughness in

as-quenched condition and significantly better toughness as the tempering temperature was increased. The improvement of blunt notch toughness for the conventionally treated 4340 steel is attributed to fine austenitic grain size.

5. The tempering behavior of 4340 steel, which has been austenitized at high temperature (1200°C) and subsequently oil-quenched, showed that toughness increased from as-quenched condition up to a tempering temperature of about 200°C, however, there was a drop in toughness for a tempering temperature as low as 225°C. On the other hand, there was no such drop in toughness in similar tempering temperature range for a 4340 steel, which had been austenitized at a conventional temperature (870°C). The 'temper embrittlement' was also associated with an intergranular fracture failure mode. It is believed that prior austenitic grain boundary segregation coupled with cementite precipitation during tempering has triggered the above embrittlement.

6. The limited bainitic heat-treatments from high temperature austenitization studied in this investigation resulted in lower fracture toughness or tensile strength than that obtained from direct quench. The poor mechanical properties produced by such heat treatments are attributed to large bainitic ferrite grain size.

APPENDIX

The appendix is provided for those readers who may be unfamiliar with certain technical terms used in the main text. However, it may be worthwhile to review the macroscopic (i.e. toughness testing) and the microscopic aspects of fracture. Current models regarding effect of notch-root radius on the toughness have also been described in details. This has been considered necessary for the anomalous toughness behavior with notch-root radius obtained in this investigation. The appendix is divided into four sections. (1) Microstructure of steel, (2) toughness testing, (3) the effect of notch-root radius on the toughness, and (4) microscopic aspects of fracture.

A.1. Microstructure of Steel - Steel has a large number of microstructural constituents namely pearlite (coarse, fine, divorced, etc.), carbide (ε-carbide, Hagg carbide, cementite, etc.), ferrite (α-ferrite, δ-ferrite), martensite, (lath, plate), bainite (upper and lower), to name a few; however from a strength and toughness viewpoint, two constituents (as far as this investigation is concerned) are important, i.e. martensite and bainite. Hence, only these two will be described briefly in the following sections.

A.1.1. Martensite - The name martensite was originally proposed by Osmon in 1895 in honor of the German metallurgist, Adolph Martens (22), to describe the microstructure found in hardened steels. Martensite is best described by a time-temperature-transformation diagram (TTT diagram)

and Fig. A.1 describes such a diagram for a .8% C steel (28). Martensite will be produced when the parent austenite is cooled at a rate faster than the critical cooling rate to avoid the nose of the TTT diagram.

Martensite transformation has many characteristics (22-27), notable among which are (a) that it is a diffusionless transformation, (b) plate-like volume transform with the speed of sound as the temperature is falling below the M_s (M_s is the highest temperature for the first martensitic nucleus to form), (c) that it generally does not form while the temperature is held constant, (d) martensite is highly strained because of super-saturation of carbon and (e) that the product has definite crystallographic habit and lattice orientation relationship with respect to the parent phase. Based on the lattice correspondence of the parent and the product phases, both Bowles and Mackenzi (27) and Lieberman, Wechsler and Read (25), postulated that the transformation from austenite to martensite involves three steps: (a) Bain distortion of the correspondence lattice, (b) inhomogeneous shear deformation by either slip or twin, (c) a rotation of the lattice, although not in sequential order.

The strength of martensite primarily depends on two factors (26), (a) high density of dislocations in the lath martensite and also at the lath boundary, (b) carbon atom redistribution leading to pinning of the dislocations.

A.1.2 Bainite - Bainite is the product formed, if the steel is held above M_s and allowed to transform (see Fig. A.1). The mechanism of bainite formation is still controversial, even 40 years after its discovery.

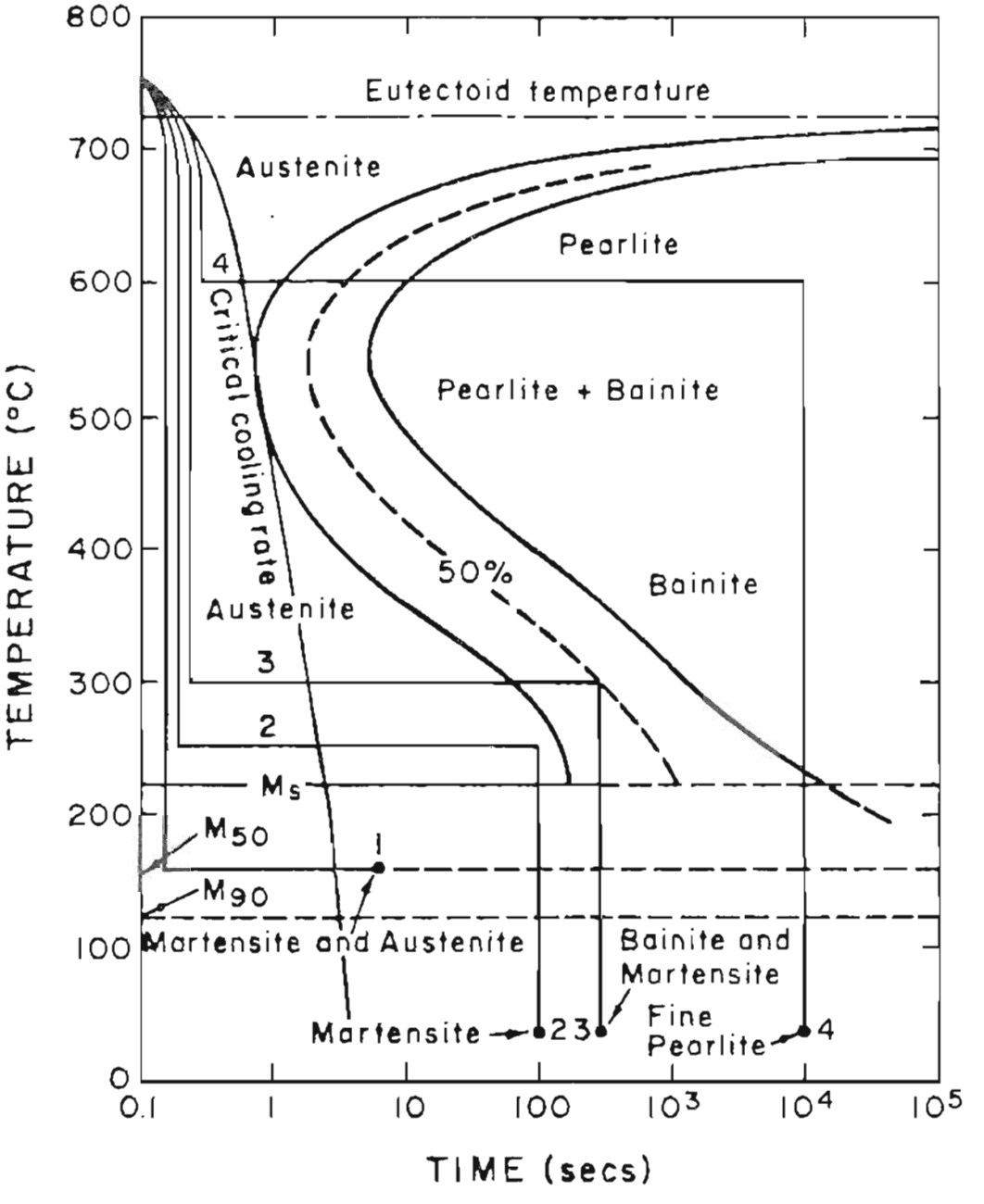

Fig. A.1. Arbitrary time-temperature paths on an isothermal transformation diagram for a 0.8% C steel.[28]

However, bainite has been found to provide good mechanical prospects in terms of tensile strength, impact transition temperature and ductility. The factors that have been agreed to characterize bainite (15,16,29-31), are:

1. The volume transformed, X vs time follows nucleation and growth type kinetics in that X initially rises slowly but at an ever increasing rate, and then finally levels off to its final value.

2. The product always consists of plates of ferrite with carbides precipitated either between plates (higher temperatures) or inside the plates (lower temperatures). The carbide in upper bainite has been identified to be cementite while that in lower bainite is ε-carbide.

3. There is a change in shape that accompanies the transformation. If a piece of austenite with an initially smooth surface is partially transformed, the bainite plates give relief markings when they form.

A.2. Toughness Testing - There are essentially five reasons (32) why toughness tests are carried out to evaluate a material's resistance to fracture:

1. To determine whether there is a strong probability that catastrophic fracture will occur in a particular material, loaded under a given set of conditions, (i.e. determination of ductile-brittle transition temperature).

2. For use in choosing between potential materials for a particular application (i.e. is material A more 'brittle' than material B?).

3. For quality control tests by the materials producer.

4. For analysis of failures that have occurred in service.

5. To obtain data that can be directly used for design purposes (i.e. maximum working stress, minimum operating temperatures, service lifetime).

There are many toughness tests such as the Charpy V-notch test, Izod test, tensile test, drop-weight test, etc. But the Charpy V-notch test is most popular because it is inexpensive, easy to carry out and consumes a nominal amount of material. Essentially it measures the energy required to break a notched test bar of given dimensions.

However, with the advent of linear elastic fracture mechanics (LEFM) some sophisticated tests like fracture toughness testing (33) have come into practice and the essence of the test is that the stress-intensity factor, which is a function of both stress and crack-length, reaches a critical value known as the fracture toughness, instantaneous crack initiation will take place. As the above two tests were used in this investigation for toughness evaluation, the relevant information on them is provided next.

A.2.1 Fracture of Charpy V-Notch Specimens - The Charpy specimen is a rectangular bar of dimensions of 0.394" x 0.394" x 2.165" with a .079" deep machined V-notch (ref. Fig. A.2). It has been used extensively

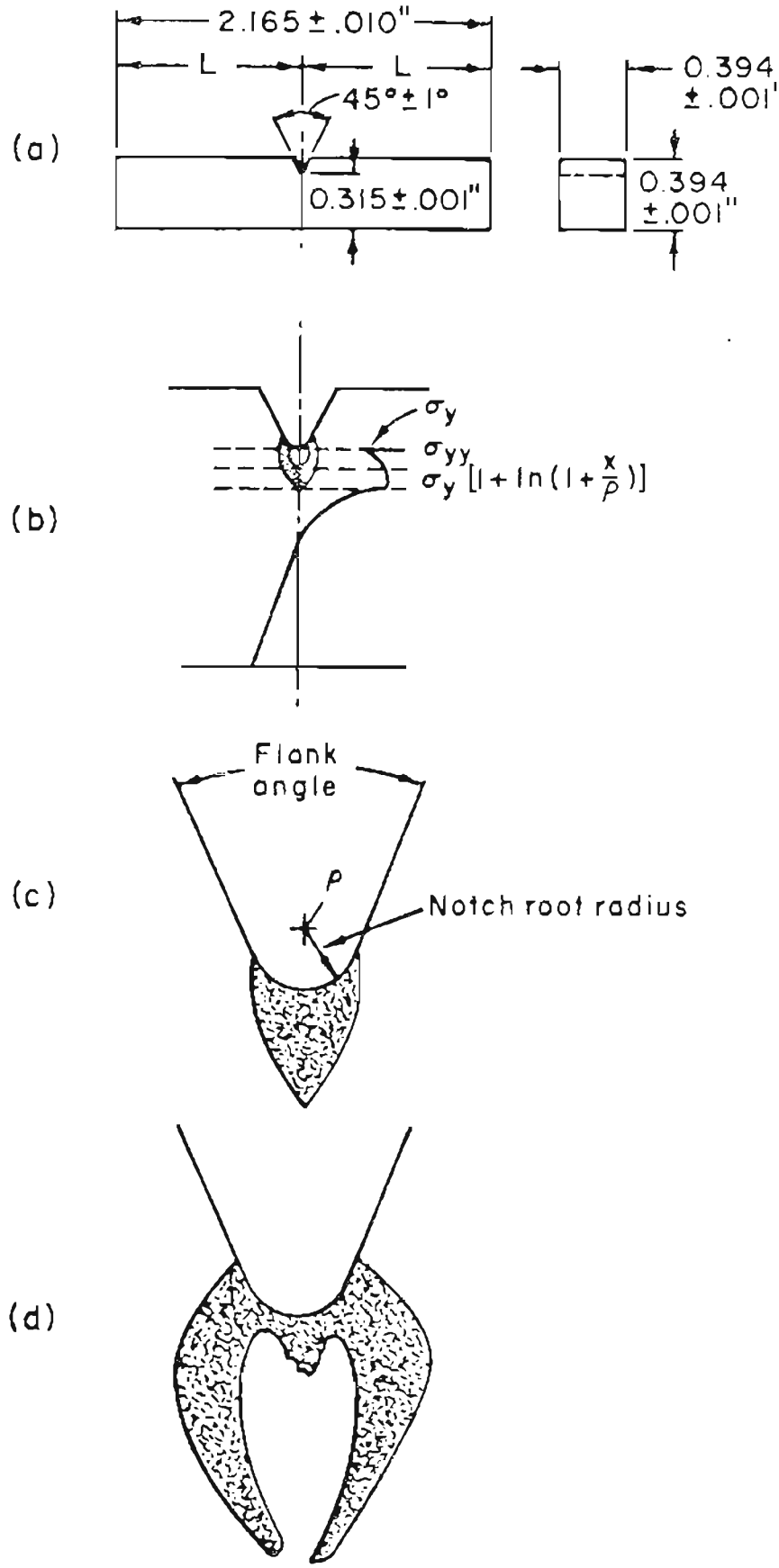

Fig. A.2 (a) Charpy specimen, (b) schematic elastic-plastic stress distribution for a notched bar in plane strain bending, (c) plastic zone shape - wedge type (logarithmic spiral), (d) hinge type.

by metallurgists to study the fracture properties of materials, and many engineering safety codes including nuclear applications are based on Charpy specimens.

The specimen is broken under the hammering action of a pendulum in three-point bend loading and the energy absorbed in breaking the specimen is known as the toughness. This is the standard ASTM test as per E-23, Part 31, 1969.

The results from standard Charpy impact tests cannot be directly correlated with tests designed from fracture mechanics principles. Hence, various Charpy tests have been developed recently, notably among which are the instrumented Charpy test and the slow-bend Charpy test. The specimens are loaded in 3-point bending as before. Both pre-cracked and standard specimens with 0.010" root radius are used, depending on the nature of the test. Since these specimens have become the common type used for fracture testing, they have been studied in detail. Deformation and fracture of Charpy specimens have been quantitatively analyzed by several people (34-36). However, no ASTM Standards are in existence for such tests.

A.2.1.1 General Yield Load - During loading of a Charpy type specimen a small region below the notch starts to yield while the rest of the material is still deforming elastically. The plastic flow-lines at this stage are of the form of logarithmic spirals and the local stress condition can be approximated by the following equation (37):

$$\sigma_{yy} = \sigma_y \left[1 + \ln \left(1 + \frac{R}{\rho}\right)\right] \qquad A\text{-}1$$

where σ_{yy} = Longitudinal stress in the y-direction σ_y = Yield strength R = Distance from the notch-root ρ = Notch root radius

On further loading, the flow pattern develops into plastic hinges (Fig. A.2) which spread across the specimen ligament at general yield load P_{GY}. At this load the entire section of the specimen is plastically deformed. P_{GY} is dependent on the geometry and is proportional to the tensile yield strength of the material. Since yield strength is strain rate dependent so is P_{GY}. The relation between yield strength and the general yield load has been given by Green and Hundy (34), for pre-cracked and also as a function of notch root radius.

Assuming Tresca's (38) criteria ($\sigma_{ys} = 2k$), k = shear yield strength, the relationship for standard Charpy may be expressed as

$$\frac{P_{GY}}{B(W-a)} = 0.242\ \sigma_y \qquad A.2$$

where B is the specimen thickness, W is the specimen width, a is the crack length (notch depth).

For a pre-cracked Charpy specimen the flank angle is close to zero and equation A.2 becomes (34)

$$\frac{P_{GY}}{B(w-a)} = 0.252\ \sigma_y \qquad A.3$$

The root radius of the notch has a very small effect on these relationships, as shown experimentally (ref. Fig. A.3) which shows that the general yield load is independent of the root radius of Charpy specimens. This result has been also observed by Wilshaw, etal (39).

A.2.1.2 Dynamic Fracture Toughness from Instrumented Charpy Test: As stated earlier, the results from standard Charpy impact tests cannot be directly used in fracture mechanics equations. However, by instrumenting the tup of the Charpy hammer with strain gages, load-time information can be obtained. which makes it possible to determine the dynamic fracture toughness, K_{Id} (40-45). An idealized load-time record is shown in Fig. A.4. Fracture toughness calculations according to linear elastic fracture mechanics principles (46) are made by the following relations:

$$K_{ID} = \frac{1.5\ YL\ (P_M)}{BW^2}\ a^{1/2} \qquad A.4$$

where

W = width. L = length. B = thickness. a = notch depth

$$Y = 1.93-3.07(a/w) + 14.53(a/w)^2 -25.11(a/w)^3 + (25.8)\ (a/w)^4,$$

and P_M is the applied load at fracture pop-in when fracture occurs before general yielding. Equation A.4 reduces to the following when the appropriate Charpy dimensions and loading are considered:

$$K_{ID} = 38.7\ Y\ (P_M)\ a^{1/2} \qquad A.5$$

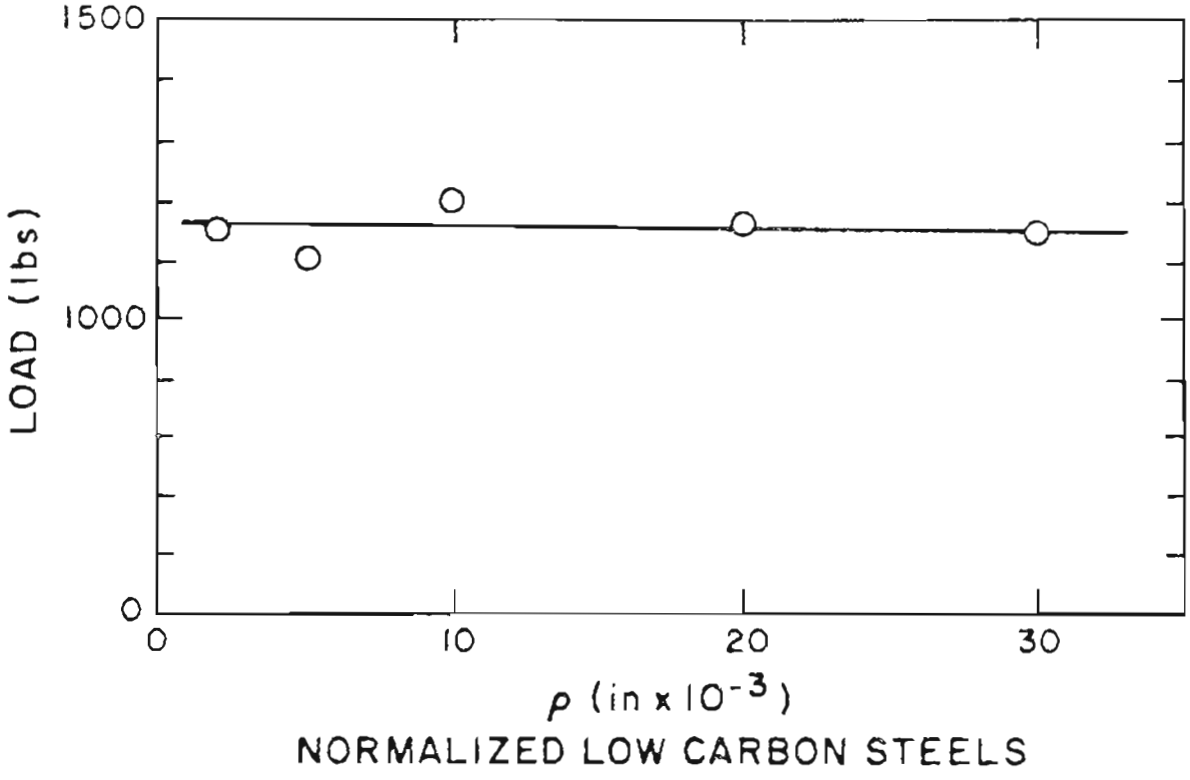

Fig. A.3 Variation of general yield load with the notch root radius for a low-carbon steel during slow bending at room temperature.

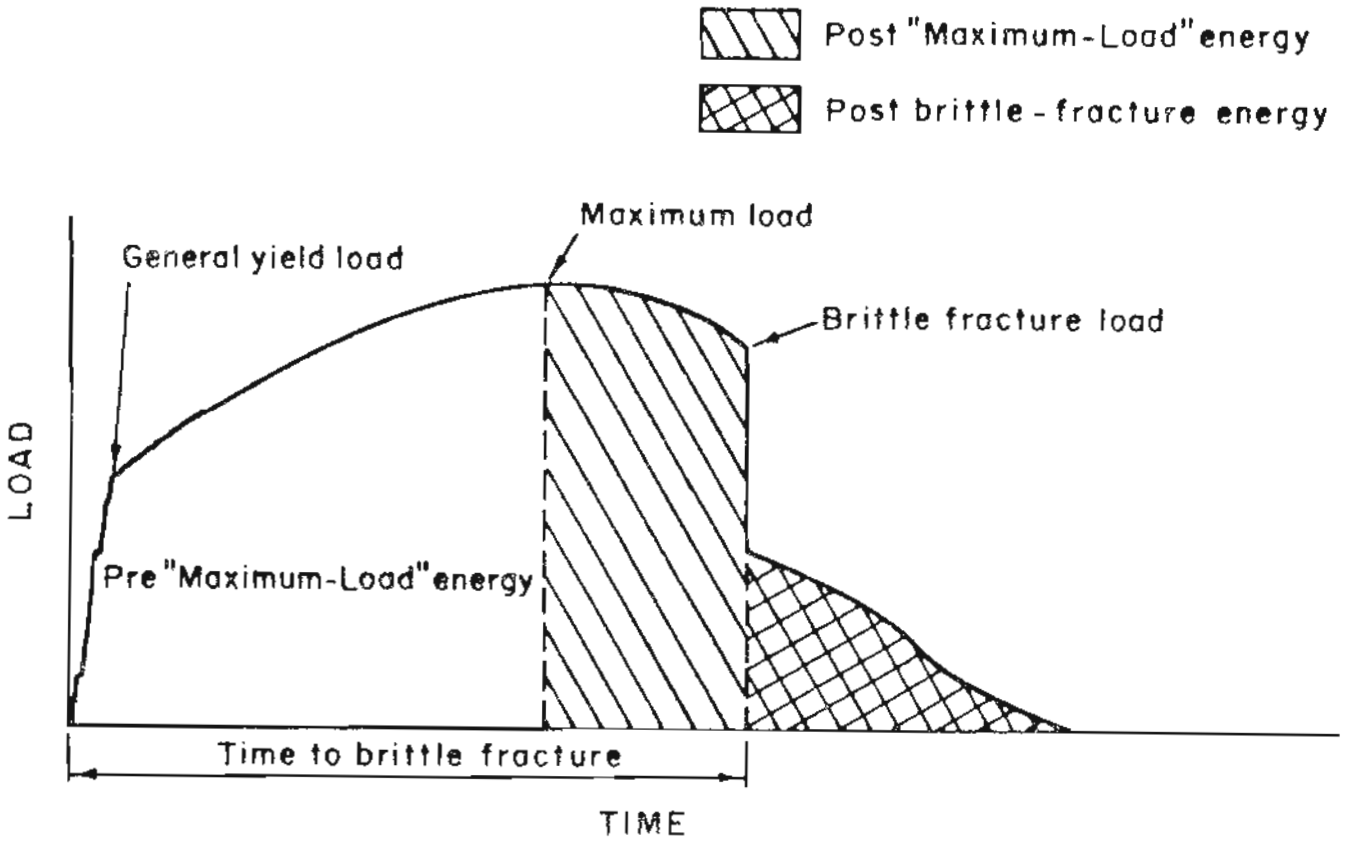

Fig. A.4 An idealized load-time trace for an impacted Charpy V-notch sample.

where K_{ID} is measured in units of psi-$in^{1/2}$, P_M in units of lbs and a in units of inches.

The instrumented Charpy test can also predict fracture toughness after general yield load, although there is considerably controversy regarding the calculations of a meaningful fracture toughness value based on data derived from a specimen which fractures after general yielding in any type of testing. The various methods (42) that can be used for fracture toughness calculations are (a) maximum load method, (b) equivalent energy approach, (c) equivalent strain energy release rate, (d) crack opening displacement, (e) J-integral method.

A.2.2 Linear Elastic Fracture Toughness Test: The fracture toughness testing is the outcome of fracture mechanics approach, first initiated by Griffith (47). In order to avoid the discrepancy between the theoretical cohesive strength and the actual fracture strength (which is always less), Griffith assumed the existence of inherent defects in the material and the crack will grow when the decrease of elastic energy just balances the increase of surface energy. His results are shown as

$$\sigma = \left[\frac{2E\gamma_s}{a}\right]^{1/2} \quad \text{for plane stress}$$

$$\sigma = \left[\frac{2E\gamma_s}{(1-\upsilon^2)\pi a}\right]^{1/2} \quad \text{for plane strain} \qquad \text{A.6}$$

E = Young's modulus, γ_s = surface energy, υ = Poisson's ratio

a = crack length, σ = fracture stress

The Griffith equation as it stands is not directly applicable to the fracture of structural metals. For brittle fracture, in which the extent of yielding at the point of instability is substantially smaller than the width of the specimens, the fracture stress is proportional to $(a)^{-1/2}$. However, the constant of proportionality is much greater than that predicted by the Griffith formula. The first explanation of this higher proportionality factor was provided by Orowan (48) and Irwin (49) who suggested that the surface tension term in Equation A.6 should be modified to include the amount of plastic work done as the crack grows.

Thus $$\sigma = \left[\frac{E(2\gamma_s + \gamma_p)}{\pi a} \right]^{1/2} \quad \text{for plane stress} \qquad A.7$$

where γ_p is a plastic work term. Since γ_p is much greater than γ_s, the latter can be neglected, and hence

$$\sigma = \left[\frac{E\gamma_p}{\pi a} \right]^{1/2} \qquad A.8$$

Toughness, as envisaged by Griffith is the rate of release of elastic energy with respect to crack lengths, and is symbolized by G. The elastic energy of a specimen containing a crack of length a and subject to a tensile stress σ, in plane strain is given as

$$W = \frac{1}{2} \sigma^2 (1-\upsilon^2) \pi a^2/E \qquad A.9$$

Hence $$G_I = \frac{dw}{da} = \sigma^2 (1-\upsilon^2) \pi a/E.$$

Another definition for toughness has been envisaged by Irwin and co-workers (50-51) as the stress-intensity factor, which is defined as $K = \sigma(\pi a)^{1/2}$ for a mode 1 load containing a crack length 2a in an infinitely wide specimen. The K parameter sometimes produces confusion because it's dimensions of stress $(\text{length})^{1/2}$ are not commonly encountered in other physical formulae. It should be emphasized that it is a factor which characterizes the intensity of the stress field ahead of a crack. For a mode 1 loading (as depicted below) the stresses for a stress intensity factor K_I are

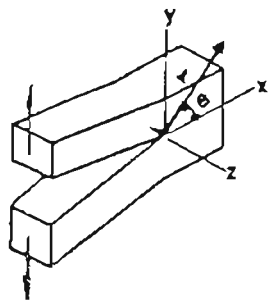

$$\sigma_x = \frac{K_I}{(2\pi r)^{1/2}} \cos\frac{\theta}{2}\left[1 - \sin\frac{\theta}{2}\sin\frac{3\theta}{2}\right]$$

$$\sigma_y = \frac{K_I}{(2\pi r)^{1/2}} \cos\frac{\theta}{2}\left[1 + \sin\frac{\theta}{2}\sin\frac{3\theta}{2}\right] \qquad \text{A.10}$$

$$\tau_{xy} = \frac{K_I}{(2\pi r)^{1/2}} \sin\frac{\theta}{2}\cos\frac{\theta}{2}\cos\frac{3\theta}{2}$$

$$\sigma_z = \nu(\sigma_x + \sigma_y) \quad \tau_{xz} = \tau_{yz} = 0$$

By substituting $K = \sigma (\pi a)^{1/2}$ in A.9 we can obtain G_I in terms of stress intensity.

$$K_I^2 = \frac{EG_I}{(1-\upsilon^2)}$$

The criterion for unstable crack growth in plane strain in terms of G from A.6 is

$$G_{Ic} = \gamma_p \text{ for } \gamma_s << \gamma_p$$

and in terms of the stress intensity is

$$K_{Ic} = \left(\frac{EG_{IC}}{1-\upsilon^2} \right)^{1/2} \qquad \text{A.11}$$

Thus both elastic energy release rate approach and the stress intensity approach are equivalent.

The previous expression, as developed by Irwin (50), provide the basis for the entire field of fracture toughness testing as long as the gross fracture stress is less than the yield strength of the material. At fracture, the stress intensity factor reaches a critical K_{Ic}, the corresponding plastic zone size has reached a critical value of R_c and the critical plastic zone size at fracture is given by (51)

$$R_c = \frac{1}{2\pi} \left(\frac{K_{Ic}}{\sigma_{ys}} \right)^2 \qquad \text{A.12}$$

Equation A.12 indicates that the tougher the material, the larger is the critical plastic zone size ahead of crack.

In order for a fracture toughness (K_{Ic}) test to be valid, the plastic zone size has to be restricted to a small value and a plane strain condition must prevail: this means that the thickness of the specimen must be large enough so that the plane strain conditions are achieved. Arbitrarily, the valid thickness (=B) has been chosen, so that $B \geq 2.5 \left(\frac{K_{Ic}}{\sigma_{ys}}\right)^2$.

For materials in which failure occurs with an extensive plastic zone, the plastic deformation at the crack tip would be large enough to invalidate the linear elastic fracture mechanics analysis. Under such conditions, the crack opening displacement, (COD), has been used in studying the fracture (Fig. A.5). During loading the crack faces move away from one another and produce a displacement at the crack tip normal to the crack plane which is called the "crack tip opening displacement" (COD). A schematic picture of crack opening displacement is given in Fig. A.5. The fracture criterion can be written such that the crack advances when the crack tip opening displacement reaches a critical value $(COD)_c$. There are several analytic treatments relating COD to the stress intensity factor (52-58). For plane strain it can be given by

$$K^2 = \frac{\lambda \sigma_y E (COD)}{(1-\upsilon^2)} \qquad A.13$$

when σ_y is the yield strength, E is the Young's modulus, υ is Poisson's ratio and λ= constant $\simeq$ 1.

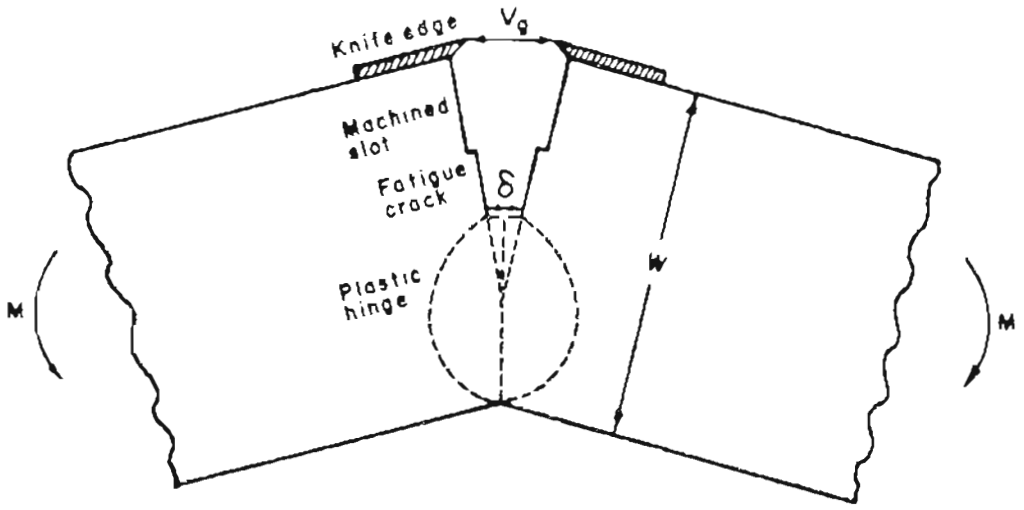

Fig. A.5 Diagram showing crack-tip displacement of a knife-edge displacement Vg.

Deformation in the plastic zone causes a transverse contraction at the crack notch tip which is called the notch root contraction (NRC) (59). Empirical relation relating NRC to COD can be determined, which allow NRC to be used as a measure of toughness. For cases where fracture occurs after general yield, NRC is a useful parameter to predict fracture toughness. However, all these toughness measurements are apparent toughness in the absence of a valid K_{Ic} test.

A.2.3 Comparison of Fracture Toughness Test and Charpy V-Notch Test - As stated earlier, in Charpy testing a specimen of specified dimensions is broken under the impact action of a swinging pendulum and the energy required to break the specimen is known as the toughness. In fracture toughness testing the strain-energy release-rate as the crack advances is calculated. Hence the parameters of the two tests are entirely different.

In Charpy testing, the energy absorbed per unit area is an integrated value across the entire fracture surface. It does not distinguish between separate events (60) in the fracture process, namely fracture initiation, propagation, the transition from plane strain to plane stress and the resistance the material offers as the crack extends; on the other hand, the plane strain fracture toughness refers to fracture initiation in the plane strain condition.

In spite of the evaluation parameter being different, there have been attempts to correlate fracture toughness data with Charpy V-notch energy data and many empirical relations have been proposed. For a 4340 steel heat treated to high strength level, which fails by a low energy

energy tear mode (61) (see Fig. A.6), such relations will be of little significance. Another factor for not adhering to such relationship in this investigation is that such statistical relationships are valid only for the steels in question. Also for 4340 steel significant microstructural changes may not be detected by Charpy test because of the low-energy tear mode type of fracture and to start with the energy absorbed value is very low (14-15 ft-lbs). Hence, in order to compare between Charpy and fracture toughness test it is necessary to measure the resistance to fracture initiation in the Charpy specimen as is done in the fracture toughness specimen either in slow-bend or instrumented Charpy test: the toughness thus obtained in Charpy specimen is known as apparent toughness, since the specimen dimensions do not conform to ASTM standards for a valid fracture toughness tests. However, for an ultra-high strength steel like 4340, the plastic zone size is quite small and hence even Charpy type specimens of small thickness closely resemble fracture toughness specimens.

In addition, there are three other important differences in these two test methods, namely (a) strain rate; the strain rate in Charpy testing is 5-6 orders higher than in K_{Ic} testing. However, in slow-bend Charpy testing, the strain rate can be approximated to K_{Ic} testing, (b) method of loading, i.e. the Charpy loading is three-point bend loading and fracture toughness testing is done both by compact tension and three-point bend specimens. When bend specimens are used in fracture toughness testing, there is no difference. However, when compact tension specimens are used, there is a difference in the method of loading between the two

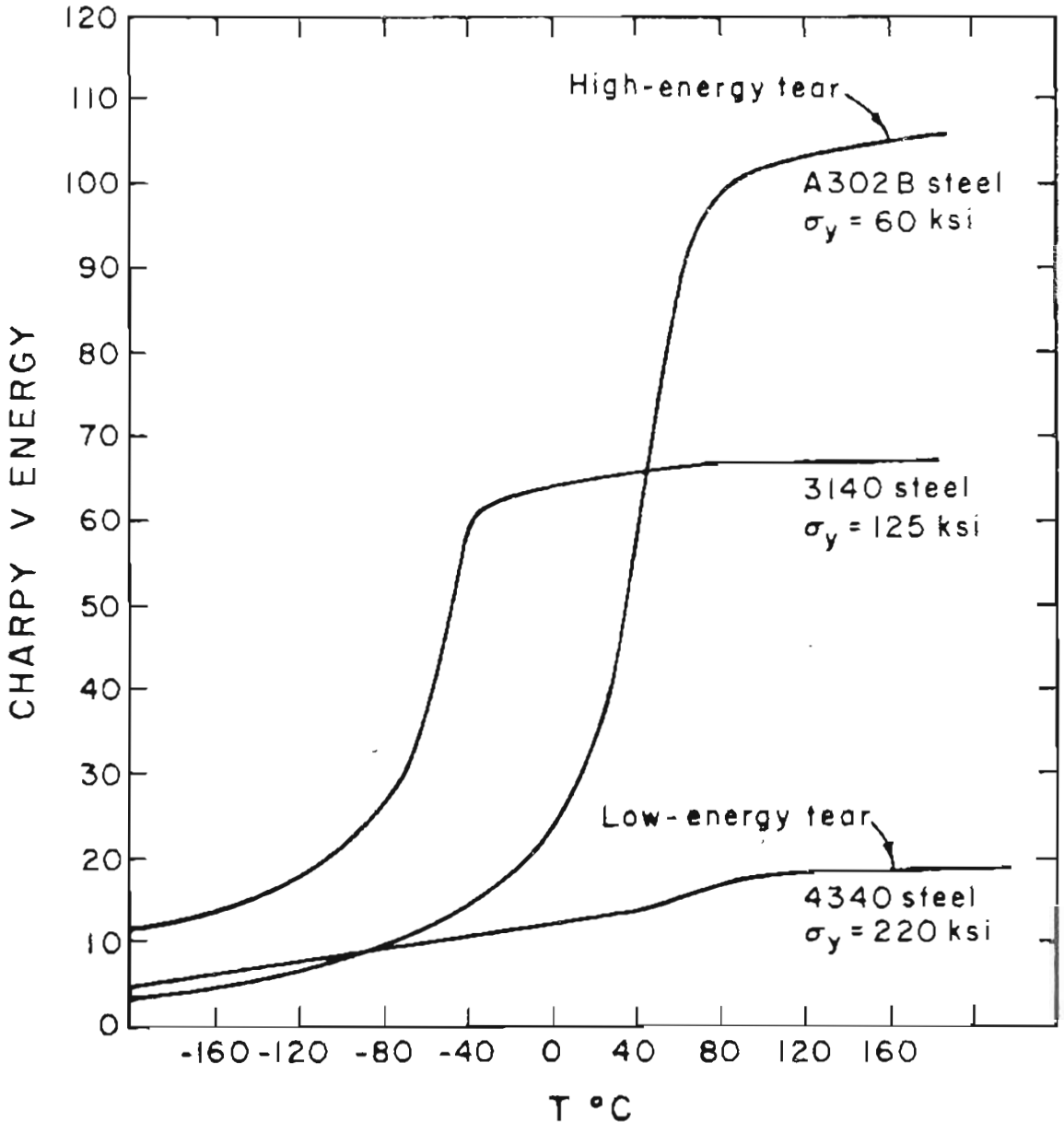

Fig. A.6. Effect of yield strength level on the shape of Charpy V notch impact curves for some typical commercial steels.

tests, (c) notch-root radius, i.e. the fracture toughness specimens contain a fatigue pre-crack, whereas the standard Charpy specimens contains a V-notch, having a root radius of 0.01 inch. This difference can be eliminated by pre-cracking the Charpy specimen before testing or having a fracture toughness specimen of root radius .01" without resorting to fatigue pre-cracking. However, by resorting to the second method, the test is not a valid ASTM fracture toughness test as ASTM-E-399.

A.3 The Effect of Notch-Root Radius on the Toughness - It has been reported (62,63) that the elastic strain energy release rate is relatively insensitive to tip root-radius in the range from a mathematical 'sharp' crack to some finite root radii. This is also expected from Irwin's analysis (64) $K = \lim_{\rho \to 0} \frac{1}{2} \sigma_m (\pi\rho)^{1/2}$, where σ_m = maximum stress at the notch, ρ = notch root radius. In this relationship K will become insensitive to root radius whenever σ_m is inversely proportional to $\rho^{1/2}$. However, experimental fracture data have shown that this is not always the case. Fracture toughness values can be significantly lower for a fatigue-cracked specimen than for a small but finite root radius specimen (65). Similar increases in toughness with increase of root radius have been observed by Rack (66) in unaged ß-titanium alloys, Myers (67), et al. in monocrystalline silicon, and Ritchi (2), in quenched and tempered 4340 steel. Different theoretical models have been proposed by several authors, which predict a linear relationship of fracture toughness with notch root radius. Current models are described below.

A.3.1 Critical Stress Model- This model (68) postulates that when the longitudinal stress ahead of a notched bar, subjected to bending, equals a stress σ_f^*, the 'microscopic cleavage stress', fracture will occur. This model employs the stresses in the plastic zone from slip-line field theory and the extent of plastic zone is estimated from fracture mechanics principles.

The longitudinal stresses along the net section within the plastic zone ($R < r$) is given by slip line field theory (37) $\sigma_{yy} = \sigma_y [1+\ln(1+\frac{R}{\rho})]$ where ρ = root radius of the notch. The maximum longitudinal stress $(\sigma_{yy})_{max}$

$$(\sigma_{yy})_{max} = \sigma_y \left[1 + \ln \left(1 + \frac{r}{\rho}\right)\right] \qquad \text{A.14}$$

so that $(\sigma_{yy})_{max}$ increases with increasing plastic zone size. The stress distribution as a function of the distance from the notch root is given in Fig. A.7 for different notch root radii. The size of plastic zone is given by

$$r = \frac{1}{\pi} \left(\frac{K_{Ic}}{\bar{\sigma}_y}\right)^2 = \frac{1}{\pi} \left(\frac{K_{Ic}}{1.68\sigma_y}\right)^2 \qquad \text{A.15}$$

where $\bar{\sigma}_y$ is replaced by 1.68 σ_y, the average contained value of σ_y in the plastic zone for plane strain. Combining equns. 1.14 and 1.15

$$K_{Ic}(\rho) = 2.89\, \sigma_y \left[\exp\left(\frac{\sigma_y^*}{\sigma_y} - 1\right) - 1\right] \rho^{1/2} \qquad \text{A.16}$$

Since for sharp crack $\rho \to 0$, $K_{Ic}(\rho) \to 0$. Hence for a sharp crack, the equation is modified to include

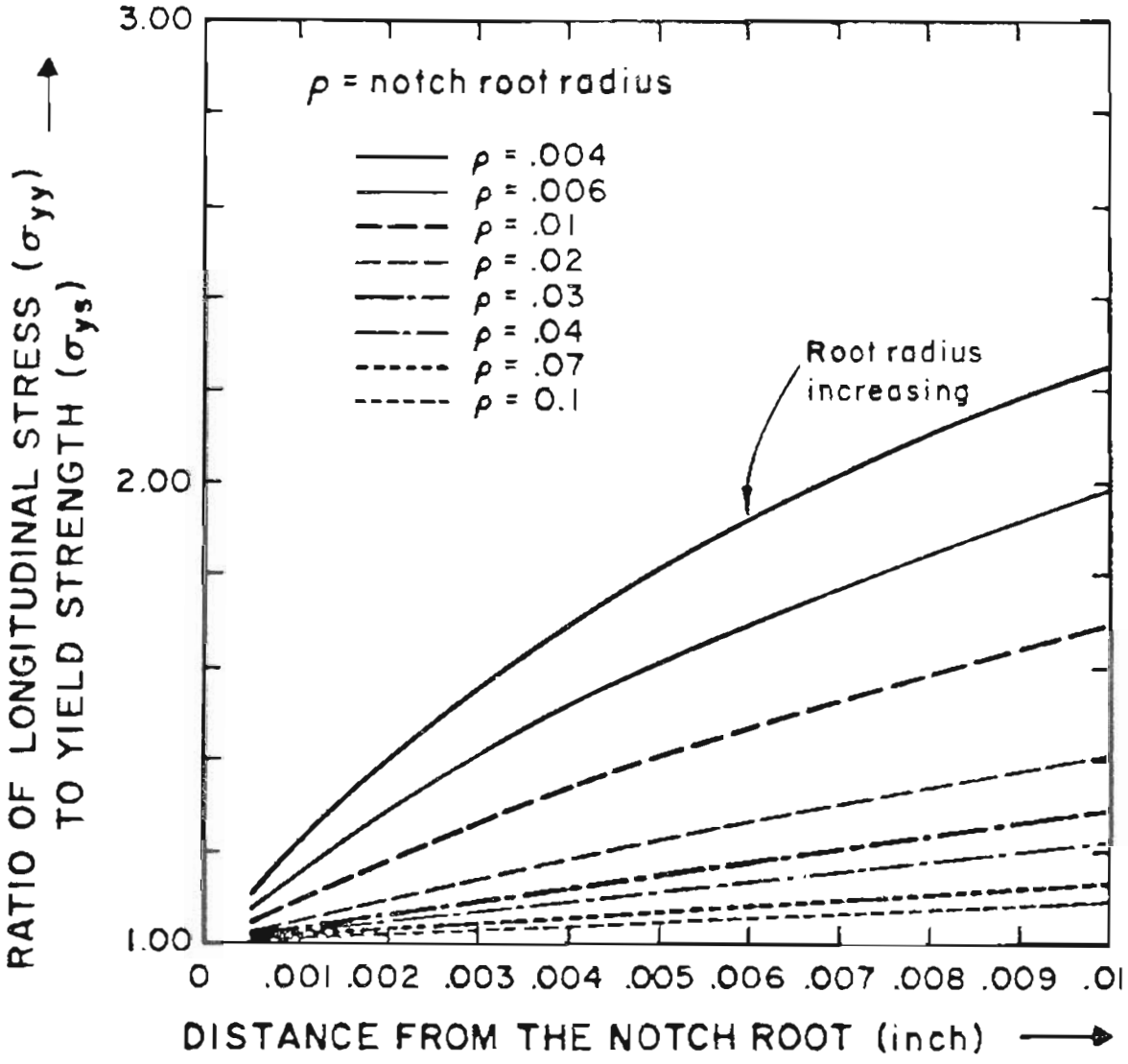

Fig. A.7 Stress distribution ahead of blunt notches of various root radii by slip-line field theory.

$$\lim_{\rho \to 0} K_{Ic}(\rho) = K_{Ic} = 2.89\, \sigma_y \left[\exp\left(\frac{\sigma_f^*}{\sigma_y} - 1\right) - 1\right] \rho_o^{1/2} \qquad A.17$$

where ρ_o = limiting root radius, i.e. from sharp crack to limiting root radius the fracture toughness should remain constant. The model also predicts an increase of fracture toughness with square root of notch-root radius.

A.3.2 Critical Strain Model - In contrast to the previous stress-controlled model, this model (68) predicts that fracture will occur when the strain ahead of the crack-tip reaches a critical value. Critical strain leads to initiation of void at the particle/matrix interface, which subsequently coalescences, leading to what is known as 'microvoid coalescence'. Particle may be an inclusion or a second phase particle. The distribution ahead of crack tip is given by

$$\varepsilon_R = \frac{F(\theta)}{R} \qquad A.18$$

where F is a function of root radius and θ is the bend angle of the specimen, R is the distance ahead of the notch. Furthermore, it has been shown by Wells (70) that the notch-tip opening displacement 2V(C) is given by $2\,V(C) = a\times\theta$, where a is the notch depth. The region at the notch tip can be treated as a 'miniature tensile specimen' of gage length 2ρ. It follows that

$2V(C) = 2\rho\, \varepsilon(c)$, where $\varepsilon(c)$ is the strain at the crack tip.

or $\varepsilon(c) = \frac{a\theta}{\rho}$

Thus, there is a finite strain at the notch root. In order to compare the above two equations, Tetelman and Wilshaw assumed that the strain is constant over a distance R^* from the notch root. Hence

$$\varepsilon(R) = \frac{V(c)\ R^*}{\rho\ R} \qquad \text{A-20}$$

Using the Dugdale-Barenblatt model (33), the following relation is obtained:

$$V(C) = \frac{4}{\pi}\ \frac{\overline{\sigma}_y}{E} \cdot r, \quad \text{where} \quad \overline{\sigma}_y = 1.68\ \sigma_y \qquad \text{A-21}$$

for plane strain, & r = plastic zone size.

Combining equations A-20 and A-21

$$\varepsilon(R) = \frac{4}{\pi}\frac{R^*}{R} \times \frac{\overline{\sigma}_y}{E}\ \frac{r}{\rho}$$

or

$$\varepsilon(R) = \frac{4}{\pi}\frac{R^*}{R}\ \left(\frac{1.68\sigma_y}{E}\right)\ \left(\frac{.12}{\rho}\right)\ \left(\frac{K}{\sigma_y}\right)^2$$

Rupture should occur when ε at r_θ reaches critical value $\varepsilon_f(r_\theta)$. This is reached when $R = 2.25\rho$ according to Wilshaw (71). Substituting results in

$$K_A(o) = \left(\frac{4.4\ E\ \sigma_y\ a\ \theta_f}{R^*}\right)^{1/2}\ \sqrt{\rho} \qquad \text{A-22}$$

Thus in this model also the fracture toughness increases with the square root of notch root radius. And, as before, a limiting root radius ρ_o is postulated for a sharp crack.

A.3.3 Other Works on Relationship of Toughness with Notch Root Radius - The effect of notch root radius on toughness has been discussed and a theoretical model based on a plastic relaxation representation of a crack has been proposed by Heald, Spink and Worthington (72). Their results are shown as

$$K_A(\rho) \frac{(\pi a)^{1/2}\sigma_u}{[1+(\rho/a)^{1/2}]} \left\{ \frac{2}{\pi}\cos^{-1} \left[\exp\left(-\frac{\pi K_{Ic}}{8\sigma_u^2 a}\right)\right] + \left(\frac{\rho}{a}\right)^{1/2} \right\} \quad A.23$$

The derivative of K_A with respect to ρ in this equation is positive, meaning thereby the toughness increases with increase in notch root radius.

Greager and Paris (73) have calculated the near-field notch tip stresses for very slender elliptical crack having a "small" root radius $\rho/a \approx (b/a)^2 \ll 1$ and for a mode 1, the stresses are as follows:

$$\sigma_x = \frac{K_I}{(2\pi r)^{1/2}} \left[\cos\frac{\theta}{2}\left(1-\sin\frac{\theta}{2}\sin\frac{3\theta}{2}\right) - \frac{\rho}{2r}\cos\frac{3\theta}{2}\right]$$

$$\sigma_y = \frac{K_I}{(2\pi r)^{1/2}} \left[\cos\frac{\theta}{2}\left(1+\sin\frac{\theta}{2}\sin\frac{3\theta}{2}\right) + \frac{\rho}{2r}\cos\frac{3\theta}{2}\right]$$

$$\tau_{xy} = \frac{K_I}{(2\pi r)^{1/2}} \left[\sin\frac{\theta}{2}\cos\frac{\theta}{2}\cos\frac{3\theta}{2} - \frac{\rho}{2r}\sin\frac{3\theta}{2}\right] \quad A\text{-}24$$

For $\theta = 0$ the variations of σ_x and σ_y with distance from the notch root are given in Fig. A-8 and Fig. A-9., respectively. From this it is also apparent that fracture toughness should increase with increase in notch root radius.

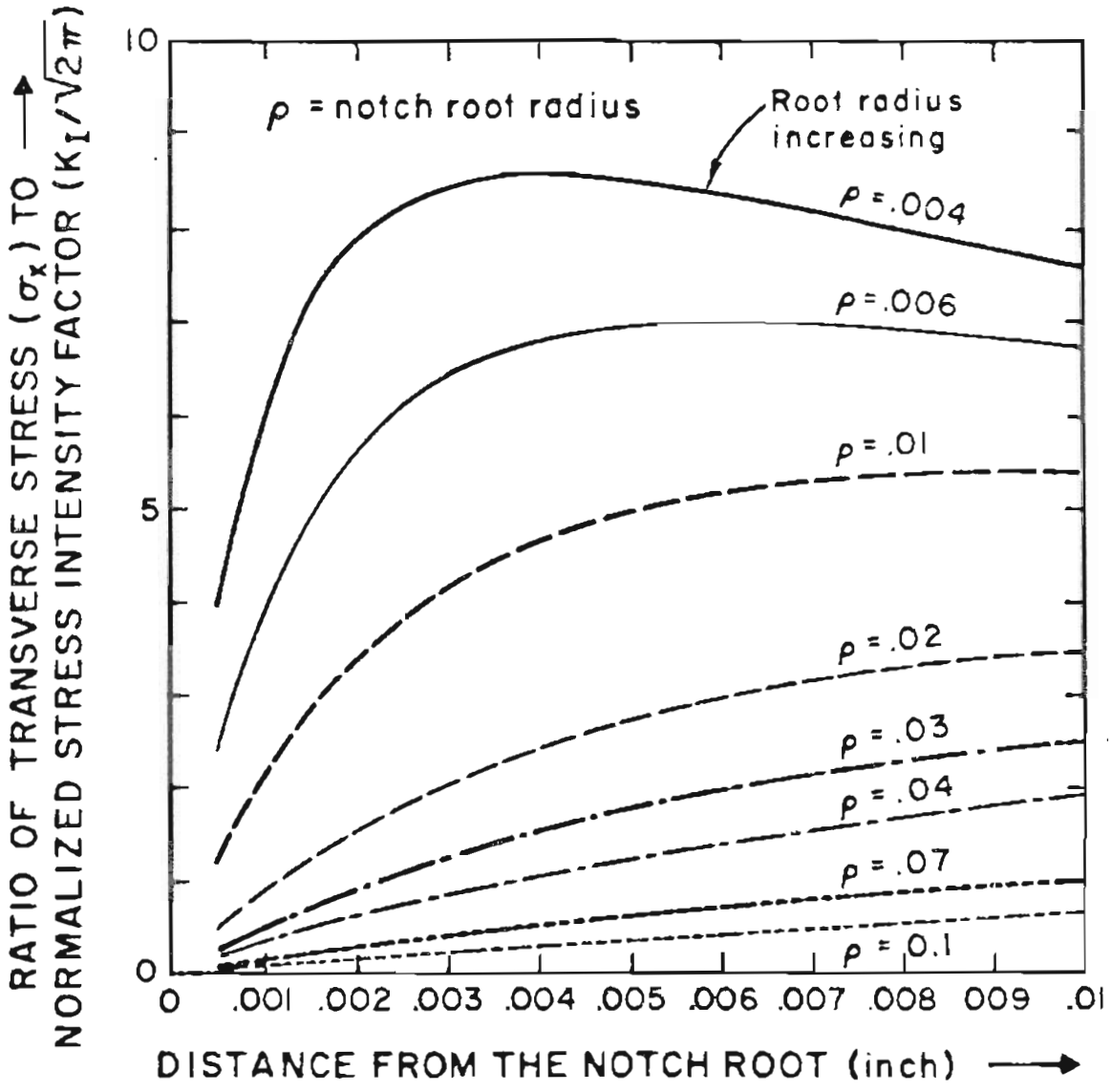

Fig. 48 Variation of σ_x with distance from the notch-root ($\theta = 0^\circ$) for different notch-root radii for a mode 1 stress intensity factor K_I.

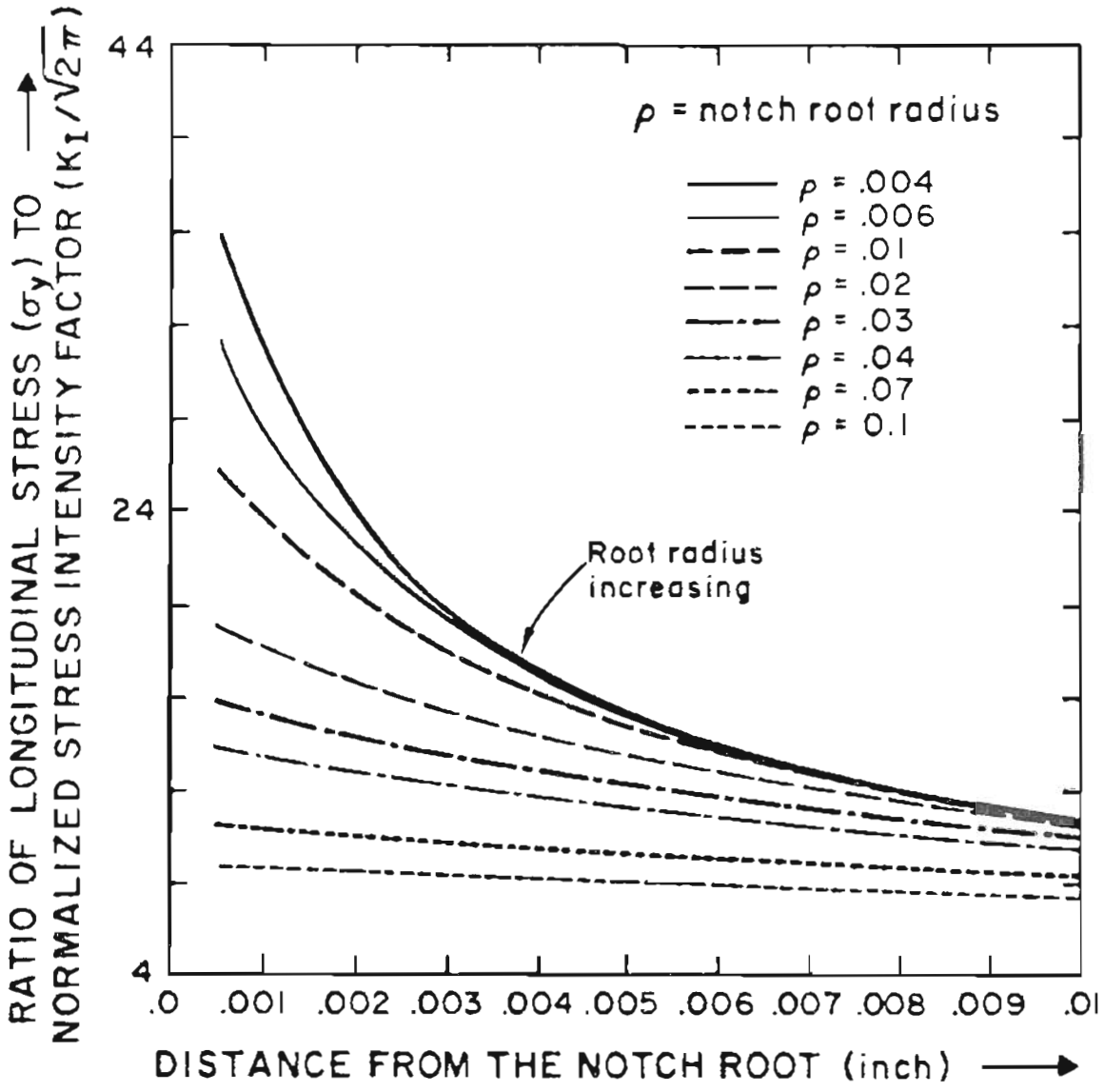

Fig. A.9 Variation of σ with distance from the notch-root ($\theta = 0^\circ$) for different notch root radii for a mode 1 stress intensity factor K_I.

An expression for the fracture toughness ahead of a blunt notch for strain controlled fracture (3) has been given as

$$K_A = \left(\frac{3}{2}\ \sigma_y\ E\ \varepsilon_f\right)^{1/2}\ \rho^{1/2} \qquad A.25$$

where σ_y = yield strength E = Young's modulus ε_f = critical strain at fracture, ρ= notch root radius. For a sharp crack, ρ is replaced again by ρ_o = limiting root radius. This relation also predicts a linear relation of toughness with notch-root radius.

Thus all the current theories predict an increase in toughness with increase in notch root radius.

A.4. Microscopic Aspects of Fracture - Fracture on a macroscopic scale is normally divided into two categories, (a) brittle fracture which occurs without any plastic deformation, (b) ductile fracture with a large amount of plastic deformation.

A.4.1 Brittle Fracture - Brittle fracture in metals occurs either by transgranular or intergranular cleavabe. Transgranular cleavage is separation along one or more crystallographic planes and intergranular cleavage occurs along weaker grain boundaries. There is extensive, experimental evidence that plastic deformation proceeds cleavage fracture. Sensitive techniques such as strain gages (74) and etch pitting (75) have been used to detect plastic flow and they confirm that microplastic deformation occurs prior to cleavage in iron and steel. The cleavage process is postulated to involve three steps which will be discussed next.

A.4.1.1 Piling up of Dislocations - In the first stage the dislocations are blocked by an obstacle. Grain boundaries, twin bands, second-phase particles, and sessile dislocations formed by dislocation reactions can all block the dislocation movement. When the pile-up is formed, the stresses at its tip become progressively more intense. Thus it can produce the required stress for crack nucleation.

A.4.1.2 Crack Nucleation - There are several mechanisms of crack nucleation by dislocation pile-up. The simplest model involves a series of edge dislocations stopped at a grain boundary or by another strong obstacle. Zener (76) suggested that as the number of dislocations in a pile up, n, increases they coalesce together at the tip of the pileup to nucleate a microcrack as shown in Fig. A.10. Cottrell (77) has proposed another mechanism of crack nucleation by dislocation for b.c.c. metals. In this model the two leading dislocations on two intersecting slip planes will react to form a sessile dislocation which then serves as an obstacle to the following dislocations. The dislocation reaction can be written as

$$a_o/2\ [111] + a_o/2\ [\bar{1}\bar{1}1] \rightarrow a_o\ [001] \qquad \text{A-26}$$

where a_o is the lattice parameter. Microscopic studies (78, 79) have revealed evidences of such sessile dislocations. On the other hand, Stroh (80) has analyzed the piling up of dislocations while other dislocations are acting as an obstacle. He has indicated that such a dislocation barrier is not sufficiently strong to nucleate a crack and the sessile dislocation would dissociate under the force of piled up dislocations.

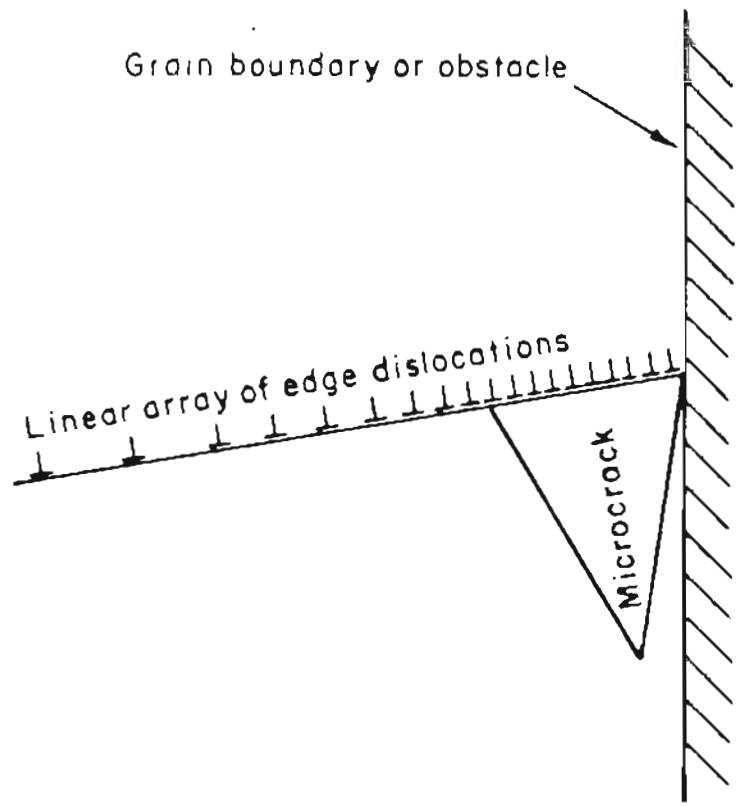

Fig. A.10 Microcrack formation at the tip of a piled-up group of edge dislocations.

Another mechanism of crack nucleation is by deformation twinning in b.c.c. metals. Such cracks have been observed in many investigations (81-84). Cracks of this type are formed at the junction of twin bands when the resolved normal stress on the cleavage plane is high.

A.4.1.3 Crack Propagation - The length of a crack nucleus is of the order of a few micrometers. The first step in crack propagation is the initial growth of the crack nucleus to a grain boundary or another obstacle. At this point the obstacle may or may not be able to stop the crack from growing. Under certain conditions a nucleated crack can grow to final fracture provided that the elastic energy released is sufficient for both the energy of the new surfaces and also for all additional fracture work. However, this is not always the case. The unstable crack could meet a tougher second phase or a strong obstacle, and be stopped. In that case, a substantially higher stress is required to restart the crack.

A.4.1.4 Theoretical Treatments of Cleavage Strength - In calculating the theoretical cleavage strength, several important points should be considered. The first one is the stress concentration at the tip of piled-up dislocations. The others are the cohesive strength and the stress relaxation produced by dislocation motions. It is also necessary to know which of the stages of the cleavage process (nucleation or crack growth) is the most difficult one to carry out. Quantitative analysis by several investigators has given the critical shear stress for cleavage (85-90) Stroh (85) assumed that crack nucleation was the major obstacle and the critical change is given by

$$\tau_c = G \left[\frac{b}{\pi^2 L} \right]^{1/2} \qquad A.27$$

where G is the shear modulus, b is the Burger's vector and L is the length of the slip band. Experimental results (91), particularly those concerning the effect of superimposed hydrostatic tension (92-93), indicate that the critical step in cleavage process is the crack growth. This led Cottrell (77) to decide that the crack propagation was likely to be the significant step.

For a polycrystalline material of grain size d, the crack growth according to Cottrell's model, occurs at a tensile stress, σ_f when

$$\sigma_f = \frac{8G\,\gamma_m}{k_y}\, d^{-1/2} \qquad A.28$$

Where γ_m is the effective surface energy, k_y is a parameter from the Hall-Petch (94,95) relationship for the yield strength of polycrystalline materials according to

$$\sigma_y = \sigma_o + k_y\, d^{-1/2} \qquad A.29$$

where σ_o is the lattice friction stress and k_y is a measure of the pinning of dislocations. Eqn. A.29 considers the contribution of grain size on cleavage strength and the other effects of the microstructure are through γ_m and k_y.

Smith (88) has considered a situation in mild steel where a nucleated crack in the carbide phase propagates through the tougher ferrite. The critical tensile stress for cleavage based on this model can be given by

$$\sigma_f = \left[\frac{4\,\gamma_m\,G}{\pi(1-\upsilon)d}\right]^{1/2} \qquad \text{A.30}$$

Reiff and Haas (90) have recently applied Cottrell's model to the condition where the fracture of grain boundary carbides act as the crack initiation. The result is given by

$$\sigma_f = \sigma_{o/2} + \left(\sigma_{o/4}^2 + \frac{8.8\,\gamma_m\,G}{d}\right)^{1/2} \qquad \text{A.31}$$

where σ_o is the lattice friction stress. γ_m, as given in the above equation, is the work done near the tip of a cleavage crack that is propagating within the grain. γ_m should be differentiated from γ_p of the Irwin formula (Eqn. A.7) in which γ_p represents the plastic work done near the tip of a propagating microcrack. Yokebari (89) has treated the problem with consideration of plastic relaxation and the critical tensile stress is given by

$$\sigma_f = k_1\sigma_o + \left[\frac{8\,k_2\gamma_m\,G}{\pi(1-\upsilon)\,d} - k_3\sigma_o^2\right]^{1/2} \qquad \text{A.32}$$

where k_1, k_2 and k_3 are constants, and all the terms are as defined above.

Some of the unsatisfactory features of the models mentioned above are (a) the dislocations are assumed to be in static equilibrium, but they actually reach their positions with finite speeds that are strongly stress dependent; (b) the strain rate effect is neglected, (c) stress relaxation is not treated explicitly, (d) the contribution of both cohesive strength and stress relaxation appear together in the energy parameter γ_m, (e) no account

is taken of the effects of microstructure. Nevertheless, the final results of these models indicate that the cleavage strength is proportional to $\left(\frac{\gamma_m G}{L}\right)^{1/2}$, where G is the shear modulus, γ_m is the effective surface energy and L is the length of the slip band.

This implies that cleavage strength increases as the required work for cleavage increases. It also indicates that a decrease in length of the slip band should increase the cleavage strength. For this reason grain refinement should increase resistance to cleavage and this has been observed experimentally.

Experimental results indicate that the cleavage strength is not strongly temperature or strain rate dependent (39,96,97). This implies that the effective surface energy and the other factors that influence the cleavage process are also not strongly temperature and strain rate dependent. An explanation for this behavior comes from the consideration of the dislocation velocity, which is one of the most stress and temperature sensitive parameters. An increase in velocity will increase the rate of piling up and thus produce higher stresses locally. However, it may also increase the rate of relaxation near the tip of the pileup which reduces the stresses locally.

The idea that cleavage strength is not strongly temperature and strain rate dependent leads to a simple criterion for brittle fracture. According to this criterion, cleavage can occur when the maximum normal stresses are larger than or equal to the cleavage strength. Numerous experimental results support this criterion for cleavage fracture (98-101).

A.4.2 Ductile Fracture - In contrast to cleavage fracture, ductile fracture occurs with a large amount of plastic deformation. It involves three stages, (a) void nucleation by the fracture of inclusions or second, phase particles or by their separation from the matrix, (b) growth of the resulting voids while they are still widely separated, and (c) coalescence of the voids to form a microcrack. The problem of ductile fracture has not received as much attention as brittle fracture due to mathematical complexity and many questions are open for investigation. The most fundamental point concerning the mechanism of ductile fracture is that it is initiated by the generation of voids at inclusions and second phase particles (102,103). These voids gradually multiply and eventually nucleate a crack by joining together. Several experimental results (104,105) have confirmed that void formation can be due to either interface failure or a result of particle fracture.

Gurland and Plateau (106) have proposed a criterion for void formation. They suggest that the energy relief due to void formation must be sufficient to produce the required surface energy to create the new free surfaces.

$$\text{or} \qquad \sigma_{void} = \frac{1}{2} \left(\frac{E\gamma}{D} \right)^{1/2} \qquad \text{A.33}$$

where σ is the stress in the matrix, D is the diameter of the void, γ is the surface energy. The value of γ depends on the surface energy of the matrix γ_m^*, the surface energy of the particle (γ_p^*) and the interface energy (γ_{mp}^*), such that the following condition holds for interface decohesion for particle fracture:

$$\gamma = \gamma_m^* + \gamma_p^* - \gamma_{mp}^* \quad \text{for interface decohesion}$$

$$\gamma = 2\,\gamma_p^* \quad \text{for particle fracture} \qquad \text{A.34}$$

Theoretical studies for the growth of nucleated voids have been made by several people (106-109). McClintock (110-111) considered uniformly spaced cylindrical holes in a linearly strain hardenable material under simple shear with superimposed hydrostatic tension. The rate of growth of these holes depends on the two transverse components of stress, σ_{xx} and σ_{yy}, the equivalent stress and strain, and on the strain hardening exponent n in the flow equation.

$$\varepsilon_f = \frac{(1-n)\ m}{\sinh\left[(1-n)\ (\sigma_{xx} + \sigma_{yy})/(2\sigma/\sqrt{3})\right]} \qquad \text{A.35}$$

where m is a parameter which depends on the size and distance between the holes. The criticism of this model is that in the presence of a relatively rigid inclusion, free deformation of the voids is limited. Another objection is that the model is two dimensional.

Since the field of ductile fracture is complex and unexplored, it has been a difficult task to express a definite microscopic criterion for fracture. Criteria based on strain alone have been proposed (111,112). This criteria, although often satisfactory, cannot be generally applicable; for example, Hoadson's (113) results indicate that the process of void formation requires critical stress, while the growth and coalescence of voids depends on hydrostatic stress and strain. A criterion that takes into account both stress and strain would be more successful. Until more

investigation on ductile fracture is carried out, no simple criteria can accurately describe the microscopic aspects of ductile fracture.

REFERENCES

1. G. Y. Lai, W. E. Wood, R. A. Clark, V. F. Zackay and E. R. Parker, Met. Trans. 1974, Vol. 5, p. 1663.

2. R. O. Ritchie, B. Francis and W. L. Server, Met. Trans. 4, 1976, Vol. 7A, p.831.

3. R. O. Ritchie and R. M. Horn, Met. Trans. A, Vol. 9A, March 1978, p. 331.

4. P. M. Kelly and J. Nutting, J.I.S.I., 197, 1961, p.199.

5. O. Johari and G. Thomas, Acta Metallurgica, Vol. 13, 1965, p.1211.

6. B. Lee, S. Millman, I.L. MacDougall, S. R. Keown and B. B. Argent, Metal Science, July 1977, p.261.

7. M. J. Yokota and G. Y. Lai, Met. Trans. A, Vol. 6A, 1975, p.1832.

8. V. F. Zackay et al., 'Strengthening mechanisms in solids', 179, 1962, Cleveland, ASM.

9. K. Kuo, Jernkontorets Ann. 1956, Vol. 140, p.854.

10. E. Tekin and P.M. Kelly, Precipitation from Iron-Base Alloys, p.173, AIME, New York, 1965.

11. A. R. Cox, Iron and Steel, 1968, Vol. 41, p.539.

12. S. Murphy and J. A. Whiteman, Met. Trans. Vol. 1, April 1970, p.843.

13. D. Huang and G. Thomas, Met. Trans, Vol. 2, 1971, p.1587.

14. D. W. Smith and R. F. Hehemann, J.I.S.I. June, 1971, p.476.

15. K. J. Irvine and F. B. Pickering, 'Physical Properties of Materials and Bainite', Special Report 93, I.S.I., 1965, p.110.

16. D. N. Shackleton and F. B. Pickering, ibid, p.126.

17. G. Y. Lai, Met. Trans A, Vol. 6A, 1975, p.1469.

18. H. I. Aaronson and H. A. Domian, Trans. of the Met. Soc. of AIME, Vol. 236, 1966, p.781.

19. G. Y. Lai, Materials Science and Engineering, 19, 1975, p.153.

20. W. E. Wood, 'Mechanisms of Enhanced Toughness in Martensitic Alloys', Technical Report N00019-77-C-0135, Feb. 1978.

21. W. E. Wood, 'Mechanism of Enhanced Toughness in Martensitic Alloys,' Contract No. N00019-76-C-0149, 1976, p.55.

22. C. M. Wayman, Introduction to the Crystallography of Martensitic Transformations, Macmillan Series, 1964.

23. B. A. Bilby and J. W. Christian, J.I.S.I., 197, 1961, 122.

24. E. C. Bain, Trans. AIME, 70, 1924, 25.

25. D. S. Lieberman, M.S. Wechsler and T. A. Read, J. App. Phys., 26, 1953, 473.

26. M. Cohen, Trans. AIME, 224, 1962, 638.

27. J. S. Bowles and J. K. Mackenzie, Acta Met., 2, 1954, 129.

28. R. E. Reed-Hill, Physical Metallurgy Principles, Litton Educational Publishing, Inc., 1973.

29. R. F. Heheman, Phase Transormations, ASM Seminar, Metals Park, Ohio, 1970.

30. L. Kaufman, V. Radcliff, and M. Cohen, Decomposition of austenite by Diffusional Processes, Interscience Publishers, Inc., New York, 1962, p.313.

31. R. H. Goodenow, R. H. Burkalow and R. F. Hehemann, special report 93, ISI, 1965, p.135.

32. A. S. Tetelman and A. J. McEvily, Fracture of Structural Materials, Wiley, New York, 1967.

33. J. F. Knott, Fundamentals of Fracture Mechanics, Wiley, New York-Toronto, 1973.

34. A. P. Green and B. B. Hundy, J. Mech. Phys. Solids, 4, 1956, p.128.

35. A. P. Green, Quart. J. Mech. and Applied Math, 6, 1953, p.223.

36. T. R. Wilshaw, JISI, 204, 1966, p.936.

37. R. Hill, Mathematical Theory of Plasticity, Oxford Press, London,1950.

38. G. E. Dieter,Jr., Mechanical Metallurgy, McGraw-Hill, New York,1961.

39. A. S. Tetelman, T. R. Wilshaw, C. A. Rau, Int. J. of Fracture Mechanics, 4, 1968, p.147.

40. W. L. Server, D. R. Ireland, R. A. Wullaert, Report No. TR-74-29-R, Effects Technology, 1974.

41. H. J. Saxton, D.R. Ireland, W.L. Server - STP 563, ASTM 1974, p.50.

42. W. L. Server and D. R. Ireland - STP 563, ASTM, 1974, p.74.

43. H. J. Pack, Journal of Testing and Evaluation, 4(3), 1976, p.176.

44. J. C. Radon and C. E. Turner, Engr. Fra. Mechanics, Vol.1, 1969, p.411.

45. P.E. Diesburg, Petroleum Mechanical Eng. Conf., Tulsa, Okla., Sept. 21-25, 1975, p.1.

46. W. F. Brown and J. E. Srawley, Am.Soc.Test.Mat., STP 381, 1965, p.133.

47. A. A. Griffith, Phil. Trans. Roy. Soc. A-221, 1920, p.163.

48. E. Orowan, Trans. Inst. Engrs. Shipbuilders, Scotland, 89, 1946, p.165.

49. G. R. Irwin, Fracture Encyclopedia of Physics, Vol. VI, Springer, Heidelberg (1958), Vol. 8, p.551.

50. G. R. Irwin, 9th Intern. Congr. of App. Mech. Univ. of Brussels, Vol. 8, 1957, p.245.

51. G. R. Irwin, App. Mater. Res. 3, 1964, p.65.

52. J. R. Rice, J. Appl. Mech. Trans. ASME, 35, 1968, p.379.

53. A. A. Wells, Proceedings of the crack propagation symposium, College of Aeronautics, Cranfield, England, 1961, Vol. 1, p.210.

54. B. A. Bilby, Proc. Roy. Soc. A272, 1963, p. 304.

55. F.M. Burdebin and D.E.W. Stone, J. Strain Analysis, 1, 1966, p.145.

56. N. Levy, Int. J. Frac. Mech. 7, 1971, p.143.

57. J. R. Rice and M. A. Johnson, Inelastic Behavior of Solids, ed. by M. F. Kanninen, et al., McGraw-Hill, New York, 1970, p.641.

58. J. G. Sumpter, Third International Conference on Fracture, Munich, Germany, April, 1973.

59. J. N. Robinson and A. S. Tetelman, Report No. UCLA-Eng. 7409, January, 1974.

60. V. Weiss and S. Yakawa, ASTM, STP 381, 1964, p.1.

61. A.S. Tetelman and A.J. McEvily, Fracture of Structure Materials, Wiley, New York, 1967, p.120.

62. G. R. Irwin, J. A. Kies and H. L. Smith, Fracture Strengths relative to Onset and Arrest of Crack Propagation, Proceedings Am. Soc. Testing Matls, Vol. 58, 1958, p.640.

63. J. D. Lubahn. Proceedings, Am. Soc. Testing Matls. Vol. 59, 1959, p. 885.

64. G. R. Irwin, Proceedings First Symp. on Naval Structure Mechanics, Pergamon Press, London and New York, NY, 1960.

65. S. Yakawa and J. G. McMulline - Transactions, Am. Soc. Mechanical Engrs., J. of Basic Eng., Vol. 83, 1961, p.451.

66. H. J. Rack, Materials Science and Eng., 24 (1976), p.165.

67. R. J. Myers and B. M. Hillberry - Fracture 1977, vol. 3, ICF 4, Waterloo, Canada, June 1977, p.19.

68. J. Malkin and A. S. Tetelman, Engr. Fracture Mechanics, 1971, vol.3, p.151.

69. F. A. McClintock and G. R. Irwin, Fracture Toughness Testing, ASTM STP 381, 1965, p.84.

70. A. A. Wells, Proc. Crack Propagation Symp., Cranfield, 1961, p.210.

71. T. R. Wilshaw, JISI, 204, 1966, p.936.

72. P.T. Heald, G.M. Spink and P.J. Worthington, Mat. Sci. Eng. 10, 1972, p.129.

73. M. Greager and P.C. Paris, International J. Frac. Mechanics. 3, 1967, p.247.

74. C. E. Richards, C. N. Reed and R.E. Smallman, Intl. Conf. Strength Metals and Alloys, Japan Inst. Met. Tokyo, 517, 1967, p.961.

75. P.J. Worthington and E. Smith, Acta Met., 14, 1966, p.35.

76. C. Zener, 'Micro Mechanisms of Fracture', Fracturing of Metals, ASTM (1949), p.3.

77. A. H. Cottrell, Trans. AIME, 212, 1958, p.192.

78. W. Carrington, Proc. Royal Soc. (London), A-259, 1960, p.203.

79. R. Honda, Acta Met., 9, 1961, p.969.

80. A.N. Stroh, Fracture, B.L. Averbach et al., eds. MIT Press, Cambridge, Mass, and Wiley, New York, 1959, p.117.

81. D. Hull, Acta Met. 8, 1960, p.11.

82. D. Hull, Fracture of Solids, Drucker and Gilman, Eds., Interscience, New York, 1963, p.417.

83. C. N. Reid, J. Less Common Metals, 9, 1965, p.105.

84. J. Hording, Proc. Royal Soc. A299, 1967, p.464.

85. A. N. Stroh, Advances in Physics, 6, 1957, p.418.

86. J. P. Esheby, F. C. Frank and F.R.N. Nabarro, Phil. Mag. 42, 1951, p.351.

87. E. Smith, Inst. Phys. and Phys. Soc, London, 1966, p.36.

88. E. Smith, Internal J. of Fracture Mechanics, Vol. 4, 1968, p.131.

89. T. Yokobari, International J. of Fracture Mechanics, Vol. 5, 1968, p.179.

90. K.H. Reiff and C. Haas, Third Intl. Conf. on Fracture, Munich, Germany, April 1973.

91. C. J. McMahon and M. Cohen, Acta Met, 13, 1965, p.591.

92. G. Guessier and R. Castro, Rev. Metall. 46, 1949, p.517.

93. E. R. Parker, Brittle Behavior of Eng. Structures, Wiley, New York, 157.

94. E. O. Hall, Proc. Phys. Soc., 64B, 1951, p.742.

95. N. J. Petch, J.I.S.I., 174, 1953, p.25.

96. J. F. Knott, J. Mech. Phys. Solids, 15, 1967, p.97.

97. B. A. Wilcox, and A. Gilbert, Conf. on refractory Metals and Alloys, Vol. 4, Ed. R. I. Jaffee, et al., Gorden and Beach, NY 1969, p.95.

98. T. R. Wilshaw, C. A. Rau and A. S. Tetelman, Engr. Fracture Mech. 1, 1968, p.191.

99. J. A. Henrickson, D. S. Wood and D. S. Clark, Trans. ASM, 51, 1959,p191

100. J. F. Knott and A. A. Cottrell, J.I.S.I. 201, 1963, p.249.

101. T. R. Wilshaw and P.L. Pratt, Proc. of the first International Conf. on Fracture, Sendai, Japan, B.111, 2, 1965, p.973.

102. E. R. Puttick, Phil. Mag. Series 8,4, 1959, p.964.

103. H. C. Rogus, AIME Trans. 218, 1960, p.498.

104. R. J. Olsen, ASM Trans. Quarterly, 62, 1969, p.711.

105. E. Ruedl, J. of Materials Science, 4, 1969, p.814.

106. J. Gurland and J. Plateau, Trans. ASM, 56, 1963, p.442.

107. P.F. Thomason, J. of Inst. of Metals, 96, 1968, p.360.

108. F. A. McClintock, Int. J. of Fracture Mechanics, 96, 1968, p.360.

109. J. R. Rice and D. M. Tracey, J. Mech. Phys. Solids, 17, 1969, p.201.

110. F. A. McClintock, J. Appl. Mech., Trans. ASME, 35, 1968, p.353.

111. F. A. McClintock, Inter. J. Fracture Mech., 4, 1968, p.101.

112. R.F. Smith and J. F. Knott, Conf. on Practical Application of Fracture Mechanics to Pressure-Vessel Technology, London, 1971, Institution of Mechanical Engineers, London, 1971, p.65.

113. E. E. Hodgson, 'An Experimental Investigation of Deformation and Fracture Mechanisms in Spheriodized Carbon Steels, Ph.D. in Engineering, Materials Science Department, Stanford University, Stanford, CA, October, 1971.

114. Annual Book of ASTM Standards (American Society for Testing Materials, Philadelphia, 1972), p.955, part 31.

115. Ibid, p.959, part 31.

116. W. E. Wood, et al., AEC Contract No. W-7405-Eng. 48 and AMMRC Contract No. DAAG46-7-C-0220, May 1973.

117. W. E. Wood, E. R. Parker and V. F. Zackay, Report No. LBL-1474, Lawrence BErkeley Laboratory, University of California, Berkeley, CA, May 1973.

118. G. C. Sih, A Special Theory of Crack Propagation, Methods of Analysis and Solutions of Crack Problems, Edited by G. C. Sih, Noordhoff International Publishing Company, Croningen (1972).

119. G. C. Sih and E. P. Chen, Journal of Composite Materials, 7 (1973), p. 230.

120. M. E. Kipp and G. C. Sih, International J. of Solids and Structures, 11 (1975), p.153.

121. Philip H. Francis and William L. Ko, International Journal of Fracture, Vol. 12, No. 2, April 1976, p.243.

122. E. D. Hondros and D. McClean, Grain Boundary Structure and Properties, ed. G. A. Chadwick, D. A. Smith, London, Academic Press, 1976, p.353.

123. J. R. Rice, Corrosion, Vol. 32, No. 1, p.22.

124. R. O. Ritchie, J. F. Knott and J. R. Rice, J. Mech. Phys. Solids, 1973, Vol. 21, p.395.

125. N. J. Petch, J.I.S.I., Vol. 25 (1953), p.173.

126. A. N. Stroh , Proc. R. Soc., A 223, 404 (1954).

127. R. F. Hehemann, K. R. Kinsman and H. I. Aaronson: Metallurgical Trans. Vol. 3, May 1972 and 1077.

128. J. W. Christian 'Symposium on Decomposition of Austenite by Diffusional Processes', New York, Interscience, 1962, p.371.

129. F. B. Pickering, Transformation and Hardenability in Steels, Climax Molybdenum Co. of Michigan (Inc.), Feb. 27-28, 1967, p.109.

130. R. O. Ritchie, J. F. Knott and L.C.E. Geniets, The Microstructure and Design of Alloys, Proc. 3rd, Intl. Conf. on Strength of Metals and Alloys, p.124.

131. G. Clark, R.O. Ritchie and J.F. Knott, Nat. Phys. Sci., Vol. 239, 1972, p.104.

132. S. K. Banerjee, C. J. McMahan, Jr., and H.C. Feng., Met. Trans. A, Vol. 9A, Feb. 1978, p.237.

133. T. Ogura, C.J. McMahon,Jr., H.C. Feng, V. Vitek, Acta. Metallurgica, Vol. 26, 1978, p.1317.

134. R.W. Cahn, Physical Metallurgy, American Elsevier Publishing Co., Inc., New York, 1970.

135. G. R. Spiech and W.C. Leslie, Met. Trans. Vol. 3, May 1972.

136. G.R. Speich, Trans. TMS-AIME, 1969, Vol. 24, p.2553.

137. R.O. Ritchie and R.M. Horn - Unpublished research, Lawrence Berkeley Laboratory, University of California, Berkeley, CA 1976.

138. R.M. Horn and R.O. Ritchie, Met. Trans. A., Vol. 9A, August 1978 p.1039.

139. G. Thomas, Met. Trans A., Vol. 9A, March 1978, p.439.

140. J.M. Capus and G. Mayer: Metallurgia, 1960, Vol. 62 and p.133, JISI 1958, Vol. 196, p.255; ibid 1963; vol. 201, p.53.

141. C.J. McMahon, Jr., Mat. Sci. Engr. 1976, Vol. 25, p.233.

142. E.B. Kula and A.A. Anctil, J. Materials, 1969, 4, p.817.